

PhD Dissertation 12/2011

**Nuclear Magnetic Resonance Studies of Molecular Transport
in Activated Carbon and Other Porous Media**

Filipe Furtado

ISSN 1860-0387



Nuclear Magnetic Resonance Studies of Molecular
Transport in Activated Carbon and Other Porous Media

Von der Fakultät für Chemie und Mineralogie

der Universität Leipzig

genehmigte

DISSERTATION

zur Erlangung des akademischen Grades

DOCTOR RERUM NATURALIUM

(Dr. rer. nat.)

vorgelegt

von Diplom-Chemiker Filipe Ricardo Correia Duarte Furtado

geboren am 24. März 1981 in Lissabon, Portugal

Angenommen aufgrund der Gutachten von:

Prof. Dr. F.-D. Kopinke (Universität Leipzig)

Prof. Dr. J. Caro (Universität Hannover)

Tag der Verleihung: 18. Juli 2011

Die vorliegende Arbeit wurde unter Leitung von Prof. Dr. Frank-Dieter Kopinke und unter Betreuung von Dr. habil. Ulf Roland am Helmholtz-Zentrum für Umweltforschung UFZ im Zeitraum von November 2006 bis November 2010 angefertigt. Der experimentelle Teil der Arbeit wurde unter Leitung von Prof. Dr. Jörg Kärger und unter Betreuung von Juniorprof. Petrik Galvosas an der Universität Leipzig durchgeführt.

Bibliographic Description

Filipe Ricardo Correia Duarte Furtado

Nuclear Magnetic Resonance Studies of Molecular Transport in Activated Carbon and Other Porous Media

University of Leipzig, Doctoral Thesis

182 pages, 171 literature references, 75 figures, 3 tables

Abstract

The present thesis focuses mainly on the investigation of diffusive transport in activated carbons with a bi-modal pore size distribution from both lignocellulosic (MAC-LMA12) and polymeric (MA2) starting materials. This was achieved by using the ability of Pulsed Field Gradient Nuclear Magnetic Resonance (PFG NMR) to trace molecular displacements in a microscopic, non-invasive way. The observed distributions of diffusion coefficients revealed mass transport resistances on a length scale much smaller than the particle size, both in the studied activated carbons but also in the purely microporous NaX zeolite which was also investigated in this work. Furthermore, sorption-desorption hysteresis phenomena in the MA2 sample were investigated. There, it was verified that strong kinetic restrictions affected both the uptake and the inner-particle diffusivity of the guest substance.

Due to the limitations of PFG NMR in the study of environmentally relevant matrices, namely due to short relaxation times, and especially at concentrations of environmental significance, an alternative NMR method based on the phenomenon of Paramagnetic Relaxation Enhancement was developed. Its feasibility was demonstrated in both homogenous and heterogeneous model systems.

Bibliographischer Beschreibung

Filipe Ricardo Correia Duarte Furtado

Kernresonanzspektroskopische Untersuchung des Stofftransports in Aktivkohle und anderen porösen Materialien

Universität Leipzig, Dissertation

182 Seiten, 171 Zitate, 75 Abbildungen, 3 Tabellen

Zusammenfassung

Die vorliegende Promotion befasst sich im Wesentlichen mit der Untersuchung von Stofftransport infolge von Diffusion in Aktivkohlen, welche eine bimodale Porengrößenverteilung aufweisen. Es wurden Aktivkohlen untersucht, die sowohl auf Lignocellulose (MAC-LMA12) als auch auf synthetischen Polymeren (MA2) basieren. Die tragende Methode zur Untersuchung war hierbei die NMR mit gepulsten magnetischen Feldgradienten (PFG NMR). Diese erlaubt die Untersuchung von molekularen Verschiebungen auf einer mikroskopischen Längenskala auf nicht invasive Weise und ist deshalb zur Untersuchung der Aktivkohlen bestens geeignet. Die ermittelten Verteilungen von Diffusionskoeffizienten untermauern die Existenz von inneren Transportwiderständen auf einer Längenskala erheblich kleiner als der Durchmesser der einzelnen Aktivkohlekörner. Vergleichbare Ergebnisse sind aus der Literatur für zeolithische Systeme bekannt, welche im Rahmen dieser Arbeit auch speziell für den Zeolithen NaX bestätigt werden konnten. Überdies wurde an der Aktivkohle MA2 die Hysterese zwischen Adsorption und Desorption untersucht, welche auf eine starke kinetische Behinderung hinweist und somit sowohl die Sorptionsrate als auch die Diffusion der sorbierten Substanz im porösen Wirtssystem beeinflusst.

Ein weiterer Teil der Arbeit befasst sich mit der Entwicklung einer NMR-Methode zur Bestimmung molekularer Beweglichkeit speziell für umweltrelevante Proben, wo PFG NMR, bedingt durch zu kurze NMR Relaxationszeiten bzw. zu geringe Konzentrationen, nicht angewendet werden kann. Sie basiert auf der Ausnutzung des Paramagnetic Relaxation Enhancement (PRE) Effektes. Die Anwendbarkeit wurde sowohl für homogene als auch für heterogene Modellsysteme nachgewiesen.

Table of Contents

1. Introduction	6
2. Publications and Results	21
Publication 1: Characterization of carbon materials with the help of NMR methods	21
Publication 2: The evidence of NMR diffusometry on pore space heterogeneity in activated carbon	45
Publication 3: Tracing pore-space heterogeneities in X-type zeolites by diffusion studies	65
Publication 4: Guest diffusion in interpenetrating networks of micro- and mesopores	79
Additional results on MA2 activated carbon	99
Publication 5: Paramagnetic relaxation enhancement (PRE) as a tool for probing diffusion in environmentally relevant porous media	113
3. Conclusions	143
4. Selected Literature	147
5. Annexes	150

1. Introduction

Generally, all solid materials have a surface which forms the interface where interactions with liquid and gaseous substances occur. The accessible surface of a solid material primarily depends on its geometrical properties, namely its shape, size and its microscopic imperfections and defects. Therefore, solids with large surface area are able to interact with many molecules simultaneously, from which a significant change in the mobility of these interacting substances may result.

Porous media, composed of porous solids or powders, have the potential to accommodate large amounts of substance and interact with various compounds. These features are related to their high surface area and to the properties of their porous structure. This has been proven to be of great importance in many natural and technological processes [1]. In the context of environmental pollution, reduced mass transfer of pollutants in porous media such as soils greatly influence their bioavailability to pollutant-degrading bacteria, thus posing a major issue in soil remediation [2-5] and complicating risk assessment [6]. On the other hand, many chemical reactions, particularly in the field of heterogeneous catalysis are controlled by the rate at which the reactants are transported to reactive sites [7,8]. The interactions between molecules and surfaces in porous media frequently lead to complex patterns of mass transfer, which poses an obstacle in the development of new materials for specific applications but also in understanding in detail the established ones. This, together with the development of new porous materials in the last decades stresses the importance of investigating mass transfer phenomena in these cases and contributing to its clarification.

The search for efficient and cost-effective solutions in adsorbents for environmental remediation and supports for chemical catalysis has increasingly brought attention to nanoporous carbon materials, particularly to activated carbon [9,10]. Generally speaking, activated carbon is produced by carbonization of a carbon rich material followed by an activation step. Currently, activated carbon is industrially produced in large amounts, and has a wide range of applications. In fact, market studies forecast that due to growing environmental awareness in industrialized

countries the worldwide demand of activated carbon may reach up to 1.15 million tons in 2012 [11,12].

Although the final properties and applications from naturally occurring forms of porous carbons such as coal greatly differ from those of activated carbon, their basic structure remains strongly related. They are formed by imperfectly stacked graphene layers (see Figure 1) with the porosity being located on the gaps between these layers. Their strong apolar character and their slit-shaped geometry, due to the carbon sp^2 hybridization state, favors the adsorption of similarly aromatic and planar molecules [9] making them rather hydrophobic materials.

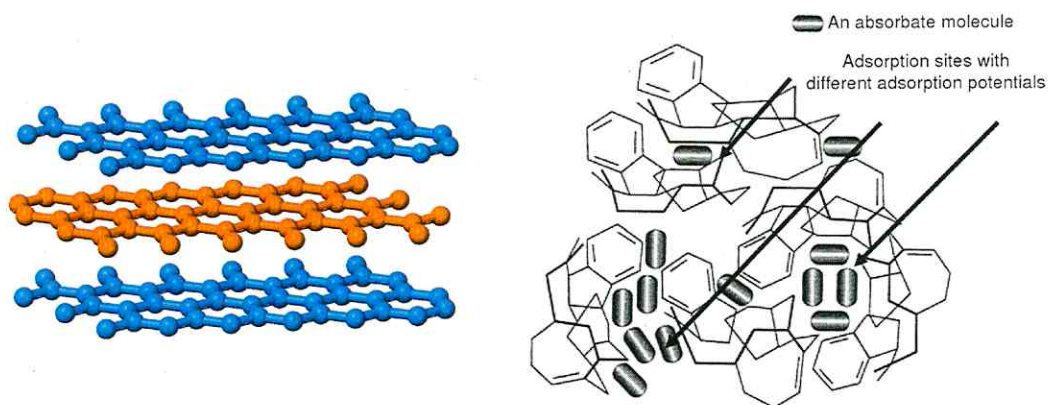


Figure 1 – Schemes of sp^2 -hybridized carbon atoms forming idealized graphene layers (left, retrieved from reference [13]) and schematic representation of a possible three-dimensional structure in activated carbon, forming pores with different sizes, shapes and showing adsorbate molecules (right, adapted from reference [9]).

The characteristics of a given activated carbon depend on the starting material and the activation process. Both natural (lignocellulosic) and synthetic materials can be used as parent materials for the carbonization step, while subsequent activation can be of thermal or chemical nature, or of a combination of these. Different gases and compounds can be used for this purpose. Together, all these variables influence the final product in texture, pore size distribution and surface

chemistry. During synthesis, particularly in dependence on the activation procedure and the precursor, various polar chemical groups are formed in the edges of these layers (Figure 2) and give these materials a potential for also adsorbing polar molecules.

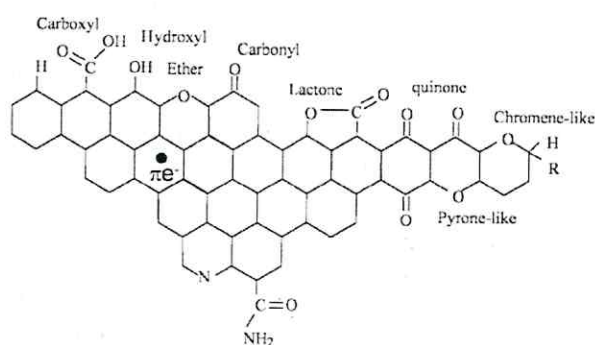


Figure 2 – Main functional groups found on the edges of the graphene layers. Adapted from reference [14]).

Typically, lignocellulosic materials have the advantages of being inexpensive and making a cost effective up-scaling in activated carbon production. However, the resulting materials retain, to some extent, the structure of their natural precursors, and typically exhibit highly developed microporosity. While this can be beneficial in remediation applications, it limits their applicability in fine chemistry and catalysis, since mesopores are known for playing a decisive role in mass transfer. For this reason, efforts have been made in the development of simultaneously micro- and mesoporous activated carbons [15], with recent years having a pronounced development of such materials, from both synthetic [16] and natural [17] precursors.

Activated carbon distinguishes itself from other porous materials by combining a very high specific surface area with different pore sizes, structure and surface chemistry, but more importantly, because of the possibility to control these by varying the starting materials and the activation processes. This makes it a particularly tailorable material, which accounts for its numerous applications in different fields of technology, ranging from water and air remediation [14],

to gas separation and storage [18], chemical catalysis [19], where it is used as a catalyst support or as catalyst *per se*.

Contrasting to activated carbons, other porous solids are regarded as highly organized in their structure. Zeolites present a rather defined structure, and are considered as crystalline materials with ordered arrangement of channels and chambers (referred to as supercages). To illustrate this, Figure 3 shows a scheme of the repeating unit and a SEM image of faujasite, one of many types of available zeolite structures. They are typically microporous materials and have been widely used as molecular sieves in gas separation and in chemical catalysis. Due to their idealized structure and its technical relevance, these materials have also served as a model system to study the adsorptive and molecular transport in porous media and associated phenomena. Literature is ever since their discovery abundant concerning these topics and there are a wide range of books on this subject [20].

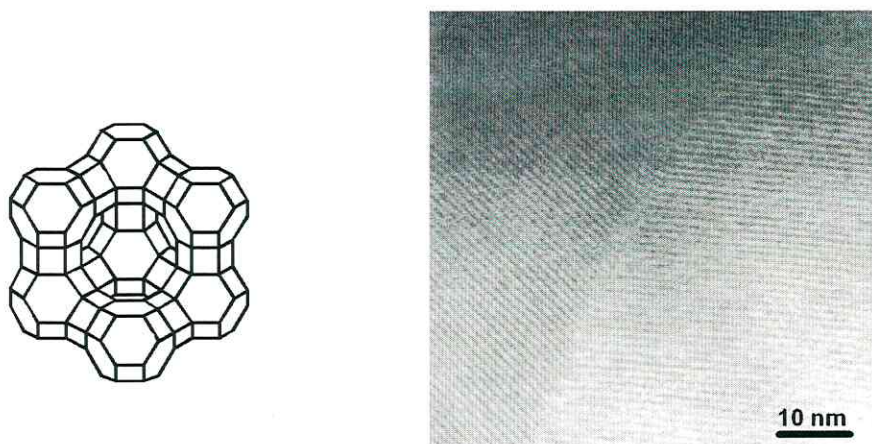


Figure 3 – Left) Scheme of faujasite (zeolites type X and Y) repeating unit (adapted from ref. [21]) and right) SEM image of faujasite where channels can be observed to have a parallel and well organized arrangement, with a 7.4 Å pore spacing [22].

Characterization of porous materials

Isothermal gas adsorption is a standard procedure to estimate the specific surface area of porous solids and powders, relying e.g., on the BET theory [21]. This method consists in recording the gas uptake from the material under study at subsequently increasing values of the applied external pressure. Since the capillary condensation of the adsorbing gas occurs as a function of pore size, different pores are filled up with liquid at different values of the externally applied pressure, thus providing qualitative information on the porosity of the material. Conversely, desorption of the guest molecules may be obtained by the stepwise reduction of the applied pressure. However, the rate at which the system equilibrates after each pressure step may differ in the case of increasing or decreasing pressures, which leads to the observation of hysteresis. This phenomenon becomes evident when different uptake values are observed for the same applied pressure on the adsorption and desorption branch. In such cases, the concentration in the system depends not only on the external applied pressure, but on other factors as well. Hysteretic behavior is typically observed in materials containing mesopores ($2 \text{ nm} < \text{pore size} < 50 \text{ nm}$) but has also been observed in microporous (pore size $< 2 \text{ nm}$) materials. The respective mechanisms are postulated to differ [21].

It is generally accepted that both hysteresis phenomena and the accessible surface area are highly dependent on the characteristics of the probe molecule, namely its size and polarity but also its mobility upon interaction with the solid matrix. Pores or spaces with diameters close to those of the probe molecules may be inaccessible or may require very long equilibration times, during adsorption experiments. Moreover, different compounds may experience different influence of the pore surface because of different adsorption potentials. These factors complicate accurate predictions on the behavior of different adsorbents by solely considering experimental data from gas adsorption isotherms.

Commonly, porous materials are characterized by combining information from different experimental techniques. However, for practical purposes and especially for technical processes

using porous media, the material itself is only a part of the system, which is also composed of the adsorbate molecules. Therefore, for characterization, it is important to consider the whole system, including the interaction between adsorbent and adsorbate, rather than the mere structure of the porous solid. Due to its structure complexity and heterogeneity, the complete characterization of activated carbons in terms of molecular adsorption and transport, is a particularly challenging task.

It has early been recognized that both adsorption and desorption on porous materials are largely controlled by the diffusive transport inside the porous matrix [23]. With time, it became widely accepted that pore and surface diffusion are fundamental in understanding phenomena such as pollutant bioavailability in natural porous media and soils [2,24] but also in heterogeneous catalytic processes [25]. For these reasons, experimental data concerning the diffusivity of gases and liquids in porous materials has become highly desirable, and different methods have been developed for this purpose. These can be divided into two sub-categories: macro- and microscopic methods. Macroscopic methods [26] involve measurements under non-equilibrium conditions, while microscopic or molecular methods refer to spectroscopic techniques, which are mostly performed in equilibrium conditions. Frequently, a discrepancy in the values obtained between these two types of experiments is observed. This has been interpreted as a direct consequence of the differing time scales in these experiments [27]. Macroscopic methods typically rely on the determination of concentration or adsorbent uptake as a function of time, from which the diffusivity can be estimated upon geometrical considerations and use of the appropriate models. These techniques include, for example, the gravimetric sorption method [26] and the time-lag approach [24], the latter consisting in measuring the flux through a porous sample by creating a concentration gradient along the sample length. In these methods, molecules must travel through the adsorbent bed before detection, which may imply long experimental times and molecular displacements over several millimeters. This contrasts with spectroscopic methods, such as Nuclear Magnetic Resonance (NMR), which has established as a method to investigate molecular dynamics. NMR line-shape and relaxation studies may provide information on the binding and interactions of the adsorbent with the

porous material [28]. With this approach one can indirectly measure molecular diffusivity, with typical time scales between 10^{-10} s and 10^{-1} s, corresponding to molecular displacements in the Angstrom (10^{-10} m) range, depending on the mobility of the probed nuclei. Relying on the use of Pulsed Field Gradients (PFG) in NMR experiments, NMR diffusometry [29,30] allows the investigation of molecular diffusion over significantly longer time scales from ms to s and corresponding molecular displacements, from nm to mm. Varying the observation time of the experiment allows studying the influence of different types of restrictions to diffusion, by pores of different sizes. This, combined with the fact that it is a nuclei-specific and non-invasive technique, makes it particularly suitable and reliable to study diffusion in porous media. Thus, it has seen extensive application in this [29-32] and other fields [33].

Despite its potential and applicability, the success of NMR diffusometry relies on sufficiently long longitudinal and transverse relaxation times, which sets the limit of both duration of the observation time and the gradient pulse, in the pulse sequence. This can be a major limitation, particularly in systems where paramagnetic species are present [34] or upon strong adsorption [35], since these are known to enhance spin-relaxation. Besides potentially containing significant amounts of paramagnetic metals and minerals, natural porous media such as coals, soils and sands may cause slow diffusivity and strong interaction of the species of interest with the pore surfaces, rendering the NMR diffusometry inadequate in such cases. Activated carbon samples contain varying ash amounts, potentially rich in paramagnetic species since, as previously mentioned, they are a product of carbonization of its starting materials. Likewise, strong adsorption and correspondingly slow diffusivities further restrict the obtainable information from PFG NMR measurements. Due to this reason, NMR diffusometry remains a less popular technique in studying activated carbon, in comparison to other porous media, such as zeolites. As a consequence, there is a lack of experimental data with activated carbons as host systems, in particular, concerning the influence of mesopores in mass transfer and hysteresis phenomenon. However, as it will be shown in the present work, the above mentioned obstacles may be circumvented, either by a careful

choice of the experimental conditions or by designing new methods which do not require the use of PFG.

Aims and overview of the presented publications and results

The study of molecular dynamics, in particular the diffusion of guest substances in different porous media, by means of different NMR methods is the central theme of the present thesis. Its main aim was the characterization of the mobility of different guest compounds by making extensive use of the ability of NMR diffusometry to trace their molecular displacements in activated carbons and, in particular, to clarify the role of mesopores in mass transfer. The present work benefits from recent hardware developments [36] and access to simultaneously micro- and mesoporous activated carbons through cooperation with the Advanced Materials Laboratory in Alicante, Spain. The diffusion in these materials, from both lignocellulosic (Publication 1) as well as from polymeric (Publication 2) origin, were investigated, and the obtained results compared to those in a microporous zeolite (Publication 3). Further studies in activated carbon include a detailed investigation of the hysteresis phenomenon, in these materials (Publication 4).

Considering the limitations of the PFG NMR technique, an additional objective of this thesis was the development of an alternative NMR method to probe molecular diffusivities with particular application to environmentally relevant systems (Publication 5).

Publication 1

This work combines NMR cryoporometry, relaxometry and diffusometry to investigate different activated carbon materials of lignocellulosic origin. These include microporous (Takeda 4A and 5A, Norit) and simultaneously micro- and mesoporous samples (MAC-LMA12, Nuchar). Textural characterization was done by nitrogen isothermal adsorption (BET). The pore size distribution for micro- and mesoporous samples was also estimated from NMR cryoporometry experiments using nitrobenzene as probe molecule. The interaction of ethanol (with high dipolar moment) and toluene

(with low dipolar moment) with the pore surface of purely microporous and simultaneously micro- and mesoporous samples was investigated by NMR-relaxometry. Furthermore, the diffusivity in these host-guest systems was measured via NMR diffusometry. These results revealed a pronounced distribution of diffusion coefficients in MAC-LMA12 sample which was not the case in strictly microporous systems. In the case of the former, the variation of the observation time produced no significant effect on the shape of the spin-echo attenuation, leading to the conclusion that the distribution on the diffusivities is caused by sample heterogeneities in the μm range. Moreover, from the initial slope of the spin-echo NMR decay, the average diffusion coefficients of ethanol, toluene, nitrobenzene, acetone and *n*-decane in MAC-LMA12 were determined. The obtained diffusivities are interpreted in light of the physico-chemical properties (bulk diffusivity and boiling point) of each of these compounds.

Publication 2

This publication presents the study of the cyclohexane diffusion properties in resin-based activated carbon (MA2). This material possesses an almost perfect mixture of micro- and mesoporosity with a particularly narrow pore size distribution in the respective regions, and is therefore an exciting model system for investigation of the interplay between these porous networks and its influence on the transport properties of the guest molecules. To do so, the self-diffusivity of cyclohexane was determined via NMR diffusometry, upon systematic variation of different parameters, as a means to obtain information on the connectivity of the pore system. This includes the dependency of *i*) the observation time and *ii*) nuclear magnetic transverse relaxation, *iii*) the effect of particle size, *iv*) the influence of substrate loading and the fraction of frozen cyclohexane in the mesopore space, by variation of *v*) the temperature of the measurement. Parameters *i*) to *iv*) revealed to have no significant influence on the observed distribution of diffusivities, while the freezing of cyclohexane led to an additional confinement of molecules in the micropores. These

observations indicate an interdependent contribution of the pore networks (micro- and mesoporous) to mass transfer in this sample.

The observed distribution of diffusivities in all loadings and corresponding temperatures is interpreted in terms of a log-normal distribution probability function, where the median diffusivity and variance serve as parameters to describe the experimentally determined diffusion coefficients. These are interpreted as a direct consequence of the sample heterogeneity and inherent transport resistivities, on a scale of around 10 μm , resembling those observed in other porous systems, such as zeolites.

Publication 3

The diffusion of *n*-butane in zeolite NaX was studied via NMR diffusometry at different loadings as a means to probe the homogeneity of the porous matrix. At lower concentrations, a broad distribution of diffusivities was observed together with an absence of observation time dependency, resembling the observations made in activated carbon systems. This confirms the existence of internal transport barriers, indicating considerable deviations from the idealized structure. These results are particularly relevant for the application of these materials in industrial processes, but also serve, in the present context, as a comparison to the results obtained in activated carbon systems known for their pore heterogeneity. Similarly to the latter system, the primary PFG NMR data obtained from *n*-butane in zeolite NaX were successfully fitted to a log-normal distribution function.

At higher loadings, *n*-butane diffusivity showed a bimodal character, rather than being log-normally distributed, accompanied by the observation of a time dependency. These results are interpreted in light of known models for inter-particle or long-range diffusion.

Publication 4

The main aim of this work was to investigate the adsorption hysteresis phenomena, in a hierarchical porous material, in this case the activated carbon MA2, by establishing an experimental correlation between the systems uptake and mass transfer occurring inside the pore structure. This was done by a procedure resembling the isothermal gas adsorption in which, upon system saturation, the external pressure of cyclohexane was varied subsequently to lower values until loading reached about 50% of the sample saturation (corresponding to empty mesopores) followed by a step-wise increase of the pressure till saturation was reached. In each pressure step, the loading of sample was determined by the initial intensity of the NMR free induction decay (FID) whereas the average diffusivity was determined by PFG NMR spectroscopy.

It was observed that with the chosen waiting times between each pressure step, the experimental data in the desorption branch significantly differed from the adsorption branch, representing a hysteresis between both loading and diffusion data. In the case of adsorption, waiting times of up to 20 h at pressures close to saturation were necessary for a significant change in the loading of the sample. Resembling purely mesoporous systems, loading and diffusivity appeared to be directly correlated with the "history" of the sample: they were found to be larger upon decreasing pressures (desorption) than on increasing pressure (adsorption). The maximum in the diffusivities observed in the adsorption branch was predicted by simple models which consider the contributions of micropores, mesopores and gas-diffusivity.

Additional results on MA2 activated carbon

The influence of temperature and loading of cyclohexane and toluene in MA2 activated carbon on the distribution of observed diffusivities was investigated by systematically fitting all the experimental data obtained to a log-normal distribution of diffusivities, in closed samples. From the fit results, the average diffusivities were plotted in an Arrhenius fashion, allowing to conclude on the

different mechanisms of molecular transport at different loadings and corresponding temperatures. These results are related to the system presented in Publication 2.

In addition to the results presented in Publication 4, the dependence of diffusivity on decreasing loading and pressure (desorption branch) was fitted by combining the determined micropore diffusivity with literature models used to describe the diffusivity in purely mesoporous materials, in which the contributions arising from both bulk liquid and the molecular transport in the Knudsen regime, are taken into account. Consideration of the estimated pore size distribution and the respective diffusivities, led to a good agreement with the experimentally obtained data.

Publication 5

Motivated by the limitations of the PFG NMR methodology concerning short relaxation times as previously described, the present work aimed to develop an alternative NMR method to investigate the molecular dynamics, providing a chance for application to environmentally relevant porous media and probe molecules. The enhancement of the relaxation rate due to the proximity to paramagnetic centers is known as Paramagnetic Relaxation Enhancement (PRE) and allowed the detection of 2,2,6,6-Tetramethylpiperidinyloxy (TEMPO) in water at concentrations as low as 70 ppm. The changes in NMR transverse relaxation times of water protons due to migration of TEMPO were measured via the CPMG pulse sequence, in homogeneous solution and in a water-saturated sand column. The transport diffusivity was estimated by applying adequate models to the two systems investigated. The method yielded results in accordance with the literature values. Thus, it opens a new approach to investigate molecular dynamics of probe molecules in low concentrations, as a method to provide information on the interactions with matrices of environmental relevance.

References

- [1] F. Schüth, K. S. W. Sing, and J. Weitkamp, *Handbook of porous solids*. Weinheim Germany: Wiley-VCH, **2002**.
- [2] National Research Council (U.S.), *Bioavailability of contaminants in soils and sediments processes, tools, and applications*. Washington D.C.: National Academies Press, **2003**.
- [3] A. Koelmans, M. Jonker, G. Cornelissen, T. Bucheli, P. Vannoort, and O. Gustafsson, Black carbon: the reverse of its dark side, *Chemosphere*, **2006**, 63, 365-377.
- [4] L. J. Ehlers and R. G. Luthy, Peer reviewed: contaminant bioavailability in soil and sediment, *Environ. Sci. Technol.*, **2003**, 37, 295A-302A.
- [5] K. Semple, K. J. Doick, K. C. Jones, P. Burauel, A. Craven, and H. Harms, Peer reviewed: defining bioavailability and bioaccessibility of contaminated soil and sediment is complicated, *Environ. Sci. Technol.*, **2004**, 38, 228A-231A.
- [6] R. Geyer, A. D. Peacock, A. Miltner, H. H. Richnow, D. C. White, K. L. Sublette, and M. Kästner, In situ assessment of biodegradation potential using biotrap amended with ¹³C-labeled benzene or toluene, *Environ. Sci. Technol.*, **2005**, 39, 4983-4989.
- [7] G. Ertl, H. Knözinger, F. Schüth, and J. Weitkamp, *Handbook of heterogeneous catalysis*. Weinheim, Chichester: Wiley-VCH, John Wiley, **2008**.
- [8] G. Swiegers, *Mechanical catalysis: methods of enzymatic, homogeneous, and heterogeneous catalysis*. Hoboken N.J.: John Wiley, **2008**.
- [9] F. Rodríguez-Reinoso and H. Marsh, *Activated carbon*. Amsterdam; Boston: Elsevier, **2006**.
- [10] P. Serp and J. L. Figueiredo, *Carbon materials for catalysis*. Hoboken N.J.: John Wiley & Sons, **2009**.
- [11] W. Storck, Activated carbon demand shows promise, *Chem. Eng. News*, **1996**, 74, 22.
- [12] Water World, New report examines world demand for activated carbon, available online at <http://www.waterworld.com>, **2008**.
- [13] Available online at <http://en.wikipedia.org/wiki/File:Graphite-layers-side-3D-balls.png>, **2010**.
- [14] T. Bandoz, *Activated carbon surfaces in environmental remediation*. Amsterdam; London: Elsevier, **2006**.
- [15] S. R. Tennison, Phenolic-resin-derived activated carbons, *Appl. Catal.*, **1998**, A: General, 173, 289-311.
- [16] J. Yang, Preparation and properties of phenolic resin-based activated carbon spheres with controlled pore size distribution, *Carbon*, **2002**, 40, 911-916.

- [17] J.M.Juárez-Galán, A. Silvestre-Albero, J. Silvestre-Albero, and F. Rodríguez-Reinoso, Synthesis of activated carbon with highly developed “mesoporosity”, *Microporous Mesoporous Mater.*, **2009**, 117, 519-521.
- [18] F. Rodríguez-Reinoso, Porous carbons in gas separation and storage, in *Combined and Hybrid Adsorbents*. J. M. Loureiro and M. T. Kartel, Eds. Springer Netherlands, **2006**.
- [19] F. Rodríguez-Reinoso, The role of carbon materials in heterogeneous catalysis, *Carbon*, **1998**, 36, 159-175.
- [20] J. Kärger and D. M. Ruthven, *Diffusion in zeolites and other microporous solids*. New York: Wiley, **1992**.
- [21] F. Rouquerol, J. Rouquerol, and K. Sing, *Adsorption by powders and porous solids principles, methodology, and applications*. San Diego : Academic Press, **1999**.
- [22] Jeol USA, Electron Optics Image Gallery, **2011**.
- [23] D. Ruthven, *Principles of adsorption and adsorption processes*. New York: Wiley, **1984**.
- [24] P. Grathwohl, *Diffusion in natural porous media: contaminant transport, sorption desorption and dissolution kinetics*. Boston: Kluwer Academic Publishers, **1998**.
- [25] C. Satterfield, *Mass transfer in heterogeneous catalysis*. Huntington N.Y.: R.E. Krieger Pub. Co.,**1981**.
- [26] D. M. Ruthven, S. Brandani, and M. Eic, Measurement of diffusion in microporous solids by macroscopic methods, in *Adsorption and diffusion*. H. G. Karge and S. Brandani, Eds. Berlin; Heidelberg: Springer, **2008**.
- [27] J. Kärger and D. M. Ruthven, On the comparison between macroscopic and n.m.r. measurements of intracrystalline diffusion in zeolites, *Zeolites*, **1989**, 9, 267-281.
- [28] V. V. Turov and R. Lebeda, Application of ¹H NMR spectroscopy method for determination of characteristics of thin layers of water adsorbed on the surface of dispersed and porous adsorbents, *Adv. Colloid Interface Sci.*, **1999**, 79, 173-211.
- [29] F. Stallmach and J. Kärger, The potentials of Pulsed Field Gradient NMR for investigation of porous media, *Adsorption*, **1999**, 5, 117-133.
- [30] F. Stallmach and P. Galvosas, Spin echo NMR diffusion studies, *Ann. Rep. NMR S.* **2007**, 61, 51– 131.
- [31] W. S. Price, NMR Diffusometry, in *Modern Magnetic Resonance - Part I*. G. A. Webb, Ed. Dordrecht: Springer Netherlands, **2006**.
- [32] T. Brandt, E. Cabrita, and S. Berger, Theory and application of NMR diffusion studies, in *Modern Magnetic Resonance - Part I*. G. A. Webb, Ed. Dordrecht: Springer Netherlands, **2006**.

- [33] P. Callaghan, *Principles of nuclear magnetic resonance microscopy*. Oxford: Clarendon Press, **1993**.
- [34] I. Foley, Effect of paramagnetic ions on NMR relaxation of fluids at solid surfaces, *Journal of Magnetic Resonance, Series A*, **1996**, 123, 95-104.
- [35] K. J. Dunn, D. J. Bergman, and G. A. Latorraca, *Nuclear magnetic resonance*. Amsterdam, London: Pergamon, **2002**.
- [36] P. Galvosas, F. Stallmach, G. Seiffert, J. Kärger, U. Kaess, and G. Majer, Generation and application of ultra-high-intensity magnetic field gradient pulses for NMR spectroscopy, *Journal of Magnetic Resonance*, **2001**, 151, 260-268.

2. Publications and Results

Publication 1: Characterization of carbon materials with the help of NMR

methods

Microporous and Mesoporous Materials, **2009**, *120*, 91

M. Krutyeva^a, F. Grinberg^a, F. Furtado^c, P. Galvosas^a, J. Kärger^a, A. Silvestre-Albero^b, A. Sepulveda-Escribano^b, J. Silvestre-Albero^b and F. Rodríguez-Reinoso^b

^aDepartment of Interface Physics, University of Leipzig, Linnéstr. 5, D-04103 Leipzig, Germany

^bLaboratorio de Materiales Avanzados, Departamento de Química Inorgánica, Universidad de Alicante, Ap.99, E-03080 Alicante, Spain

^cHelmholtz Centre for Environmental Research, Leipzig, Permoserstr. 15, D-04318 Leipzig, Germany

Abstract

Combined NMR cryoporometry, relaxometry and diffusometry were applied to characterize porous carbon materials. Pore space characterization in NMR cryoporometry is based on the measurement of melting-point depression of the confined liquids, whereas NMR relaxometry and diffusometry explore the random motion of the molecules under confinement by the pore space. We demonstrate compatibility between the evidence of classical sorption experiments and NMR cryoporometry on pore size distribution. There is a distribution in both the nuclear magnetic relaxation rates and diffusion coefficients. These distributions have to be referred to heterogeneities in the pore space. Since they can only be observed if their influence is not averaged out on the diffusion paths covered by the molecules during the respective measurements, the spatial extension of the regions with structural differences (as evidenced by the differences in diffusion and nuclear magnetic relaxation of the probe molecules) may be estimated to be at least of the order of 20 μm .

Keywords: activated carbons, porous structure, NMR, diffusion, liquids

1. Introduction

Nanoporous carbon materials are used in a wide range of industrial applications, including heterogeneous catalysis, separation, storage of gases and fluid purification. These materials are characterized by a complex porous network constituted of micropores with pore widths of less than 2 nm, mesopores with pore widths between 2 and 50 nm and macropores with pore width greater than 50 nm. Such a three-dimensional pore structure results in a material that exhibits a high surface area together with a high pore volume. Additionally, carbon materials can accommodate heteroatoms (mainly oxygen surface groups) on structural defects (e.g. boundaries of the graphene layer) which affect the surface chemistry of the material. A main advantage of porous carbons in respect to other porous solids is that, both the porous structure and the surface chemistry can be tailored by pre- and post-synthesis treatments. This helps to achieve the properties required for a particular application [1].

The proportion of micropores and mesopores on carbon materials strongly depends on the synthesis procedure used. Microporous carbons can be prepared from a wide variety of lignocellulosic precursors (olive stones, coconut shell, etc.) using either physical (CO_2 , H_2O , etc.) or chemical (H_3PO_4 , ZnCl_2 , etc.) activation [2-4]. Although the presence of microporosity is required to achieve a high surface area, i.e. a high adsorption capacity, the presence of some mesoporosity is quite often desirable. Mesopores are very useful, not only for processes involving larger molecules, but also because they constitute channels for speeding up the access to the inner microporosity. Carbon materials with a highly developed mesoporosity can be prepared using different approaches, such as combination of chemical and physical activation, use of nanocasting (hard and soft template strategy) technology, etc. [5,6,7].

Textural characterization of nanoporous carbon materials is commonly performed using adsorption of probe molecules (He, Ar, N_2 , CO_2 , etc.). Among them, N_2 adsorption at 77 K and CO_2 adsorption at 273 K are the most widely used to assess both the total microporosity (< 2 nm) and

the narrow microporosity (< 0.7 nm), respectively [8]. Additionally, application of several mathematical models to the adsorption isotherms can provide information about the “apparent” surface area, pore size distribution, etc. (e.g. Brunauer-Emmett-Teller equation to the N₂ adsorption isotherm). Although the correct characterization of the textural properties is of paramount importance to understand the behavior of carbon materials in a certain application, their effectiveness in adsorption processes will also be highly depending on the transport (diffusion) of adsorptives to the inner pore system.

NMR methods have proven to be an efficient tool to study micro- and mesoporous materials and surface interactions of confined liquids [9]. A combination of several NMR techniques is especially useful as it allows for elucidation of a multitude of important system characteristics. As an example, the properties of sorbate molecules in contact with the liquid/solid interfaces at pore walls were studied with the help of NMR cryoporometry and relaxometry [10,11]. NMR cryoporometry provides information on the distribution of the pore size. NMR relaxometry is especially sensitive to surface interactions. The aim of this work is the characterization of mesoporous carbons by combination of the three NMR techniques: cryoporometry, relaxometry and diffusometry. Various adsorptive molecules were used for this study. One of the accents was put on monitoring molecular transport of the confined liquids in the porous space of the investigated materials. Direct measurements of molecular self-diffusion were performed with the help of Pulsed Field Gradient (PFG) NMR permitting one to obtain an in-depth information on both transport properties of the confined liquids and the structure characteristics of the host material.

2. Experimental

2.1. Materials

Two carbon molecular sieves (Takeda 4A and Takeda 5A, Takeda Chemical Industries Ltd.) and three different activated carbons (PK13, RGC30 and MAC-LMA12) have been used in this

study. The selection of these samples is based on their different textural properties. While carbon molecular sieves and the activated carbon PK13 (Norit) are mainly microporous, the samples RGC30 (Nuchar) and MAC-LMA12 exhibit both micro- and mesoporosity.

Carbon molecular sieves Takeda 4A and Takeda 5A and activated carbons PK13 and RGC30 are commercially available carbon materials. Sample MAC-LMA12 (MAC: mesoporous activated carbon; LMA: Laboratorio de Materiales Avanzados; x=12: production number) was prepared from olive stones as a raw material. Firstly, the olive stones were crashed, sieved to 3 mm and washed with diluted H_2SO_4 (10%) to remove the majority of inorganic impurities. The clean sample was impregnated with an aqueous solution of CaCl_2 (7 wt.%) for 7 h in a thermostatic water bath at 358 K. After 7 h, the temperature was increased up to 373 K and held at this temperature until the level of water became similar to that of olive stone, the remaining water being removed by filtration. The impregnated sample was dried for 24 h at 353 K in an air recirculation oven and then it was submitted to an activation treatment in a horizontal furnace using CO_2 (100 ml/min) at 1043 K for 6 h. After the activation, the sample was outgassed in a vacuum oven for 4h at 323 K, in order to remove the remaining CO_2 adsorbed, and subsequently washed with hot HCl (5%) in order to remove the remaining calcium; a final washing with distilled water until pH=7 was performed.

In order to avoid interferences in the diffusion process from inorganic species remaining on the carbon structure, all carbon materials have been washed with HCl (10%) at 353 K for 3h. After the acid treatment, carbon samples have been washed with distilled water until pH=7 and subsequently dried overnight at 353 K. After the washing treatment, the total ash content is mainly nil for RGC30, MAC-LMA12, Takeda 4A and Takeda 5A samples, while it is around 2 wt % for sample PK13.

2.2. Sample characterization

N₂ and CO₂ adsorption isotherms were determined in a Coulter Omnisorb-610 equipment at 77 K and 273 K, respectively. Prior to the adsorption measurement, samples were outgassed under vacuum (10⁻³ Pa) at 523 K for 4h. Dubinin-Radushkevich (DR) equation was applied to the N₂ and CO₂ adsorption isotherms in order to obtain both the total micropore volume (V₀) and the volume of narrow microporosity (V_n), respectively [12]. Total pore volume (V_t) was obtained from the amount adsorbed at P/P₀ ~ 0.99 on the N₂ isotherm, while the mesopore volume (V_{meso}) was calculated from the difference between (V_t) and (V₀). The “apparent” surface area (S_{BET}) was determined applying the Brunauer-Emmett-Teller (BET) equation to the N₂ adsorption isotherms.

2.3. NMR analysis

All NMR measurements were performed with the help of the home-built PFG NMR spectrometer FEGRIS NT, operating at a ¹H resonance frequency of 125 MHz [13]. High-intensity magnetic field gradients (up to 35 Tm⁻¹) were applied.

The construction of the melting curves in the experiments on NMR cryoporometry was based on the temperature dependences of the NMR signal intensity. The latter was evaluated as the maximal spin echo amplitude produced by the standard Hahn echo radio frequency pulse sequence (90° - τ - 180°). The value of τ was set to 2 ms. All measured echo amplitudes were normalized by the value of the (echo) amplitude at the highest temperature (above the bulk melting point). The range of investigated temperatures was between 165 K and 298 K. The experiments were started at the lowest temperature and then the temperature was increased in steps of 5 K. The relaxation rates of the adsorbate molecules in the investigated samples were determined using the Carr-Purcell-Mejboom-Gill (CPMG) pulse sequence. The measurement of diffusion coefficients in PFG NMR was performed with the help of the standard three 90°- pulse sequence (also known as the “stimulated echo” pulse sequence).

The preparation of the samples for the NMR experiments was performed as follows. The host material was introduced into the sample tubes with an outer diameter of 7.5 mm. After that, the tubes with the material were heated at 383 K during 24 h in an oven under atmospheric conditions. Then the samples were connected to the vacuum system and dehydrated under high vacuum (less than 10^{-2} Pa) at 523 K for around 4 h. While evacuating, a certain amount of liquid was injected into the tubes. For relaxation and diffusion experiments, the amount of the sorbate was adjusted to achieve full loading of the pores (100% of the total pore volume). For the NMR cryoporometry experiments, the amount of sorbate (nitrobenzene in our work) was supplied in excess, thus allowing an oversaturation of the host material. Finally, the sample tubes were sealed.

3. Results and discussion

3.1. Textural characterization

Figure 1 shows the N_2 adsorption isotherms for the different samples studied. As it can be observed, all carbon materials exhibit a high nitrogen uptake at low relative pressures ($P/P_0 < 0.01$), which mainly corresponds to the adsorption on micropores. After the sharp knee in the N_2 isotherms, samples PK13 and MAC-LMA12 exhibit a near-plateau with a small slope but, above $P/P_0 \sim 0.6$, the sample MAC-LMA12 exhibits an important increase in the amount adsorbed and a hysteresis loop suggesting the additional presence of some mesoporosity. The situation becomes different for sample Nuchar RGC30. This activated carbon exhibits a continuous increase in the amount adsorbed over the whole relative pressure range (up to $P/P_0 = 0.97$), which corresponds to the combined presence of microporosity together with a well-developed mesoporosity. These findings are clearly reflected on Table 1. The micropore volume, obtained from the N_2 (V_0) and CO_2 (V_n) adsorption isotherms for sample Norit PK13 is quite similar, thus reflecting the presence of a narrow pore size distribution on this sample [14]. This difference between V_0 and V_n becomes slightly more evident for the synthesized activated carbon, denoted MAC-LMA12, in which the total

pore volume is constituted by about 70% mesopores and 30% micropores. Last but not least, sample RGC30 exhibits very different values for V_0 and V_n , which confirms the presence of a broad micropore size distribution with combination of both micropores and mesopores (the proportion of narrow micropores being less important than for the other carbons).

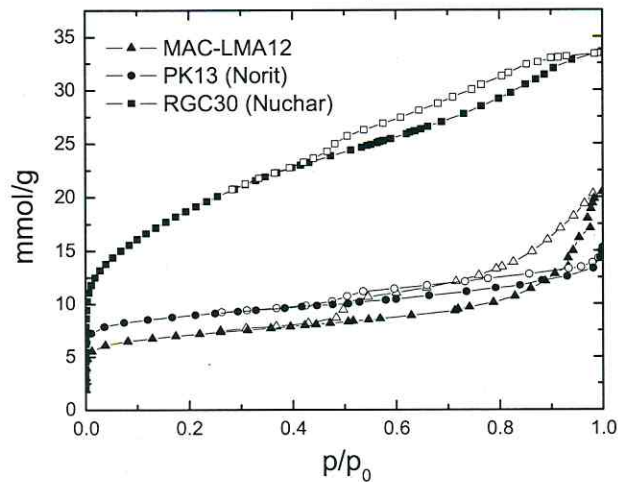


Fig.1 N_2 adsorption isotherms at 77 K for samples Nuchar RGC30, Norit PK13 and MAC-LMA12.

As it has been mentioned before, carbon molecular sieves Takeda 4A and Takeda 5A have been also considered for this study due to the pure microporous nature of these samples (more than 90% of the pore volume is in the range of microporosity), with the mesopore volume in these materials being almost nil [15]. The micropore volumes V_0 obtained from N_2 adsorption isotherms at 77 K are $0.22 \text{ cm}^3\text{g}^{-1}$ and $0.33 \text{ cm}^3\text{g}^{-1}$, for samples Takeda 4A and Takeda 5A, respectively. The two carbon molecular sieves Takeda 4A and Takeda 5A differentiate from each other by the size of the mouth in the microporous space: 0.4 and 0.5 nm, respectively [1].

	$S_{\text{BET}} / \text{m}^2 \text{g}^{-1}$	$V_0 (\text{N}_2) / \text{cm}^3 \text{g}^{-1}$	$V_{\text{meso}} / \text{cm}^3 \text{g}^{-1}$	$V_t / \text{cm}^3 \text{g}^{-1}$	$V_n (\text{CO}_2) / \text{cm}^3 \text{g}^{-1}$
MAC-LMA12	569	0.23	0.48	0.71	0.21
Norit PK13	738	0.29	0.24	0.53	0.26
Nuchar RGC30	1521	0.52	0.64	1.16	0.34

Table 1 “Apparent” surface area (S_{BET}), micropore volume V_0 , mesopore volume V_{meso} and total pore volume V_t in the samples studied, as obtained from the N_2 adsorption measurements at 77 K and the pore volume determined by CO_2 adsorption experiment V_{CO_2} at 273 K.

3.2. NMR cryoporometry

NMR cryoporometry exploits the melting point depression of liquids confined in mesopores [16]. The melting temperature T_m of a liquid frozen in pores is lower than that of a bulk liquid as a consequence of the smaller crystal sizes and the enhanced surface-to-volume ratio. This effect is larger for smaller pores. According to the Gibbs-Thomson equation [17] the difference between the normal (bulk) and the depressed melting points (in pores) is inversely proportional to the pore diameter d :

$$\Delta T_m(d) = T_m - T_m(d) = k/d, \quad (1)$$

where k is a constant related to the thermodynamic properties of the confined liquid. In materials with a distribution of pore diameters, the melting temperature of the confined liquid will vary with the pore size. In NMR cryoporometry, one only observes the NMR signal due to the

molecules in the liquid state. Therefore, at each temperature below the bulk melting point, the measured signal intensity is proportional to the volume of the non-frozen liquid confined in the pores. Analyzing the NMR response as a function of the temperature permits to determine the distribution of the pore sizes using the

$$\frac{\Delta v}{\Delta d} = \frac{k \Delta v}{\Delta T_m(d) d^2} \quad (2)$$

where v is the total volume of pores with diameters $\leq d$. Hence, $\frac{\Delta v}{\Delta d}$ is nothing else than the pore size distribution, which, owing to Eq. (2), becomes directly experimentally accessible. The parameter k should be known (or calibrated) in advance. This method is limited to pore sizes exceeding 1 nm and is efficient in characterizing the pores on the mesoscopic length scale.

The transverse nuclear magnetic relaxation of guest molecules within the micropores was typically small (≤ 2 ms) so that the contribution of these molecules to the observed NMR signal could be neglected. It is, therefore, exclusively the size distribution of the mesopores which is traced in our present cryoporometry studies.

In this work, the so-called melting curves, i.e. the temperature dependences of the NMR signal intensity, were measured for nitrobenzene confined in MAC-LMA12, Nuchar RGC30 and Norit PK13. Figure 2 shows the melting curves of all three samples in the range of temperatures between 165 K and 298 K. The bulk melting point of nitrobenzene at 279 K is indicated as the vertical line. A step-like decrease in the vicinity of this temperature observed for all three samples is attributed to the bulk liquid component (outside the pores). Obviously, in sample MAC-LMA12 this decay merges with the decay in large mesopores and macropores which introduces a large uncertainty in pore size distribution resulting from this part of the melting curve. For two samples, MAC-LMA12 and RGC30, a change of the signal intensity was also observed at lower temperatures, i.e. below the bulk step. This change refers to melting of nitrobenzene confined in the mesoporous space of these materials. In Norit PK13, melting in the mesopores was not observed.

This indicates that the mesoporous volume in PK13 is small in comparison to the other two samples, in agreement with the adsorption results (see Table 1).

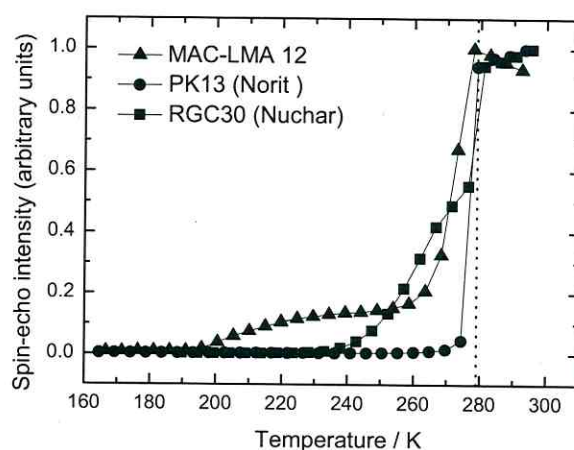


Fig.2 Temperature dependence of the NMR spin-echo signal intensity (“melting curves”) of nitrobenzene in Nuchar RGC30, Norit PK13 and MAC-LMA12 carbon materials. The signal intensity is proportional to the total amount of liquid within the sample at the given temperature. The vertical line indicates the bulk melting point of nitrobenzene.

The pore size distributions of RGC30 and MAC-LMA12 calculated from the melting curves are shown in Figure 3. The mean pore diameters could roughly be estimated from the peaks of the distribution functions as ~ 2 nm and ~ 7 nm for MAC-LMA12 and RGC30 samples, respectively. Figure 3 shows that the distribution around these values is broader for RGC30 than for MAC-LMA12. In the latter sample, there is an additional broad peak centered at around 15 nm. It corresponds to the first steep decay in the melting curves, close to the bulk melting point. Due to the limited resolution in this range of our melting curve, this peak does only indicate the presence of some larger mesopores and macropores and is not suitable for quantitative analysis.

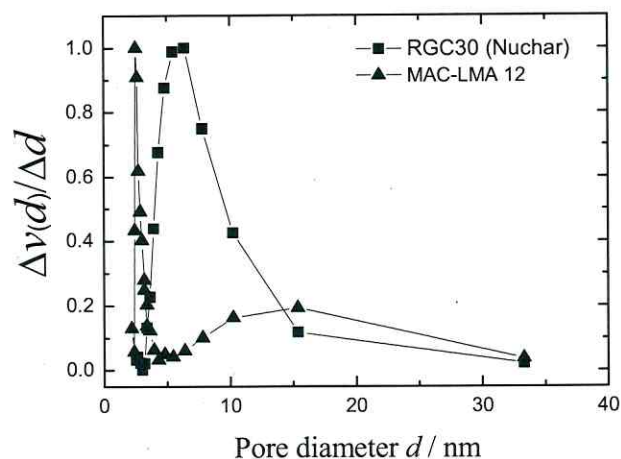


Fig.3 Pore size distribution in Nuchar RGC30 and MAC-LMA12 samples calculated from the melting curves shown in Fig. 2.

3.3. NMR relaxometry

In addition to NMR cryoporometry which is sensitive to pore space geometry, NMR relaxometry can provide valuable information on molecular dynamics of the confined liquid and on surface interactions. The adsorbate molecules probe the pore structure and surfaces via translational diffusion between the surface sites and the internal volume of the pore. In the vicinity of the solid surface, the transverse relaxation time T_2 of a liquid tends to decrease in comparison to the bulk state. The decrease is the larger the stronger is the surface interaction and is usually more pronounced for polar liquids. In pores with characteristic sizes of a few or a few tens of nanometers the exchange between the surface sites and the pore interior is fast on the time scale of the NMR experiment. The measured transverse relaxation rate T_2^{-1} of a liquid in the mesopores, therefore, will represent an average of the bulk-like liquid relaxation rate $T_{2,\text{bulk}}^{-1}$ and the enhanced surface

relaxation rate, weighted according to the surface-to-volume ratio of the pore. Brownstein and Tarr calculated T_2^{-1} of a liquid confined in a simple spherical pore with a volume V and a surface S :

$$\frac{1}{T_2} = \frac{1}{T_{2,\text{bulk}}} + \rho \frac{S}{V} \quad (3)$$

where S/V is the surface-to-volume ratio and ρ is the surface relaxivity [18]. Equation (3) contains quantities related both to geometrical characteristics (surface-to-volume ratio) and to surface interactions (surface relaxivity). The amplitude of the transverse magnetization in a system with equally sized pores and uniform surface interactions will be a simple exponential function of time:

$$\Psi(t) = I(t)/I(0) = \exp\left(-\frac{t}{T_2}\right) \quad (4)$$

where $I(t)$ is the intensity of the transverse magnetization at time t . In our experiments, it was evaluated from a series of spin echoes produced by the CPMG pulse sequence [19]. If there is a distribution of the pore sizes, the relaxation function will result as the integral of the contributions of the individual pores [20]:

$$\Psi(t) = \int f(T_2^{-1}) \exp\left(-\frac{t}{T_2}\right) d(T_2^{-1}) \quad (5)$$

where $f(T_2^{-1})$ denotes the distribution function of the relaxivities. The mean relaxation rate can be determined from the initial slope of the relaxation curve according to

$$\langle T_2^{-1} \rangle = -\lim_{t \rightarrow 0} \frac{\partial}{\partial t} (\Psi(t)) = \int T_2^{-1} f(T_2^{-1}) d(T_2^{-1}) \quad (6)$$

Typically, the transverse relaxation time of a bulk liquid (seconds) is much larger than that of a liquid near the pore wall (milliseconds or below). Therefore, the measured relaxation rate in Eq. (3) is determined solely by the second term. Provided the distribution of relaxivities $f(T_2^{-1})$ is due to

distribution of the pore sizes only, the latter can be deduced from the measured relaxation function, Eq. (5). This was demonstrated, for example, for a series of silica gels in Ref. [11].

Figure 4 shows the attenuations of transverse magnetization of ethanol, nitrobenzene and toluene in MAC-LMA12 as a function of time. Deviations from the exponential behavior were observed. A closer inspection shows that the curves can be decomposed into two components

$$\Psi(t) = \Psi_{\text{fast}}(t) + \int f(T_2^{-1}) \exp\left(-\frac{t}{T_2}\right) d(T_2^{-1}) \quad (7)$$

where $\Psi_{\text{fast}}(t)$ refers to the “fast” attenuation component visible at short times, see inset in Figure 4. This component is relevant for a quite small fraction of molecules (10-20%) and, therefore, cannot be analyzed in more detail as it is masked by the dominating “slower” component. The latter refers to 80-90% of molecules and exhibits a moderate deviation from the exponential behavior. The existence of two components in the relaxation curves indicates the presence of two species of molecules with different dynamic properties. The species with the faster relaxation and smaller population should probably be attributed to the liquid confined in the microporous space. The larger fraction with slower relaxation should then be attributed to the liquid in the mesopores. It is worth noting that the exchange between the two species is hindered. This is in spite of the large diffusion path lengths of more than 100 nm, notably exceeding the pore sizes. In turn, this should mean that as soon as the molecules enter the microporous space (or some specific areas of this space) they tend to stay in this space and not easily exchange with the molecules in the mesopores.

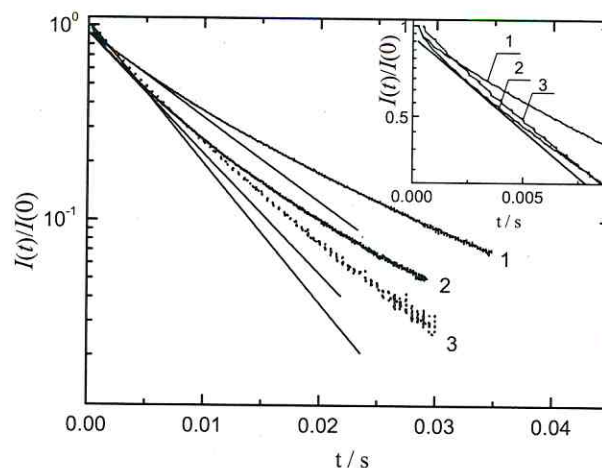


Fig.4 Attenuation of the transverse magnetization of toluene (1), ethanol (2), and nitrobenzene (3) at 298 K confined in MAC-LMA12. The initial parts of these plots are presented in the inset. The attenuation curves were measured by the CPMG pulse sequence.

The mean relaxation rates were determined from the initial slopes of the slow components of the relaxation curves according to Eq. (4). The corresponding inverse values, $1/\langle T_2^{-1} \rangle$, for toluene, ethanol and nitrobenzene were 10 ms, 7 ms and 6 ms, respectively. The fact that the relaxation times of ethanol and nitrobenzene were shorter than in toluene correlates with the much stronger polarity of these liquids in comparison with toluene. This is due to the stronger surface interactions of polar molecules giving rise to enhanced relaxivity at the surface and, hence, to shorter overall transverse relaxation times [11].

PFG NMR diffusion studies reveal molecular displacements of order of micrometers during the experimental observation times (see Section 3.4). Therefore, a non-exponential relaxation behavior can only be observed if the sample consists of sub-regions of different pore characteristics (e.g. mean pore sizes) with extensions over at least tens of micrometers.

The analysis of the molecular dynamics in the microporous space of the MAC-LMA12 material was approached by separate studies of the microporous carbon materials Takeda 4A and Takeda 5A. The relaxation curves of ethanol and toluene in these materials are shown in Figure 5. Only slight deviations from the exponential behavior are observed. The relaxation times (obtained as the inverse values of the mean relaxation rates, $1/\langle T_2^{-1} \rangle$) were 1.2 ms and 2 ms for ethanol, and 0.5 ms and 0.8 ms for toluene in Takeda 4A and Takeda 5A, respectively. Again the trends in the relaxation rates exhibit the expected behavior. The relaxation times become the smaller, the more rigid are the formed guest-host complexes: both an increase in the guest size (from ethanol to toluene) and a decrease in the host "cage" size (from Takeda 5A to Takeda 4A; in parallel with an enhancement of the surface-to-volume ratio) lead to slower relaxation times.

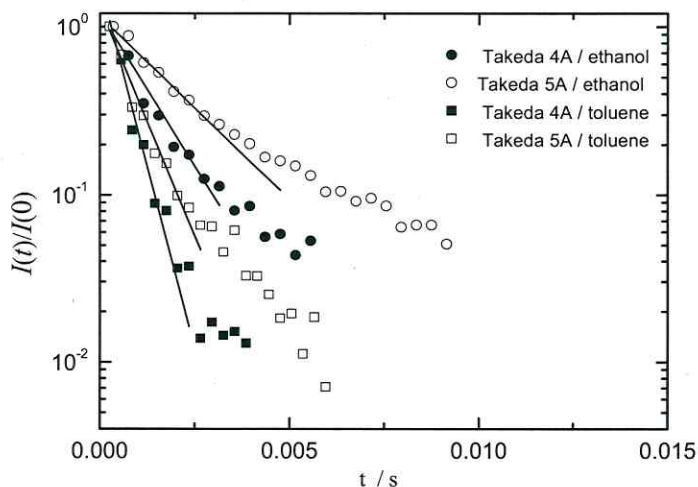


Fig.5 Attenuation of the transverse magnetization of ethanol and toluene at 298 K confined in Takeda 4A and Takeda 5A. The attenuation curves were measured by the CPMG pulse sequence.

3.4. NMR diffusometry

The PFG NMR technique provides information about the pore structure via the transport properties of the adsorbed molecules. The attenuation of the NMR signal is related to the “propagator” $P(x, t)$ (the probability distribution of molecular displacements along the axis of gradient direction x during the time t) according to

$$\Psi(q, t) = \int P(x, t) \cos(qx) dx, \quad (8)$$

where $q = \gamma \delta g$, and γ is the nuclear gyromagnetic ration, with g and δ denoting the amplitude and the duration of the magnetic field gradients, respectively. In isotropic homogeneous systems, the propagator is typically represented by a Gaussian function

$$P(x, t) = (4\pi Dt)^{-1/2} \exp\left(-\frac{x^2}{4Dt}\right), \quad (9)$$

where D is the diffusion coefficient. The latter correlates the mean square displacement and time according to the Einstein equation [21] for “normal” diffusion

$$\langle x^2(t) \rangle = 2Dt. \quad (10)$$

By inserting Eq. (9) into Eq. (8), the PFG NMR signal attenuation for normal diffusion is found to be:

$$\Psi(q, t) = \exp(-q^2 t D). \quad (11)$$

For a distribution of diffusivities, a multi-exponential attenuation curve will result:

$$\Psi(q, t) = \int f(D) \exp(-q^2 t D) dD, \quad (12)$$

where $f(D)$ denotes the distribution function of diffusivities, i.e. the probability that the diffusion path of an arbitrary selected molecules during the observation time may be characterized by a diffusivity D . Depending on the size of the regions within the samples, to which these different diffusivities D . Depending on the size of the regions within the samples, to which these different diffusivities may be attributed, this distribution may be a function of the observation time, tending to become

smaller with increasing observation time. The mean diffusivity $\langle D \rangle$ can be evaluated from the initial slopes of the attenuation curves:

$$\langle D \rangle = - \lim_{(q^2 t) \rightarrow 0} \frac{\partial(\ln \Psi(q, t))}{\partial(q^2 t)} = \int f(D) D dD. \quad (13)$$

In this work, we investigated the diffusion of several liquids confined in MAC-LMA12. The sorbate molecules were ethanol, toluene, nitrobenzene, acetone and n-decane. As an example, Fig. 6 shows the diffusion attenuation curve for ethanol at 298 K. The observed behavior is typical of all liquids considered. It exhibits a clear deviation from the exponential function and can tentatively be analyzed in terms of two components:

$$\Psi(q, t) = \int f(D) \exp(-q^2 t D) dD + f_{\text{slow}} \exp(-q^2 t D_{\text{slow}}) \quad (14)$$

where f_{slow} and D_{slow} denote the relative fraction and the diffusivity of molecules contributing to the slowly attenuating component of the curve, $f(D)$ is the distribution of diffusivities related to the dominating (faster) component. (The relative fractions of the fast and slow component are normalized as $\int f(D) dD + f_{\text{slow}} = 1$). The values of f_{slow} and D_{slow} , as evaluated from the fits of the exponential function to the slow component of the curve in Figure 6, were 0.062 and $4 \times 10^{-13} \text{ m}^2 \text{ s}^{-1}$.

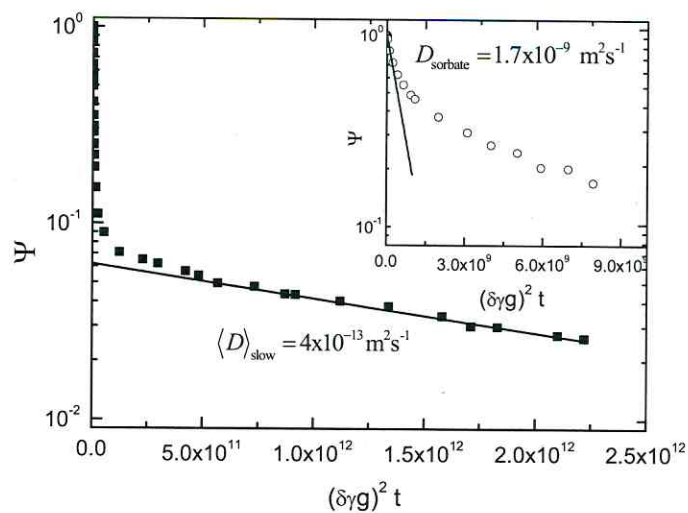


Fig.6 Diffusion attenuation curve of ethanol in MAC-LMA12 at 298 K measured with an observation time of 10 ms (squares). D_{slow} is the minimal value of the diffusion coefficient allowed by the NMR equipment. $D_{\text{sorbate}} = \langle D \rangle$ is the mean diffusion coefficient evaluated from the initial slope of the attenuation which was obtained after subtraction of the slow component from the total attenuation curve (circles in the inset).

The two constituents of the diffusion attenuation indicate that, over the observation time, the molecules exist in essentially two different dynamical states, as observed already above in context of nuclear magnetic relaxation. Again, we attribute the smaller fraction with the smaller diffusivities to molecules confined in the micropores and the dominating fraction with the larger diffusivities to the liquid in the mesopore space.

The faster attenuating component, obtained after subtraction of the slow component from the total attenuation is shown in the inset, Figure 6. It exhibits a clear deviation from the exponential dependence, thus indicating a distribution of diffusivities as incorporated by the first term in Eq.

(14). The mean diffusion coefficient $\langle D \rangle$ referring to the fast component was determined from the initial slope. It equals approximately $1.7 \times 10^{-9} \text{ m}^2 \text{ s}^{-1}$ and thus is four orders of magnitude larger than D_{slow} .

The slow diffusion component is to be compared with the diffusion behavior of the same liquid in the microporous Takeda samples. Figure 7 shows the diffusion attenuation curves of ethanol in Takeda 4A and Takeda 5A at 298 K. In Takeda 5A, the attenuation curves were exponential over the covered range of more than one order of magnitude. In Takeda 4A, the signal intensity was so small (as a consequence of the fast transverse relaxation) so that the data points could be measured only in a limited range, not below 50% of the initial amplitude. In this range, the observed attenuations were exponential as well. The diffusion coefficient of ethanol in Takeda 5A, evaluated from the exponential fits to the data points, was $8 \times 10^{-12} \text{ m}^2 \text{ s}^{-1}$. In Takeda 4A, the evaluated diffusivity was $9 \times 10^{-13} \text{ m}^2 \text{ s}^{-1}$, nearly one order of the magnitude smaller than in Takeda 5A. This finding complies with the shorter relaxation time observed in Takeda 4A and quantifies the effect of the more severe restriction to diffusion due to the smaller pores in this material, as compared with Takeda 5A.

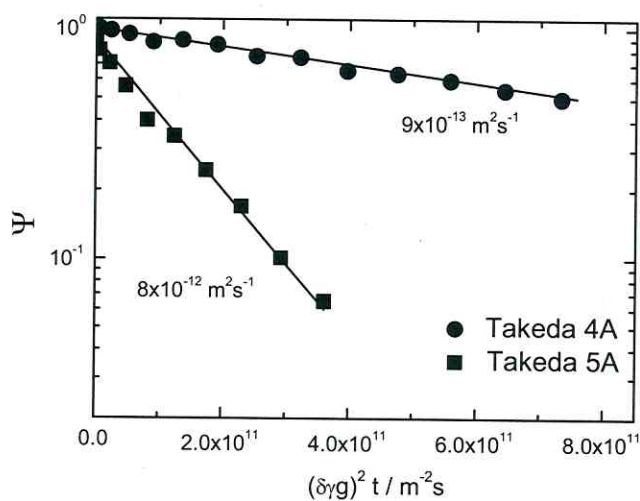


Fig.7 Diffusion attenuation curves of ethanol in Takeda 4A and Takeda 5A at 298 K. The observation time was equal to 10 ms.

Figure 8 shows the diffusion attenuation curves of toluene in MAC-LMA12 for various observation times in the range between 10 ms and 300 ms. No time dependence of the attenuations was observed for both the slow and fast (see inset) components. The molecular displacements monitored in our experiments were between 60 nm for the slower component and 23 μm for the faster component. On the one hand, the absence of the time dependence indicates that there is practically no exchange between the two different species as it was suggested on the basis of the relaxation studies. On the other hand, it provides evidence that the mesopores in MAC-LMA12 represent a well interconnected space, rather than a system of closed separated pores. In the latter case one would have to expect a decrease of the curve slopes with increasing observation times.

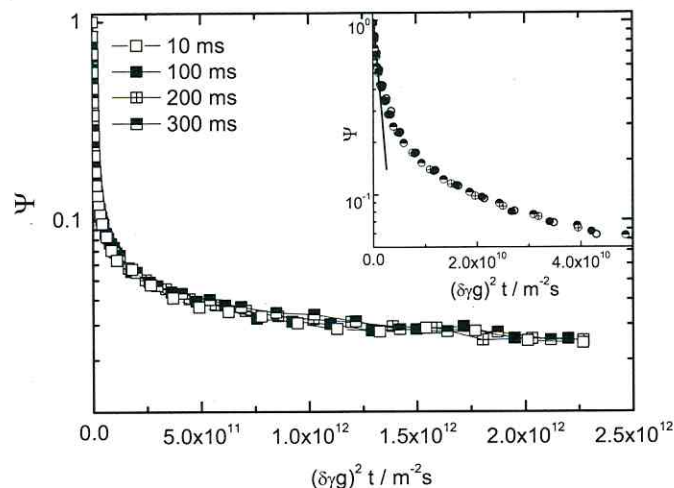


Fig.8 Diffusion attenuation curves of toluene in MAC-LMA12 at 298 K with different observation times (10, 100, 200, 300 ms). The inset shows the fast component obtained after subtracting the slow component from the total attenuation curve. The observation time was 10 ms.

The diffusion behavior of several liquids (acetone, ethanol, toluene, n-decane and nitrobenzene) confined in MAC-LMA12 was compared. Table 2 provides the comparison of the resulting mean diffusivities D_{sorbate} with the bulk diffusivities of these liquids D_{liquid} . Depending on the particular guest, the diffusivities within the pore system are found to be both larger and smaller than the bulk diffusivities. This finding may be related to the fact that due to the presence of the host lattice, guest diffusion may occur both in a liquid (phase 1) attached to the pore system and through the free space (phase 2). With the respective relative amounts of molecules p_i and diffusivities D_i , the mean diffusivity as accessible by PFG NMR will result to be [22]

$$D_{\text{sorbate}} = p_1 D_1 + p_2 D_2 \quad (15)$$

The diffusivity D_1 in the free space, following gas-phase or Knudsen diffusion [9, 22], is notably larger and the diffusivity D_2 in the liquid phase, due to the tortuosity of the pore space, is

smaller than the diffusivity D_{liquid} in the bulk phase. Thus, depending on the relative contributions p_1 and p_2 , D_{sorbate} may in fact assume larger or smaller values than D_{liquid} . The magnitude of p_1 increases in proportion with the vapor phase pressure and, hence, also the contribution of the first term in Eq. (15). Hence, it is in complete agreement with our understanding that, as shown in Table 2, a decrease in the boiling point (which corresponds to a decrease in the vapor pressure at a given temperature) is accompanied with a decrease in D_{sorbate} . The latter, according to Eq. (15), reflects a decrease in p_1 , i.e. in the contribution of the fast (gas-phase) mode of molecular propagation.

	$D_{\text{sorbate}} \times 10^{-9}$ m^2s^{-1}	$D_{\text{liquid}}, \times 10^{-9} \text{m}^2\text{s}^{-1}$	$D_{\text{sorbate}}/D_{\text{liquid}}$	Boiling point $^{\circ}\text{C}$
acetone	5	4.6	1.1	56.5
ethanol	1.7	1.1	1.5	78.4
toluene	0.6	2.3	0.26	111
n-decane	0.24	1.4	0.17	174
nitrobenzene	0.09	0.8	0.11	211

Table 2 Diffusion coefficients of the liquids when confined in carbon MAC-LMA12 (D_{sorbate}) and in the bulk (D_{liquid}) and their ratio, in comparison with their boiling temperature. The diffusion coefficient of the liquid in pores $D_{\text{sorbate}} = \langle D \rangle$ is the mean value of the diffusivity in the pores and was calculated from the initial slope of the attenuation curve.

4. Conclusions

Carbon materials containing different proportions of micro- and mesoporosity were studied. The combination of different NMR methods was used to explore the pore structure and the interaction of the adsorbate with the pore walls. Pore size distribution in samples RGC30 and MAC-LMA12 was determined by NMR cryoporometry. In MAC-LMA12, a narrow pore size distribution was observed, with a mean pore size of about 2 nm; RGC30 sample has a broad pore size distribution, centered around a mean pore size of about 7 nm. These two values reflect the differences observed in the N₂ (77 K) and CO₂ adsorption isotherms.

In microporous Takeda 4A, the sorbate relaxation rates were larger and the diffusivities smaller than in Takeda 5A. This evidences that sorbate molecules in Takeda 4A experience stronger restrictions in both their re-orientational and translational motions than in Takeda 5A, as a consequence of the smaller pore size of Takeda 4A. In MAC-LMA12, two molecular species with different relaxation and diffusion properties were observed. The dominating part of molecules confined in MAC-LMA12 exhibited much smaller relaxation rates and larger diffusivities than in Takeda samples. This is attributed to the presence of mesopores which tend to confine the dominating part of the liquid. Besides, diffusion experiments showed the existence of the quite broad distribution of the diffusivities. This is attributed to heterogeneities of the material on length scales notably exceeding the characteristic molecular displacements (in the range of micrometers).

5. Acknowledgements

The authors thank Dr. R. Valiullin and A. Khohlov for useful discussions. The work was supported by the European Network of Excellence (NoE) Inside Pores (NMP3-CT2004-500895). Financial support from project (MAT2007-61734) is acknowledged.

6. References

- [1] H. Marsh and F. Rodríguez-Reinoso, *Activated Carbon*, Elsevier, London (2006).
- [2] F. Rodríguez-Reinoso, J.M. Martín-Martínez, M. Molina-Sabio, R. Torregrosa and J. Garrido-Segovia, *J. Colloid Interface Sci.* **106** (1985) 315.
- [3] J.C. Gonzalez, M.T. Gonzalez, M. Molina-Sabio, F. Rodríguez-Reinoso and A. Sepúlveda-Escribano, *Carbon* **33** (1995) 1175.
- [4] M. Molina-Sabio and F. Rodríguez-Reinoso, *Colloids and Surfaces A: Physicochem. Eng. Aspects* **241** (2004) 15.
- [5] R. Ryoo, S. Hoon Joo and S. Jun, *J. Phys. Chem. B* **103** (1999) 7743.
- [6] C. Liang and S. Dai, *J. Am. Chem. Soc.* **128** (2006) 5316.
- [7] J.M. Juárez-Galán, A. Silvestre-Albero, J. Silvestre-Albero and F. Rodríguez-Reinoso, *MicroMesoMater.* **117** (2009) 519.
- [8] F. Rodríguez-Reinoso and M. Molina-Sabio, *Adv. Colloid Interface Sci.* **76–77** (1998) 271.
- [9] J. Kärger and D.M. Ruthven, *Diffusion in Zeolites*, Wiley & Sons, New York (1992).
- [10] J. Mitchell, S.C. Stark and J.H. Strange, *J. Phys. D: Appl. Phys.* **38** (2005) 1950.
- [11] R.M.E. Valckenborg, L. Pel and K. Kopinga, *J. Phys. D: Appl. Phys.* **35** (2002) 249.
- [12] J. Garrido, A. Linares-Solano, J.M. Martín-Martínez, M. Molina-Sabio, F. Rodríguez-Reinoso and R. Torregrosa, *Langmuir* **3** (1987) 76.
- [13] P. Galvosas, F. Stallmach, G. Seiffert, J. Kärger, U. Kaess and G. Majer, *J. Magn. Reson.* **151** (2001) 260.
- [14] F. Rodríguez-Reinoso, J. Garrido, J.M. Martín-Martínez, M. Molina-Sabio and R. Torregrosa, *Carbon* **27** (1989) 23.
- [15] R.V.R.A. Rios, J. Silvestre-Albero, A. Sepúlveda-Escribano, M. Molina-Sabio and F. Rodríguez-Reinoso, *J. Phys. Chem. C* **111** (2007) 3803.
- [16] J.H. Strange, M. Rahman and E.G. Smith, *Phys. Rev. Lett.* **71** (1993) 3589.
- [17] C.L. Jackson and G.B. McKenna, *J. Chem. Phys.* **93** (1990) 9002.
- [18] K. Brownstein and C. Tarr, *Phys. Rev. A* **19** (1979) 2446.
- [19] H. Carr and E. Purcell, *Phys. Rev.* **94** (1954) 630.
- [20] M. Cohen and K. Mendelson, *J. Appl. Phys.* **53** (1982) 1127.
- [21] A. Einstein, *Ann. Phys.* **17** (1905) 549.
- [22] J. Kärger, H. Pfeifer and W. Heink, *Adv. Magn. Reson.* **12** (1988) 2.

**Publication 2: The evidence of NMR diffusometry on pore space
heterogeneity in activated carbon**

Microporous and Mesoporous Materials, 2011, 141, 184

F. Furtado^{a,b}, P. Galvosas^{b,c}, M. Gonçalves^d, F.-D. Kopinke^a, S. Naumov^b, F. Rodríguez-Reinoso^d,
U. Roland^a, R. Valiullin^b, J. Kärger^b

^aDepartment of Environmental Engineering, UFZ – Helmholtz-Centre for Environmental Research, Permoserstr. 15, 04318 Leipzig, Germany

^bDepartment of Interface Physics, University of Leipzig, Linnéstr. 5, D-04103 Leipzig, Germany

^cSchool of Chemical and Physical Sciences, Victoria University of Wellington, P.O. Box 600, Wellington 6140, New Zealand

^dDepartamento de Química Inorgánica, Universidad de Alicante, Apartado 99, 03080 Alicante, Spain

Abstract

With the advent of nanoporous materials with hierarchical pore structure, pore space exploration becomes an increasingly complex task which depends on the successful inclusion of novel techniques of sample characterization, in addition to the established ones. We present the results of an in-depth pulsed field gradient (PFG) NMR study of guest diffusion in an activated carbon with a two-modal pore structure (MA2). The pronounced distribution of the local diffusivities is taken as an indication of notable sample heterogeneities. The options of their further characterization by intentionally varying the parameters and conditions of the diffusion measurements are discussed.

Keywords: PFG NMR, Diffusion, Activated carbon, Pore heterogeneity

1. Introduction

Diffusion, i.e. the irregular movement of atoms and molecules, is among the fundamental and omnipresent phenomena in nature and technology and occurs in all states of matter. A particular fascination is provided with systems where the sizes of the diffusing molecules are comparable with the characteristic length scale of the host systems by which they are accommodated. This is in particular true for mass transfer in nanoporous materials [1]. Their technological benefit is based on the compatibility of their pore diameters with the size of the guest molecules, by which either catalytic conversion or adsorptive separation is exploited for the generation of value-added products [2,3]. Equally important, the similarity of molecular and pore diameters gives rise to numerous phenomena of fundamental relevance for soft-matter interaction with solid surfaces [4,5], in particular for a better understanding of the conditions for molecular reorientation and redistribution under confinement [68].

Being determined by the pore architecture, the rate of molecular propagation may – in turn – be considered as a source of information about pore architecture. In the present study, we have explored these potentials by the application of the pulsed field gradient technique of nuclear magnetic resonance (PFG NMR) to studying molecular diffusion of cyclohexane in an activated carbon with a two-modal pore structure (MA2). The potentials of PFG NMR for this type of studies are based on two unique properties of this technique. Being able to directly record the probability of molecular displacements during well-defined time intervals (of typically milliseconds till seconds), PFG NMR provides direct information about the rate of molecular propagation (the diffusivity) over distances from about 100 nm to 100 μm [9,10]. In addition, PFG NMR may as well distinguish whether this rate is uniform or whether, over the whole of the sample, there is a distribution of the local propagation patterns giving rise to a sample-related distribution of local diffusivities [11,12]. We are going to exploit this distribution of local diffusivities as a measure of sample heterogeneity.

2. Experimental

2.1 The sample under study

The carbon MA2 (see Fig. 1) has been prepared by carbonisation and subsequent CO₂-activation (43% activation burn-off) of a spherical porous resin obtained by cross-linking of phenol-formaldehyde Novolac precursor with hexamethylenetetramine and with ethylene glycol as solvent-pore former [13]. Figure 2 shows the N₂ adsorption, at 77 K. The high N₂ uptake at P/P_0 values below 0.1 and over 0.8, reveal high micro- and mesoporosity, each one occupying approximately 50% of total pore volume.

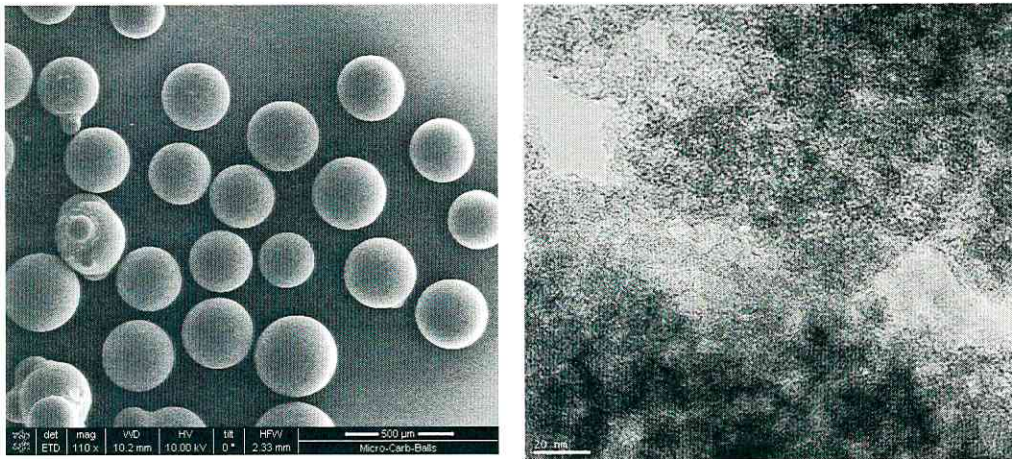


Fig. 1 (Left) SEM picture of the carbon particles. (Right) TEM picture where both micropore and mesopore structures can be seen.

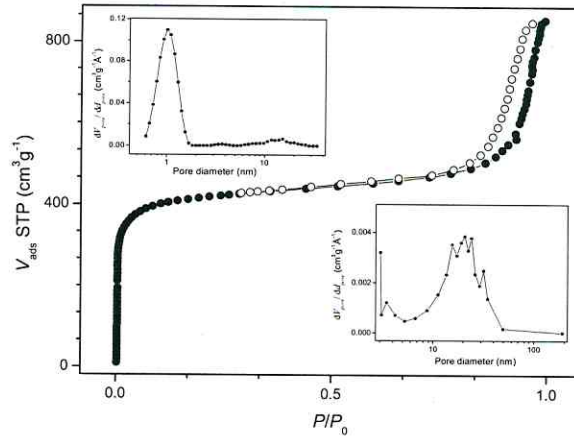


Fig. 2 N_2 adsorption isotherm at 77 K for the carbon sample under study, with closed and open symbols corresponding to the adsorption and desorption branch, respectively. P_0 corresponds to the N_2 saturated vapor pressure at 77 K. The inserts show the micropore and mesopores pore size distribution (upper left side and lower right side, respectively) as obtained by DFT (micropore distribution) and BJH (mesopores distribution).

2.2 PFG NMR diffusion studies

The PFG NMR diffusion studies have been performed with the 13-interval pulse sequence [14] at a proton resonance frequency of 125 MHz by means of the home-built PFG NMR diffusion spectrometer FEGRIS NT [15,16]. Assuming isotropic, normal diffusion and separation times t (between the two gradient pulse pairs, determining the “observation” time) notably exceeding those between one gradient pulse pair, the attenuation of the NMR signal (the “spin echo”) obeys eq. (1) [9,14-16]

$$\Psi(t, g\delta) = \exp(-\gamma^2 (2\delta)^2 g^2 D t) \quad (1)$$

with g and δ denoting the amplitude and the duration of one magnetic field gradient pulse and with γ denoting the gyromagnetic ratio ($2.675 \times 10^8 \text{ T}^{-1} \text{ s}^{-1}$ for hydrogen). The self-diffusivity D is related by the Einstein equation [6,17]

$$\langle x^2(t) \rangle = 2Dt \quad (2)$$

to the mean squared molecular displacement $\langle x^2(t) \rangle$ in gradient direction during the observation time t . Eq. (1) implies homogeneity of the sample under study with respect to a length scale of the order of the molecular displacements under study [18]. This means that, on the average, the probe molecules “experience” the identical pore space on their trajectories during the PFG NMR experiments. If the system deviates from this requirement, instead of eq. (1) one has to consider

$$\Psi(t, g\delta) = \int_0^{\infty} p(D) \exp(-\gamma^2 (2\delta)^2 g^2 D t) dD \quad (3)$$

where $p(D)dD$ denotes the probability that the diffusivity of the guest molecules within an arbitrarily selected space element (of the order of the considered displacements) is within the interval $D \dots D + dD$. More correctly, one has even to take into account that, due to differences in the nuclear magnetic relaxation times [9,15,16], not only the diffusivities but also the contribution of the molecules to the observed PFG NMR signal from different sample regions may be different. Hence, the function $p(D)$ must be considered to be weighted by differences in the relaxation properties of the different sample regions.

If the PFG NMR signal attenuation follows eq. (1) a semi-logarithmic plot of the signal intensity versus $\gamma^2 (2\delta)^2 g^2 t$ yields a straight line with the diffusivity as its negative slope. In

isotropic systems – as in the case considered, deviations from linearity may indicate deviations from sample homogeneity. This becomes especially true when this deviation will not depend on the observation time t . In this case, the mean diffusivity can be derived from the initial slope of the semi-logarithmic plot of the signal intensity, i.e. for sufficiently small values of $\gamma^2(2\delta)^2 g^2 t$. We shall extensively make use of this option.

The experimental data as acquired with the PFG NMR technique may be described by a log-normal distribution of diffusion coefficients [19,20]

$$p(D) = \frac{1}{D\sigma\sqrt{2\pi}} \exp\left[-\frac{(\ln D - \ln D_0)^2}{2\sigma^2}\right] \quad (4)$$

Here, D_0 denotes the median of the diffusivity and σ gives the multiplicative standard deviation, which can empirically be correlated to the degree of heterogeneity of the system under study. It has to be noted that we do not have any particular arguments in favor of Eq.4, except that it reasonably reproduces the experimental data and has a relatively simple meaning. The obtained parameters D_0 and σ are used to characterize the properties of the diffusion process under study regardless of its actual nature.

For the PFG NMR diffusion studies, a given amount of the host material was filled into sample tubes of 7.5 mm outer diameter and heated in an oven to 383 K in contact with the atmosphere over 24 h. Subsequently, the samples were connected to a vacuum system and dehydrated under high vacuum (of less than 10^{-2} Pa) at 523 K for around 4 h. After cooling down, the sample was connected to a vessel of known volume, with a given vapor pressure of the diffusant, corresponding to the desired loading amount. After loading was complete, the sample was then cooled to the temperature of liquid nitrogen thus allowing the sealing of the sample.

3. Results and Discussion

Irrespective of their great technological relevance, molecular diffusion in activated carbons has never been investigated with the same effort compared to the study of diffusion in zeolites [21]. This is mainly related to the fact that, in contrast to zeolites, activated carbon is not available in the form of well-shaped crystallites. In conventional uptake and release studies this complicates or even excludes the transformation of the directly observable rate constants into well-defined diffusivities. Though, as a technique sensitive to the rate of molecular transportation in the particle interior, PFG NMR is not affected by this complication, its application is severely handicapped by the generally very short transverse nuclear magnetic relaxation times of these materials. Hence, owing to recent improvement of the PFG NMR methodology and the increasing amount of novel structure types also in the field of activated carbons [22], only very recently [23] PFG NMR diffusion studies have been performed with NMR signal attenuations over more than one order of magnitude. There, for the first time, together with the present work indications for a deviation of the attenuation function from the simple exponential dependence as predicted by eq. (1) for diffusion in a homogeneous system could be observed, opposing previous ones in related systems [24,25].

3.1 Distribution of guest diffusivities in activated carbon of type MA2

Fig. 3 displays the PFG NMR attenuation curve of cyclohexane in MA2 at room temperature for 100% pore filling and an observation time of $t = 10$ ms. The curve is shown to be nicely approximated by eq. (3) with a distribution function of the local diffusivities as given by eq. (4). During the fitting procedure, variation of the signal-to-noise ratios (S/N) from 125 to 500 produced the respective variation of resulting D_0 and σ of less than 1% and 9%, respectively. The results presented do refer to S/N inferred from the experimental data which is about 475. Best fit is attained with $D_0 = (2.80 \pm 0.03) \times 10^{-10} \text{ m}^2\text{s}^{-1}$ and a distribution width $\sigma = 0.60 \pm 0.02$. With these parameters

it is possible to calculate the average diffusion coefficient $D_m = D_0 e^{\sigma^2/2}$, yielding $D_m = 3.36 \times 10^{-10} \text{ m}^2\text{s}^{-1}$, which would as well follow via eq. (1) from the slope of the initial decay of the attenuation curve.

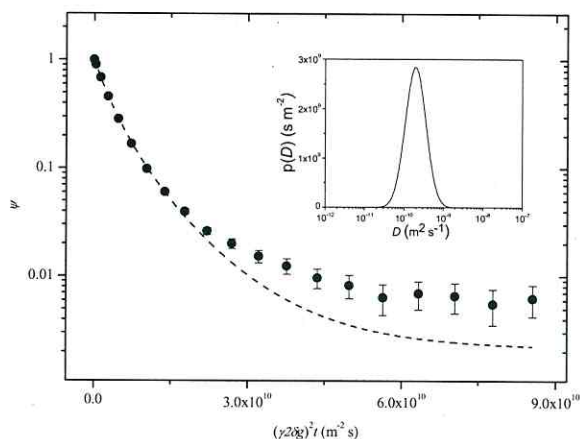


Fig. 3 Spin-echo attenuation of cyclohexane in a fully loaded MA2 sample, at 298 K ($t = 10$ ms) and best fit by eq. (3), assuming a log-normal distribution of diffusion coefficients (eq. 4). The insert shows the distribution of the diffusion coefficients (eq. 4).

With eq. (4), this result is easily seen to be equivalent with the statement that 68.3% of the measured diffusion coefficients fall into the interval $[D_m/\sigma, D_m/\sigma]$ i.e. $[2.0 \times 10^{-10}, 5.6 \times 10^{-10} \text{ m}^2\text{s}^{-1}]$. Inserting this result into eq. (2) yields an interval of the square root of mean square displacement considering the range of observation times used from 2.0 μm till 3.3 μm .

It is noteworthy to emphasize that the diffusion path lengths and, hence, the extensions of these regions are much larger than the diameters of both the micro- and mesopores. The trajectories of all molecules considered will, therefore, consist of displacements within both the

micropores and macropores. The diffusivities of molecules confined to pore spaces are known to depend on numerous influences, including the nature of the pore surface, the pore diameters and the tortuosity of the pore space. In the subsequent sections we are going to describe different series of experiments while changing selected influences as a parameter. It is our aim to specify the possible origin of the particular distribution in the diffusivities by exploring the influence of these variations on the resulting diffusivities.

3.2 Variation of the observation time

If one varies the observation time for a diffusion experiment the range of molecular displacement will change until the diffusion path is obstructed. Without obstruction, the mean square displacement will increase according to eq. (2) and the distribution of diffusion becomes time independent. Fig. 4a represents the spin-echo decays for an observation time range of 5 ms to 250 ms. The shape of the echo attenuation, which holds the information on the diffusion coefficient distribution is identical for all observation times within the accuracy of the acquired NMR data. We therefore conclude that the sample morphology is homogeneous for subregions of 2 to 13 μm , since no observation time dependence for the corresponding mean square displacements from 3 to 170 μm^2 were observed (see Fig. 4b for the linear increase of $\langle x^2 \rangle$ with increasing observation time, as given by eq. (2)).

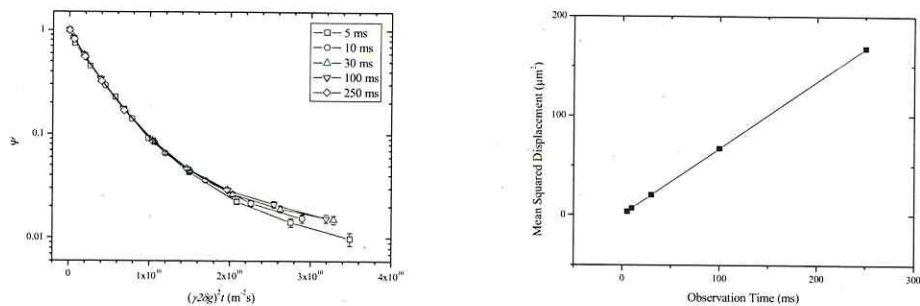


Fig. 4 (a) Left) Spin-echo attenuation of cyclohexane in a fully loaded MA2 sample, at 298 K for different observation times (t) and (b) right) mean squared displacement for the respective observation times.

As a result, even with the largest diffusion path lengths attainable in the present diffusion studies no change in the distribution function of the resulting local diffusivities could be observed. This means that the correlation lengths of sample homogeneity, i.e. the distance after which a notable change in the host structure will have occurred, have to be much larger than these distances.

3.3 Variation of particle sizes

After the estimate of a lower limit of the correlation length, one may also consider the opposite limiting case, i.e. whether the individual particles (with diameters between 0.15 to 0.50 mm, see fig. 1) are essentially homogeneous (i.e. with homogeneity correlation lengths notably exceeding their diameters) and that the distribution in the observed diffusivity is caused by a distribution in the structural properties (and, hence, in the diffusion properties) from particle to particle. Their small size prohibits PFG NMR diffusion measurements with each individual host particle.

This problem may be circumvented, however, if the structural peculiarities are correlated with the particle sizes. For the exploration of this option, we have compared the diffusivities in samples

containing different particle size fractions. The resulting attenuation plots are shown in fig. 5. Again, in all samples the attenuation plots and, hence, the distribution functions for the local diffusivities are found to be essentially identical. Hence, any correlation between the size of the host particles and their structural properties may be excluded.

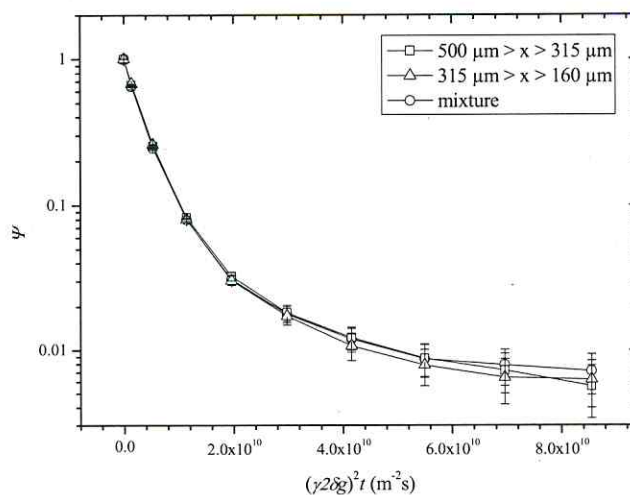


Fig. 5 Effect of particle size on the spin-echo attenuation of cyclohexane in fully loaded samples, at 298 K ($t = 10$ ms).

3.4 Variation of the impact of nuclear magnetic relaxation

The distribution in the diffusivities has to be referred to locally varying properties of the host structure. For the exploration of their nature, it would be interesting to find out whether these variations in the host structure give also rise to a distribution of further key parameters of the host-guest system, in addition to the guest diffusivities. In this context, the nuclear magnetic relaxation times are of particular interest since they are known to depend very sensitively on the pore sizes and the pore wall chemistry, generally decreasing with increasing surface-to-volume ratios [5,26]. If

the variation in the diffusivities is caused by corresponding variations in the pore geometry and pore wall chemistry, one should, therefore, expect correlations between the diffusivities and nuclear magnetic relaxation times.

Fig. 6 displays PFG NMR attenuation curves where the signal intensity has been modified by dramatically changing the contributions of the two nuclear magnetic relaxation mechanisms. Keeping the observation time (and, hence, the time interval relevant for longitudinal nuclear magnetic relaxation) approximately constant, the PFG NMR pulse sequence was modified in such a way that the time interval relevant for transverse nuclear magnetic relaxation was increased by a factor of 4 (which, in effect, has led to a decrease of the NMR signal (the spin echo) by about 1 order of magnitude). Note, that we have negligible influence of T_1 on the signal intensity for the parameter variations in these experiments. Fig. 6 shows that this significant variation in the contributions of the two relaxation mechanisms did not yield any perceptible effect on the shape of the attenuation curve. This means that the contributions of the regions with different diffusivities have in no way been affected by the variation in the weights of the relaxation mechanisms. It is therefore unlikely that the differences in the diffusivities are correlated with a corresponding variation in the pore geometry and pore wall chemistry.

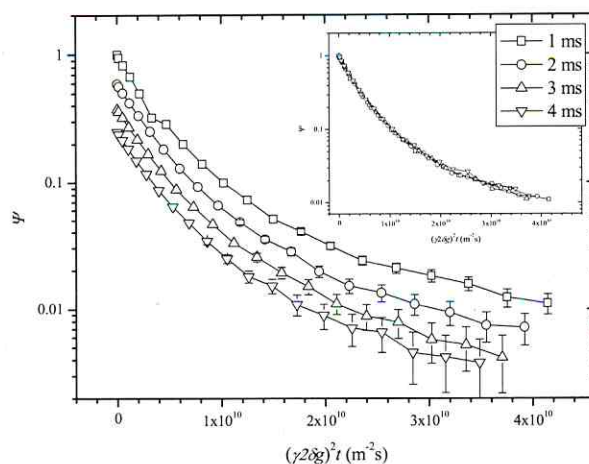


Fig. 6 Spin-echo attenuation of cyclohexane in a fully loaded sample, with different T_2 relaxation windows (variation of the interval between the pair of gradients with opposite sign in the 13-interval pulse sequence [14]). The insert shows the same data, normalized to the echo intensity for the lowest gradient used, for each data set.

3.5 Variation of substrate loading and temperature

The host material under study is known to contain interpenetrating networks of micro- and mesopores as illustrated in section 2.1. Molecular propagation over distances of micrometers as relevant for the PFG NMR measurements, includes therefore displacements in both pore spaces. The contribution of molecular migration in either of these spaces to the overall mass transfer through the host particles as recorded by PFG NMR depends on both the loading and the temperature of measurement. It is, therefore, worthwhile to explore up to which extent the distribution in the diffusivities is affected by a variation of loading and temperature, in particular the effect of these on the liquid-solid phase transition of geometrically confined cyclohexane.

As an example, fig. 7 shows the PFG NMR attenuation curves for cyclohexane at four different temperatures and for pore loadings varying from 20 % to complete saturation. For better

comparability, the attenuation curves have been plotted versus $g^2 t D_m$ so that differences in the attenuation curves caused by differences in the absolute values of the diffusivities are compensated. For both the measurements at 0°C and 40°C, the shape of the attenuation curve is found to remain essentially unaffected by increasing the loading from the lowest value of 20 % (where the mesopores are essentially empty) up to complete saturation. The distribution in the diffusivities is thus found to remain unchanged, irrespective of the dramatic difference in the nature of the pore spaces involved.

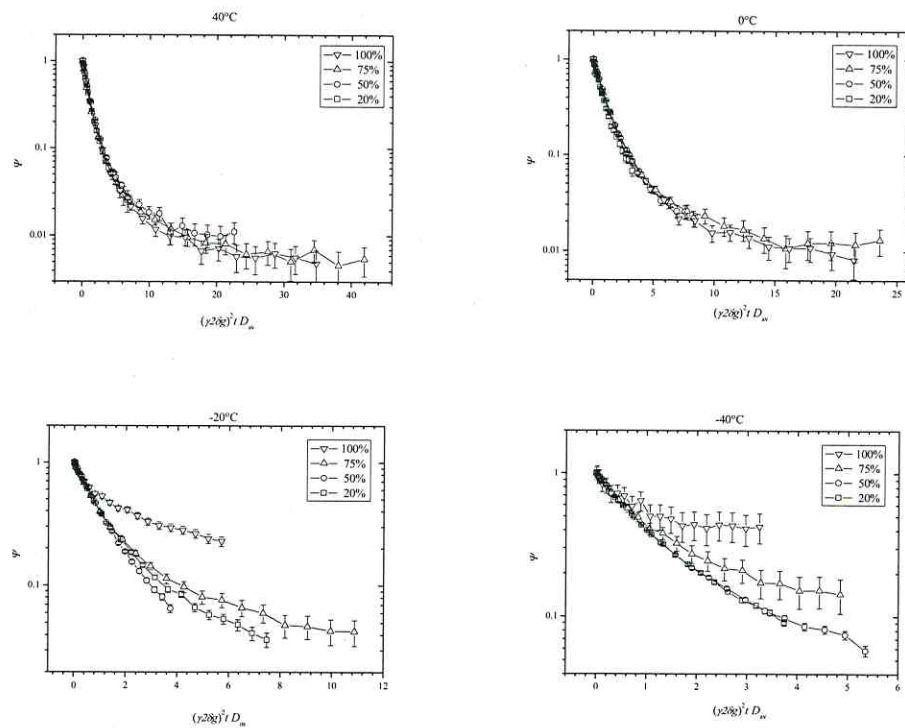


Fig. 7 Influence of temperature on cyclohexane spin-echo attenuation, for different loadings.

This finding is complementary to the message of the diffusion studies with varying impact of nuclear magnetic relaxation in section 3.4. Irrespective of a significant variation of the contribution

of the two pore spaces to overall mass transfer, the shape of the PFG NMR attenuation curves, and hence the distribution of the diffusivities, is found to remain essentially unchanged. One has to exclude, therefore, the possibility that the variation in the diffusivities over the sample may be attributed to a variation of the ratio of the local meso- and microporosity over the sample. In this case, the transition from dominating micro- to dominating mesopore transport should lead to much more distinct changes in the diffusivity distributions.

It is interesting to note that the compatibility in the attenuation curves for different loadings is not preserved with further temperature decrease. At -20°C , after coinciding in their initial slopes (as the consequence of the unifying representation vs. g^2tD_m), the attenuation curve of the fully saturated sample is found to notably deviate from those with lower loadings, yielding a progressively decreasing slope. With eqs.(1) and (3), this finding has to be attributed to molecules with notably reduced diffusivities. Fig. 8 compares the relative intensity of the first spin echo, at different temperatures and corresponding loadings.

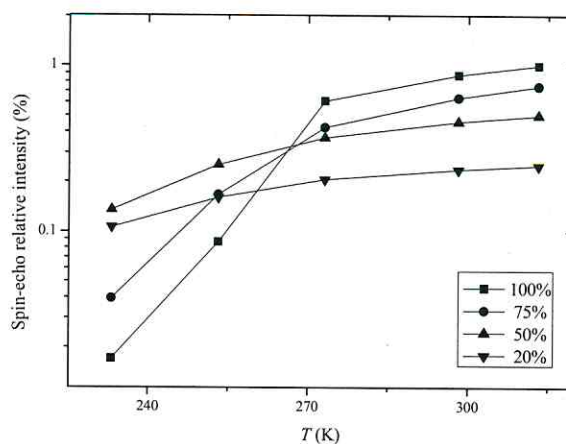


Fig. 8 - Temperature dependency of the relative intensity of the first echo of the 13-interval pulse sequence, for different loadings. The intensities are normalized to the value obtained for the fully loaded sample at 313.15 K.

Samples with lower loadings where mesopores remain partially empty (20 % and 50 %), are less affected by temperature decrease whereas more saturated samples reveal a drastic dependency on temperature. For rationalizing such a behavior we have to recognize that the suppression of the freezing point T_f in pores of diameter d from the bulk value T_{fb} (6.6°C for cyclohexane) is related by following the Gibbs-Thompson equation [27,28]

$$T_f = T_{fb} - K/d, \quad (5)$$

where K is a calibration constant, characteristic of the system under study. Consequently, the phase change will occur at larger pores, which severely reduces the transverse relaxation time, thus suppressing the contribution of the frozen phase to the overall signal intensity. This can clearly be observed on the steep decrease in signal intensity from 0°C to -20°C. Indeed, in the fully

saturated sample, a large fraction of the liquid in the mesopores is already frozen (signal intensity loss > 80%). At these low temperatures, it is important to note that the spin-echo signal intensity on fig. 8, represents almost exclusively the liquid in the micropores, due to sufficiently short transverse relaxation times in mesopores, at these high loadings. This effect is more pronounced with decreasing temperatures, with the additional solid phase leading to an additional confinement of the remaining fluid phase, reflected by a decrease not only in the transverse relaxation time but also in the diffusivities in these regions and thus in the decaying slope of the PFG NMR signal attenuation curve. In complete agreement with this reasoning, at -40°C this effect is found to be even more pronounced since now the freezing process is extended to smaller mesopores, leading to an even larger effect of confinement for the remaining fluid phase.

4. Conclusions

With cyclohexane as probe molecules, molecular diffusion in activated carbon MA2 revealed a broad distribution of the local diffusivities as recorded by PFG NMR measurements sensitive to root mean square displacements of up to 13 μm . This distribution was found to remain essentially unaffected by significant variations in the measuring conditions, including observation time, substrate loading, the conditions of nuclear magnetic relaxation and temperature. Deviations below the bulk freezing temperature may be easily referred to an extra-confinement due to the additionally formed frozen phase. We tentatively attribute the observed distribution of diffusivities to internal transport barriers as observed in zeolites. It is – just due to the observed invariance of the attenuation curves with the experimental conditions – even rather unlikely that this variance is correlated with some local properties of the pore system (such as the mean pore diameters, the pore wall chemistry or the relative density of the micro- and macropores) with correlation lengths of at least the considered displacements of about 10 μm . With its well established application to

biological systems [29-31] Fourier transformed q -space plots may be regarded as an alternative methodology for providing further information on the present system, as it also provides information on the micrometer range.

One can rationalize that in addition to the influence of the “regular” pore space, the rate of molecular migration may be affected by further influences, including transport resistances in the form of planes of reduced permeability traversing the host bulk phase. In zeolites, the existence of such “internal transport barriers” has been suggested long time ago to explain the discrepancy between the results of micro- and macroscopic diffusion measurements [32]. Very recently [33], the occurrence of such resistances could be directly evidenced in comparative studies by transmission electron microscopy and PFG NMR diffusion measurements. While it is premature to attribute the observed behavior in the present case of activated carbon to these additional resistances, as found in zeolites, it may provide an explanation to the experimental evidence and, therefore, be acceptable as a working hypothesis.

5. Acknowledgements

Financial support from Marie Curie Early Stage Training Program “Risk Assessment and Environmental Safety Affected by Compound Bioavailability in Multiphase Environments” (RAISEBIO) and by the Deutsche Forschungsgemeinschaft in the frame of the International Research Training Group “Diffusion in Porous Materials” is gratefully acknowledged. We also thank Dr. José Luis Barzola Quiquia for the SEM picture presented in this work.

6. References

- [1] F. Schuth, K.S.W. Sing and J. Weitkamp, *Handbook of Porous Solids*, Wiley-VCH, Weinheim, Germany (2002).
- [2] D.M. Ruthven In: J. Kärger, Editor, *Leipzig, Einstein, Diffusion*, Leipziger Univ.-Verl., Leipzig (2010), pp. 123–143.
- [3] J. Weitkamp, *Catalysis and Zeolites: Fundamentals and Applications*, Springer, New York (1999).
- [4] F. Feil, C. Jung, J. Kirstein, J. Michaelis, C. Li, F. Nolde, K. Müllen and C. Bräuchle, *Micropor. Mesopor. Mater.* 125 (2009), pp. 70–78.
- [5] N. Nestle, A. Kühn, K. Friedemann, C. Horch, F. Stallmach and G. Herth, *Micropor. Mesopor. Mater.* 125 (2009), pp. 51–57.
- [6] D.M. Ruthven In: H.G. Karge and J. Weitkamp, Editors, *Adsorption and Diffusion*, Springer, Berlin, Heidelberg (2008) pp. 1–43.
- [7] J.R. Sangoro, A. Serghei, S. Naumov, P. Galvosas, J. Kärger, C. Wespe, F. Bordusa and F. Kremer, *Phys. Rev. E* 77 (2008), p. 051202.
- [8] K. Seehamart, T. Nanok, R. Krishna, J.V. Baten, T. Remsungnen and S. Fritzsche, *Micropor. Mesopor. Mater.* 125 (2009), pp. 97–100.
- [9] J. Kärger In: H.G. Karge and J. Weitkamp, Editors, *Adsorption and Diffusion*, Springer, Berlin, Heidelberg (2008) pp. 85–133.
- [10] B. Blümich, *Essential NMR for Scientists and Engineers*, Springer, Berlin (2005).
- [11] P.T. Callaghan, S. Godefroy and B.N. Ryland, *Magn. Reson. Imaging* 21 (2003), pp. 243–248.
- [12] P.T. Callaghan, S. Godefroy and B.N. Ryland, *J. Magn. Reson.* 162 (2003), pp. 320–327.
- [13] S.R. Tennison, O.P. Kozynchenko, V.V. Strelko, A.J. Blackburn, *Porous Carbons*, US 2004/0024074 A1.
- [14] R. Cotts, M. Hoch, T. Sun and J. Markert, *J. Magn. Reson.* 83 (1989), pp. 252–266.
- [15] F. Stallmach and P. Galvosas, *Annu. Rep. NMR Spectrosc.* 61 (2007), pp. 51–131.
- [16] P. Galvosas, F. Stallmach, G. Seiffert, J. Kärger, U. Kaess and G. Majer, *J. Magn. Reson.* 151 (2001), pp. 260–268.
- [17] J. Kärger, *Leipzig, Einstein, Diffusion*, Leipzig: Leipziger Univ.-Verl., 2007.
- [18] J. Kärger and S. Vasenkov, *Micropor. Mesopor. Mater.* 85 (2005), pp. 195–206.
- [19] M. Nydén and O. Söderman, *Macromolecules* 31 (1998), pp. 4990–5002.

- [20] G. Fleischer, F. Rittig, J. Kärger, C.M. Papadakis, K. Mortensen, K. Almdal and P. Štěpánek, *J. Chem. Phys.* 111 (1999), p. 2789.
- [21] H.G. Karge and J. Weitkamp, *Adsorption and Diffusion*, Springer, Berlin, Heidelberg (2008).
- [22] F. Rodríguez-Reinoso, H. Marsh, *Activated Carbon*, Amsterdam, Boston: Elsevier, 2006.
- [23] M. Krutyeva, F. Grinberg, F. Furtado, P. Galvosas, J. Kärger, A. Silvestre-Albero, A. Sepulveda-Escribano, J. Silvestre-Albero and F. Rodríguez-Reinoso, *Micropor. Mesopor. Mater.* 120 (2009), pp. 91–97.
- [24] M. Dubinin, R. Vartapetian, A. Voloshchuk, J. Karger and H. Pfeifer, *Carbon* 26 (1988), pp. 515–520.
- [25] J. Kärger and H. Spindler, *J. Am. Chem. Soc.* 113 (1991), pp. 7571–7574.
- [26] K. Brownstein and C. Tarr, *Phy. Rev. A* 19 (1979), pp. 2446–2453.
- [27] R. Valiullin, S. Naumov, P. Galvosas, J. Kärger, H. Woo, F. Porcheron and P.A. Monson, *Nature* 443 (2006), pp. 965–968.
- [28] J. Strange, M. Rahman and E. Smith, *Phys. Rev. Lett.* 71 (1993), pp. 3589–3591.
- [29] P.W. Kuchel, T.R. Eykyn and D.G. Regan, *Magn. Reson. Med.* 52 (2004), pp. 907–912.
- [30] A. Bar-Shir and Y. Cohen, *NMR Biomed.* 21 (2008), pp. 165–174.
- [31] G. Pages, T.W. Yau and P.W. Kuchel, *Magn. Reson. Med.* 64 (2010), pp. 645–652.
- [32] J. Kärger and D.M. Ruthven, *Zeolites* 9 (1989), pp. 267–281.
- [33] A. Feldhoff, J. Caro, H. Jobic, J. Ollivier, C.B. Krause, P. Galvosas and J. Kärger, *Chem. Phys. Chem.* 10 (2009), pp. 2429–2433.

Publication 3: Tracing pore-space heterogeneities in X-type zeolites by diffusion studies

Langmuir, 2011, 27, 416

Ziad Adem,[†] Jürgen Caro,[‡] Filipe Furtado,[†] Petrik Galvosas,^{†,§} Cordula B. Krause,[†] Jörg Kärger[†]

[†]Department of Interface Physics, University of Leipzig, Linnéstrasse 5, 04103 Leipzig, Germany,

[‡]Institute of Physical Chemistry and Electrochemistry, Leibniz University Hanover, Callinstrasse 3-3A, 30167 Hannover, Germany

[§]MacDiarmid Institute for Advanced Materials and Nanotechnology, School of Chemical and Physical Sciences, Victoria University of Wellington, PO Box 600, Wellington, New Zealand

Abstract

Pore space homogeneity of zeolite NaX was probed by pulsed field gradient (PFG) NMR diffusion studies with *n*-butane as a guest molecule. At a loading of 0.75 molecules per supercage, a wide spectrum of diffusivities was observed. Guest molecules in the (well-shaped) zeolite crystallites were thus found to experience pore spaces of quite different properties. After loading enhancement to 3 molecules per supercage, however, molecular propagation ideally followed the laws of normal diffusion in homogeneous media. At sufficiently high guest concentrations, sample heterogeneity was thus found to be of no perceptible influence on the guest mobilities anymore.

Introduction

The introduction of novel synthesis concepts¹ and the refinement of established ones²⁻⁴ to attain transport-optimized nanoporous materials lead to unprecedented options of their technological application in mass separation and heterogeneous catalysis⁵. As one of the rate-limiting processes during application, molecular diffusion in such systems has become one of the favorite subjects of investigation⁶. Thus it was observed that the bulk phase of zeolite crystallites may notably deviate from the ideal textbook structure. By varying the “observation” time of the measurements, the intracrystalline space was found to be traversed by transport resistances which lead to decreasing “effective” diffusivities, the larger the displacements are which are followed in the experiments⁷⁻⁹. Deviating from the “conventional” view that, if at all, additional transport barriers may only occur as “surface barriers”^{10, 11} diffusion studies provided severe evidence of the possibility that such transport resistances, acting in addition to the “drag” exerted by the genuine pore space, may also occur in the crystal interior. Recent high-resolution transmission electron microscopy investigations¹² revealed stacking faults of mirror-twin type on (111)-type planes of the cubic framework of FAU-type zeolites. By the detection of these faults, for the first time direct evidence of deviations in the structural homogeneity of zeolites was provided which, so far, could only be suggested as a possible hypothesis for explaining the discrepancy between “macroscopic” and “microscopic” diffusivities¹³.

Recently, the pulsed field gradient (PFG) technique of NMR¹⁴ has been applied to diffusion studies in mesoporous host-guest systems. The guest diffusivities could be exploited as a most sensitive probe of the molecular configurations in pore space, exhibiting quite different features in dependence on loading, temperature and sample “history”. In the present investigation, we have benefited from these special features of PFG NMR by evaluating the deviations from sample homogeneity in detailed diffusion studies with *n*-butane as a probe molecule in large crystals of zeolite NaX.

Materials and Methods

Sample synthesis and characterization

The giant X-type zeolite crystals were synthesized following a modified Charnell procedure¹⁵. The gel composition 1.7 Na₂O : Al₂O₃ : 1.3 SiO₂ : 300 H₂O : 10 triethanolamine gave after 5 weeks crystallization at 85 °C 70 – 80 µm large crystals (Fig. 1a). To adjust the reactivity of the silicate and aluminate species, metallic aluminium and colloidal silica (LUDOX) have been used. All solutions were filtered using Millipore filters (0.22 µm), the starting hydrogels were prepared at 0 °C, and quickly heated to crystallization temperature. Powder X-ray diffraction (Fig. 1b) proves the high crystallinity of the X-type crystals prepared (for comparison see ref 16). This high crystallinity does as well appear in the well-shaped form of the crystals (Fig. 1a).

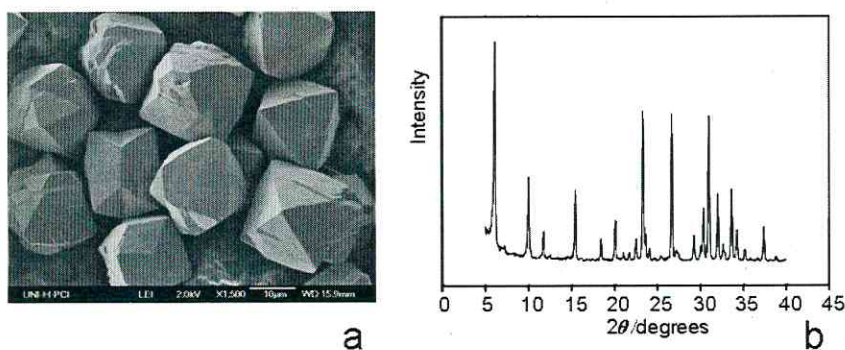


Figure 1. Scanning electron micro-image (Jeol JSM 6700F) (a) and X-ray diffraction pattern (b) of the NaX-type sample under study.

PFG NMR diffusion studies

The diffusion measurements were performed by means of the homebuilt PFG NMR spectrometer FEGRIS 400¹⁷ with the 13-interval pulse sequence¹⁸. In this technique, the two gradient pulses of conventional PFG NMR are replaced by pairs of alternating gradient pulses

separated by high-frequency π pulses. In this way, the disturbing influence of the permanent internal field gradients due to indispensable sample heterogeneities is reduced. The observation time was varied between 5 ms and 1 sec and the mean molecular displacements covered in the studies ranged from about 200 nm up to 20 μm . For diffusion in homogeneous, isotropic media, the signal intensity in PFG NMR experiments is known to obey the relation^{6,14,17,18}

$$\Psi(\delta g, t) = \exp(-\gamma^2 \delta^2 g^2 Dt) = \exp(-\gamma^2 \delta^2 g^2 \langle r^2(t) \rangle / 6) \quad (1)$$

with g , δ and t ($\gg \delta$) denoting the amplitude, duration and separation of the gradient pulses (where, in the 13-interval pulse sequence, δ stands for the sum of the durations of the two gradients of a pair, to ensure conformity with the notation of the simple stimulated echo¹⁷). The second equation results from Einstein's relation⁶

$$\langle r^2(t) \rangle = 6Dt \quad (2)$$

implying proportionality between the mean square displacement and the observation time. The self-diffusion coefficient D appearing in this relation coincides with the tracer diffusivity defined by Fick's 1st law.

For the PFG NMR diffusion studies, the zeolite material is contained in closed sample tubes. It is loaded with a well-defined amount of *n*-butane molecules which were introduced into the activated samples by chilling from a calibrated gas volume by means of liquid nitrogen. The samples were activated by heating (10 K/hour) under evacuation and by leaving the sample, under continued evacuation, at the final temperature of 400 °C for additional 10 hours.

Results and Discussion

Figure 2 provides typical examples of the primary data observed in our diffusion experiments. As their most striking feature, the attenuation plots for loadings with 3 molecules per supercage (Fig. 2c) are found to follow, essentially, the dependence of eq. (1), while there are significant

deviations for the smaller loading with 0.75 molecules per supercage (Fig. 2a, b). From eq. (1) the slope of the attenuation plots is easily seen to be proportional to the diffusivity and, hence, via eq. (2), to the mean square displacements. Correspondingly, at an average loading of 3 molecules per cavity (which corresponds to a relative pore filling of about one half), anywhere within the sample the guest molecules propagate at identical diffusion rates, while, at the lower loadings, notable differences become perceptible. This means that, within the pore space of the sample accommodated by the guest molecules, there have to be substantial differences which, at low loadings, give rise to the differences observed in the diffusivities. The coincidence in the attenuation curves for different observation times appearing from Figs. 2a and b indicates that, during the covered diffusion times, there is essentially no guest exchange between the regions of different mobilities.

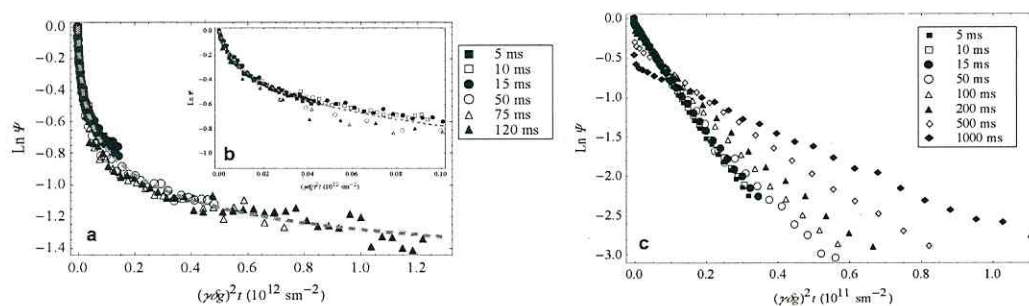


Figure 2. PFG NMR spin-echo attenuation curves for n-butane in the NaX sample under study for different observation times as indicated by the different symbols at 298 K and for guest loadings of 0.75 (a, b) and 3 (c) molecules per cavity. The broken line in Figs. a and b represents the best fit of the attenuation curves for a log-normal distribution of the diffusivities (eqs. (3) and (4)) to the data points.

The effect of heterogeneity may be quantified by introducing a probability function $p(D)$ with $p(D) dD$ indicating the probability that the diffusivity of a guest molecule, arbitrarily selected within

the sample, is in the interval $D...D+dD$. In this case, eq. (1) may be transferred into the more general form

$$\Psi(\delta g, t) = \int_0^{\infty} p(D) \exp(-\gamma^2 \delta^2 g^2 D t) dD. \quad (3)$$

Often, the so-called log-normal distribution¹⁹⁻²¹

$$p(D) = \frac{1}{D\sigma\sqrt{2\pi}} \exp\left[-\frac{(\ln D - \ln D_m)^2}{2\sigma^2}\right] \quad (4)$$

is found to serve as a reasonable first-order approach for systems where molecular diffusion has to be described by a distribution of diffusivities rather than by a single one. Here D_m stands for the mean and σ for the width of the distribution. In the limiting case of infinitely narrow distributions, i.e. with $p(D)$ equal to Dirac's delta function, eq. (3) coincides with eq. (1). This approach is also in the present case found to yield a good fit to the data points as shown in Figs. 2a and b by the broken line which corresponds to values of $D_m = 2.54 \times 10^{-11} \text{ m}^2\text{s}^{-1}$ and $\sigma = 2.6$. For rationalizing this result we may recollect²¹ that the interval $D_m/\sigma... D_m \times \sigma$ comprises 68.3 % of the distribution. In the present contents, this means that the sample heterogeneity appears in a variation of the local diffusivities over a factor of about 7 in two thirds of the total pore space, and that the deviation of the diffusivities in the remaining parts is even more significant!

In Fig. 2c, the slope of the signal attenuation and hence, via eq. (1), the effective diffusivity is seen to decrease with increasing observation time. Exactly this behavior has to be required as a consequence of the fact that intracrystalline diffusion proceeds within the finite volume of the individual crystallites of zeolite NaX rather than in an infinitely extended medium. The confinement leads to mean square displacements $\langle r^2(t) \rangle$ lagging progressively behind the displacements in an infinitely extended corresponding medium with increasing observation time t leading, with eq. (2), to the observed decrease in the diffusivities. For a quantitative proof of this interrelation one may consider these diffusivities as a function of the square root of the observation time as displayed in

Fig. 3. . For diffusion in spheres of radius R in second-order approximation this dependency obeys the following analytical expression,²²

$$\frac{D_{\text{eff}}}{D_0} \approx 1 - \frac{4}{3R} \left(\frac{D_0 t}{\pi} \right)^{1/2} - \frac{D_0 t}{2R^2} \quad (5)$$

with D_0 denoting the genuine diffusivity, unaffected by boundary effects. Figure 3 shows the best fit of eq. (3) to the initial four data points, yielding $D_0 = 7.6 \times 10^{-11} \text{ m}^2 \text{ s}^{-1}$ and a value of $R = 6.4 \text{ }\mu\text{m}$ for the mean crystal radius, which is of the order of magnitude expected from crystal micro-images shown in Fig. 1a. The approach provided by eq. (5) implies that the molecular diffusion path lengths during observation time are still notably exceeded by the crystal radii, i.e. $(D_0 t)^{1/2} \ll R$. Effective diffusivities with further increasing observation times are, therefore, beyond the limits of the applicability of eq. (5).

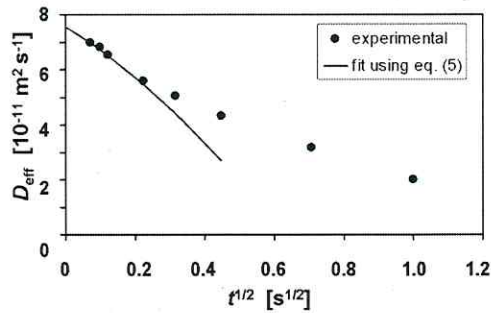


Figure 3. Effective diffusivities in the NaX specimen at 298 K (as resulting, via eq. (1), from the slopes of the representation of Fig. 2b) and comparison with the best fit of the second-order approach of their time dependence under confinement by spheres (eq. (5)).

As another feature of Fig. 2c, the signal attenuation curves are found to start with an abrupt drop which is increasing with increasing observation time. This first steep decay has to be attributed to that part of the molecules which, during the observation, was able to escape into the intercrystalline space and which, correspondingly, were able to cover particularly long

displacements. The contributions to the signal decay are proportional to the fractions of molecules which, respectively, remain inside the crystals or are able to leave. In the so-called NMR tracer desorption technique^{6,23} this additional information of PFG NMR experiments with beds of nanoporous materials is used to explore the existence of surface barriers. Assuming an exponential approach

$$p(t) = \exp(-t/\tau) \quad (6)$$

for the relative number of molecules which have remained within one and the same crystallite during the whole observation time t , one may introduce a mean molecular life time τ . This quantity can be compared with the mean life time resulting under the assumption that molecular exchange is exclusively determined by intracrystalline diffusion,^{23,24}

$$\tau_{\text{Diff}} = \frac{R^2}{15D_0} \quad (7)$$

The values resulting in the present study are $\tau = 1.5$ s and $\tau_{\text{Diff}} = 36$ ms. Intercrystalline exchange is thus found to be controlled by the permeation of a surface resistance on the individual zeolite crystals rather than by diffusion through the crystal bulk phase. With this finding, belatedly, we also justify the application of eq. (5), which does only hold in the limiting case of ideally reflecting boundaries. In the other extreme, namely for diffusion-limited exchange, the right-hand side would maintain its structure, however, with slightly modified pre-factors.^{22,25}

To facilitate the discussion of the differences observed with the two loadings, Fig. 4 compares the present data with the results of previous diffusion measurements with a sample of NaX stemming from the celebrated laboratory of Professor Zhdanov, Leningrad/St. Petersburg²⁶. Diffusion measurements with this material revealed, after as long as 30 years, a remarkable reproducibility yielding, with one and the same zeolite specimen, essentially identical diffusivity data²⁷. Moreover, the diffusion data in these materials were found to be in good agreement with theoretical predictions based on the pore space geometry of the ideal NaX structure.^{28,29} It is in particular the decrease in the mobilities with increasing loading which was widely accepted as a

quite general feature of *n*-alkane diffusion in zeolite NaX,³⁰ caused by the diminishing “free volume”. In addition to the much smaller values of the diffusivities, at room temperature, now also this loading tendency is found to be reversed.

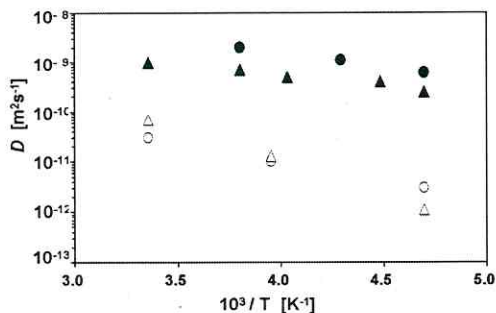


Figure 4. Comparison of the diffusivities of *n*-butane in zeolite NaX (full symbols: specimens synthesized by S.P. Zhdanov,^{26,28} open symbols: this study, sample shown in Fig. 1a) at loadings of 0.75 (circles) and 3 (triangles) molecules per large cavity. The size of the symbols corresponds to the uncertainty in the diffusivities.

Assuming that the diffusivities in the Zhdanov samples are exclusively determined by the friction exerted by the genuine NaX pore network, the lower diffusivities in the zeolites considered in this study (and, most likely, also in numerous other products of zeolite synthesis considered in the past) must additionally be influenced by transport resistances in the interior of the crystals, possibly similarly to the stacking faults revealed in the TEM studies of ref 12. With locally varying separation l between these resistances and, possibly, permeabilities α through these resistances (defined as the ratio between the particle flux through the resistance and the difference in the concentrations on either side^{31,33}), they would give rise to the observed distribution in the diffusivities as soon as the studied displacements exceed these separations but are still short enough to avoid an averaging over the whole spectrum of permeabilities and separations. In such cases, the effective diffusivity simply results by reciprocal addition of the two impeding mechanisms³¹

$$\frac{1}{D_{\text{eff}}} = \frac{1}{D} + \frac{1}{\alpha l}. \quad (8)$$

Hence, increasing permeabilities would reduce the contribution of the second term on the right hand side of eq. (8) to the overall diffusivity. Since, in general, the activation energies for permeation through the intracrystalline transport resistances exceed those for diffusion through the genuine pore space,^{12,32} the contribution of the second term on the right hand side of eq. (8) is expected to decrease with increasing temperature. The observation that the effective diffusivities in the present samples increase more strongly with increasing temperature than the diffusivities in the genuine NaX samples considered in ref 28 is in complete agreement with this consideration.

In a similar way one may also rationalize that at the higher loadings the influence of sample heterogeneity is not visible anymore. It is well known that in narrow pores the diffusivities generally increase with increasing loading (type-v pattern of concentration dependence^{30,33}). Since the formation of internal transport resistances is associated with constrictions in the pore space the permeability through these barriers is expected to increase with increasing guest concentrations. Hence, with increasing concentration, the weight of barrier permeation (second term in eq. (8)) on the effective diffusivity is decreasing, while the first term, as a consequence of the well-known decrease of *n*-alkane diffusivities in the genuine pore space of NaX²⁸, becomes more and more dominating so that, eventually, the influence of the additional transport resistances and, hence, of sample heterogeneities due to structure defects becomes negligibly small – as experimentally observed.

Conclusion

Exploiting *n*-butane as a probe molecule, well-shaped crystals of zeolite NaX are found to exhibit a remarkable heterogeneity. This heterogeneity appears in a broad distribution of the butane

diffusivities at low loadings, covering an order of magnitude. These diffusion data are by one to two orders of magnitude below the diffusivities observed in NaX specimens which are generally assumed to be close to perfect crystallinity²⁶. One has to conclude, therefore, that in the NaX specimens considered in the present study, guest diffusion is also controlled by internal transport resistances ("barriers") which act in addition to the permanent "drag" exerted on the diffusing molecules by the genuine pore space. Thus, a variation in both the spacing and the intensity of these resistances over the sample may easily explain the observed distribution in the observed diffusivities. It is interesting to note that these differences disappear with increasing loading. However, such a behavior is not unexpected since in narrow-pore media the diffusivities (and, hence, also the permeabilities) are known to generally increase with increasing loading. As a consequence, the influence of these barriers will decrease with increasing loadings so that, eventually for sufficiently large concentrations, sample heterogeneity will disappear in the diffusion patterns.

In addition to previous studies revealing sample heterogeneities by recording time-dependent intracrystalline diffusivities^{9,34} or by combining the PFG NMR diffusion data with the results of quasi-elastic neutron scattering and high-resolution microscopy¹², we have observed that, for one and the same guest molecule, the effect of sample heterogeneity on the observed diffusion patterns may dramatically depend on the loading. The decrease of this influence with increasing loading is shown to be in agreement with quite general features of mass transfer in pore spaces.³⁰

Crystals which, judging from both their external habit and their x-ray diffraction patterns, appear to be ideal are thus found to occur with vast differences in their real structure, ranging from perfect crystallinity as observed, e.g., with the diffusion measurements in ref 28 and their repetition in ref 27, to pronounced heterogeneities as substantiated with the present studies following previous comparative diffusion measurements by QENS and PFG NMR and investigations by high-resolution transmission electron microscopy¹². It is noteworthy that in these studies, both ideal crystallinity and deviations from crystallinity have been observed irrespective of the size of the given

crystals. The correlation between the deviations from ideal crystallinity and the resulting diffusion patterns is thus expected to be quite complex and should be kept in mind quite generally in diffusion studies with such materials.

Acknowledgement

Financial support by Deutsche by Deutsche Forschungsgemeinschaft (International Research Group „Diffusion in Zeolites“) and by „Fonds der Chemischen Industrie“ are gratefully acknowledged. Xiaobo Yang (Hanover) is thanked for NaX synthesis, Aisheng Huang (Hanover) for taking the XRD and SEM.

References

- (1) Kaskel, S. In Handbook of Porous Solids; Schüth, F., Sing, K. S. W., Weitkamp, J., Eds.; Wiley-VCH: Weinheim, 2002; Vol. 2, pp 1190– 1249.
- (2) Choi, M.; Srivastava, R.; Ryoo, R. *Chem. Commun.* **2006**, 4380– 4382
- (3) Sel, O.; Kuang, D.; Thommes, M.; Smarsly, B. *Langmuir* **2006**, *22*, 2311– 2322
- (4) Sun, L. H.; Shan, Z.; Maschmeyer, T.; Coppens, M. O. *Langmuir* **2003**, *19*, 8395
- (5) Ertl, G.; Knözinger, H.; Schüth, F.; Weitkamp, J. Handbook of Heterogeneous Catalysis; Wiley-VCH: Weinheim, 2008.
- (5) Karge, H. G.; Weitkamp, J. Adsorption and Diffusion; Springer: Berlin, 2008; Vol. 7, p 400.
- (7) Takaba, H.; Yamamoto, A.; Hayamizu, K.; Oumi, Y.; Sano, T.; Akiba, E.; Nakao, S. *Chem. Phys. Lett.* **2004**, *393*, 87– 91
- (8) Takaba, H.; Yamamoto, A.; Hayamizu, K.; Nakao, S. *J. Phys. Chem. B* **2005**, *109*, 13871– 13876
- (9) Vasenkov, S.; Böhlmann, W.; Galvosas, P.; Geier, O.; Liu, H.; Kärger, J. *J. Phys. Chem. B* **2001**, *105*, 5922– 5927

- (10) Barrer, R. M. *Langmuir* **1987**, *3*, 309– 315
- (11) Kärger, J. *Langmuir* **1988**, *4*, 1289– 1292
- (12) Feldhoff, A.; Caro, J.; Jobic, H.; Krause, C. B.; Galvosas, P.; Kärger, J. *Chem. Phys. Chem.* **2009**, *10*, 2429– 2433
- (13) Kärger, J.; Ruthven, D. M. *Zeolites* **1989**, *9*, 267– 281
- (14) Naumov, S.; Valiullin, R.; Monson, P.; Kärger, J. *Langmuir* **2008**, *24*, 6429– 6432
- (15) Yang, X.; Albrecht, D.; Caro, J. *Microporous Mesoporous Mater.* **2006**, *90*, 53– 61
- (16) Database of Zeolite Structures: Powder Patterns, homepage of the International Zeolite Association, www.iza-structure.org
- (17) Galvosas, P.; Stallmach, F.; Seiffert, G.; Kärger, J.; Kaess, U.; Majer, G. *J. Magn. Reson.* **2001**, *151*, 260– 268
- (18) Cotts, R. M.; Hoch, M. J. R.; Sun, T.; Markert, J. T. *J. Magn. Reson.* **1989**, *83*, 252– 266
- (19) Nydén, M.; Soderman, O. *Macromolecules* **2002**, *35*, 4990– 5002
- (20) Fleischer, G.; Rittig, F.; Kärger, J.; Papadakis, C. M.; Mortensen, K.; Almdal, K.; Štěpánek, P. *J. Chem. Phys.* **1999**, *111*, 2789– 2796
- (21) Limpert, E.; Stahel, W. A.; Abbt, M. *BioScience* **2001**, *51*, 341– 352
- (22) Mitra, P. P.; Sen, P. N.; Schwartz, L. M. *Phys. Rev. B* **1993**, *47*, 8565– 8574
- (23) Krutyeva, M.; Kärger, J. *Langmuir* **2008**, *24*, 10474– 10479
- (24) Barrer, R. M. *Zeolites and Clay Minerals as Sorbents and Molecular Sieves*; Academic Press: London, 1978; p 497.
- (25) Geier, O.; Snurr, R. Q.; Stallmach, F.; Kärger, J. *J. Chem. Phys.* **2004**, *120*, 367
- (26) Zhdanov, S. P.; Khvostchov, S. S.; Feoktistova, N. N. *Synthetic Zeolites*; Gordon and Breach: New York, 1990.
- (27) Ulrich, K.; Freude, D.; Galvosas, P.; Krause, C.; Kärger, J.; Caro, J.; Poladli, P.; Papp, H. *Microporous Mesoporous Mater.* **2009**, *120*, 98– 103
- (28) Kärger, J.; Pfeifer, H.; Rauscher, M.; Walter, A. *J. Chem. Soc., Faraday Trans. 1* **1980**, *76*, 717– 737
- (29) Auerbach, S. M.; Bull, L. M.; Henson, N. J.; Metiu, H. I.; Cheetham, A. K. *J. Phys. Chem.* **1996**, *100*, 5923– 5930
- (30) Keil, F. J.; Krishna, R.; Coppens, M. O. *Rev. Chem. Eng.* **2000**, *16*, 71– 197
- (31) Crick, F. *Nature* **1970**, *225*, 420
- (32) Paoli, H.; Méthivier, A.; Jobic, H.; Krause, C.; Pfeifer, H.; Stallmach, F.; Kärger, J. *Microporous Mesoporous Mater.* **2002**, *55*, 147– 158

(33) Kärger, J.; Ruthven, D. M. *Diffusion in Zeolites and Other Microporous Solids*; Wiley & Sons: New York, 1992.

(34) Vasenkov, S.; Kärger, J. *Microporous Mesoporous Mater.* 2002, 55, 139–145

Publication 4: Guest diffusion in interpenetrating networks of micro- and mesopores

The Journal of the American Chemical Society, **2011**, 133, 2437

F. Furtado^{a,b}, P. Galvosas^{b,c}, M. Gonçalves^d, F.-D. Kopinke^a, S. Naumov^b, F. Rodríguez-Reinoso^d, U. Roland^a, R. Valiullin^{b,*}, J. Kärger^b

^aDepartment of Environmental Engineering, UFZ – Helmholtz-Centre for Environmental Research, Permoserstr. 15, 04318 Leipzig, Germany

^bDepartment of Interface Physics, University of Leipzig, Linnéstr. 5, D-04103 Leipzig, Germany

^cSchool of Chemical and Physical Sciences, Victoria University of Wellington, P.O. Box 600, Wellington 6140, New Zealand

^dDepartamento de Química Inorgánica, Universidad de Alicante, Apartado 99, 03080 Alicante, Spain

Abstract

Pulsed field gradient NMR is applied for monitoring the diffusion properties of guest molecules in hierarchical pore systems after pressure variation in the external atmosphere. Following previous studies with purely mesoporous solids, also in the material containing both micro- and mesopores (activated carbon MA2), the diffusivity of the guest molecules (cyclohexane) is found to be most decisively determined by the sample "history": at a given external pressure diffusivities are always found to be larger if they are measured after pressure decrease (i.e. on the "desorption" branch) rather than after pressure increase (adsorption branch). Simple model consideration reproduces the order of magnitude of the measured diffusivities as well as the tendencies in their relation to each other and their concentration dependence.

Keywords: Activated carbon, diffusion, pulsed field gradient NMR, hierarchical pore systems

Introduction

The need for transport-optimized materials for molecular separation and for molecular conversion by heterogeneous catalysis has initiated the development of novel strategies for the production of such materials¹. Combining the benefit of micropores for molecular separation and conversion and of mesopores for transport acceleration, materials of hierarchical pore architecture have attained particular interest². The interpenetration of micro- and mesopore spaces leads to very special patterns of mass transfer which, in such complex systems, are by far more complicated to be assessed than in purely microporous or mesoporous materials. This includes, in particular, the exploration of the interrelation between sorption hysteresis and mass transfer. In the literature, time-dependent hysteresis is referred to both structural changes (such as deformations and swelling) in the host material^{3,4} and diffusion resistances in the pore space⁵. To the best of our knowledge, never before mass transfer and sorption hysteresis in hierarchical pore systems has been directly correlated by experimental measurement.

The present study is dedicated to this issue, exploiting the pulsed field gradient technique of NMR (PFG NMR)⁶⁻⁸ as a sophisticated tool for the in-situ observation of molecular displacements over microscopic dimensions. The covered diffusion path lengths are thus large enough to ensure tracing the combined effect of mass transfer in the micro- and mesopores. They are small enough, however, to remain unaffected by the influence of unwanted boundary effects by the external surface of the host particles and the interparticle space.

Materials and Methods

The host system under study was an activated carbon (MA2), prepared by carbonisation and subsequent CO₂ activation (43% activation burn-off) of spherical porous resin obtained by cross-

linking of phenol-formaldehyde Novolac precursor with hexamethylenetetramine and with ethylene glycol as solvent - pore former^{9,10}. It consists of spherical particles (Figure 1.a) with diameters of 0.15-0.50 μm (mean 0.32 μm).

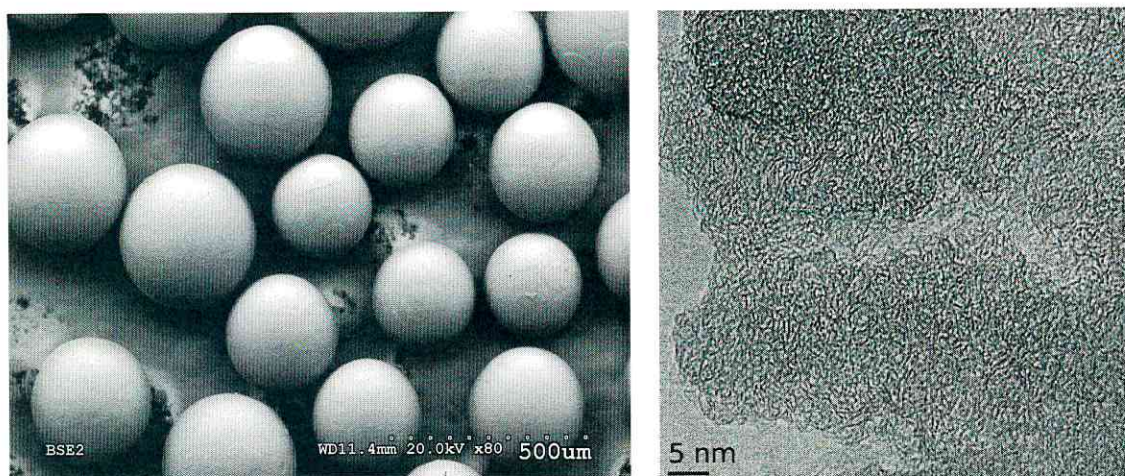


Figure 1. Images of the host system under study (activated carbon of type MA2^{9,10}) as obtained by (a), left) scanning electron microscopy and (b), right) by transmission electron microscopy, revealing both micro- and mesopores.

In both nitrogen adsorption at 77 K (Figure 2) and transmission electron microscopy (Figure 1.b), micro- and mesoporosity appear in an almost perfect mixture (1:1), with respective volumes $V_{\text{micro}}=0.64 \text{ cm}^3\text{g}^{-1}$ and $V_{\text{meso}}=0.59 \text{ cm}^3\text{g}^{-1}$, which correspond to two pore diameter ranges centered around 1 nm and 20 nm, in the obtained pore size distributions (inserts to Figure 2). Furthermore, the micropore volume was also accessed by CO_2 adsorption at 273 K giving rise to an expected slightly lower value of $V_{\text{micro}}=0.57 \text{ cm}^3\text{g}^{-1}$. This value remains in good agreement with the estimation from the N_2 adsorption data, since the adsorption of CO_2 at 273 K is limited to the narrow ($< 1 \text{ nm}$) micropores^{11,12}; the distinction of narrow and wide microporosity is clear in the DFT¹³ pore size distribution inset of Figure 2.

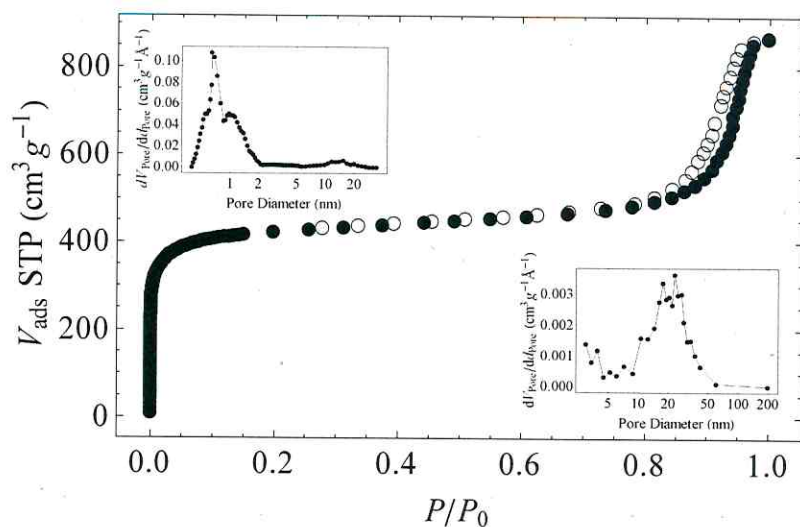


Figure 2. N_2 adsorption isotherm at 77 K for the carbon sample under study, with closed and open symbols corresponding to the adsorption and desorption branch, respectively. The insets show the micropore and mesopores pore size distributions (upper left side and lower right side, respectively) as obtained by DFT¹³ (micropore distribution) and BJH¹⁴ (mesopores distribution). Note that the area under both peaks, in the upper-left inset, is approximately the same.

The diffusion measurements have been performed by means of the pulsed field gradient (PFG) NMR technique⁶⁻⁸, using cyclohexane (with a saturation pressure of $P_0=130$ mbar, at 298 K) as a probe molecule. By considering large ensembles of molecular entities, experiments of this type are complementary to single-molecule observation¹⁵ and yield the complete statistical information relevant for the selected space and time scales. The primary quantity recorded by PFG NMR is the intensity of the NMR signal (the spin echo). This quantity, plotted as a function of the intensity of the field gradient pulses, is the Fourier transform of the propagator⁷, i.e. the probability distribution of molecular displacements as a function of the observation time. Typical space and time scales as accessible by PFG NMR are micrometers and milliseconds. The mean square displacement $\langle r^2(t) \rangle$

results as the mean squared width of this distribution and follows directly from the signal attenuation in the limit of sufficiently small gradient intensities (initial decay of the NMR signal intensity in a semi-logarithmic representation versus the squared magnetic field gradient intensity^{6,7}).

PFG NMR diffusion data in complex systems are commonly represented by so-called effective diffusivities defined by the relation

$$D_{\text{eff}} = \langle r^2(t) \rangle / 6t \quad (1)$$

as the ratio between the mean square displacement $\langle r^2(t) \rangle$ of the molecules under study and the observation time t . In homogeneous systems, Eq. (1) represents Einstein's diffusion equation^{16,17} and D_{eff} coincides with the genuine coefficient of self-diffusion (also referred to as the self-diffusivity). In heterogeneous systems, D_{eff} is the mean value of the diffusivities of all probe molecules under study. The diffusion measurements have been performed with the 13-interval pulse sequence¹⁸ at a proton resonance frequency of 125 MHz by means of the home-built PFG NMR diffusion spectrometer FEGRIS NT^{19,20}. Prior to the measurements, the host material under study was kept in an oven at 383 K in contact with atmosphere over 24 h and, subsequently, under high vacuum ($< 10^{-2}$ Pa) at 523 K for 4 h. The diffusion measurements were generally performed by connecting the sample with a reservoir containing the guest molecule under well-defined pressure. By varying the pressure, a continuous variation of the sample loading was possible. By approaching a certain pressure either from smaller or larger values (i.e. by adsorption or desorption) different sample "histories" could be considered. Since the intensity of the NMR signal following the first ($\pi/2$) pulse of the PFG NMR pulse sequence (the "free induction decay") is directly proportional to the number of guest molecules, the NMR technique may as well be exploited to determine the guest loading. This occurs under exactly those conditions under which the diffusion experiments are performed and allows the immediate correlation of diffusion and adsorption under a well-defined external atmosphere²¹.

Complementary to these studies, selected diffusion measurements have been performed in closed PFG NMR samples as well. After subjecting the host material to exactly the same activation procedure as described above, these samples have been prepared by introducing a well-defined amount of guest molecules into the host material by freezing with liquid nitrogen and subsequent sealing of the sample tubes.

Results

Figure 3 provides a survey of the diffusivities (D_{eff}) of cyclohexane in activated carbon MA2 measured under variation of the external gas phase pressure, jointly with the corresponding loadings (Θ). The loadings are represented as the ratio between the amount actually adsorbed and its maximum value attained by guest pressures close to saturation. Inevitable long-term instabilities cause the uncertainty indicated for the loadings. The uncertainty in the measured diffusivities relative to each other is smaller than the size of the symbols.

Usually, the measurements were performed 10 minutes after the pressure step. The development of the loading during this time interval is represented by the development of the free induction decay (FID) shown in Figure 4. Pressure steps during adsorption (Figure 4.a) are found to lead to an only slight change in loading, which must be expected to continue after the considered time interval of 10 minutes. In general pressure steps during desorption are followed by a much more pronounced change in loading (Figure 4.b). The normalized representation in Figure 4.c shows that this effect is particularly pronounced for pressure steps around $P/P_0 = 0.7$.

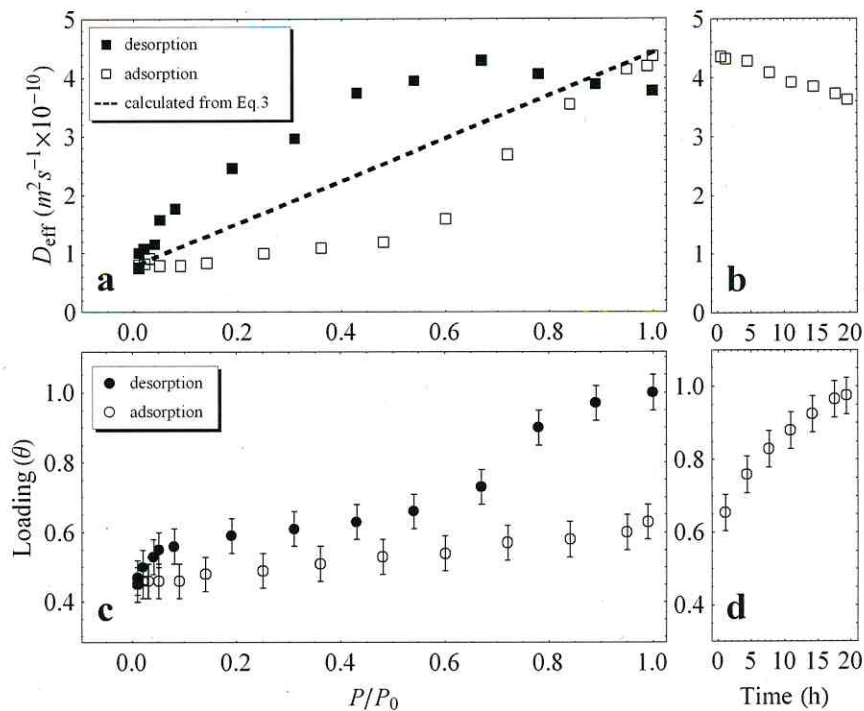


Figure 3. a) Diffusivities of cyclohexane at 298 K in MA2 as a function of the relative external pressure during adsorption and desorption and the diffusivities resulting via Equation 3 (dashed line). b) Evolution of the diffusivities with time after the last pressure step (to $P/P_0 \approx 1$) on the adsorption branch. c) Cyclohexane loading isotherm at 298 K in MA2 as a function of the external pressure during adsorption and desorption, measured 10 min after each pressure variation. d) Loading evolution with time after the pressure step to $P/P_0 \approx 1$ on the adsorption branch.

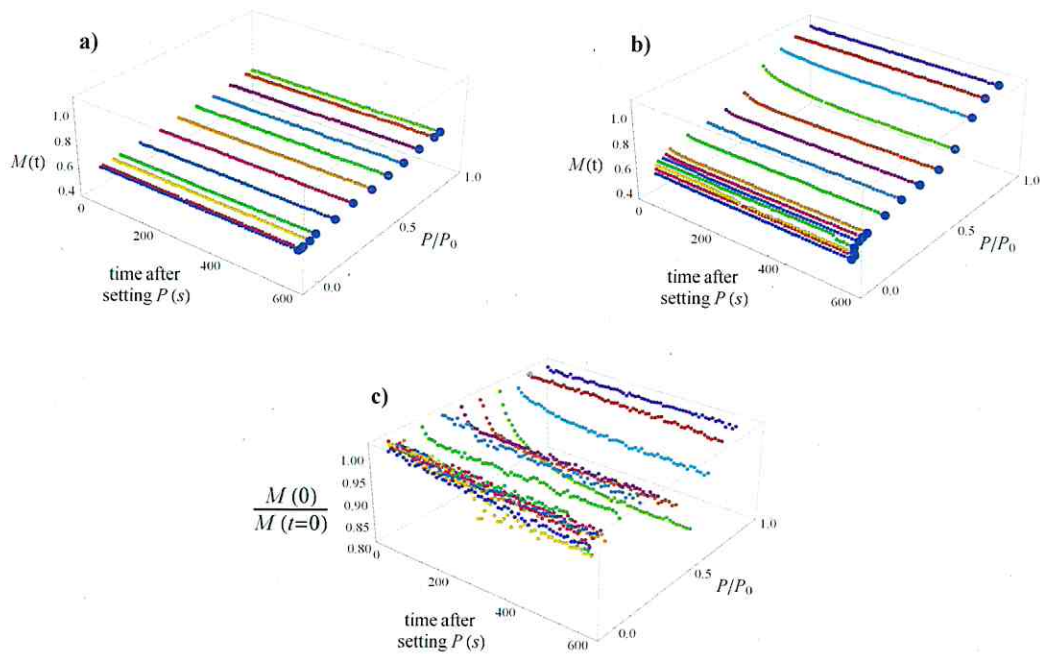


Figure 4. Changes in loading of the host material following pressure steps during adsorption (a) and desorption (b, c). The blue data points are used as loading in Figure 3.c).

Limitation in the measuring time allowed an extension of the equilibration time only for selected cases. One example is provided by Figures 3.b and d, where the final adsorption step to saturation is found to require equilibration times of days, accompanied by distinct changes in the diffusivities. A second experiment of this type has been performed during desorption following the pressure step from $P/P_0 = 0.74$ to 0.67 . Here, following the initial change as displayed by Figure 4.c, during the considered time interval of 20 hours no further change in loading and diffusivity became visible within the accuracy of these measurements ($\pm 5\%$).

Complementary to the diffusion measurements at well-defined external pressures, Figure 5 provides a survey of the diffusivity data obtained for the closed samples. Also included in this representation are the diffusivity data of Figure 3a. The error bars in the loading (resulting by

turning the vertical error bars of Figure 3c into horizontal direction) are omitted. Note that diffusion measurements with loadings notably below saturation of the micropores could not be performed by the experimental set-up designed for pressure variation (data of Figure 3a). The spatial constraint given by the PFG NMR spectrometer did not allow a satisfactorily accurate adjustment and maintenance of the small guest pressures necessary for attaining these low loadings.

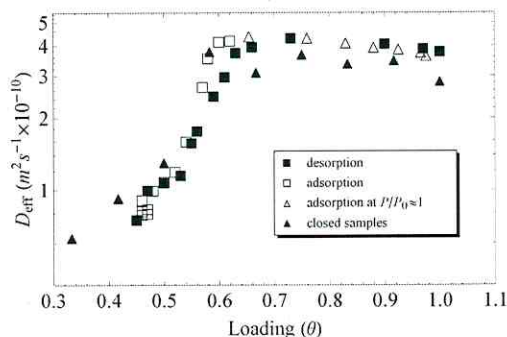


Figure 5. Measured diffusivities as a function of sample loading, obtained by continually varying the external pressure and on closed samples, prepared with a defined amount of cyclohexane.

Discussion

Following investigations with purely mesoporous host systems (Vycor porous glass)²² and system containing both meso- and macro-porosity²³, with the data shown in Figure 3a for the first time hysteresis effects are also observed for diffusion in hierarchical pore networks involving both micro- and mesoporous spaces. It turns out that, for a given external pressure, the measured diffusivities notably depend on the “history” of the system: if the pressure is attained by pressure decrease from larger values (i.e. on the “desorption branch”), the diffusivities are found to be

notably larger than after approaching the same pressure from lower values, i.e. on the adsorption branch.

For rationalizing the observed diffusion behavior, we have to correlate the experimentally accessible quantity, the mean square displacement, with its constituents, i.e. the displacements in the micro- and mesopores. The distances over which, in PFG NMR measurements, the guest molecules are followed are typically of the order of micrometers so that the diffusion paths consist, in general, of displacements in both the micro- and mesoporous spaces. We, correspondingly, note

$$\langle r^2(t) \rangle = \langle (r_{\text{micro}}(t) + r_{\text{meso}}(t))^2 \rangle = \langle r_{\text{micro}}^2(t) \rangle + \langle r_{\text{meso}}^2(t) \rangle \quad (2)$$

where $r_{\text{micro}}(t)$ and $r_{\text{meso}}(t)$ represent the (vector) sum over all individual constituents of overall displacement in the micro- and mesoporous spaces, respectively, during time t . The second relation holds rigorously if subsequent displacements in the micro- and mesopores are uncorrelated. This requirement is fulfilled for mutually interpenetrating pore networks and corresponds to the model of parallel diffusion resistances. Dividing Eq.(2) by the observation time and comparison with Eq.(1) finally yields

$$D_{\text{eff}} = \frac{t_{\text{micro}}}{t} D_{\text{micro}} + \frac{t_{\text{meso}}}{t} D_{\text{meso}} = p_{\text{micro}} D_{\text{micro}} + p_{\text{meso}} D_{\text{meso}} \quad (3)$$

where the quantities $t_{\text{micro(meso)}}$, $D_{\text{micro(meso)}}$ and $p_{\text{micro(meso)}}$ denote, respectively, the total life time (during t), the self-diffusivity and the relative amount of molecules in the micro- (meso-) mesopores. The second equation results in consequence of the detailed-balance requirement $p_{\text{micro}}/t_{\text{micro}} = p_{\text{meso}}/t_{\text{meso}}$.

With Eq. (3), the general tendency in the variation of the diffusivities with varying loading, as revealed by Figure 5, may be easily rationalized. For loadings sufficiently below total filling of the

microporous space (i.e. up to $\Theta \approx 0.5$), the pressure and, hence, the relative amount p_{meso} of molecules in the mesopores is so small that the second term in Eq. (3) may be neglected. Mass transfer in the pore system is essentially controlled, therefore, by micropore diffusion. The increase with increasing loading observed in this loading range corresponds to the well-known pattern III of the concentration dependence of pore space diffusion as discussed by Kärger and Ruthven²⁴ and may be referred to the (transport-impeding) influence of strong adsorption sites which decreases with increasing loading.

In Figure 5, this range of micropore-controlled diffusion is followed by a region ($0.5 < \Theta < 0.6$) of steep increase of the diffusivity with increasing loading: loading enhancement by 20 % increases the diffusivity by a factor of 5. This enhancement may immediately be attributed to the onset and a dramatic increase of the contribution of mesopore diffusion to mass transfer, i.e. to the second term on the right-hand side of Eq. (3). We have to note that the relative amount of molecules in the mesopores is still much smaller than in the micropores ($p_{\text{meso}} \ll p_{\text{micro}}$). This, however, is now becoming to be overcompensated by the fact that molecular propagation in the (still empty) mesopores is much larger than in the micropores and that, therefore, $D_{\text{meso}} \gg D_{\text{micro}}$.

The steep increase in the diffusivity for $0.5 < \Theta < 0.6$ is followed by a moderate decrease in the diffusivities, which attain their minimum for $\Theta = 1$. This behavior appears even more pronounced in the presentations of Figure 3 and is immediately correlated with the onset of capillary condensation. Again the behavior may be rationalized by Eq. (3): capillary condensation leads to a break down in the mesopore diffusivity from Knudsen to bulk diffusion. As a consequence, the decrease in D_{meso} may effect that, irrespective of an increase of p_{meso} towards (for the given system) $p_{\text{meso}} \approx p_{\text{micro}} \approx 0.5$, the second term on the right hand side of Eq.(3) decreases with further increasing loading.

As already discussed, Figure 3 shows that cyclohexane diffusivity plotted versus external pressure does remarkably depend on the sample preparation history. It should be noted that Figure 5 rather indicates that the measured diffusivities on the desorption and adsorption branches, as well

as on closed samples in this particular system do not significantly differ from each other (within the experimental precision), for a given loading. Therefore, provided that the system has been given enough time to equilibrate, on the basis of the results obtained, one may anticipate that sample preparation history should not affect the diffusivity of the guest molecule. This, however, is a matter of ongoing discussions in the literature with a particular emphasis that, in random mesoporous structures no thermal equilibration can be obtained on the laboratory time scale^{22,30}.

The scenario of molecular dynamics as deduced from the experimental data may be supported by an order-of-magnitude estimates which can be shown to cover the two limiting cases in which the guest molecules are assumed to accommodate the mesopores exclusively in either the gaseous or liquid state. Disregarding any mass transfer along the inner surface of the mesopores, in the first case the relative amount of molecules in the mesopores may be noted as a function of the volumes V_{meso} and V_{micro} of the meso- and micropores and the pressure P in the mesopores by the relation²¹

$$p_{\text{meso}} = \frac{V_{\text{meso}}}{V_{\text{micro}} + V_{\text{meso}}} \frac{MP}{RT\rho_{\text{liq}}} \ll 1 \quad (4)$$

with R denoting the gas constant, T the absolute temperature, M the molecular weight and ρ_{liq} the density of liquid cyclohexane. Mesopore diffusion may be approached by the classical Knudsen relation

$$D_{\text{meso}} = D_{\text{Knudsen}} / \tau = \frac{d}{3\tau} \sqrt{\frac{8RT}{\pi M}} \quad (5)$$

where, in addition, a tortuosity factor τ has been introduced to take account of an additional enhancement of the diffusion path lengths due to pore tortuosity²⁵.

Figure 3.a shows the effective diffusivities resulting from Eq.(3), in combination with Eqs. (4) and (5), by the dashed straight line. The starting point in the low-pressure region is chosen to

coincide with the effective diffusivity which may be attributed to micropore diffusion at micropore saturation. By assuming that the mesopores are exclusively filled by gas phase, p_{meso} remains much less than p_{micro} (i.e., $p_{\text{meso}} \ll p_{\text{micro}} \approx 1$, with the latter relation following due to $p_{\text{micro}} + p_{\text{meso}} = 1$). With Eqs. (3) to (5), D_{eff} thus results as a function linearly increasing with the pressure. Its slope is given by the ratio d/τ . With a pore diameter of $d = 20$ nm (see Figure 2), the effective diffusivity is found to reach the experimental value at saturation pressure by assuming a tortuosity factor of $\tau = 1.3$. Since our estimates had to neglect possible contributions of surface diffusion to mass transfer in the mesopores, including correlation effects which may affect the applicability of Eq. (5)²⁶⁻²⁸, the resulting tortuosity factor is only an estimate of the lower limit and thus in satisfactory agreement with the values (about 2 to 4) commonly found in the literature²⁵.

With the onset of capillary condensation, after a waiting time of 20 h (Figure 3.b), the effective diffusivity decreases to a value of $D_{\text{eff}} = 3.6 \times 10^{-10} \text{ m}^2 \text{ s}^{-1}$. In the limiting case of micro- and mesopore saturation, Eq. (3) becomes

$$D_{\text{eff}} = \frac{V_{\text{micro}}}{V_{\text{micro}} + V_{\text{meso}}} D_{\text{micro}} + \frac{V_{\text{meso}}}{V_{\text{micro}} + V_{\text{meso}}} D_{\text{meso}} \quad (6)$$

where, for simplicity, the guest densities in the two pore spaces are assumed to coincide. With the relevant values of $D_{\text{micro}} = 7.9 \times 10^{-11} \text{ m}^2 \text{ s}^{-1}$, $V_{\text{micro}} = 0.64 \text{ cm}^3 \text{ g}^{-1}$ and $V_{\text{meso}} = 0.59 \text{ cm}^3 \text{ g}^{-1}$, Eq. (6) is found to yield the experimentally determined value of $D_{\text{eff}} = 3.6 \times 10^{-10} \text{ m}^2 \text{ s}^{-1}$ by implying a value of $D_{\text{meso}} = 6.6 \times 10^{-10} \text{ m}^2 \text{ s}^{-1}$ for the liquid diffusivity in the mesopores. This value is by a factor of 2 below the diffusivity in the bulk liquid ($D_{\text{cyclohexane}} = 1.4 \times 10^{-9} \text{ m}^2 \text{ s}^{-1}$)²⁹ which, again, may be easily referred to the effect of tortuosity. The order of magnitude of the measured diffusivities is thus found to be nicely reflected by our simplifying model based on Eq.(3) and by considering the two extreme cases that mass transfer in the mesopores is controlled by either Knudsen diffusion (mesopores

exclusively containing gas phase) or by bulk diffusion (mesopores exclusively containing liquid phase).

As the most remarkable feature of Figure 3.a, the measured diffusivities are found to deviate in a well-defined way from the straight line which, via Eqs. (3) to (5), represents the diffusivities predicted by assuming that the gas pressure within the mesopores coincides with the pressure externally applied. The experimental results deviate to smaller values on the adsorption branch, i.e. in a sequence of steps with increasing pressure, while they are above this line on the desorption branch. Such history dependence in the measured diffusivities ("diffusion hysteresis") has, for the first time, been observed in purely mesoporous systems²².

With the present study, this phenomenon is now as well demonstrated to occur in hierarchical pore networks. In contrast to the purely mesoporous materials, in the hierarchical materials under study the mesoporous space is imbedded in a microporous matrix. The micropores provide the system with additional diffusion pathways, the efficiency of which may be quantified by the micropore diffusivities also measured in this study (diffusivities in Figure 5 for $\Theta < 0.5$). The additional diffusion pathways provided by the micropores may be expected to promote equilibration. It turns out, however, that this effect is not strong enough and does not prevent the formation of hysteresis effects. This finding confirms the conclusion of the previous studies with purely mesoporous materials²²: system equilibration during hysteresis is not correlated with the guest diffusivities. It is the rate of collective rearrangement of molecular ensembles rather than of individual molecules which promotes the systems into states of lower free energy. It is well established that the propagation rate of the latter process is dramatically decreasing with increasing time^{22,30-32} excluding equilibrium establishment over feasible observation times.

Deviating from the observations with the pure mesoporous material (Vycor porous glass, see Figure 1b of ref. (22)), the diffusivities on the desorption branch are now (Figure 3a) found to be notably larger (rather than smaller) than those on the adsorption branch. This difference, however, may be nicely referred to a quite general pattern of diffusion hysteresis which may be deduced from

both the previous studies with the purely mesoporous material²² and the present investigations with hierarchical pore spaces: since, upon pressure variation, the system tends to remain in the old state the diffusivities likewise tend to be shifted towards the previously measured values. The relation between the diffusivities on the adsorption and desorption branches may therefore easily be correlated with the overall trends in the concentration dependence. In Vycor porous glass²², the diffusivity at saturation is found to be notably smaller than over most of the covered pressure range while, just vice versa, in the material considered in this study, the diffusivity at complete saturation is notably larger than over most of the pressure range considered.

The deviation of the experimental data from the theoretical estimate (broken line in Figure 3a) towards larger values on the desorption branch and towards smaller values on the adsorption branch is in complete agreement with the understanding that, upon pressure decrease, the actual pressure within the mesopores is above the external pressure, while it is below the external pressure upon pressure increase: system "memory" tends to maintain the previous state. The time interval between pressure variation and measurement (in general 10 min) has thus turned out to be too small to ensure complete equilibration.

Figures 3b and 3d and Figure 4 display the experimental data which have been obtained in selected series of measurement with observation times extended to 20 hours. As a most intriguing difference in system evolution, pressure steps are found to lead to a pronounced short-term response during desorption (Figures 4.b and 4.c) while, during adsorption (Figures 3.b and 3.d, Figure 4.a), loading and diffusivities vary extremely slowly with increasing observation time. A reliable explanation of this difference requires long-term measurements with correspondingly long observation times which are under consideration for future studies. Possible explanations may include variations in the host structure upon sorption³ and/or kinetic restrictions in the micropore space as suggested in ref. (33).

For the time constant (“first statistical moment”³⁴) of the decay following the desorption step at $PI/P_0 = 0.67$ in Figures 4.b and 4.c one obtains a value of $\tau_{des} \approx 100$ s. For diffusion-limited desorption by spherical particles of radius R , this time constant is given by the relation³⁴

$$\tau_{des}^{diff} = \frac{R^2}{15D_{des}} \quad (7)$$

with D_{des} denoting the diffusivity relevant for the desorption process considered. With a mean radius of 0.16 mm as relevant for our host particles and the above value of $\tau_{des} \approx 100$ s, Eq. (7) yields a diffusivity $D_{des} = 1.7 \times 10^{-11} \text{ m}^2\text{s}^{-1}$. It is interesting to note that this value is still – though slightly smaller – of the order of the micropore diffusivities ($D_{micro} = 7.9 \times 10^{-11} \text{ m}^2\text{s}^{-1}$). The given differences might, moreover, be referred to the different nature of the two diffusivities: the self-diffusivity resulting by PFG NMR is an equilibrium quantity while D_{des} results from the rate of desorption and is, therefore, generally referred to as a transport (or Fickian) diffusivity^{28,35}. On the basis of the experimental data so far available, however, the indicated correlation with the short-time behavior in the relaxation curves shown in Figure 4.b and 4.c cannot be anything more than a tentative approach. Similarly, there is no sound basis to exclude that the observed fast relaxation is followed by another, very slow one, with time constants far too large to be accessible in our measurements. The possibility of diverging time constants is well established in the literature^{22,36}.

Conclusions

In the course of the last decades, diffusion measurements in apparently simple materials such as purely microporous solids revealed a multitude of diverging results^{37,38} and, eventually, led to the insight that the real structure of such materials may notably deviate from the patterns resulting from conventional structure analysis and generally found in text books^{39,40}. It is worthwhile mentioning

that, in general, these complications do not concern diffusion measurements by Quasi-Elastic Neutron Scattering (QENS⁴¹) where the covered diffusion paths are of the order of nanometers. Structural deviations such as stacking faults⁴⁰ which may become rate controlling in PFG NMR diffusion measurements (and even more pronounced in the more “macroscopic” techniques) would thus affect an only negligibly fraction of the recorded trajectories and would not appear in the QENS diffusion data. This virtue of QENS is impressively demonstrated by the excellent agreement between QENS measurement of guest diffusion in zeolites and Molecular Dynamics simulations which are based on the ideal pore structure⁴².

Mesoporous and in particular hierarchical host materials may additionally complicate the conditions for reliable diffusion measurements. Since the range of diffusion measurement by QENS is, at the best, limited to distances comparable with the mesopore diameters, this technique is unable to provide direct information about the rate of long-range diffusion within the individual host particles.

Covering diffusion path lengths from fractions to hundreds of micrometers, PFG NMR is the method of choice for the measurement of molecular transport in such systems. Following previous studies with purely mesoporous materials^{22,43,44}, PFG NMR has now been employed to investigate the mobility of guest molecules in a material with an interpenetrating network of micro- and mesopores as a function of the sample history. Over essentially the whole pressure range covered in the experiments, for one and the same externally applied pressure the molecular diffusivities measured on the desorption branch, i.e. following a decrease in the external pressure, notably exceeded the diffusivities on the adsorption branch. We were able to rationalize both the trends in the concentration dependence and the relation between the diffusivities on the basis of simple microkinetic models.

The waiting times of generally 10 minutes, as allowed by the conditions under which the experiments had to be performed, not unexpectedly turned out to be much too short for equilibration. Even with waiting times of up to 20 hours, allowed for in selected cases, there was no

clear evidence of final equilibration. We have confined ourselves to weak conjectures about the mechanisms behind the ongoing equilibration process, including the option of sorption-induced structural changes in the host material, and hope that the presented experimental data help to intensify investigations on a challenging field of current research.

References

- (1) Schüth, F.; Sing, K. S. W.; Weitkamp, J. *Handbook of Porous Solids*; Wiley-VCH: Weinheim, Germany, 2002.
- (2) Wang, G.; Johannessen, E.; Kleijn, C.; Deleeuw, S.; Coppens, M. *Chem. Eng. Sci.* **2007**, *62* (18–20) 5110– 5116
- (3) Gregg, S. *Adsorption, Surface Area, And Porosity*; Academic Press: London, New York, 1982.
- (4) Tvardovski, A. J. *Colloid Interface Sci.* **2001**, *241* (2) 297– 301
- (5) Ravikovitch, P. I.; Neimark, A. V. *Adsorption* **2005**, *11* (S1) 265– 270
- (6) Dvoyashkin, M.; Valiullin, R.; Kärger, J.; Einicke, W. D.; Gläser, R. *J. Am. Chem. Soc.* **2007**, *129* (34) 10344– 10345
- (7) Kärger, J.; Pfeifer, H.; Heink, W. *Adv. Magn. Reson.* **1988**, *12*, 2– 89
- (8) Stejskal, E. O.; Tanner, J. E. *J. Chem. Phys.* **1965**, *42* (1) 288
- (9) Rodríguez-Reinoso, F.; Marsh, H. *Activated Carbon*; Elsevier: Amsterdam, Boston, 2006.
- (10) Tennison, S. R.; Kozynchenko, O. P.; Strelko, V. V.; Blackburn, A. J. *Porous carbons*. U.S. Patent 2004, /0024074 A1.
- (11) Garrido, J.; Linares-Solano, A.; Martin-Martinez, J. M.; Molina-Sabio, M.; Rodríguez-Reinoso, F.; Torregrosa, R. *Langmuir* **1987**, *3* (1) 76– 81
- (12) Rodríguez-Reinoso, F.; Garrido, J.; Martinmartinez, J.; Molinasabio, M.; Torregrosa, R. *Carbon* **1989**, *27* (1) 23– 32
- (13) Lastoskie, C.; Gubbins, K. E.; Quirke, N. *J. Phys. Chem.* **1993**, *97* (18) 4786– 4796
- (14) Barrett, E. P.; Joyner, L. G.; Halenda, P. P. *J. Am. Chem. Soc.* **1951**, *73* (1) 373– 380
- (15) Jung, C.; Kirstein, J.; Platschek, B.; Bein, T.; Budde, M.; Frank, I.; Müllen, K.; Michaelis, J.; Bräuchle, C. *J. Am. Chem. Soc.* **2008**, *130* (5) 1638– 1648
- (16) Einstein, A. *Ann. Phys. (Berlin)* **1905**, *322* (8) 549– 560

- (17) Kärger, J. *Leipzig, Einstein, Diffusion*; Leipziger University-Verlag: Leipzig, 2007.
- (18) Cotts, R.; Hoch, M.; Sun, T.; Markert, J. *J. Magn. Reson.* **1989**, *83* (2) 252–266
- (19) Galvosas, P.; Stallmach, F.; Seiffert, G.; Kärger, J.; Kaess, U.; Majer, G. *J. Magn. Reson.* **2001**, *151* (2) 260–268
- (20) Stallmach, F.; Galvosas, P. *Annu. Rep. NMR Spectrosc.* **2007**, *61*, 51–131.
- (21) Valiullin, R.; Kortunov, P.; Kärger, J.; Timoshenko, V. *J. Chem. Phys.* **2004**, *120* (24) 11804–11814
- (22) Valiullin, R.; Naumov, S.; Galvosas, P.; Kärger, J.; Woo, H. J.; Porcheron, F.; Monson, P. A. *Nature* **2006**, *443* (7114) 965–968
- (23) Valiullin, R.; Dvoyashkin, M.; Kortunov, P.; Krause, C.; Kärger, J. *J. Chem. Phys.* **2007**, *126* (5) 054705
- (24) Kärger, J.; Ruthven, D. M. *Diffusion in Zeolites and Other Microporous Solids*; Wiley: New York, 1992.
- (25) Satterfield, C. *Mass Transfer in Heterogeneous Catalysis*; R.E. Krieger Pub. Co.: Huntington, N.Y., 1981.
- (26) Ruthven, D. M.; DeSisto, W. J.; Higgins, S. *Chem. Eng. Sci.* **2009**, *64* (13) 3201–3203
- (27) Bhatia, S. K.; Nicholson, D. *AIChE J.* **2006**, *52* (1) 29–38
- (28) Krishna, R. *J. Phys. Chem. C* **2009**, *113* (46) 19756–19781
- (29) Holz, M.; Heil, S. R.; Sacco, A. *Phys. Chem. Chem. Phys.* **2000**, *2* (20) 4740–4742
- (30) Naumov, S.; Valiullin, R.; Monson, P. A.; Kärger, J. *Langmuir* **2008**, *24* (13) 6429–6432
- (31) Woo, H. J.; Monson, P. *Phys. Rev. E* **2003**, *67* (4) 041207
- (32) Neimark, A. V.; Ravikovitch, P. I.; Vishnyakov, A. *Phys. Rev. E* **2002**, *65* (3 Pt 1) 031505
- (33) Nguyen, T. X.; Bhatia, S. K. *Langmuir* **2008**, *24* (1) 146–154
- (34) Barrer, R. *Zeolites and Clay Minerals As Sorbents and Molecular Sieves*; Academic Press: London, New York, 1978.
- (35) Chmelik, C.; Bux, H.; Caro, J.; Heinke, L.; Hibbe, F.; Titze, T.; Kärger, J. *Phys. Rev. Lett.* **2010**, *104*, 8
- (36) Dvoyashkin, M.; Khokhlov, A.; Valiullin, R.; Kärger, J. *J. Chem. Phys.* **2008**, *129* (15) 154702
- (37) Kärger, J. *Adsorption* **2003**, *9*, 29–35
- (38) Ruthven, D. M. *Molecular Sieves—Science and Technology: Adsorption and Diffusion*; Springer-Verlag: Berlin, Heidelberg; 2008; Vol. 7.
- (39) Agger, J. R.; Hanif, N.; Cundy, C. S.; Wade, A. P.; Dennison, S.; Rawlinson, P. A.; Anderson, M. W. *J. Am. Chem. Soc.* **2003**, *125* (3) 830–839

- (40) Feldhoff, A.; Caro, J.; Jovic, H.; Ollivier, J.; Krause, C. B.; Galvosas, P.; Kärger, J. *ChemPhysChem* **2009**, *10* (14) 2429–2433
- (41) Jovic, H. *Molecular Sieves—Science and Technology: Adsorption and Diffusion*; Springer-Verlag: Berlin, Heidelberg; 2008; Vol. 7.
- (42) Jovic, H.; Theodorou, D. N. *Microporous Mesoporous Mater.* **2007**, *102* (1–3) 21–50
- (43) Valiullin, R.; Kärger, J.; Gläser, R. *Phys. Chem. Chem. Phys.* **2009**, *11* (16) 2833
- (44) Dvoyashkin, M.; Khokhlov, A.; Naumov, S.; Valiullin, R. *Microporous Mesoporous Mater.* **2009**, *125* (1–2) 58–62

Additional results on MA2 activated carbon

The results presented in this section were accomplished after the submission and acceptance of the publications concerning the MA2 activated carbon. They provide additional information complementary to the published results and are, for this reason, presented and discussed in this supplementary section.

Effect of temperature and loading on diffusion

This section deals with the influence of temperature and loading (Θ) on the diffusivity of both cyclohexane and toluene in activated carbon MA2. The distribution of diffusion coefficients was obtained by fitting the spin-echo attenuation to a log-normal distribution.

Fitting results

All spin echo-attenuation decays collected at different temperatures were fitted by combining Eq. 3 and 4, as referred to presented in Publications 2 and 3. The noise floor and the experimental uncertainty were considered for each decay curve independently. All considered loadings have an uncertainty of around 5%. The collected data and the respective fitting are shown in Annex 1. The spin-echo attenuation curves are nicely fitted by assuming of a log-normal distribution of the diffusivities, till around 10% of its value. However for attenuations higher than ($0\% < \psi < 10\%$) this was not always the case. This deviation from the log-normal distribution is likely to be associated with a reflective nature of the activated carbon particle surfaces and a consequent reduced surface permeability. In this case, molecules would encounter an additional restriction to diffusion, which would be reflected by a slow component the spin-echo attenuation curve. Higher loadings and

temperatures have been observed to increase the diffusivity in this system, causing molecules to travel greater distances and correspondingly increasing the probability to encounter the particle surface. This is in agreement with the experimental observations since, as shown in Annex 1, the deviations from the fit with the log-normal model occur particularly in measurements where the sample loading and the temperature were higher.

Variation of σ with loading and temperature

The standard deviation (σ) of the log-normal distribution did not significantly vary throughout the probed temperatures and loadings with values mostly in the range of 0.5 and 0.7, as shown in Figure 1 for both cyclohexane and toluene. Concerning the results obtained with cyclohexane, it should however be noted, that there is a greater dispersity than in the values observed with toluene, in particularly for low temperatures (-40°C, -20°C), where the value of σ tends to increase with increasing loadings. This tendency can be understood by considering that for loadings greater than 50% significant cyclohexane freezing is observed for temperatures lower than 0°C (see Figure 8, in Publication 2). The fitting results yield a higher value of σ at -20°C than the one obtained at -40°C, but this remains a rather uncertain result, due to the low signal-to-noise ratio (large error bars, on Figure 7, in Publication 2) on the spin-echo attenuation measured at -40°C. Within the experimental uncertainty, the data on the fully loaded sample at these low temperatures are very similar, and a similar value of sigma should also be expected. As previously discussed, the freezing in mesopores led to an additional confinement in micropores, which render shorter relaxation times and worsens the conditions of the measurement. This is not observed for toluene, since the probed temperatures are well above the freezing temperature of toluene (see Annex 2).

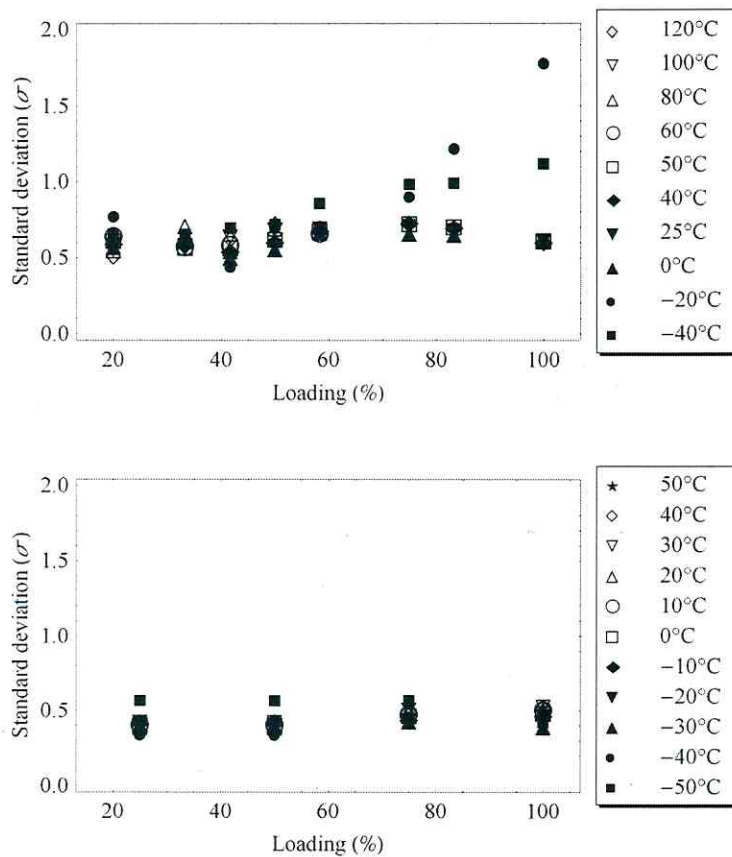


Figure 1 – Variation of the standard deviation (σ) with temperature and loading for cyclohexane (above) and toluene (below). The scale on both graphics was chosen to be the same in order to emphasize the greater dispersion of the values obtained for cyclohexane.

Variation of D_m with loading and temperature

Figure 2 shows the influence of temperature and loading on the average diffusivity (D_m), calculated by inserting the obtained parameters (D_0 , σ) in the relation $D_m = D_0 e^{\sigma^2/2}$. In the case of cyclohexane, it can be observed that the diffusivity increases with temperature and loading, reaching a maximum value between 50% and 75% loadings. Therefore, by considering the values obtained on the sample with a loading of 58% it can be concluded that this increase, compared to a loading of 20%, ranges from factors of 6 to 8, for measurements at -40°C and 50°C , respectively. For loadings greater than 58%, the diffusivity at temperatures greater than 0°C tends to decrease, with increasing loading. Below this value, no significant change with temperature on the average diffusivity is observed. Thus, the decrease with increasing loading occurs with factors of 1.3 to 1.7, at the corresponding temperatures of 25°C and 50°C . The results obtained with toluene show a similar trend as cyclohexane, but no maximum value in the diffusivities from 50% to 75% is observed. In this range, a large increase in the diffusivities of approximately a factor of 4 is observed at all probed temperatures, followed by a slight increase, from 75% to 100%. Over the whole loading range, the minimal and maximum toluene diffusivities differ by factors of 8 and 6, respectively, at the lowest (-50°C) and highest (50°C) temperatures probed.

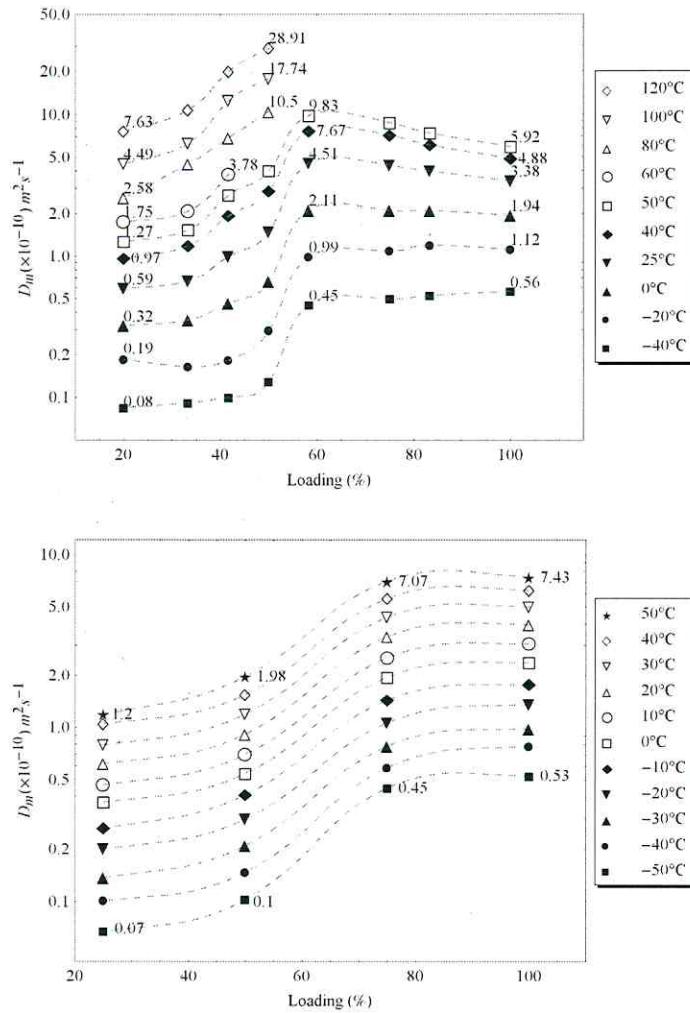


Figure 2 – Variation of the average diffusivity (D_m) with temperature and loading, as calculated from the obtained parameters with the log-normal fitting (D_0 , σ), for cyclohexane (above) and toluene (below). The lines are indicators of the experimental isothermal points.

Arrhenius Relation

If the activation enthalpy for the diffusion ($\Delta_D H$) is independent of the temperature, then its value may be estimated with the Arrhenius Relation (Equation 1):

$$D = D^0 \exp\left(-\frac{\Delta_D H}{RT}\right) \quad (1)$$

where D^0 denotes the pre-exponential factor, $\Delta_D H$ the activation enthalpy of diffusion, R the gas constant and T is the absolute temperature. Figures 3 and 4 show the best fit for cyclohexane and toluene using Equation 1, respectively. In these figures, the diffusivity D is plotted in a semi-logarithmic scale against the $1/T$, implying that a greater slope corresponds to a higher activation enthalpy ($\Delta_D H$).

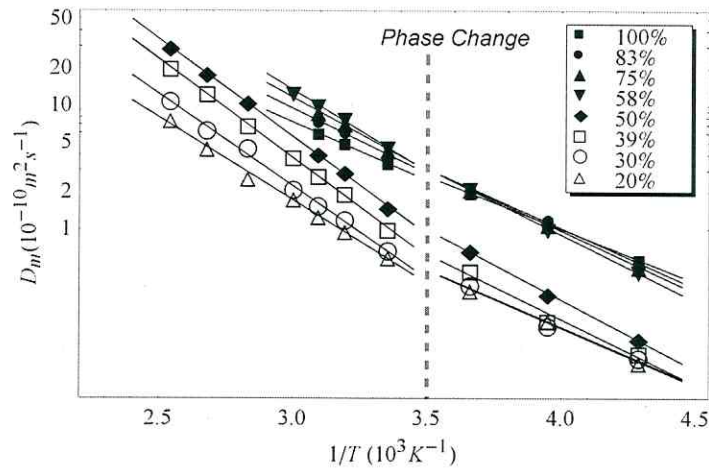


Figure 3 – Arrhenius plot for different cyclohexane loadings. The dashed line represents a rough estimate of the freezing point of liquid cyclohexane (at 6.6°C). The best fit for each data is shown represented by the full lines.

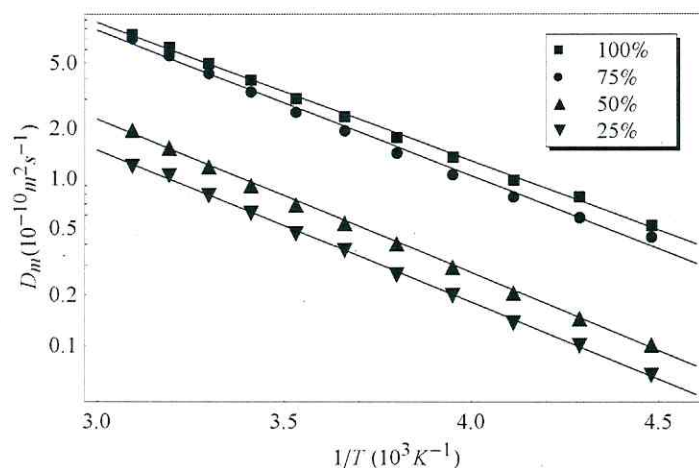


Figure 4 – Arrhenius plot for different toluene loadings. The best fit for each data is represented by the full lines.

Two temperature intervals were considered, corresponding to the temperature ranges above and below the freezing temperature of liquid cyclohexane (Figure 3). Toluene phase change is not expected at the probed temperatures and, accordingly, data shows an Arrhenius-like behavior over the whole measured temperature range (see Figure 4). The results for both cyclohexane and toluene are summarized in Figure 5, where the obtained activation enthalpies are related to the corresponding sample loadings.

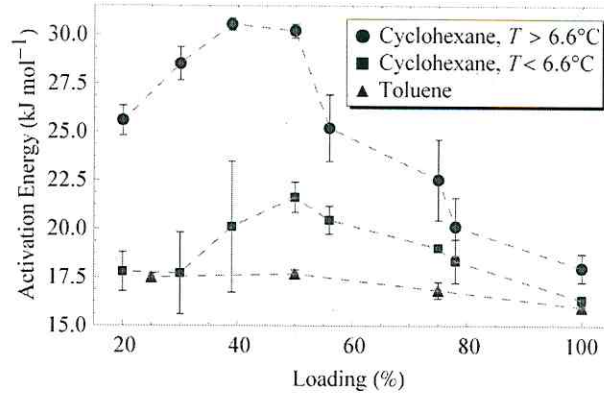


Figure 5 – Activation enthalpies of diffusion ($\Delta_D H$) for cyclohexane (for temperatures above and below 6.6°C) and toluene.

The activation enthalpies estimated for toluene remain essentially constant with increasing loadings while cyclohexane reveals a rather different tendency: for both temperature domains considered, a maximum in the activation energy is observed around 50% loading, more pronounced in the case of the measurements taken at $T > 6.6^\circ\text{C}$. At around 50% loading, mesopores are essentially filled with gaseous cyclohexane, and the measured diffusivities are given by the relation:

$$D_m = p_{gas} D_{gas} + p_{micro} D_{micro} \quad (2)$$

Therefore, the temperature dependency of measured D_m will be influenced by both processes, but in particular by gas diffusion, since micropore diffusion is known to be much slower than gas diffusivity, in the present system (as discussed Publication 4). Additionally, it is known from the literature [1] that the pressure dependency on temperature is given by:

$$p_{gas} = p_{sat} \exp \left[-\frac{\Delta_v H}{R} \left(\frac{1}{T} - \frac{1}{T_v} \right) \right] \quad (3)$$

where p_{sat} denotes the saturated vapor pressure, $\Delta_v H$ the vaporization enthalpy and T_v the boiling point. The maximum, observed at loadings of 39% and 50% (see Figure 5) corresponds to $\Delta_D H = 30.5 \text{ kJ mol}^{-1}$, which is in good agreement with the literature value of the vaporization enthalpy of cyclohexane ($\Delta_v H = 33 \text{ kJ mol}^{-1}$). Also, Equation 3 shows that $\ln(p_{\text{gas}})$ increases linearly with the temperature (T), thus revealing that the influence of gas-phase transport should be higher at higher temperatures, implying a more pronounced dominance of the factor p_{gas} in Equation 2. This corresponds to the results in Figure 5, where higher activation energies are observed in the data measured at higher temperatures ($T > 6.6^\circ\text{C}$).

With increasing loadings, the growing liquid phase will cause gas diffusivity to decrease its overall weight in the measured activation energies, and Figure 5 shows that the data sets collected at $T < 6.6^\circ\text{C}$ and $T > 6.6^\circ\text{C}$ tend to the same value of $\Delta_D H$, with increasing loading.

A slight decrease with sample loading is also observed in the toluene data, but in this case saturated vapor pressure is smaller by a factor 4 than that of cyclohexane, resulting in a much smaller effect. It should additionally be noted that at full sample saturation the values obtained for cyclohexane remain close to the result obtained for toluene, which reflects the similarity in the activation energy values for the pure liquids (see Table A, in Annexe 2).

In light of these results, it is interesting to notice, that the ratio between minimum and maximum values of D_m diffusivities is between 6 and 8 for cyclohexane, while for toluene only a factor of 4 is observed. This agrees, once again, with the validity of Eq. 2 in this system, reflecting the role of gas phase transport. A more accurate modeling of these results would in principle be possible, if the pressure inside de sample would be known. However, all measurements on this section were performed on sealed samples, and therefore a merely qualitative analysis based on the influence of the gas phase on mass transport (Equations 2 and 3) is discussed.

Summary

The contribution of mass transport occurring in gaseous phase is demonstrated in these experiments by comparing the dependency of cyclohexane and toluene diffusivity, with loading and temperature. A maximum value in the diffusivities and activation energies of cyclohexane was observed, at intermediate loadings, while this effect was not significant in the case of toluene.

Modeling the Measured Diffusivities on the Desorption Branch

In the experiments presented on this section, both cyclohexane loading (Θ) and the diffusivity (D_{eff}) were measured at different values of applied cyclohexane pressure (P/P_0). In a tentative approach, Equations 4 and 5 in Publication 4 considered the influence of external pressure on the diffusivity, showing that a linear dependency is expected, in absence of further molecular uptake, as observed in the adsorption branch (see Figure 3, a) and c), in Publication 4). However, in the referred Publication, we did not set out to model the diffusivities on the desorption branch. In this case, the sample loading changes significantly within the same time scale (10 minutes waiting time, between pressure changes) and a more elaborate model should be used, in which the transition between full saturation and onset of Knudsen diffusivity due to cyclohexane evaporation are taken into account.

The diffusivities on the desorption branch will be dominated by the effects of *i*) the decreasing liquid phase and *ii*) the decreasing external applied pressure on the gas diffusivity. A favorable combination of these effects qualitatively explains the appearance of a maximum in the measured diffusivities, observed at $P/P_0=0.74$. To account for these effects, it needs to be considered that the effective pore size for molecules in the Knudsen regime will increase until the mesopore space is depleted from liquid ($\Theta < 0.48$; $\Theta_{\text{meso}}=0$), after which, the effective pore diameter will equal the actual pore diameter (i.e., the diameter d , in Equation 5, Publication 4). Following the same

approach as in references [2,3], D_{meso} can be adapted to accommodate the influence for both liquid and gas phases in the mesopore space, thus being defined by

$$D_{\text{meso}} = p_{\text{gas}} D_{\text{gas}} + p_{\text{liq}} D_{\text{liq}} \quad (4)$$

where

$$p_{\text{gas}} = \frac{1 - \Theta_{\text{meso}}}{\Theta_{\text{meso}}} \frac{MP}{RT\rho_{\text{liq}}} \quad (5)$$

and

$$D_{\text{gas}} = D_{\text{Knudsen}} / \tau = \frac{d\sqrt{1 - \Theta_{\text{meso}}}}{3\tau} \sqrt{\frac{8RT}{\pi M}} \quad (6)$$

with the parameter $d\sqrt{1 - \Theta_{\text{meso}}}$ representing the effective diameter of a cylindrical pore. The density of the liquid phase in micro- and mesopores is assumed to be the same and therefore Θ_{meso} can be estimated from the FID by considering that $\Theta_{\text{meso}} \propto \text{FID}_{\text{meso}}$ (see Figure 3.c), in Publication 4).

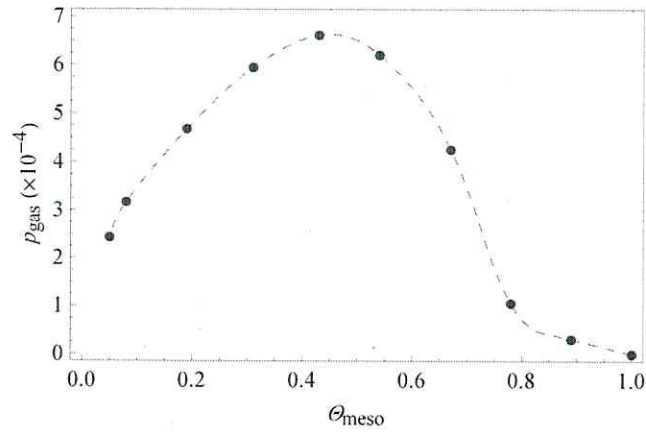


Figure 6 – Contribution of the gas phase (p_{gas}) as a function of mesopore loading, as calculated by Equation 5.

Furthermore, Equations 4 and 5 can be combined using the equality $p_{\text{liq}} = 1 - p_{\text{gas}}$, giving

$$D_{meso} = D_{liq} + \frac{1 - \Theta_{meso}}{\Theta_{meso}} \frac{MP}{RT\rho_{liq}} (D_{gas} - D_{liq}) \quad (7)$$

The distribution of the pore diameters as provided by the inset on the lower right side of Figure 2 (BJH plot) should also be taken into account since, as shown by Equation 6, $D_{gas} \propto d$. For this purpose the probability of a given pore size in the sample can be estimated by fitting the BJH result with a log-normal function of the form

$$p(d) = \frac{1}{d\sigma\sqrt{2\pi}} \exp\left[-\frac{(\ln d - \ln d_m)^2}{2\sigma^2}\right] \quad (8)$$

where d_m is the median of the pore diameters and σ the multiplicative standard deviation. The figure below shows the results of the best obtained fit with Equation 8: $d_m = (24.3 \pm 0.9)$ nm, $\sigma = 0.44 \pm 0.03$.

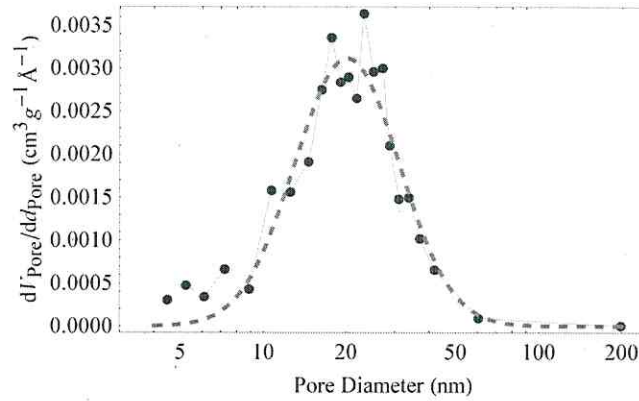


Figure 7 – Pore size distribution obtained by BJH and fit using Equation 8 (gray, dashed line).

Thus, Equation 6 may be replaced by:

$$\begin{aligned} D_{gas} &= \sum_i p(d_i) D_{Knudsen, d_i} / \tau \\ &= \sum_i p(d_i) \frac{d_i \sqrt{1 - \Theta_{meso}}}{3\tau} \sqrt{\frac{8RT}{\pi M}} \end{aligned} \quad (9)$$

with i ranging from the pore sizes obtained by the BJH distribution (from 4.5 till 200 nm). From Equation 9 is possible to plot the D_{gas} as a function of the mesopore loading:

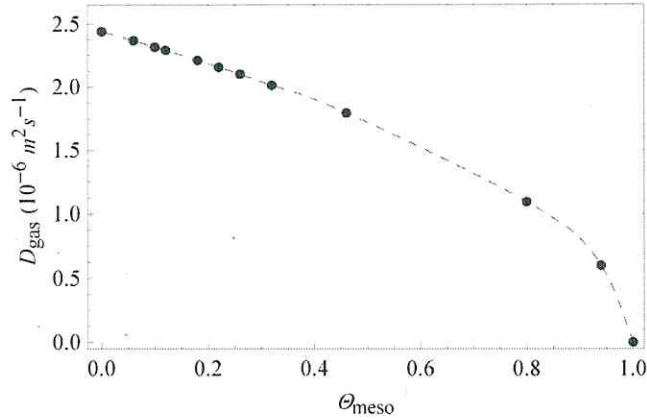


Figure 8 – Diffusivities in the gas phase, as a function of mesopore loading, as calculated from Equation 9.

Combining Equations 7 and 9 gives the diffusivity in the mesopores:

$$D_{\text{meso}} = D_{\text{liq}} + \frac{1 - \Theta_{\text{meso}}}{\Theta_{\text{meso}}} \frac{MP}{RT\rho_{\text{liq}}} \left(\sum_i p(d_i) \frac{d_i \sqrt{1 - \Theta_{\text{meso}}}}{3\tau_{\text{gas}}} \sqrt{\frac{8RT}{\pi M}} - D_{\text{liq}} \right) \quad (10)$$

Considering the micro- and mesopore contributions (Equation 6, Publication 4) and a tortuosity factor of $\tau_{\text{gas}}=1.5$, yielded the simulation of the diffusivities measured in the desorption branch (Figure 9).

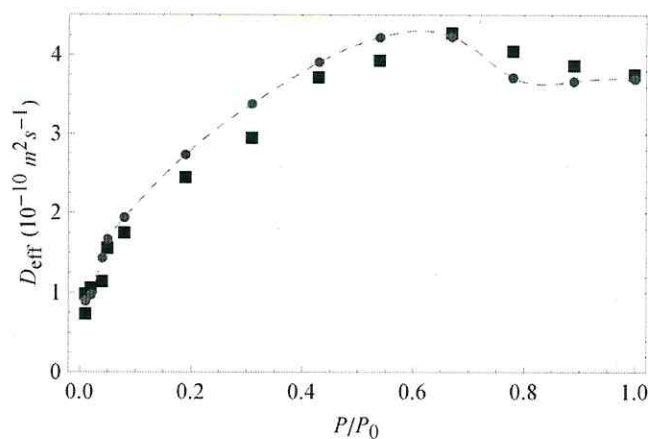


Figure 9 – Comparison between effective diffusivities: experimentally determined (black squares) and calculated from Equation 4 to 6 (Reference [2]) and considering D_{eff} as defined by Equation 10 (gray dots, dashed line).

Summary

By using literature models applied to purely mesoporous materials and considering the respective proportions of micro- and mesoporosity in activated carbon MA2, allowed a successful fit of the experimental diffusivity data in the desorption branch, presented on Publication 4. Moreover, this result yielded a value of tortuosity experienced by molecules on the gas phase ($\tau_{gas}=1.5$) which is in good agreement with the value obtained for the fully saturated system ($\tau=1.3$).

References

- [1] P. Atkins, *Atkins' Physical Chemistry*. Oxford; New York: Oxford University Press, **2002**.
- [2] Valiullin, R.; Kortunov, P.; Kärger, J.; Timoshenko, V. *J. Chem. Phys.* **2004**, *120*, 11804.
- [3] R. Valiullin, J. Kärger, and R. Gläser, *Phys. Chem. Chem. Phys.* **2009**, *11*, 16, 2833.

Publication 5: Paramagnetic relaxation enhancement (PRE) as a tool for probing diffusion in environmentally relevant porous media

Submitted for publication in *Environmental Science & Technology*

Filipe Furtado,^{†,‡} Petrik Galvosas,^{‡,§} Frank Stallmach,[‡] Ulf Roland,[†] Jörg Kärger,[‡] Frank-Dieter Kopinke[†]

[†]Department of Environmental Engineering, UFZ – Helmholtz Centre for Environmental Research, Permoserstr. 15, 04318 Leipzig, Germany

[‡]Department of Interface Physics, University of Leipzig, Linnéstr. 5, 04103 Leipzig, Germany

[§]MacDiarmid Institute for Advanced Materials and Nanotechnology, School of Chemical and Physical Sciences, Victoria University of Wellington, P.O. Box 600, Wellington 6140, New Zealand

Abstract

The transport diffusivity of the paramagnetic molecule 2,2,6,6-tetramethylpiperidine-1-oxyl (TEMPO) was measured by monitoring its influence on the NMR transverse relaxation time (T_2) on surrounding water protons - also known as Paramagnetic Relaxation Enhancement (PRE). Due to the nature of the PRE effect, few paramagnetic molecules are able to simultaneously reduce the T_2 of many NMR active nuclei, which represents a significant gain in sensitivity. In an aqueous solution, the minimal detectable TEMPO concentration was around 70 ppm. The value of the diffusivity was estimated by fitting the relaxation data, collected as a function of time, with the appropriate solutions of the second Fick's law in respect to the corresponding sample geometry and dimensions. Considering the experimentally determined TEMPO relaxivity in water ("TEMPO-water relaxivity"; $R_{\text{TEMPO}} = (1.05 \pm 0.12) \times 10^{-3} \text{ ppm}^{-1} \text{ s}^{-1}$), the obtained diffusion coefficients (D) of TEMPO in homogeneous solution and in a water saturated sand column ($D_{\text{bulk}} = (6.7 \pm 0.4) \times 10^{-10} \text{ m}^2 \text{ s}^{-1}$ and $D_{\text{pore}} = (1.4 \pm 0.5) \times 10^{-10} \text{ m}^2 \text{ s}^{-1}$, respectively) are in good agreement with the expected values (Literature values.: $D_{\text{bulk}} = 6.6 \times 10^{-10} \text{ m}^2 \text{ s}^{-1}$ and $(1.3 < D_{\text{pore}} < 2.3) \times 10^{-10} \text{ m}^2 \text{ s}^{-1}$). This new approach enables one to determine the diffusivity of paramagnetic molecules in aqueous solution and in

heterogeneous porous media with basic NMR equipment, at low concentrations and in a non-invasive manner.

Keywords: NMR-Relaxometry, Paramagnetic Relaxation Enhancement (PRE), TEMPO, T_2 Relaxation, Relaxivity, Diffusivity, Porous Media

Introduction

Mass transfer processes in porous media are of fundamental importance in describing and understanding phenomena such as pollutant bioavailability and biodegradation in soils. Likewise, they are decisive for an efficient removal of organic compounds in the context of soil remediation. Molecular diffusion (thermal Brownian movement and transport diffusion), plays a major role in these processes, but is a challenging quantity to access experimentally. In this context, nuclear magnetic resonance (NMR) spectroscopy and in particular pulsed field gradient (PFG) NMR spectroscopy are appropriate, non-invasive and nuclei selective methods which allow the assessment of the diffusivity of a particular substance in a heterogeneous sample (1-5). PFG NMR has been extensively used for investigating the self-diffusivity in a variety of systems such as polymers (6,7), zeolites (8-10) and soils (11,12). Despite the value of the information provided, there are a number of experimental difficulties in using this approach. PFG NMR has been improved to overcome difficulties in measuring slowly diffusing species (13) and the implications arising from internal magnetic field gradients (5,14-16). However, this is achieved at the cost of signal intensity loss due to enhanced relaxation time weighting. Indeed, short transverse relaxation

times (T_2) of the molecules of interest may completely hinder PFG NMR experiments. Short T_2 may result from strong adsorption or entrapment of the target compounds in the matrix (17,18) and the presence of paramagnetic species in the sample (19). Magic angle spinning (MAS) PFG NMR (20,21) has been applied for reducing the dipolar interaction between the matrix and the probe molecule thus opening the option to study samples which were difficult to measure using the conventional PFG NMR.

For studying environmental samples and transport processes especially in the context of soil pollution and remediation, the typical concentration range (often only some mg kg^{-1}) of hazardous compounds is an additional challenge when applying NMR spectroscopy. The corresponding spin densities are far below the values occurring in the NMR applications described before. However, both longitudinal (T_1) and transverse (T_2) relaxation times are strongly influenced by the presence of paramagnetic molecules, even in such low concentrations. This effect is known as Paramagnetic Relaxation Enhancement (PRE) (22,23) and has been used in different studies by deliberately introducing (24-26) or generating (27) paramagnetic species in the sample and exploiting their influence on the relaxation of the NMR-active nuclei. Contrary to conventional PFG NMR, PRE does not require a complex and expensive apparatus for data acquisition.

As an alternative to PFG NMR experiments, a new methodology based on established NMR methods is proposed in the present study which enables monitoring the transport of organic compounds in homogenous and heterogeneous media. It is applicable for low concentrations which until now were hardly accessible to NMR methods and for systems leading to relatively short relaxation times thus excluding conventional PFG NMR methods. Collecting T_2 relaxation data as a function of time and making use of PRE in combination with a suitable model for data analysis, the migration of probe molecules can be detected.

Exemplarily, the procedure is demonstrated for diffusion of TEMPO in aqueous solution. TEMPO and related compounds have been widely studied and used (28,29) in PRE studies due to their relatively high stability at room temperature (30) and their chemical versatility. In principle, a

range of physical properties of the tracer compound can be covered by appropriate derivatives of TEMPO, such that the behavior of environmentally relevant pollutants is represented. The NMR samples are prepared with a concentration gradient of the paramagnetic species. Afterwards equilibration is followed by monitoring the relaxation properties of the system, namely the relaxation of the water molecules being influenced by TEMPO in their vicinity. By considering adequate models of molecular transport the diffusivity of small amounts of TEMPO becomes experimentally accessible.

Experimental Section

Influence of porosity on relaxation

Due to the fast molecular motion in the liquid state (31,32), pure isotropic liquids usually show only one characteristic transverse relaxation time T_2 which we will denote as $T_{2,liq}$. However, liquids confined in porous media have relaxation times shorter than its corresponding bulk phase, mainly due to the influence of the surface relaxation in the pore system (33-35). The measured T_2 is given by:

$$\frac{1}{T_2} = \frac{1}{T_{2,liq}} + \frac{\rho S}{V} \quad (1)$$

where ρ is the surface relaxivity ($m\ s^{-1}$) and S/V is the surface-to-volume ratio (m^{-1}) characteristic for the pore system filled with the liquid.

Different pore sizes and geometries will have different S/V ratios and therefore, assuming the same surface relaxivity, lead to different relaxation times. Consequently, a pore size distribution will be accompanied by a relaxation time distribution (36,37). Considering that T_2 relaxation is an

exponential process with respect to the time (see Supporting Information, SI-1) it follows that for a given pore size distribution the decay of the initial magnetization (M_0) will have a multi-exponential character:

$$\frac{M(t)}{M_0} = \sum_i p_i \exp\left[-\frac{t}{T_{2,i}}\right] \quad (2)$$

where p_i denotes the fraction of spins which interacts with a given pore i having a characteristic surface-to-volume ratio. Equation 2 is equivalent to a discrete approximation of a Laplace integral, and the relaxation time distribution can, therefore, be obtained by inverse Laplace transformation (ILT) of the relaxation data (38).

NMR relaxation paramagnetic enhancement

As known from the literature (23,39-42), the presence of paramagnetic species strongly reduces both relaxation time constants T_1 and T_2 through dipole-dipole interactions. This is because the magnetic moment of an electron spin is almost three orders of magnitude larger than that of a nuclear spin. Hence, in isotropic liquids, the concentration of the paramagnetic species (e.g. TEMPO molecules) is related to T_2^{-1} of the surrounding molecules described by a constant R referred to as relaxivity in literature (23), as shown by Equation 3:

$$\frac{1}{T_{2,c}} = \frac{1}{T_{2,c_0}} + C_{TEMPO} \cdot R_{TEMPO} \quad (3)$$

where $T_{2,c(c_0)}$ is the transverse relaxation time at a given concentration (at zero concentration). Therefore, it is possible to indirectly estimate the concentration of a given paramagnetic species by

measuring T_2 of the surrounding nuclei provided that the relaxivity is known and all other parameters are kept constant. The relaxation data can then be described by replacing $T_{2,lq}$ in Equation 1 by $T_{2,c}$, in Equation 3 leading to:

$$\frac{1}{T_{2,c}} = \frac{1}{T_{2,c_0}} + \frac{\rho S}{V} + c_{TEMPO} \cdot R_{TEMPO} \quad (4)$$

Experimental Setup and Data Acquisition

Materials. TEMPO from Sigma-Aldrich was used as a paramagnetic probe molecule. Deionized water was ultrafiltered through a 0.22 μm Millipore membrane prior to use. Quartz sand (Fluka, mesh 40/150; BET surface area below 0.1 $\text{m}^2 \text{g}^{-1}$ as determined by N_2 adsorption using a Belsorp-mini device from BEL, Japan) was used after washing with deionized water. The porosity ε was estimated by the ratio of the water volume needed to saturate the interparticle volume of the sand and its total volume. A value of about 0.45 was obtained.

Samples for determining the TEMPO-water relaxivity, experiment a): A saturated stock solution (43) was prepared by dissolving 9.7 mg of TEMPO in 1 mL of deionized water in a 2 mL vial. 0.2 mL of this solution were transferred to an NMR sample tube for relaxation measurements. Dilutions of the stock solution were prepared with concentrations ranging from saturation till 0.02 ppm by diluting each individual sample, adding 0.5 mL of water to 0.5 mL of the previously prepared solution.

Sample for determining diffusion in homogenous media, experiment b): 0.1 mg of TEMPO was placed carefully on the bottom of a 1 mm inner diameter quartz tube avoiding contact with the

tube walls, then covered with 12 μL of water and subsequently sealed. A sample tube of such reduced inner diameter was chosen to prevent the onset of convection, which would interfere with the outcome of the experiments (see references 44, 45 and explanation in Supporting Information, SI-2). A scheme of the prepared sample is shown in the Supporting Information, Figure SI-1. A sample without TEMPO (B1) was prepared by analogously filling 12 μL of deionized water into an identical quartz tube.

Sample for determining diffusion in heterogeneous media, experiment c): Sand was filled in an NMR tube with an inner diameter of 5.6 mm up to a filling height of 1 cm corresponding to a sand mass of 507.5 mg. Water was then added and the sample was subsequently centrifuged (2000 RPM) for 3 min, ensuring complete water saturation of the pore space. After removing the free water phase above the sand bed, 20 μL of the TEMPO-saturated stock solution was carefully added on the top of the sand layer (see Figure SI-2 in Supporting Information). Subsequently, the sample was sealed and placed in the NMR spectrometer. A sample without TEMPO (B2) was prepared in an analogous way, namely by adding 20 μL pure water instead of a TEMPO solution.

NMR data acquisition. All measurements were performed at 298 K on the home-built 400 MHz proton frequency FT spectrometer FEGRIS (13). PRE can be observed in both T_1 and T_2 relaxation processes, as described in the Supporting Information (SI-1). However, the commonly used inversion-recovery pulse sequence for studying T_1 relaxation relies on multiple excitations (and corresponding waiting times between pulses) for data acquisition, which would necessarily correspond to long time intervals compared to the multi-echo CPMG pulse sequence (46) (one excitation), used for T_2 relaxation. For this reason, the latter relaxation mechanism (T_2) was in the focus of this study.

The data in experiment a) were collected using an echo spacing (τ) varying from 0.15 ms to 1.2 ms in order to achieve comparable attenuation of the magnetization for each sample. The data

of both time-dependent experiments, b) and c), were measured with $\tau = 0.24$ ms. In these experiments, data were collected every 12 min after sealing the samples.

Analysis of the relaxation data

Time-independent relaxation data. The data collected from Experiment a) for homogeneous solutions were fitted to a mono-exponential function. The samples B1 and B2 without TEMPO in experiments b) and c) respectively, were analyzed by a bi-exponential function and by performing ILT using the commercially available software Prospa[®] v.2.1 from Magritek Limited.

Time-dependent relaxation data. During experiments b) and c), a series of CPMG measurements was taken at different times. The TEMPO concentration at a given distance from the source will be a function of diffusion time and of TEMPO diffusivity. The acquired relaxation data of the water molecules reflect the TEMPO concentration along the sample height. Therefore, for a known TEMPO relaxivity, it is possible to model these concentration profiles as function of the diffusion coefficient. In order to be able to use known solutions of the diffusion equation for this process it is assumed that during the experimental time (i) the relaxivity of TEMPO does not change and (ii) TEMPO molecular displacement does not cover the full length of the sample for both systems under study.

Furthermore, concerning experiment b) and regarding the TEMPO crystal at the bottom of the NMR sample tube to act as a constant and infinite TEMPO source, Equation 5 represents the solution of Fick's law (47), for the corresponding initial conditions:

$$c_r = c_s \operatorname{erfc}\left(\frac{r}{2\sqrt{Dt}}\right) \quad (5)$$

c_s denotes the concentration at the source, c_r is the concentration at a distance r from the source, t is the time of diffusion and D is the TEMPO diffusion coefficient. The relaxation data can, therefore, be described by a sum of exponential decays with varying relaxation times depending on the local TEMPO concentration. The summation has to take into account the contributions of the differently relaxing water species present in the full length of the sample. The relaxation rate for a given TEMPO concentration at the source c_s , at a given distance to the source r , is obtained replacing c_{TEMPO} in Equation 3, with c_r in Equation 5, giving:

$$\frac{1}{T_{2,c}} = \frac{1}{T_{2,c_0}} + c_s \operatorname{erfc}\left(\frac{r}{2\sqrt{Dt}}\right) \cdot R_{\text{TEMPO}} \quad (6)$$

Integration over the whole length (r) of the sample yields for the magnetization decay due to T_2 relaxation:

$$\frac{M(t_{\text{CPMG}})}{M_0} = \int_0^r \exp\left[-t_{\text{CPMG}} \cdot \left(\frac{1}{T_{2,c_0}} + c_s \operatorname{erfc}\left(\frac{r}{2\sqrt{Dt}}\right) \cdot R_{\text{TEMPO}}\right)\right] dr \quad (7)$$

In this study, Equation 7 was the starting equation used to fit the measured relaxation data, having D as a fitted parameter.

For the experiment c), where a droplet of saturated TEMPO solution was added on top of a water-saturated sand sample, the solution of Fick's law is (47)

$$c(h,r) = \frac{c_s}{2} \left[\operatorname{erf}\left(\frac{h+r}{2\sqrt{Dt}}\right) + \operatorname{erf}\left(\frac{h-r}{2\sqrt{Dt}}\right) \right] \quad (8)$$

where, in addition to the already defined parameters, h is the thickness of the TEMPO-saturated water layer (see Figure SI-2 in Supporting Information). It is important to note that Equation 8 takes into account the decrease in concentration at the source because the limited amount of TEMPO initially present in the range of length h is distributed over the sample. In contrast, in experiment b) the mass of the TEMPO crystal is rather irrelevant, as long as it is not dissolved completely, which is the case during the considered experimental time.

Similarly to the Equation 6, the relaxation rate in the sand sample for a given initial TEMPO concentration c_s , at a given distance r to the source, is obtained by replacing c_{TEMPO} in Equation 3, with Equation 8

$$\frac{1}{T_{2,c}^i} = \frac{1}{T_{2,c_0}^i} + \frac{c_s}{2} \left[\operatorname{erf} \left(\frac{h+r}{2\sqrt{Dt}} \right) + \operatorname{erf} \left(\frac{h-r}{2\sqrt{Dt}} \right) \right] R_{TEMPO} \quad (9)$$

where i indicates the corresponding phase, contained in the region 0 to h (homogeneous bulk phase, $i = \text{bulk}$) or in the region h to r (heterogeneous sand phase, $i = \text{sand}$). As already mentioned, the values of T_{2,c_0}^i are different, and need to be determined experimentally (see Results and Discussion section).

Combining this result with the general relaxation equation (see Supporting Information SI-1) and integrating over the respective lengths r and h lead to:

$$\frac{M(t_{CPMG})}{M_0} = \int_0^h \exp \left[-\frac{t_{CPMG}}{T_{2,c}^{bulk}} \right] dh + \int_0^r \exp \left[-\frac{t_{CPMG}}{T_{2,c}^{sand}} \right] dr \quad (10)$$

Replacing T_{2,c_0}^{bulk} and T_{2,c_0}^{sand} from Equation 9 gives the result:

$$\frac{M(t_{CPMG})}{M_0} = \int_0^h \exp \left[-t_{CPMG} \cdot \left(\frac{1}{T_{2,e_0}^{bulk}} + \left[\frac{c_s}{2} \left[\operatorname{erf} \left(\frac{h+r}{2\sqrt{Dt}} \right) + \operatorname{erf} \left(\frac{h-r}{2\sqrt{Dt}} \right) \right] \right] \cdot R_{TEMPO} \right) \right] dh + \int_h^r \exp \left[-t_{CPMG} \cdot \left(\frac{1}{T_{2,e_0}^{sand}} + \left[\frac{c_s}{2} \left[\operatorname{erf} \left(\frac{h+r}{2\sqrt{Dt}} \right) + \operatorname{erf} \left(\frac{h-r}{2\sqrt{Dt}} \right) \right] \right] \cdot R_{TEMPO} \right) \right] dr \quad (11)$$

which is the general equation used to fit the experimental data from experiment c).

Results and Discussion

Influence of the TEMPO concentration on relaxation of bulk water, experiment a)

These data sets invariably reveal a mono-exponential behavior (see Supporting Information, Figure SI-3). This leads to the conclusion that on the time scale of these measurements and independently of the concentration, the TEMPO molecules are homogeneously distributed in the sample, leading to a uniform T_2 reduction of all water molecules. In Figure 1, the transverse relaxation time T_2 obtained by a mono-exponential fit is plotted as a function of TEMPO concentration. It can be seen that the minimal detectable concentration is approximately 70 ppm, corresponding to an average distance between TEMPO molecules of about 15 nm.

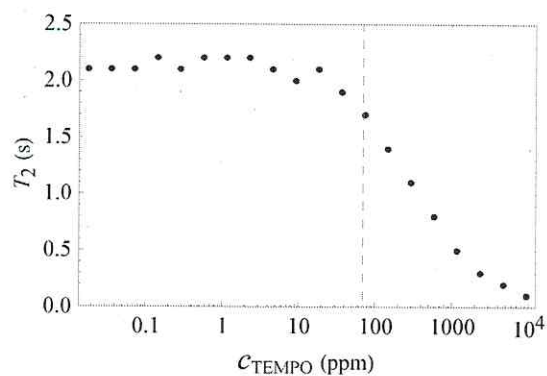


Figure 1 – Transverse relaxation time (T_2) of water in dependence on the TEMPO concentration. The detection limit for the relaxation effect of TEMPO is indicated by the gray dashed line.

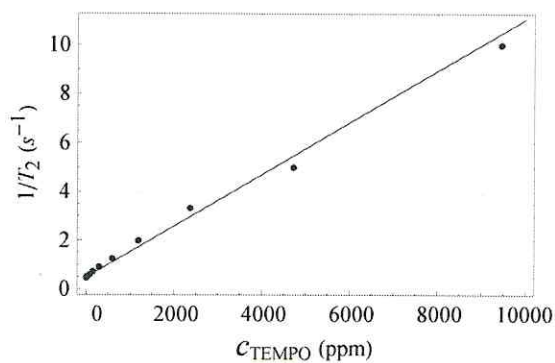


Figure 2 – Transverse relaxation rate ($1/T_2$) of water in dependence on the TEMPO concentration.

The inverse of the measured T_2 as a function of concentration (Figure 2) yields a linear dependence in which the slope corresponds to the TEMPO relaxivity and the ordinate to the relaxation rate ($1/T_2$) of the bulk liquid, as described by Equation 3. The obtained values are $R_{\text{TEMPO}} = (1.05 \pm 0.12) \times 10^{-3} \text{ ppm}^{-1} \text{ s}^{-1}$ and $T_{2,\text{H}_2\text{O}} = (2.11 \pm 0.01) \text{ s}$.

Determination of TEMPO bulk diffusivity, experiment b)

First, the accurate value of T_{2,c_0} in this system was determined by measuring the blank sample (B1). The data deviate slightly from a mono-exponential decay, which reflects a significant S/V ratio of the 1 mm tube (see Supporting Information SI-4). The calculated parameters from a bi-exponential fit are $p_a = 0.838 \pm 10^{-3}$, $p_b = 0.162 \pm 10^{-3}$, $T_{2,c_0}^a = (1.562 \pm 2 \times 10^{-3}) \text{ s}$, $T_{2,c_0}^b = (0.219 \pm 10^{-3}) \text{ s}$. Therefore, the previously presented solution of the diffusion equation in this system (Equation 5) has to be combined with a distribution of T_2 at $c_{\text{TEMPO}} = 0$ (Equation 2) and integrated over the whole sample length which gives

$$\frac{M(t_{\text{CPMG}})}{M_0} = \int_0^r \sum_i p_i \exp \left[-t_{\text{CPMG}} \cdot \left(\frac{1}{T_{2,c_0}^i} + c_0 \operatorname{erfc} \left(\frac{r}{2\sqrt{Dt}} \right) \cdot R_{\text{TEMPO}} \right) \right] dr \quad (12)$$

with i representing, in this case, the indexes a and b , from the bi-exponential fit. The semi-logarithmic plots of the time dependent relaxation data (Experiment b) and the result of the fit using Equation 12 using the T_2 values from the blank sample are shown in Figure 3.

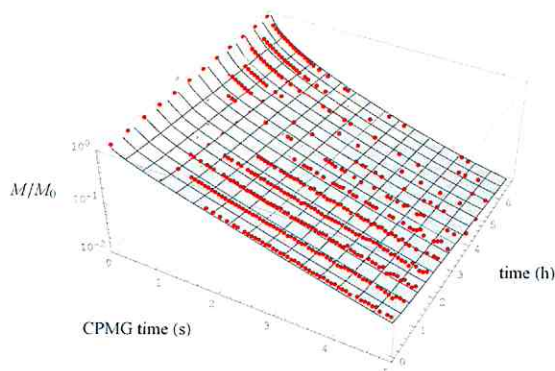


Figure 3 – Measured CPMG data of experiment b) as a function of diffusion time (●) and fitted data according to Eq. 12 (semi-transparent surface \times).

It is observed that for longer periods after starting the diffusion experiments the CPMG data deviate from a mono-exponential (linear) character towards a multi-exponential (non-linear) one. This fact is attributed to the continuous dissolution of the TEMPO crystal, which increases the dissolved concentration close to the source ($r = 0$), and spreading over the whole cross section of the tube. Using the length coordinate along the tube axis, the estimated parameters from the blank sample (ρ_a , ρ_b , T_{2,c_0}^a , T_{2,c_0}^b), the TEMPO concentration at saturation of the water phase and the previously estimated value for TEMPO-water relaxivity allows to fit the experimental data by the equations above, having the diffusion coefficient D as a fitted parameter. The result of the fit is represented by the semi-transparent surface from which a value for the diffusion coefficient of $D = (6.7 \pm 0.4) \times 10^{-10} \text{ m}^2 \text{ s}^{-1}$ is obtained. It is in good agreement with the value $D = 6.6 \times 10^{-10} \text{ m}^2 \text{ s}^{-1}$ obtained by Ciszowska et al. (48).

Using the determined diffusion coefficient and the diffusion equations, the concentration profiles being established throughout the sample in the course of the experiment can be calculated. The concentrations as a function of distance from the source (as shown in Supporting Information, Figure SI-6) reveal that the concentration at the largest distance from the source (at the end of the

tube) is still negligible for the longest observation times of the experiment, i.e. after 7 h. This result is a confirmation of assumption (ii) and thus validates the used model (Equation 5).

Determination of TEMPO diffusivity through a sand bed, experiment c)

Determination of the influence of the sand on water relaxation. The accurate distribution of T_{2,c_0}^i values was again determined by measuring the corresponding sample without TEMPO (B2). Figure 4 shows the T_2 distribution obtained from fitting the CPMG data (see Supporting Information SI-5) by ILT.

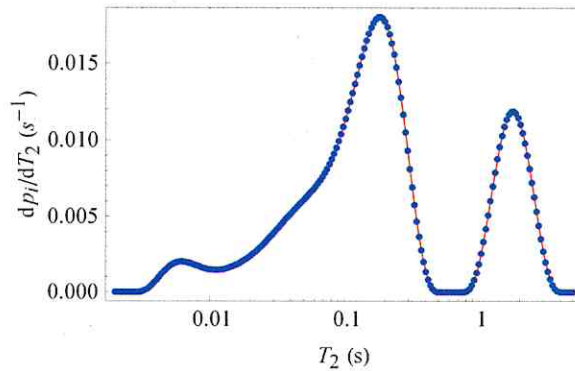


Figure 4 – Transverse relaxation time (T_2) distribution of water in a sand bed (sample B2) obtained by ILT of the relaxation data.

In Figure 4, the peak centered at $T_2 = 1.8$ s can be attributed to the bulk water layer ($i = \text{bulk}$) over the sand column, whereas the broad peak at $T_2 < 0.6$ s corresponds to the water phase between the sand grains ($i = \text{pore}$). Equation 10 was derived considering that the phases i have only one discrete value of T_2 (pore or bulk). However, Figure 4 indicates that we have to take into

account a relaxation time distribution for each given concentration of TEMPO instead. Thus, we have to generalize Equation 10 and account for T_2 distributions (based on the discrete values obtained from ILT leading to the sum terms):

$$\frac{M(t_{CPMG}, r)}{M_0} = \int_0^h \sum_j p_j \exp\left[-\frac{t_{CPMG}}{T_{2,c}^{bulk,j}}\right] dh + \int_0^r \sum_k p_k \exp\left[-\frac{t_{CPMG}}{T_{2,c}^{pore,k}}\right] dr \quad (13)$$

where j and k represent the T_2 distribution in the bulk and in the pore water phase, respectively. Replacing $T_{2,c}^{bulk,j}$ and $T_{2,c}^{pore,k}$ from Equation 13 we obtain:

$$\begin{aligned} \frac{M(t_{CPMG})}{M_0} = & \int_0^h \sum_j p_j \exp\left[-t_{CPMG} \left(\frac{1}{T_{2,c_0}^{bulk,j}} + \left[\frac{c_0}{2} \left[\operatorname{erf}\left(\frac{h+r}{2\sqrt{Dt}}\right) + \operatorname{erf}\left(\frac{h-r}{2\sqrt{Dt}}\right) \right] \right] R_{TEMPO} \right)\right] dh + \\ & \int_0^r \sum_k p_k \exp\left[-t_{CPMG} \left(\frac{1}{T_{2,c_0}^{pore,k}} + \left[\frac{c_0}{2} \left[\operatorname{erf}\left(\frac{h+r}{2\sqrt{Dt}}\right) + \operatorname{erf}\left(\frac{h-r}{2\sqrt{Dt}}\right) \right] \right] R_{TEMPO} \right)\right] dr \end{aligned} \quad (14)$$

from which the diffusivity D can be extracted. The obtained value of the TEMPO diffusion coefficient in the pore space is $D = (1.4 \pm 0.5) \times 10^{-10} \text{ m}^2 \text{ s}^{-1}$. The semi-logarithmic plots of the experimental data and the fit are shown in Figure 5.

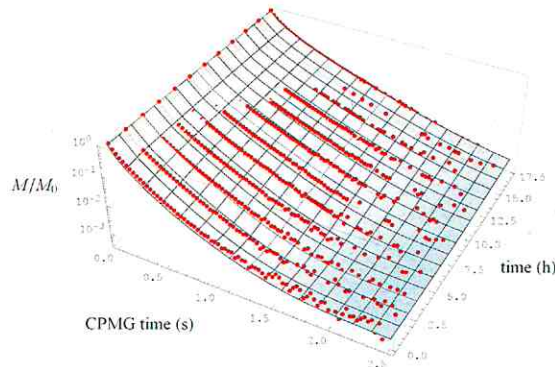


Figure 5 – Measured CPMG data of experiment c) (●) and fitted data according to Eq. 14 (semi-transparent surface \times).

From the diffusion coefficient and Equation 8, again the concentration profiles in the sample can be estimated. As it can be seen in Figure 6, at time zero (grey dashed line) all TEMPO molecules are contained at the top of the sand layer, in the region between 0 and h (integration range i). At longer diffusion times, molecules migrate from the bulk phase into the pore space of the sand bed, lowering the concentration in the bulk phase and increasing it in the pore water. The fact that the concentration remains approximately 0 close to the maximum depth of the sand layer at all experimental times confirms assumption (ii) and thus validates the used model (Equation 8).

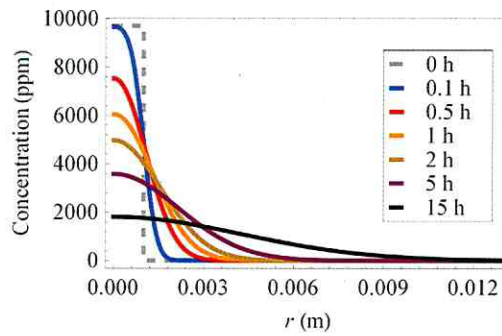


Figure 6 – Calculated TEMPO concentrations from NMR measurements at different distances from the source for diffusion times between 0.1 and 15 hours after sample preparation.

The resulting value for the diffusion coefficient can be related to the porosity of the system (ε) (48) through the empirical Archie relation with the empirical constant m following the relation

$$\frac{D_{TEMPO,pore}}{D_{TEMPO,bulk}} = \varepsilon^m \quad (15)$$

This calculation yields $m = 1.9$, which is in the range of literature data for unconsolidated sand, from 1.3 to 2.0, as reviewed by Grathwohl et al. (49,50).

Our study presents self-contained sets of data, which can be fitted and interpreted by the introduced models. The low specific surface area of the quartz sand used justifies neglecting the adsorption of TEMPO on the sand surface on data fitting and in the relaxivity determination. In other cases, where the porous matrices under study have a high specific surface area or a higher affinity for the used probe molecule, different models may need to be used, taking into account the adsorption in the pores (49,50). Adsorption may not only cause an additional barrier for transport, hence reducing the observed effective diffusion coefficient, and a deviation from the idealized system where only one diffusion process occurs, but can as well have an effect on the relaxivity of the water molecules (29,51). It is known that the immobilization of paramagnetic molecules on the surface of the solid matrix may change the surface relaxivity of the matrix itself (52).

The presented methodology allows the estimation of the diffusion of a given probe molecule in a heterogeneous porous medium. Relying on the strong effect of the diffusive species present in low concentrations on the bulk phase spin relaxation, in this case that of water protons, and using a relatively simple CPMG pulse sequence for relaxation measurement, opens a new opportunity to study transport processes under environmentally relevant conditions. The proposed method is non-invasive. Data analysis and fitting is achieved using the appropriate solutions for the diffusion equations to estimate concentration profiles and the resulting influence on the relaxation rate of the surrounding water molecules.

The method was demonstrated to be successfully applicable for TEMPO as paramagnetic relaxation enhancer in two model systems (point source in a homogeneous water phase and sand column with TEMPO-containing phase at the boundary). This method can be applied to a variety of paramagnetic compounds with varying properties such as polarity, size, chemical nature, sorption affinity, water solubility etc. and being present in low concentrations. Thus, specific information on transport of a variety of chemicals in complex matrices can be obtained, which is of great relevance in the prognosis of the fate of chemical compounds in the environment.

Acknowledgments

Financial support by the Marie Curie-Early Stage Training project RAISEBIO (Risk Assessment and Environmental Safety Affected by Compound Bioavailability in Multiphase Environments) and by the Deutsche Forschungsgemeinschaft (International Research Training Group "Diffusion in Porous Materials") is gratefully acknowledged.

Supporting Information Available

on the basic theory of NMR relaxation, experimental conditions as well as with figures showing relaxation data and a sketch of the prepared samples.

Literature Cited

- (1) Stejskal, E. O.; Tanner, J. E. Spin diffusion measurements: spin echoes in the presence of a time-dependent field gradient. *J. Chem. Phys.* **1965**, *42*, 288.
- (2) Callaghan, P. *Principles of nuclear magnetic resonance microscopy*; Clarendon Press: Oxford, 1993.
- (3) Stallmach, F.; Kärger, J. The potentials of Pulsed Field Gradient NMR for investigation of porous media. *Adsorption* **1999**, *5*, 117-133.
- (4) Stallmach, F.; Galvosas, P. Spin echo NMR diffusion studies. **2007**, *61*, 51-131.
- (5) Price, W. S. *NMR Studies of Translational Motion*; Cambridge University Press: Cambridge, 2009.
- (6) Walderhaug, H. PFG NMR Study of polymer and solubilizate dynamics in aqueous isotropic mesophases of some poloxamers. *J. Phys. Chem. B* **1999**, *103*, 3352-3357.
- (7) Matsukawa, S.; Ando, I. A study of self-diffusion of molecules in polymer gel by Pulsed-Gradient Spin-Echo ^1H NMR. *Macromolecules* **1996**, *29*, 7136-7140.
- (8) Gupta, V. Evidence for single file diffusion of ethane in the molecular sieve $\text{AlPO}_4\text{-5}$. *Chem. Phys. Lett.* **1995**, *247*, 596-600.
- (9) Kärger, J. Diffusion measurement by NMR techniques. In *Adsorption and Diffusion*. Springer Berlin Heidelberg: Berlin, Heidelberg, **2008**, *7*, 85-133.

- (10) Menjoge, A.; Bradley, S. A.; Galloway, D. B.; Low, J. J.; Prabhakar, S.; Vasenkov, S. Observation of intraparticle transport barriers in FAU/EMT intergrowth by pulsed field gradient NMR. *Micropor. Mesopor. Mat.* **2010**, *135*, 30-36.
- (11) Schaumann, G. E.; LeBoeuf, E. J. Glass transitions in peat: their relevance and the impact of water. *Environ. Sci. Technol.* **2005**, *39*, 800-806.
- (12) Simpson, A. J. Determining the molecular weight, aggregation, structures and interactions of natural organic matter using diffusion ordered spectroscopy. *Magn. Reson. Chem.* **2002**, *40*, S72-S82.
- (13) Galvosas, P.; Stallmach, F.; Seiffert, G.; Kärger, J.; Kaess, U.; Majer, G. Generation and application of ultra-high-intensity magnetic Field Gradient Pulses for NMR spectroscopy. *J. Magn. Reson.* **2001**, *151*, 260-268.
- (14) Cotts, R.; Hoch, M.; Sun, T.; Markert, J. Pulsed field gradient stimulated echo methods for improved NMR diffusion measurements in heterogeneous systems. *J. Magn. Reson.* **1989**, *83*, 252-266.
- (15) Gibbs, S. J.; Johnson, C. S. A PFG NMR experiment for accurate diffusion and flow studies in the presence of eddy currents. *J. Magn. Reson.* **1991**, *93*, 395-402.
- (16) Galvosas, P.; Stallmach, F.; Kärger, J. Background gradient suppression in stimulated echo NMR diffusion studies using magic pulsed field gradient ratios. *J. Magn. Reson.* **2004**, *166*, 164-173.
- (17) Daughney, C. J.; Bryar, T. R.; Knight, R. J. Detecting sorbed hydrocarbons in a porous medium using proton Nuclear Magnetic Resonance. *Environ. Sci. Technol.* **2000**, *34*, 332-337.
- (18) Simpson, M. J.; Simpson, A. J.; Hatcher, P. G. Noncovalent interactions between aromatic compounds and dissolved humic acid examined by nuclear magnetic resonance spectroscopy. *Environ. Toxicol. Chem.* **2004**, *23*, 355.
- (19) Kleinberg, R. L. Pore size distributions, pore coupling, and transverse relaxation spectra of porous rocks. *Magn. Reson. Imaging* **1994**, *12*, 271-274.
- (20) Fomba, K. W.; Galvosas, P.; Roland, U.; Kärger, J.; Kopinke, F.-D. New option for characterizing the mobility of organic compounds in humic acids. *Environ. Sci. Technol.* **2009**, *43*, 8264-8269.
- (21) Gratz, M.; Hertel, S.; Wehring, M.; Stallmach, F. and Galvosas, P. Mixture diffusion of adsorbed organic compounds in Metal-Organic Frameworks as studied by MAS PFG NMR. *New Journal of Physics*, **2011**, accepted for vol. 13.

- (22) Clore, G. M.; Iwahara, J. Theory, Practice, and applications of paramagnetic relaxation enhancement for the characterization of transient low-population states of biological macromolecules and their complexes. *Chem. Rev.* **2009**, *109*, 4108-4139.
- (23) Helm, L. Relaxivity in paramagnetic systems: Theory and mechanisms. *Prog. Nucl. Magn. Reson. Spectrosc.* **2006**, *49*, 45-64.
- (24) Weckhuysen, B. Chemical imaging of spatial heterogeneities in catalytic solids at different length and time scales. *Angew. Chem. Int. Edit.* **2009**, *48*, 4910-4943.
- (25) Deczky, K.; Langford, C. H. Application of water nuclear magnetic resonance relaxation times to study of metal complexes of the soluble soil organic fraction fulvic acid. *Can. J. Chemistry* **1978**, *56*, 1945-1951.
- (26) Melton, J.; Kantzas, A.; Langford, C. Nuclear magnetic resonance relaxometry as a spectroscopic probe of the coordination sphere of a paramagnetic metal bound to a humic acid mixture. *Anal. Chim. Acta* **2007**.
- (27) Mitreiter, I.; Oswald, S. E.; Stallmach, F. Investigation of iron(III)-release in the pore water of natural sands by NMR relaxometry. *Open Magn. Reson. J.* **2010**, *3*, 46-51.
- (28) Vallet, P.; van Haverbeke, Y.; Bonnet, P. A.; Subra, G.; Chapat, J. P.; Muller, R. N. Relaxivity enhancement of low molecular weight nitroxide stable free radicals: Importance of structure and medium. *Magn. Reson. Med.* **1994**, *32*, 11-15.
- (29) Bennett, H. F.; Brown, R. D.; Koenig, S. H.; Swartz, H. M. Effects of nitroxides on the magnetic field and temperature dependence of $1/T_1$ of solvent water protons. *Magn. Reson. Med.* **1987**, *4*, 93-111.
- (30) Ciriano, M. V.; Korth, H. G.; van Scheppingen, W. B.; Mulder, P. Thermal stability of 2,2,6,6-tetramethylpiperidine-1-oxyl (TEMPO) and related *N*-alkoxyamines. *J. Am. Chem. Soc.* **1999**, *121*, 6375-6381.
- (31) Bergman, D. J.; Dunn, K. J. NMR of diffusing atoms in a periodic porous medium in the presence of a nonuniform magnetic field. *Phys. Rev. E* **1995**, *52*, 6516.
- (32) Levitt, M. *Spin dynamics: basics of nuclear magnetic resonance*; John Wiley & Sons: Chichester; New York, 2001.
- (33) Brownstein, K.; Tarr, C. Importance of classical diffusion in NMR studies of water in biological cells. *Phys. Rev. A* **1979**, *19*, 2446-2453.
- (34) Dunn, K. J.; Bergman, D. J.; Latorraca, G. A. *Nuclear magnetic resonance*; Pergamon: Amsterdam, London, 2002.
- (35) Vogt, C.; Galvosas, P.; Klitzsch, N.; Stallmach, F. Self-diffusion studies of pore fluids in unconsolidated sediments by PFG NMR. *J. Appl. Geophys.* **2002**, *50*, 455-467.

- (36) Latour, L. Pore-Size Distributions and Tortuosity in Heterogeneous Porous Media. *J. Magn. Reson., Series A* **1995**, *112*, 83-91.
- (37) Jaeger, F.; Bowe, S.; Van As, H.; Schaumann, G. E. Evaluation of ^1H NMR relaxometry for the assessment of pore-size distribution in soil samples. *Eur. J. Soil Sci.* **2009**, *60*, 1052-1064.
- (38) Venkataramanan, L.; Song, Y.Q.; Hurlimann, M. D. Solving Fredholm integrals of the first kind with tensor product structure in 2 and 2.5 dimensions. *IEEE Trans. Signal Process.* **2002**, *50*, 1017-1026.
- (39) Bakhmutov, V. *Practical NMR relaxation for chemists*; Wiley: Chichester West Sussex England; Hoboken NJ, 2004.
- (40) Banci, L. *Nuclear and electron relaxation: the magnetic nucleus-unpaired electron coupling in solution*. VCH: Weinheim, New York, 1991.
- (41) Bertini, I. *Solution NMR of paramagnetic molecules: applications to metalloproteins and models*. Elsevier Science Ltd.: Amsterdam; New York, 2001.
- (42) Yazyev, O. V.; Helm, L. Nuclear Spin relaxation parameters of MRI contrast agents - insight from quantum mechanical calculations. *Eur. J. Inorg. Chem.* **2008**, *2008*, 201-211.
- (43) Merck Chemicals. 2,2,6,6-Tetramethylpiperidinyloxy security data sheet. Merck Chemicals, **2008**.
- (44) Hedin, N. Temperature imaging by ^1H NMR and suppression of convection in NMR probes. *J. Magn. Reson.* **1998**, *131*, 126-130.
- (45) Goux, W. The impact of Rayleigh-Benard convection on NMR pulsed-field-gradient diffusion measurements. *J. Magn. Reson.* **1990**, *88*, 609-614.
- (46) Meiboom, S.; Gill, D. Modified spin-echo method for measuring nuclear relaxation times. *Rev. Sci. Instrum.* **1958**, *29*, 688.
- (47) Crank, J. *The mathematics of diffusion*; Clarendon Press: Oxford [Eng], 1979.
- (48) Zhang, W.; Ma, C.; Ciszowska, M. Mass transport in thermoresponsive poly(*N*-isopropylacrylamide-co-acrylic acid) hydrogels studied by electroanalytical techniques: swollen gels. *J. Phys. Chem. B* **2001**, *105*, 3435-3440.
- (49) Förstner, U.; Grathwohl, P. *Ingenieurgeochemie*; Springer Berlin Heidelberg: 2007.
- (50) Boving, T. Tracer diffusion coefficients in sedimentary rocks: correlation to porosity and hydraulic conductivity. *J. Contam. Hydrol.* **2001**, *53*, 85-100.
- (51) Gussoni, M.; Greco, F.; Ferruti, P.; Ranucci, E.; Ponti, A.; Zetta, L. Poly(amidoamine)s carrying TEMPO residues for NMR imaging applications. *New J. Chem.* **2008**, *32*, 323.

(52) Bryar, T. Paramagnetic effects of Iron(III) species on nuclear magnetic relaxation of fluid protons in porous media. *J. Magn. Reson.* **2000**, *142*, 74-85.

Supporting Information

SI-1: NMR relaxation

Generally speaking, relaxation is the return from an excited state to a thermodynamically more favorable equilibrium state. In NMR, after spin ensembles are magnetized by radio-frequency pulses, they can subsequently lose their magnetization by two distinct processes: by exchanging energy with the lattice (an enthalpy-related process) and by losing the phase they attained from the received pulse (a rather entropic process). Both these processes are of exponential nature with respect to the time following the excitation (see Equations 1 and 2). They are referred to as longitudinal or spin-lattice relaxation, characterized by a T_1 time constant and transverse or spin-spin relaxation, characterized by a T_2 time constant:

$$\frac{M(t)}{M_0} = 1 - 2 \exp\left[-\frac{t}{T_1}\right] \quad (1)$$

$$\frac{M(t)}{M_0} = \exp\left[-\frac{t}{T_2}\right] \quad (2)$$

The existence of a spin phase is dependent on whether the system is in an excited state thus implying that T_2 will always be equal or shorter than T_1 . In liquids, the experimental values for these constants are frequently the same, because there are no internal magnetic gradients in the homogenous sample. In porous media, this might not be the case. Due to the differences in magnetic susceptibility between liquid and the solid material, internal gradients may be present in

the sample. Consequently, if the echo time in the CPMG pulse sequence is not sufficiently short to cancel out the influence of molecular diffusion between these two phases, additional spin dephasing may occur (1), making the measurable T_2 significantly shorter than T_1 . Such effect is proportional to the external magnetic field (1). Since the diffusivity only affects spin coherence and therefore T_2 , it will deviate more from T_1 also at higher fields.

The presence of paramagnetic species strongly reduces both relaxation time constants T_1 and T_2 through dipole-dipole interactions. The effectiveness of this mechanism depends on the interaction between the nuclear and the electronic spins, μ_1 and μ_2 , namely the angle γ and the distance d between them according to (2):

$$E^{dip} = -\frac{\mu_0}{4\pi} \frac{\mu_1 \mu_2}{d^3} (3 \cos^2 \gamma - 1) \quad (3)$$

In the present system, the interactions between electronic and the nuclear spins, (i.e. between TEMPO and the water protons) depend on the random encounters of these in the sample space, which is known to be a diffusion-controlled process (3). In this case, the transverse relaxation rate is said to be dominated by the so called "Outer-Sphere" relaxivity mechanism (2,3,4):

$$\frac{1}{T_2} = c_{TEMPO} \frac{16}{405} \frac{\pi N_A}{1000} \left(\frac{\mu_0}{4\pi} \right)^2 \frac{\gamma_I^2 g_e^2 \mu_B^2 S(S+1)}{d_{\min}^3 (D_M + D_L)} \times \{4J(0) + 13J(\omega_S) + 3J(\omega_I)\} \quad (4)$$

where the spectral density functions are given by

$$J(\omega) = \frac{1 + \frac{5z}{8} + \frac{z^2}{8}}{1 + z + \frac{z^2}{2} + \frac{z^3}{6} + \frac{4z^4}{81} + \frac{z^5}{81} + \frac{z^6}{648}} \quad (5)$$

with

$$z = (2\omega\tau_D)^{1/2} \quad (6)$$

In these results N_A is the Avogadro Number, d_{\min} is the so-called “distance of closest approach”, D_{TEMPO} and D_{water} are the diffusion coefficients for TEMPO and water, respectively, μ_0 is the permeability of the free space, γ_1 is the proton gyromagnetic ratio, g_e is the electron g factor, μ_B is the electron Bohr magneton, S is the electron spin quantum number, ω_1 and ω_S are the angular frequency of the proton and electron, respectively, and τ_D is the diffusional correlation time, which is defined as:

$$\tau_D = \frac{d_{\min}}{D_{\text{TEMPO}} + D_{\text{water}}} \quad (7)$$

where D_{TEMPO} and D_{water} stand for the TEMPO and water diffusivities, respectively. It should be noted, that Equation 4 shows a direct dependency on the enhancement of the relaxation rate with increasing concentration, also reflected in Equation 3, in the article text.

SI-2: Experimental Considerations

Sample preparation

The transport diffusion neutralizing an initially present concentration gradient in a liquid is described by first Fick's law (5). However, in many such systems convection may also take place, if the phases have different densities due to the differences in concentration or if temperature gradients exist in the sample. For experimental estimation of diffusion, it becomes, therefore, crucial to minimize the factors which influence the onset of convection. For a pure liquid in a cylindrical

container in which its length is much larger than its radius, convection is predicted to occur when the Rayleigh number Ra_{tube} , as given by Equation 8, exceeds a critical value Ra_c (6,7)

$$Ra_{tube} = \frac{g\alpha}{\kappa\nu} r_{tube}^4 \nabla T \quad (8)$$

The parameters α , ν , and κ are the coefficients of thermal expansion, kinematic viscosity, and thermal diffusivity of the fluid, respectively and are characteristic properties of the liquid, implying that the geometry of the sample (radius of the tube r_{tube}) and the temperature gradient ∇T have to be adequately adjusted in order to minimize convection. Since $Ra_{tube} \propto r_{tube}^4$ holds, reducing the inner diameter of the tube is of great importance. For this reason, a quartz tube with 1 mm inner diameter was used in experiment b) which involves the dissolution of a crystal into a liquid phase. Additionally, the sample was placed inside a second 5.6 mm quartz tube, which acted not only as a sample holder but also minimized the probability of temperature gradients due to the air stream from the spectrometer applied for temperature stabilization during NMR experiments.

SI-3: Additional Figures

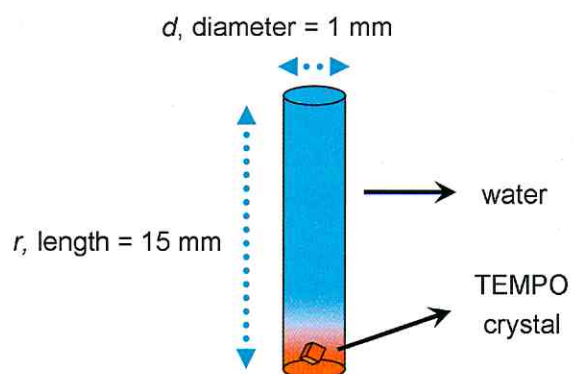


Figure SI-1 – Scheme of the sample used in experiment b)

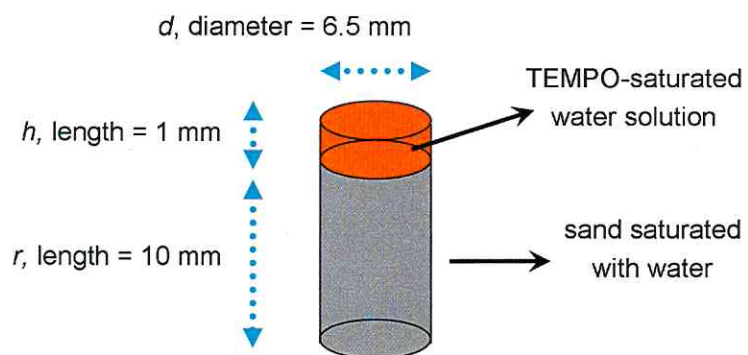


Figure SI-2 – Scheme of the sample used in experiment c)

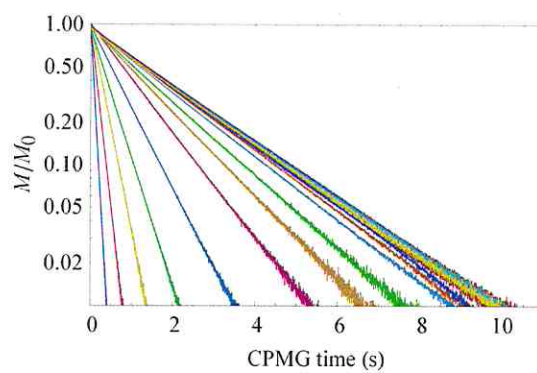


Figure SI-3 – CPMG data: relative magnetization in dependency on the TEMPO concentration in aqueous solution

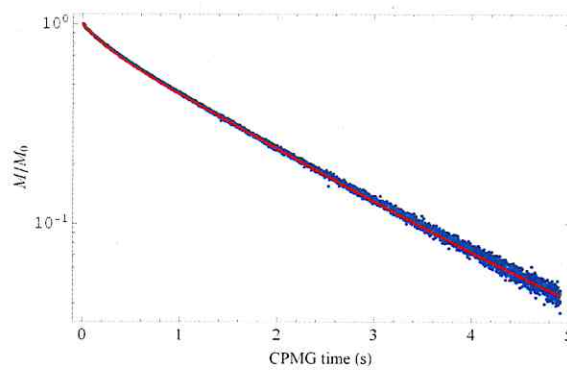


Figure SI-4 – Measured transverse relaxation decay (blue) and the bi-exponential fit (red) for water in a sample without TEMPO (B1) from experiment b).

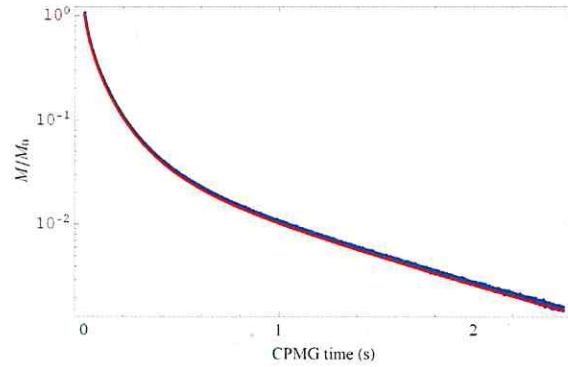


Figure SI-5 - Experimental (blue) and simulated (red) CPMG decays. The simulated data were calculated from the obtained T_2 distribution obtained by ILT as shown in Figure 4.

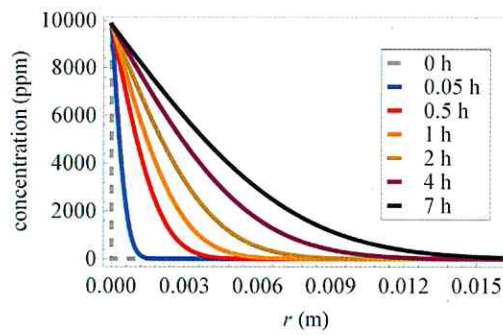


Figure SI-6 – Calculated TEMPO concentration at different distances to the source, at experimental times between 3 min (corresponding changes also in the inset) and 7 hours.

Literature Cited

- (1) D. J. Bergman and K. J. Dunn, NMR of diffusing atoms in a periodic porous medium in the presence of a nonuniform magnetic field, *Phys. Rev. E*, **1995**, 52, 6516-6535.

- (2) P. Vallet, Y. van Haverbeke, P. A. Bonnet, G. Subra, J. P. Chapat, and R. N. Muller, Relaxivity enhancement of low molecular weight nitroxide stable free radicals: importance of structure and medium *Magn. Reson. Med.*, 1994, 32, 11-15.
- (3) Bertini, I. Solution NMR of paramagnetic molecules: applications to metalloproteins and models; Elsevier Science Ltd.: Amsterdam; New York, 2001.
- (4) Helm, L. Relaxivity in paramagnetic systems: theory and mechanisms. *Prog. Nucl. Magn. Reson. Spectrosc.* **2006**, 49, 45-64.
- (5) A. Fick, Ueber Diffusion, *Ann. Phys. Chem.*, **1855**, 170, 59-86.
- (6) N. Hedin, Temperature imaging by ^1H NMR and suppression of convection in NMR probes, *J. Magn. Reson.*, **1998**, 131, 126-130.
- (7) W. Goux, The impact of Rayleigh-Benard convection on NMR pulsed-field-gradient diffusion measurements, *J. Magn. Reson.*, **1990**, 88, 609-614.

3. Conclusions

Throughout this work, different types of materials were investigated using NMR methods. NMR diffusometry was used to measure the diffusivity of different guest molecules in activated carbons of both lignocellulosic (MAC-LMA12) and polymeric (MA2) origin. These studies focused on the investigation of the heterogeneity of the pore space as well as the influence of sample loading history on the hysteresis phenomena in hierarchical porous carbons. The heterogeneity of the porous matrix was also investigated in zeolite NaX. Hysteresis phenomena were investigated in the MA2 activated carbon, where both strong kinetic restrictions in molecular uptake and gas-phase mass transfer played a significant role in the measured diffusivities in this hierarchical pore system. Furthermore, and bearing the study of environmental systems in mind, the phenomenon of PRE was used to develop a new NMR-based approach to investigate molecular transport in water-saturated porous media, without recurring to the use of PFG.

Sample morphology

The broad distribution of both toluene and cyclohexane diffusivities reflects the heterogeneity of the pore space in hierarchical activated carbons MAC-LMA12 and MA2. Concerning the latter sample, the assumption of a log-normal distribution of diffusion coefficients served as a reliable model to evaluate the diffusion data of these experiments. The same behavior was observed in NaX zeolite at measurements made with reduced loading of *n*-butane, in contrast to the observations made on other microporous materials, namely the Takeda activated carbons samples. While the spin-echo attenuation of both toluene and cyclohexane in MA2 showed a particularly strong curvature implying a more pronounced distribution of diffusivities with increasing loading, it is interesting to note that concentration studies of *n*-butane in zeolite NaX revealed the opposite trend. A distribution in diffusivities was observed at lower loadings (0.75 molecules per supercage), with no influence of observation time. This situation changed at higher loadings (3 molecules per

supercage): the spin-echo attenuation was dependent on observation time and was associated with interparticle diffusion. It could be described by a bi-exponential model. Clearly, in both systems, the diffusivity increases with increasing loading, but while in NaX zeolite, the increase in loading effectively averaged the influence of internal transport resistances. This was not the case on activated carbon. It is interesting to note that, despite the structural differences concerning carbon and zeolite materials, a log-normal distribution of diffusivities successfully described the experimental data. This suggests that in both systems transport barriers have a multiplicative effect on the self-diffusivity of guest molecules, rather than an additive effect which would give rise to a different distribution. While zeolites were long considered as nearly perfect crystallites this is known not to be the case in activated carbon samples and, therefore, the existence of internal transport barriers is not surprising. In the present work, the existence of such barriers is experimentally demonstrated, via diffusion measurements.

Hysteresis and gas-phase molecular transport

The diffusivity and cyclohexane loading in activated carbon MA2 were measured as a function of external pressure by PFG NMR and the signal intensity of the FID, respectively. The measured diffusivities and loadings measured on the desorption branch remarkably differed from those on the adsorption branch, where waiting times as long as 20 h were necessary to observe significant equilibration. In both cases (adsorption and desorption) and in agreement with measurements in purely mesoporous materials, the average diffusivity is observed to be related to the "history" of the system: loadings and diffusivities on the desorption branch are greater than those measured upon pressure increase.

The maximum value of cyclohexane diffusivity in these experiments was predicted by considering the influence of transport in the Knudsen-regime for the given pore system. While only a rough estimate was possible for the adsorption branch, a more detailed analysis was carried out in the case of the desorption branch, since the chosen waiting time between each pressure step

seemed to be sufficient for a significant equilibration of the system. On the basis of considering the pore size distribution of the sample as obtained by BJH analysis of the N₂ adsorption, an established model for purely mesoporous materials was extended to the present system under study, where diffusion also occurs in the microporous space.

The diffusivities on the whole desorption branch were successfully predicted, yielding a tortuosity value ($\tau_{des}=1.5$) which is in good agreement with that found to explain the maximum on diffusivity observed in the adsorption branch ($\tau_{ads}=1.3$). Upon complete system saturation, the diffusivities from micro- and mesopores were estimated based on their known relative volumes, from the N₂ adsorption isotherm. Mesopore diffusivity was found to be reduced by a factor of 2, which shows a good agreement to values of tortuosity found for both adsorption and desorption in the gas phase.

The estimations provided concerning both adsorption and desorption strongly relate to the interdependency of the empty space inside sample pores and Knudsen-regime diffusivity. This supports the observations made in studies on closed samples: in both MAC-LMA12 and in MA2 the role of gas-phase transport was demonstrated by relating of the obtained results with the physico-chemical properties of the guest molecules.

The notorious resistance to external pressure changes, in the case of adsorption, is tentatively proposed to relate to changes in the internal porous network, but further experiments would be needed to confirm this. More than merely rising fundamentally scientific questions, the presented observations have direct implications on the applicability of the material in processes involving cyclohexane adsorption which was demonstrated to be kinetically hindered under the chosen experimental conditions.

PRE as to tool to measure diffusion

A method based on the PRE of the water protons by TEMPO was demonstrated to successfully measure the diffusivities in homogenous and heterogeneous systems, solely by collection of relaxation data. The homogeneous system consisted of a water column, whereas the heterogeneous one of a water-saturated quartz sand, thereby serving as a model for soil systems. The obtained values for each respective system were well within the expected ranges.

This approach may be particularly useful in studying the interactions of different molecules with pore surfaces, for instance, by performing similar experiments with different TEMPO derivatives and for exploring the effect of a particular functional group, on the overall molecular transport in the case of specific interactions with the matrix. The proposed method is, in principle, applicable in more complex porous matrices. Due to its selective and non-invasive nature, it may be performed with mixtures of compounds, at different pH and temperature.

Final Remarks

The present work shows different aspects of the applicability of NMR methods in studying molecular dynamics, with emphasis on, but not limited to, NMR diffusometry. The difficulties in using the latter technique under experimentally challenging conditions due to the intrinsic properties of the activated carbons were successfully overcome and a significant contribution to understand mass transfer phenomena in systems with bi-modal pore size distributions has been given. While further theoretical and experimental investigations would be needed to fully clarify the hysteretic behavior observed in the investigated system, the present work adds an important experimental contribution on this topic. The newly developed methodology represents a feasible alternative to the use of PFG and brings NMR methods closer to environmentally relevant applications, opening new possibilities to investigate such complex systems, at low concentrations.

4. Selected Literature

1. NMR-Relaxometry and Paramagnetic Relaxation Enhancement (PRE)

V. Bakhmutov, *Practical NMR relaxation for chemists*. Chichester West Sussex England; Hoboken NJ: Wiley, **2004**.

L. Banci, *Nuclear and electron relaxation: the magnetic nucleus-unpaired electron coupling in solution*. Weinheim; New York: VCH, **1991**.

I. Bertini, *Solution NMR of paramagnetic molecules: applications to metalloproteins and models*. Amsterdam; New York: Elsevier Science Ltd., **2001**.

K. J. Dunn, D. J. Bergman, and G. A. Latorraca, *Nuclear magnetic resonance*. Amsterdam, London: Pergamon, **2002**.

I. Foley, Effect of paramagnetic ions on NMR relaxation of fluids at solid surfaces, *J. Magn. Reson., Ser. A*, **1996**, 123, 95-104.

L. Helm, Relaxivity in paramagnetic systems: theory and mechanisms, *Prog. Nucl. Magn. Reson. Spectrosc.*, **2006**, 49, 45-64.

S. Meiboom and D. Gill, Modified spin-echo method for measuring nuclear relaxation times, *Rev. Sci. Instrum.*, **1958**, 29, 688.

P. Vallet, Y. van Haverbeke, P. A. Bonnet, G. Subra, J. P. Chapat, and R. N. Muller, Relaxivity enhancement of low molecular weight nitroxide stable free radicals: importance of structure and medium, *Magn. Reson. Med.*, **1994**, 32, 11-15.

B. Weckhuysen, Chemical imaging of spatial heterogeneities in catalytic solids at different length and time scales, *Angew. Chem. Int. Ed.*, **2009**, 48, 4910-4943.

2. NMR diffusometry

T. Brandt, E. Cabrita, and S. Berger, Theory and Application of NMR Diffusion Studies, in *Modern Magnetic Resonance - Part I*. G. A. Webb, Ed. Dordrecht: Springer Netherlands, **2006**.

P. Callaghan, *Principles of nuclear magnetic resonance microscopy*. Oxford: Clarendon Press, **1993**.

P. Galvosas, F. Stallmach, and J. Kärger, Background gradient suppression in stimulated echo NMR diffusion studies using magic pulsed field gradient ratios, *J. Magn. Reson.*, **2004**, 166, 164-173.

P. Galvosas, F. Stallmach, G. Seiffert, J. Kärger, U. Kaess, and G. Majer, Generation and application of ultra-high-intensity magnetic field gradient pulses for NMR spectroscopy, *J. Magn. Reson.*, **2001**, *151*, 260-268.

W. S. Price, NMR Diffusometry, in *Modern Magnetic Resonance - Part I*. G. A. Webb, Ed. Dordrecht: Springer Netherlands, **2006**.

F. Stallmach and P. Galvosas, Spin echo NMR diffusion studies, *Ann. Rep. NMR S.* **2007**, *61*, 51–131.

F. Stallmach and J. Kärger, The potentials of Pulsed Field Gradient NMR for investigation of porous media, *Adsorption*, **1999**, *5*, 117-133.

3. Activated Carbon

F. Rodríguez-Reinoso and H. Marsh, *Activated carbon*. Amsterdam; Boston: Elsevier, **2006**.

F. Rodríguez-Reinoso, Porous carbons in gas separation and storage, in *Combined and Hybrid Adsorbents*. J. M. Loureiro and M. T. Kartel, Eds. Springer Netherlands, **2006**.

F. Rodríguez-Reinoso, The role of carbon materials in heterogeneous catalysis, *Carbon*, **1998**, *36*, 159-175.

F. Rodríguez-Reinoso, J. Garrido, J. Martín-Martínez, M. Molinasabio, and R. Torregrosa, The combined use of different approaches in the characterization of microporous carbons, *Carbon*, **1989**, *27*, 23-32.

F. Rodríguez-Reinoso, J. Martín-Martínez, M. Molina-Sabio, R. Torregrosa, and J. Garrido, Evaluation of the microporosity in activated carbons by n-nonane preadsorption, *J. Colloid Interface Sci.*, **1985**, *106*, 315-323.

P. Serp and J. L. Figueiredo, *Carbon materials for catalysis*. Hoboken N.J.: John Wiley & Sons, **2009**.

S. R. Tennison, Phenolic-resin-derived activated carbons, *Appl. Catal., A: General*, **1998**, *173*, 289-311.

4. Zeolites

A. Feldhoff, J. Caro, H. Jobic, J. Ollivier, C. B. Krause, P. Galvosas, and J. Kärger, Intracrystalline transport resistances in nanoporous zeolite X, *ChemPhysChem*, **2009**, *10*, 2429-2433.

R. Barrer, Zeolites and clay minerals as sorbents and molecular sieves. London; New York: Academic Press, **1978**.

J. Kärger and D. M. Ruthven, Diffusion in zeolites and other microporous solids. New York: Wiley, **1992**.

F. Keil, R. Krishna, and M.-O. Coppens, Modeling of diffusion in zeolites, *Rev. Chem. Eng.*, **2000**, *16*, 71-197.

5. Hysteresis and gas-phase molecular transport

S. K. Bhatia and D. Nicholson, Transport of simple fluids in nanopores: theory and simulation, *AIChE J.*, **2006**, *52*, 29-38.

T. X. Nguyen and S. K. Bhatia, Kinetic restriction of simple gases in porous carbons: Transition-state theory study, *Langmuir*, **2008**, *24*, 146-154.

R. Valiullin, S. Naumov, P. Galvosas, J. Kärger, H. J. Woo, F. Porcheron, and P. A. Monson, Exploration of molecular dynamics during transient sorption of fluids in mesoporous materials, *Nature*, **2006**, *443*, 965-968.

R. Valiullin, J. Kärger, and R. Gläser, Correlating phase behaviour and diffusion in mesopores: perspectives revealed by pulsed field gradient NMR, *Phys. Chem. Chem. Phys.*, **2009**, *11*, 2833-2853.

R. Valiullin, P. Kortunov, J. Kärger, and V. Timoshenko, Concentration-dependent self-diffusion of liquids in nanopores: a nuclear magnetic resonance study, *J. Chem. Phys.*, **2004**, *120*, 11804-11814.

6. Bioavailability

A. Koelmans, M. Jonker, G. Cornelissen, T. Bucheli, P. Vannoort, and O. Gustafsson, Black carbon: The reverse of its dark side, *Chemosphere*, **2006**, *63*, 365-377.

K. Semple, K. J. Doick, K. C. Jones, P. Burauei, A. Craven, and H. Harms, Peer Reviewed: Defining Bioavailability and Bioaccessibility of Contaminated Soil and Sediment is Complicated, *Environ. Sci. Technol.*, **2004**, *38*, 228A-231A.

5. Annexes

Annex 1 – Fit Results of Cyclohexane and Toluene in MA2

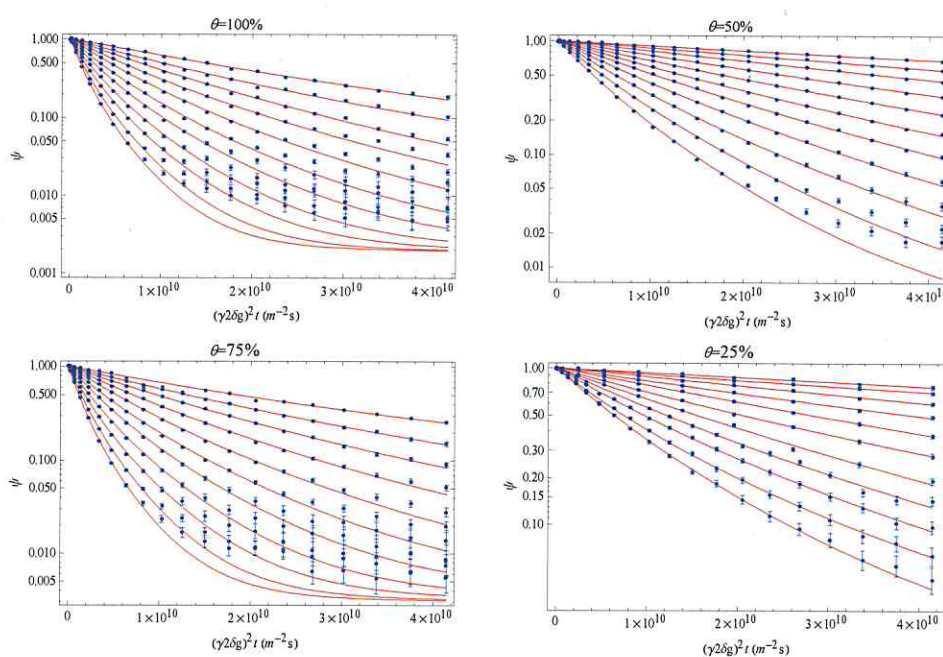


Figure A - Fitting assuming a log-normal distribution of toluene diffusivities, at different loadings. For each corresponding loading, a steeper slope represents a lower temperature (ranging from $-50^\circ C$ to $50^\circ C$).

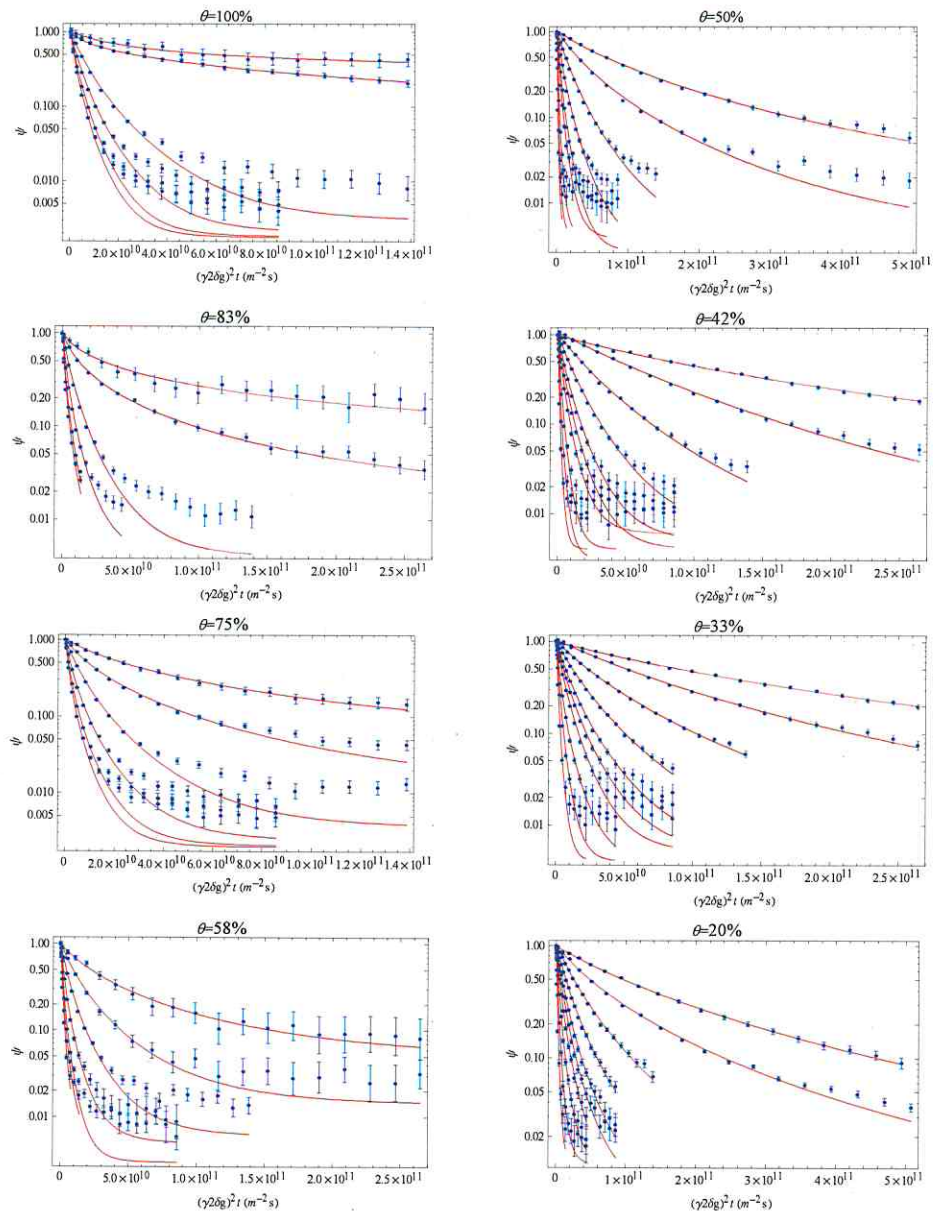


Figure B - Fitting assuming a log-normal distribution of cyclohexane diffusivities, at different loadings. For each corresponding loading, a steeper slope represents a lower temperature (ranging from -40°C to 120°C).

Annex 2 – Physical Constants for Cyclohexane and Toluene

	Toluene	Cyclohexane
Molecular Mass (g mol ⁻¹)	92.14	84.16
Liquid Self-Diffusivity (25°C) (x 10 ⁻⁹ m ² s ⁻¹)	2.66	1.4
Activation Enthalpy for Liquid Diffusion (kJ mol ⁻¹)	10.9 (from ref. [1])	19.1 (from ref. [2])
Freezing Point (°C)	-95	6.6
Vapor Pressure (20°C) (mbar)	29	104
Vaporization Enthalpy (kJ mol ⁻¹)	38	33
Boiling Point (°C)	111	81

[1] Pickup, S., Blum, F. D., Self-diffusion of toluene in polystyrene solutions, *Macromolecules*, **1989**, 22, 3961

[2] McCall, D. W., Douglass, D. C., Anderson, E. W., Diffusion in liquids, *J. Chem. Phys.*, **1959**, 31, 1555

Publication and Contribution List

Publication 1 – "**Characterisation of carbon materials with the help of NMR methods**", Margarita Krutyeva, Farida Grinberg, Filipe Furtado, Petrik Galvosas, Jörg Kärger, Ana Silvestre-Albero, Antonio Sepulveda-Escribano, Joaquín Silvestre-Albero, Francisco Rodríguez-Reinoso, *Microporous and Mesoporous Materials*, 2009, 120, 91.

- Planning and execution of the experiments shown in Figures 6 and 8
 - Participation in the revision of the manuscript
- Supervision: Juniorprof. Petrik Galvosas, Prof. Dr. Jörg Kärger

Publication 2 – "**The evidence of NMR diffusometry on pore space heterogeneity in activated carbon**", Filipe Furtado, Petrik Galvosas, Maraisa Gonçalves, Frank-Dieter Kopinke, Sergej Naumov, Francisco Rodríguez-Reinoso, Ulf Roland, Rustem Valiullin, Jörg Kärger, *Microporous and Mesoporous Materials*, 2011, 141, 184.

- Participation in the conceptual design of the work
 - Planning and execution of all experiments as well as modelling of the obtained results. Exceptions are the results shown in Figure 1.a, Figure 1.b and Figure 2 (TEM, SEM, nitrogen adsorption data and respective pore size distributions of the material under study)
 - Participation in the writing of the manuscript as well as in applying the requested modifications during the revision process
 - Participation in the final revision of the manuscript
- Supervision: Juniorprof. Petrik Galvosas, Prof. Dr. Jörg Kärger, Dr. habil. Ulf Roland and Prof. Dr. Frank-Dieter Kopinke

Publication 3 – "**Tracing pore-space heterogeneities in X-type zeolites by diffusion studies**", Ziad Adem, Jürgen Caro, Filipe Furtado, Petrik Galvosas, Cordula B. Krause, Jörg Kärger, *Langmuir*, 2011, 27, 416.

- Modelling of the experimental data shown in Figures 2 and 3 and elaboration of related literature research
 - Participation in the revision of the manuscript
- Supervision: Prof. Dr. Jörg Kärger

Publication 4 – “**Guest Diffusion in Interpenetrating Networks of Micro- and Mesopores**”, Filipe Furtado, Petrik Galvosas, Maraisa Gonçalves, Frank-Dieter Kopinke, Sergej Naumov, Francisco Rodríguez-Reinoso, Ulf Roland, Rustem Valiullin, Jörg Kärger, *Journal of the American Chemical Society*, 2011, 133, 2437.

- Participation in the conceptual design of the work
- Planning and execution of all experiments, with exception of the results shown on Figures 1 and 2 (TEM, SEM, nitrogen adsorption data and respective pore size distributions of the material under study)

- Elaboration of the literature research and modelling of the experimental data

- Participation in the writing of the manuscript as well as in applying the requested modifications during the revision process

- Participation in the final revision of the manuscript

Supervision: Juniorprof. Petrik Galvosas, Prof. Dr. Jörg Kärger, Dr. habil. Ulf Roland and Prof. Dr. Frank-Dieter Kopinke

Publication 5 – “**Paramagnetic Relaxation Enhancement (PRE) as a tool for probing diffusion in environmentally relevant porous media**”, Filipe Furtado, Petrik Galvosas, Frank Stallmach, Ulf Roland, Jörg Kärger, Frank-Dieter Kopinke, *Environmental Science & Technology*, submitted.

- Participation in the conceptual design of the work

- Planning and execution of all experiments

- Elaboration of the literature research

- Modelling of the experimental data

- Writing of the manuscript

Supervision: Juniorprof. Petrik Galvosas, Prof. Dr. Jörg Kärger, Dr. habil. Ulf Roland and Prof. Dr. Frank-Dieter Kopinke

Lebenslauf

Persönliche Daten	
Nachname, Vorname	Correia Duarte Furtado, Filipe Ricardo
Geburtsdatum und -ort	24.03.1981, Lissabon (Portugal)
Berufserfahrung	
Beruf	Doktorand - Marie Curie Stipendium (Early Stage Training)
11.2006 – 11.2010	Department für Technische Umweltchemie, Helmholtz-Zentrum für Umweltforschung - UFZ (Prof. Frank-Dieter Kopinke) im Zusammenarbeit mit der Abteilung Grenzflächenphysik, Universität Leipzig (Arbeitskreis: Prof. Jörg Kärger)
Studium	
Qualifikation	Diplom Angewandte Chemie, mit Schwerpunkt Organische Chemie
09.1999 – 01.2006	Faculdade de Ciências e Tecnologia - Universidade Nova de Lisboa (Lissabon, Portugal)
Praktika	
12.2004 – 12.2005	Faculdade de Ciências e Tecnologia - Universidade Nova de Lisboa, im Arbeitskreis von Ass. Prof. Eurico Cabrita (Lissabon, Portugal)
Schwerpunkt	Strukturelle Charakterisierung von Oxozolinonen- und Imidazolydinonen mit verschiedenen NMR-Methoden
03.2005 – 08.2005	ERASMUS Programme: Institut für Analytische Chemie - Universität Leipzig, im Arbeitskreis von Prof. Stefan Berger (Leipzig)
Schwerpunkt	Untersuchung der Tertiärstruktur von Peptiden mit verschiedenen NMR-Methoden
Schulzeit	
1987-1999	Grundschule (Seixal, Portugal) und Gymnasium (Almada, Portugal).

Acknowledgments

Resulting from a cooperation project, the time during which this work was developed allowed me to have contact with a great variety of people, from different institutes, research fields, ages and nationalities. I would like to express my gratitude to all the people in the TUCHEM and GFP departments, from the UFZ and the University of Leipzig, respectively, for actively contributing to this enriching experience. I especially would like to acknowledge the following people:

Prof. Dr. Frank-Dieter Kopinke and Dr. habil. Ulf Roland for accepting me into their research group and for their dedicated supervision and assistance, thus making the present work possible.

Prof. Dr. Jörg Kärger for sharing his knowledge and his enthusiasm in this field of research, and for all the energy invested in me and in my project.

Juniorprof. Petrik Galvosas for his assistance in tackling with the experimental aspects of this work but especially for his guidance and advice.

Prof. Dr. Francisco Rodríguez-Reinoso and Dr. Maraisa Gonçalves, from the University of Alicante, Spain for a most cordial and fruitful cooperation.

Prof. Dr. Mathias Kästner and all the members of the RAISEBIO research group, for a great working environment.

Prof. Dr. Roger Gläser for accepting me in the International Research Training Group (IRTG) "Diffusion in Porous Materials".

Dr. Margarita Krutyeva, and Dr. Rustem Valiullin, who played a crucial role at different stages of my work, for all their assistance and helpful considerations.

Dr. habil. Frank Stallmach for many helpful discussions and suggestions.

Dr. Wadinga Fomba, Dr. Sergej Naumov and Dr. Ivonne Mitreiter for their readiness in sharing their own knowledge and experiences with me.

To Dr. Rico Rockmann, Dr. habil. Gritt Kalies and Dr. José Luis Barzola Quiquia for all the help and discussions on the characterization of activated carbon samples.

To Birgit Forkert, Dr. Frank Holzer and Dr. Ulf Trommler, not only for their generosity in providing assistance in the laboratory work but also for contributing to an easy going working environment.

To Stefan Schlayer, Lutz Moschkowitz and Peter Fatum, for technical assistance.

At this point, I sincerely would like to thank Dr. Eurico Cabrita for suggesting the city of Leipzig as my destination as an undergraduate exchange student, and to Prof. Stefan Berger, for his kindness in welcoming me in his work group. My personal experience during that time greatly contributed for my wish to return to this city, from which the present work resulted.

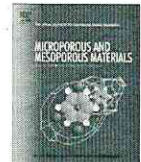
Finally and especially, I would like to thank my friends and my family for their warmth and support.

Publikationsausdrucke



Contents lists available at ScienceDirect

Microporous and Mesoporous Materials

journal homepage: www.elsevier.com/locate/micromeso

Characterization of carbon materials with the help of NMR methods

M. Krutyeva^a, F. Grinberg^{a,*}, F. Furtado^c, P. Galvosas^a, J. Kärger^a, A. Silvestre-Albero^b,
A. Sepulveda-Escribano^b, J. Silvestre-Albero^b, F. Rodríguez-Reinoso^b

^a Department of Interface Physics, University of Leipzig, Linnéstrasse 5, D-04103 Leipzig, Germany

^b Laboratorio de Materiales Avanzados, Departamento de Química Inorgánica, Universidad de Alicante, Ap. 99, E-03080 Alicante, Spain

^c Helmholtz Centre for Environmental Research, Leipzig, Permoserstrasse 15, D-04318 Leipzig, Germany

ARTICLE INFO

Article history:

Received 15 May 2008

Received in revised form 11 December 2008

Accepted 11 December 2008

Available online 25 December 2008

Keywords:

Activated carbons
Porous structure
NMR
Diffusion
Liquids

ABSTRACT

Combined NMR cryoporometry, relaxometry and diffusometry were applied to characterize porous carbon materials. Pore space characterization in NMR cryoporometry is based on the measurement of melting point depression of the confined liquids, whereas NMR relaxometry and diffusometry explore the random motion of the molecules under confinement by the pore space. We demonstrate compatibility between the evidence of classical sorption experiments and NMR cryoporometry on pore size distribution. There is a distribution in both the nuclear magnetic relaxation rates and diffusion coefficients. These distributions have to be referred to heterogeneities in the pore space. Since they can only be observed if their influence is not averaged out on the diffusion paths covered by the molecules during the respective measurements, the spatial extension of the regions with structural differences (as evidenced by the differences in diffusion and nuclear magnetic relaxation of the probe molecules) may be estimated to be at least of the order of 20 μm .

Published by Elsevier Inc.

1. Introduction

Nanoporous carbon materials are used in a wide range of industrial applications, including heterogeneous catalysis, separation, storage of gases and fluid purification. These materials are characterized by a complex porous network constituted of micropores with pore width of less than 2 nm, mesopores with pore widths between 2 and 50 nm and macropores with pore width of greater than 50 nm. Such a three-dimensional pore structure results in a material that exhibits a high surface area together with a high pore volume. Additionally, carbon materials can accommodate heteroatoms (mainly oxygen surface groups) on structural defects (e.g. boundaries of the graphene layer) which affect the surface chemistry of the material. A main advantage of porous carbons in respect to other porous solids is that, both the porous structure and the surface chemistry can be tailored by pre- and post-synthesis treatments. This helps to achieve the properties required for a particular application [1].

The proportion of micropores and mesopores on carbon materials strongly depends on the synthesis procedure used. Microporous carbons can be prepared from a wide variety of lignocellulosic precursors (olive stones, coconut shell, etc.) using either physical (CO_2 , H_2O , etc.) or chemical (H_3PO_4 , ZnCl_2 , etc.) activation [2–4]. Although the presence of microporosity is required to achieve a

high surface area, i.e. a high adsorption capacity, the presence of some mesoporosity is quite often desirable. Mesopores are very useful, not only for processes involving larger molecules, but also because they constitute channels for speeding up the access to the inner microporosity. Carbon materials with a highly developed mesoporosity can be prepared using different approaches, such as combination of chemical and physical activation, use of nanocasting (hard and soft template strategy) technology, etc. [5–7].

Textural characterization of nanoporous carbon materials is commonly performed using adsorption of probe molecules (He, Ar, N_2 , CO_2 , etc.). Among them, N_2 adsorption at 77 K and CO_2 adsorption at 273 K are the most widely used to assess both the total microporosity (<2 nm) and the narrow microporosity (<0.7 nm), respectively [8]. Additionally, application of several mathematical models to the adsorption isotherms can provide information about the “apparent” surface area, pore size distribution, etc. (e.g. Brunauer–Emmett–Teller equation to the N_2 adsorption isotherm). Although the correct characterization of the textural properties is of paramount importance to understand the behaviour of carbon materials in a certain application, their effectiveness in adsorption processes will also be highly depending on the transport (diffusion) of adsorptives to the inner pore system.

NMR methods have proven to be an efficient tool to study micro- and mesoporous materials and surface interactions of confined liquids [9]. A combination of several NMR techniques is especially useful as it allows for elucidation of a multitude of important system characteristics. As an example, the properties

* Corresponding author. Tel.: +49 (0) 341 97 32504; fax: +49 (0) 341 97 32549.
E-mail address: grinberg@physik.uni-leipzig.de (F. Grinberg).

of sorbate molecules in contact with the liquid/solid interfaces at pore walls were studied with the help of NMR cryoporometry and relaxometry [10,11]. NMR cryoporometry provides information on the distribution of the pore size. NMR relaxometry is especially sensitive to surface interactions. The aim of this work is the characterization of mesoporous carbons by combination of the three NMR techniques: cryoporometry, relaxometry and diffusometry. Various adsorptive molecules were used for this study. One of the accents was put on monitoring molecular transport of the confined liquids in the porous space of the investigated materials. Direct measurements of molecular self-diffusion were performed with the help of Pulsed Field Gradient (PFG) NMR permitting one to obtain an in-depth information on both transport properties of the confined liquids and the structure characteristics of the host material.

2. Experimental

2.1. Materials

Two carbon molecular sieves (Takeda 4A and Takeda 5A, Takeda Chemical Industries Ltd.) and three different activated carbons (PK13, RGC30 and MAC-LMA12) have been used in this study. The selection of these samples is based on their different textural properties. While carbon molecular sieves and the activated carbon PK13 (Norit) are mainly microporous, the samples RGC30 (Nuchar) and MAC-LMA12 exhibit both micro- and mesoporosity.

Carbon molecular sieves Takeda 4A and Takeda 5A and activated carbons PK13 and RGC30 are commercially available carbon materials. Sample MAC-LMA12 (MAC: mesoporous activated carbon; LMA: Laboratorio de Materiales Avanzados; x = 12: production number) was prepared from olive stones as a raw material. Firstly, the olive stones were crashed, sieved to 3 mm and washed with diluted H_2SO_4 (10%) to remove the majority of inorganic impurities. The clean sample was impregnated with an aqueous solution of $CaCl_2$ (7 wt.%) for 7 h in a thermostatic water bath at 358 K. After 7 h, the temperature was increased up to 373 K and held at this temperature until the level of water became similar to that of olive stone, the remaining water being removed by filtration. The impregnated sample was dried for 24 h at 353 K in an air recirculation oven and then it was submitted to an activation treatment in a horizontal furnace using CO_2 (100 ml min^{-1}) at 1043 K for 6 h. After the activation, the sample was outgassed in a vacuum oven for 4 h at 323 K, in order to remove the remaining CO_2 adsorbed, and subsequently washed with hot HCl (5%) in order to remove the remaining calcium; a final washing with distilled water until pH 7 was performed.

In order to avoid interferences in the diffusion process from inorganic species remaining on the carbon structure, all carbon materials have been washed with HCl (10%) at 353 K for 3 h. After the acid treatment, carbon samples have been washed with distilled water until pH 7 and subsequently dried overnight at 353 K. After the washing treatment, the total ash content is mainly nil for RGC30, MAC-LMA12, Takeda 4A and Takeda 5A samples, while it is around 2 wt.% for sample PK13.

2.2. Sample characterization

N_2 and CO_2 adsorption isotherms were determined in a Coulter Omnisorb-610 equipment at 77 K and 273 K, respectively. Prior to the adsorption measurement, samples were outgassed under vacuum (10^{-3} Pa) at 523 K for 4 h. Dubinin-Radushkevich (DR) equation was applied to the N_2 and CO_2 adsorption isotherms in order to obtain both the total micropore volume (V_0) and the volume of narrow microporosity (V_n), respectively [12]. Total pore volume

(V_t) was obtained from the amount adsorbed at $P/P_0 \sim 0.99$ on the N_2 isotherm, while the mesopore volume (V_{meso}) was calculated from the difference between V_t and V_0 . The “apparent” surface area (S_{BET}) was determined applying the Brunauer–Emmett–Teller (BET) equation to the N_2 adsorption isotherms.

2.3. NMR analysis

All NMR measurements were performed with the help of the home-built PFG NMR spectrometer FEGRIS NT, operating at a 1H resonance frequency of 125 MHz [13]. High-intensity magnetic field gradients (up to 35 Tm^{-1}) were applied.

The construction of the melting curves in the experiments on NMR cryoporometry was based on the temperature dependences of the NMR signal intensity. The latter was evaluated as the maximal spin-echo amplitude produced by the standard Hahn echo radio frequency pulse sequence ($90^\circ-\tau-180^\circ$). The value of τ was set to 2 ms. All measured echo amplitudes were normalized by the value of the (echo) amplitude at the highest temperature (above the bulk melting point). The range of investigated temperatures was between 165 K and 298 K. The experiments were started at the lowest temperature and then the temperature was increased in steps of 5 K. The relaxation rates of the adsorbate molecules in the investigated samples were determined using the Carr–Purcell–Mejboom–Gill (CPMG) pulse sequence. The measurement of diffusion coefficients in PFG NMR was performed with the help of the standard three 90° - pulse sequence (also known as the “stimulated echo” pulse sequence).

The preparation of the samples for the NMR experiments was performed as follows. The host material was introduced into the sample tubes with an outer diameter of 7.5 mm. After that, the tubes with the material were heated at 383 K during 24 h in an oven under atmospheric conditions. Then the samples were connected to the vacuum system and dehydrated under high vacuum ($<10^{-2}$ Pa) at 523 K for around 4 h. While evacuating, a certain amount of liquid was injected into the tubes. For relaxation and diffusion experiments, the amount of the sorbate was adjusted to achieve full loading of the pores (100% of the total pore volume). For the NMR cryoporometry experiments, the amount of sorbate (nitrobenzene in our work) was supplied in excess, thus allowing an oversaturation of the host material. Finally, the sample tubes were sealed.

3. Results and discussion

3.1. Textural characterization

Fig. 1 shows the N_2 adsorption isotherms for the different samples studied. As it can be observed, all carbon materials exhibit a high nitrogen uptake at low relative pressures ($P/P_0 < 0.01$), which mainly corresponds to the adsorption on micropores. After the sharp knee in the N_2 isotherms, samples PK13 and MAC-LMA12 exhibit a near-plateau with a small slope but, above $P/P_0 \sim 0.6$, the sample MAC-LMA12 exhibits an important increase in the amount adsorbed and a hysteresis loop suggesting the additional presence of some mesoporosity. The situation becomes different for sample Nuchar RGC30. This activated carbon exhibits a continuous increase in the amount adsorbed over the whole relative pressure range (up to $P/P_0 = 0.97$), which corresponds to the combined presence of microporosity together with a well-developed mesoporosity. These findings are clearly reflected on Table 1. The micropore volume obtained from the N_2 (V_0) and CO_2 (V_n) adsorption isotherms for sample Norit PK13 is quite similar, thus reflecting the presence of a narrow micropore size distribution on this sample [14]. This difference between V_0 and V_n becomes slightly more evi-

dent for the synthesized activated carbon, denoted MAC-LMA12, in which the total pore volume is constituted by about 70% mesopores and 30% micropores. Last but not least, sample RGC30 exhibits very different values for V_0 and V_m , which confirms the presence of a broad micropore size distribution with combination of both micropores and mesopores (the proportion of narrow micropores being less important than for the other carbons).

As it has been mentioned before, carbon molecular sieves Takeda 4A and Takeda 5A have been also considered for this study due to the pure microporous nature of these samples (more than 90% of the pore volume is in the range of microporosity), with the mesopore volume in these materials being almost nil [15]. The micropore volume (V_0) obtained from N_2 adsorption isotherms at 77 K is $0.22 \text{ cm}^3 \text{ g}^{-1}$ and $0.33 \text{ cm}^3 \text{ g}^{-1}$, for samples Takeda 4A and Takeda 5A, respectively. The two carbon molecular sieves Takeda 4A and Takeda 5A differentiate from each other by the size of the mouth in the microporous space: 0.4 and 0.5 nm, respectively [1].

3.2. NMR cryoporometry

NMR cryoporometry exploits the melting point depression of liquids confined in mesopores [16]. The melting temperature T_m of a liquid frozen in pores is lower than that of a bulk liquid as a consequence of the smaller crystal sizes and the enhanced surface-to-volume ratio. This effect is larger for smaller pores. According to the Gibbs–Thomson equation [17] the difference between the normal (bulk) and the depressed melting points (in pores) is inversely proportional to the pore diameter d

$$\Delta T_m(d) = T_m - T_m(d) = k/d, \quad (1)$$

where k is a constant related to the thermodynamic properties of the confined liquid. In materials with a distribution of pore diameters, the melting temperature of the confined liquid will vary with the pore size. In NMR cryoporometry, one only observes the NMR

signal due to the molecules in the liquid state. Therefore, at each temperature below the bulk melting point, the measured signal intensity is proportional to the volume of the non-frozen liquid confined in the pores. Analyzing the NMR response as a function of the temperature permits to determine the distribution of the pore sizes using the

$$\frac{\Delta v}{\Delta d} = \frac{k \Delta v}{\Delta T_m(d) d^2} \quad (2)$$

where v is the total volume of pores with diameters $\leq d$. Hence, $\frac{\Delta v}{\Delta d}$ is nothing else than the pore size distribution, which, owing to Eq. (2), becomes directly experimentally accessible. The parameter k should be known (or calibrated) in advance. This method is limited to pore sizes exceeding 1 nm and is efficient in characterizing the pores on the mesoscopic length scale.

The transverse nuclear magnetic relaxation of guest molecules within the micropores was typically small (≤ 2 ms) so that the contribution of these molecules to the observed NMR signal could be neglected. It is, therefore, exclusively the size distribution of the mesopores which is traced in our present cryoporometry studies.

In this work, the so-called melting curves, i.e. the temperature dependences of the NMR signal intensity, were measured for nitrobenzene confined in MAC-LMA12, Nuchar RGC30 and Norit PK13. Fig. 2 shows the melting curves of all three samples in the range of temperatures between 165 K and 298 K. The bulk melting point of nitrobenzene at 279 K is indicated as the vertical line. A step-like decrease in the vicinity of this temperature observed for all three samples is attributed to the bulk liquid component (outside the pores). Obviously, in sample MAC-LMA12 this decay merges with the decay in large mesopores and macropores which introduces a large uncertainty in pore size distribution resulting from this part of the melting curve. For two samples, MAC-LMA12 and RGC30, a change of the signal intensity was also observed at lower temperatures, i.e. below the bulk step. This change refers to melting of nitrobenzene confined in the mesoporous space of these materials.

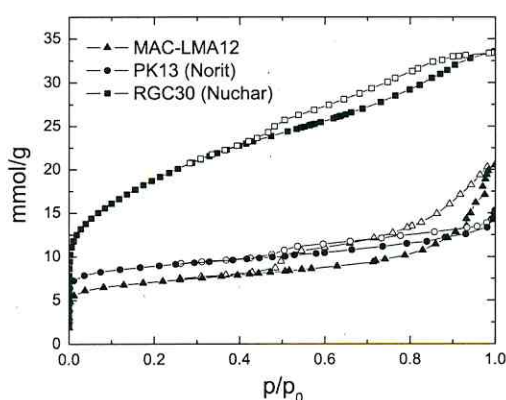


Fig. 1. N_2 adsorption isotherms at 77 K for samples Nuchar RGC30, Norit PK13 and MAC-LMA12.

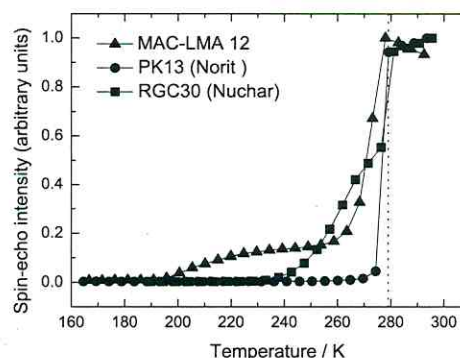


Fig. 2. Temperature dependence of the NMR spin-echo signal intensity ("melting curves") of nitrobenzene in Nuchar RGC30, Norit PK13 and MAC-LMA12 carbon materials. The signal intensity is proportional to the total amount of liquid within the sample at the given temperature. The vertical line indicates the bulk melting point of nitrobenzene.

Table 1

"Apparent" surface area (S_{BET}), micropore volume (V_0), mesopore volume (V_{meso}) and total pore volume (V_t) in the samples studied, as obtained from the N_2 adsorption measurements at 77 K and the narrow micropore volume (V_n) determined by CO_2 adsorption experiments at 273 K.

	$S_{\text{BET}}/\text{m}^2 \text{ g}^{-1}$	$V_0 (\text{N}_2)/\text{cm}^3 \text{ g}^{-1}$	$V_{\text{meso}}/\text{cm}^3 \text{ g}^{-1}$	$V_t/\text{cm}^3 \text{ g}^{-1}$	$V_n (\text{CO}_2)/\text{cm}^3 \text{ g}^{-1}$
MAC-LMA12	569	0.23	0.48	0.71	0.21
Norit PK13	738	0.29	0.24	0.53	0.26
Nuchar RGC30	1521	0.52	0.64	1.16	0.34

In Norit PK13, melting in the mesopores was not observed. This indicates that the mesoporous volume in PK13 is small in comparison to the other two samples; in agreement with the adsorption results (see Table 1).

The pore size distributions of RGC30 and MAC-LMA12 calculated from the melting curves are shown in Fig. 3. The mean pore diameters could roughly be estimated from the peaks of the distribution functions as ~ 2 nm and ~ 7 nm for MAC-LMA12 and RGC30 samples, respectively. Fig. 3 shows that the distribution around these values is broader for RGC30 than for MAC-LMA12. In the latter sample, there is an additional broad peak centered at around 15 nm. It corresponds to the first steep decay in the melting curves, close to the bulk melting point. Due to the limited resolution in this range of our melting curve, this peak does only indicate the presence of some larger mesopores and macropores and is not suitable for quantitative analysis.

3.3. NMR relaxometry

In addition to NMR cryoporometry which is sensitive to pore space geometry, NMR relaxometry can provide valuable information on molecular dynamics of the confined liquid and on surface interactions. The adsorbate molecules probe the pore structure and surfaces via translational diffusion between the surface sites and the internal volume of the pore. In the vicinity of the solid surface, the transverse relaxation time T_2 of a liquid tends to decrease in comparison to the bulk state. The decrease is the larger the stronger is the surface interaction and is usually more pronounced for polar liquids. In pores with characteristic sizes of a few or a few tens of nanometers the exchange between the surface sites and the pore interior is fast on the time scale of the NMR experiment. The measured transverse relaxation rate T_2^{-1} of a liquid in the mesopores, therefore, will represent an average of the bulk-like liquid relaxation rate $T_{2,\text{bulk}}^{-1}$ and the enhanced surface relaxation rate, weighted according to the surface-to-volume ratio of the pore. Brownstein and Tarr calculated T_2^{-1} of a liquid confined in a simple spherical pore with a volume V and a surface S

$$\frac{1}{T_2} = \frac{1}{T_{2,\text{bulk}}} + \rho \frac{S}{V} \quad (3)$$

where S/V is the surface-to-volume ratio and ρ is the surface relaxivity [18]. Eq. (3) contains quantities related both to geometrical characteristics (surface-to-volume ratio) and to surface interactions (surface relaxivity). The amplitude of the transverse magnetization in a system with equally sized pores and uniform surface interactions will be a simple exponential function of time

$$\Psi(t) = I(t)/I(0) = \exp\left(-\frac{t}{T_2}\right) \quad (4)$$

where $I(t)$ is the intensity of the transverse magnetization at time t . In our experiments, it was evaluated from a series of spin echoes produced by the CPMG pulse sequence [19]. If there is a distribution of the pore sizes, the relaxation function will result as the integral of the contributions of the individual pores [20]

$$\Psi(t) = \int f(T_2^{-1}) \exp\left(-\frac{t}{T_2}\right) d(T_2^{-1}) \quad (5)$$

where $f(T_2^{-1})$ denotes the distribution function of the relaxivities. The mean relaxation rate can be determined from the initial slope of the relaxation curve according to

$$\langle T_2^{-1} \rangle = -\lim_{t \rightarrow 0} \frac{\partial}{\partial t} (\Psi(t)) = \int T_2^{-1} f(T_2^{-1}) d(T_2^{-1}) \quad (6)$$

Typically, the transverse relaxation time of a bulk liquid (seconds) is much larger than that of a liquid near the pore wall (milliseconds or below). Therefore, the measured relaxation rate in Eq. (3) is determined solely by the second term. Provided the distribution of relaxivities $f(T_2^{-1})$ is due to distribution of the pore sizes only, the latter can be deduced from the measured relaxation function, Eq. (5). This was demonstrated, for example, for a series of silica gels in Ref. [11].

Fig. 4 shows the attenuations of transverse magnetization of ethanol, nitrobenzene and toluene in MAC-LMA12 as a function of time. Deviations from the exponential behaviour were observed. A closer inspection shows that the curves can be decomposed into two components

$$\Psi(t) = \Psi_{\text{fast}}(t) + \int f(T_2^{-1}) \exp\left(-\frac{t}{T_2}\right) d(T_2^{-1}) \quad (7)$$

where $\Psi_{\text{fast}}(t)$ refers to the "fast" attenuation component visible at short times, see inset in Fig. 4. This component is relevant for a quite small fraction of molecules (10–20%) and, therefore, cannot be analysed in more detail as it is masked by the dominating "slower" component. The latter refers to 80–90% of molecules and exhibits a moderate deviation from the exponential behaviour. The existence of two components in the relaxation curves indicates the presence of two species of molecules with different dynamic properties. The species with the faster relaxation and smaller population should probably be attributed to the liquid confined in the microporous space. The larger fraction with slower relaxation should then be attributed to the liquid in the mesopores. It is worth noting that the exchange between the two species is hindered. This

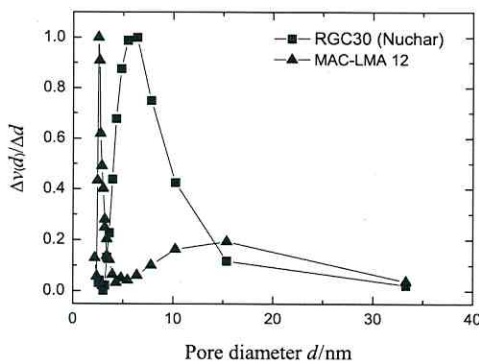


Fig. 3. Pore size distribution in Nuchar RGC30 and MAC-LMA12 samples calculated from the melting curves shown in Fig. 2.

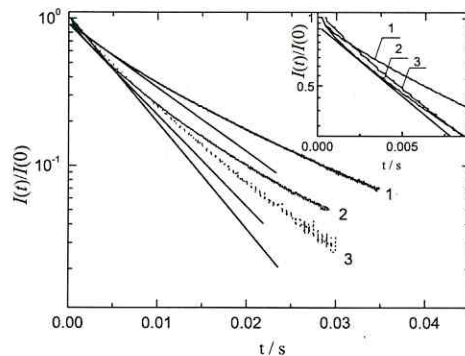


Fig. 4. Attenuation of the transverse magnetization of toluene (1), ethanol (2), and nitrobenzene (3) at 298 K confined in MAC-LMA12. The initial parts of these plots are presented in the inset. The attenuation curves were measured by the CPMG pulse sequence.

is in spite of the large diffusion path lengths of more than 100 nm, notably exceeding the pore sizes. In turn, this should mean that as soon as the molecules enter the microporous space (or some specific areas of this space) they tend to stay in this space and not easily exchange with the molecules in the mesopores.

The mean relaxation rates were determined from the initial slopes of the slow components of the relaxation curves according to Eq. (4). The corresponding inverse values, $1/(T_2^{-1})$, for toluene, ethanol and nitrobenzene were 10 ms, 7 ms and 6 ms, respectively. The fact that the relaxation times of ethanol and nitrobenzene were shorter than in toluene correlates with the much stronger polarity of these liquids in comparison with toluene. This is due to the stronger surface interactions of polar molecules giving rise to enhanced relaxivity at the surface and, hence, to shorter overall transverse relaxation times [11].

PFG NMR diffusion studies reveal molecular displacements of order of micrometers during the experimental observation times (see Section 3.4). Therefore, a non-exponential relaxation behaviour can only be observed if the sample consists of sub-regions of different pore characteristics (e.g. mean pore sizes) with extensions over at least tens of micrometers.

The analysis of the molecular dynamics in the microporous space of the MAC-LMA12 material was approached by separate studies of the microporous carbon materials Takeda 4A and Takeda 5A. The relaxation curves of ethanol and toluene in these materials are shown in Fig. 5. Only slight deviations from the exponential behaviour are observed. The relaxation times (obtained as the inverse values of the mean relaxation rates, $1/(T_2^{-1})$) were 1.2 ms and 2 ms for ethanol, and 0.5 ms and 0.8 ms for toluene in Takeda 4A and Takeda 5A, respectively. Again the trends in the relaxation rates exhibit the expected behaviour. The relaxation times become the smaller, the more rigid are the formed guest-host complexes: both an increase in the guest size (from ethanol to toluene) and a decrease in the host “cage” size (from Takeda 5A to Takeda 4A; in parallel with an enhancement of the surface-to-volume ratio) lead to slower relaxation times.

3.4. NMR diffusometry

The PFG NMR technique provides information about the pore structure via the transport properties of the adsorbed molecules. The attenuation of the NMR signal is related to the “propagator” $P(x, t)$ (the probability distribution of molecular displacements along the axis of gradient direction x during the time t) according to

$$\Psi(q, t) = \int P(x, t) \cos(qx) dx, \quad (8)$$

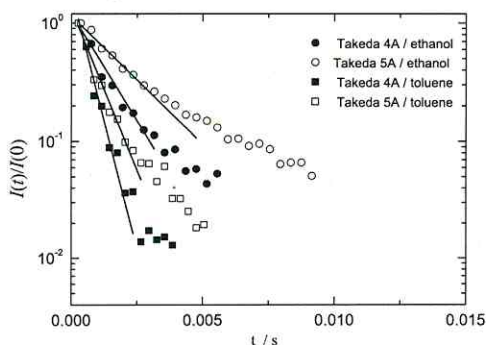


Fig. 5. Attenuation of the transverse magnetization of ethanol and toluene at 298 K confined in Takeda 4A and Takeda 5A. The attenuation curves were measured by the CPMG pulse sequence.

where $q = \gamma \delta g$, and γ is the nuclear gyromagnetic ration, with g and δ denoting the amplitude and the duration of the magnetic field gradients, respectively. In isotropic homogeneous systems, the propagator is typically represented by a Gaussian function

$$P(x, t) = (4\pi Dt)^{-1/2} \exp\left(-\frac{x^2}{4Dt}\right), \quad (9)$$

where D is the diffusion coefficient. The latter correlates the mean square displacement and time according to the Einstein equation [21] for “normal” diffusion

$$\langle x^2(t) \rangle = 2Dt. \quad (10)$$

By inserting Eq. (9) into Eq. (8), the PFG NMR signal attenuation for normal diffusion is found to be:

$$\Psi(q, t) = \exp(-q^2 t D). \quad (11)$$

For a distribution of diffusivities, a multi-exponential attenuation curve will result:

$$\Psi(q, t) = \int f(D) \exp(-q^2 t D) dD, \quad (12)$$

where $f(D)$ denotes the distribution function of diffusivities, i.e. the probability that the diffusion path of an arbitrary selected molecules during the observation time may be characterized by a diffusivity D . Depending on the size of the regions within the samples, to which these different diffusivities may be attributed, this distribution may be a function of the observation time, tending to become smaller with increasing observation time. The mean diffusivity ($\langle D \rangle$) can be evaluated from the initial slopes of the attenuation curves:

$$\langle D \rangle = - \lim_{(q^2 t) \rightarrow 0} \frac{\partial(\ln \Psi(q, t))}{\partial(q^2 t)} = \int f(D) D dD. \quad (13)$$

In this work, we investigated the diffusion of several liquids confined in MAC-LMA12. The sorbate molecules were ethanol, toluene, nitrobenzene, acetone and n-decane. As an example, Fig. 6 shows the diffusion attenuation curve for ethanol at 298 K. The observed behaviour is typical of all liquids considered. It exhibits a clear deviation from the exponential function and can tentatively be analysed in terms of two components:

$$\Psi(q, t) = \int f(D) \exp(-q^2 t D) dD + f_{\text{slow}} \exp(-q^2 t D_{\text{slow}}) \quad (14)$$

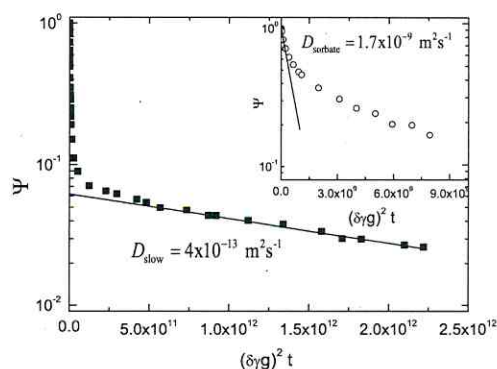


Fig. 6. Diffusion attenuation curve of ethanol in MAC-LMA12 at 298 K measured with an observation time of 10 ms (squares). D_{slow} is the minimal value of the diffusion coefficient allowed by the NMR equipment. $D_{\text{sorbate}} = \langle D \rangle$ is the mean diffusion coefficient evaluated from the initial slope of the attenuation which was obtained after subtraction of the slow component from the total attenuation curve (circles in the inset).

where f_{slow} and D_{slow} denote the relative fraction and the diffusivity of molecules contributing to the slowly attenuating component of the curve. $f(D)$ is the distribution of diffusivities related to the dominating (faster) component. (The relative fractions of the fast and slow component are normalized as $\int f(D)dD + f_{\text{slow}} = 1$). The values of f_{slow} and D_{slow} , as evaluated from the fits of the exponential function to the slow component of the curve in Fig. 6, were 0.062 and $4 \times 10^{-13} \text{ m}^2 \text{ s}^{-1}$.

The two constituents of the diffusion attenuation indicate that, over the observation time, the molecules exist in essentially two different dynamical states, as observed already above in context of nuclear magnetic relaxation. Again, we attribute the smaller fraction with the smaller diffusivities to molecules confined in the micropores and the dominating fraction with the larger diffusivities to the liquid in the mesopore space.

The faster attenuating component, obtained after subtraction of the slow component from the total attenuation is shown in the inset, Fig. 6. It exhibits a clear deviation from the exponential dependence, thus indicating a distribution of diffusivities as incorporated by the first term in Eq. (14). The mean diffusion coefficient (D) referring to the fast component was determined from the initial slope. It equals approximately $1.7 \times 10^{-9} \text{ m}^2 \text{ s}^{-1}$ and thus is four orders of magnitude larger than D_{slow} .

The slow diffusion component is to be compared with the diffusion behaviour of the same liquid in the microporous Takeda samples. Fig. 7 shows the diffusion attenuation curves of ethanol in Takeda 4A and Takeda 5A at 298 K. In Takeda 5A, the attenuation curves were exponential over the covered range of more than one order of magnitude. In Takeda 4A, the signal intensity was so small (as a consequence of the fast transverse relaxation) so that the data points could be measured only in a limited range, not below 50% of the initial amplitude. In this range, the observed attenuations were exponential as well. The diffusion coefficient of ethanol in Takeda 5A, evaluated from the exponential fits to the data points, was $8 \times 10^{-12} \text{ m}^2 \text{ s}^{-1}$. In Takeda 4A, the evaluated diffusivity was $9 \times 10^{-13} \text{ m}^2 \text{ s}^{-1}$, nearly one order of the magnitude smaller than in Takeda 5A. This finding complies with the shorter relaxation time observed in Takeda 4A and quantifies the effect of the more severe restriction to diffusion due to the smaller pores in this material, as compared with Takeda 5A.

Fig. 8 shows the diffusion attenuation curves of toluene in MAC-LMA12 for various observation times in the range between 10 ms and 300 ms. No time dependence of the attenuations was observed for both the slow and fast (see inset) components. The molecular displacements monitored in our experiments were between 60 nm for the slower component and 23 μm for the faster compo-

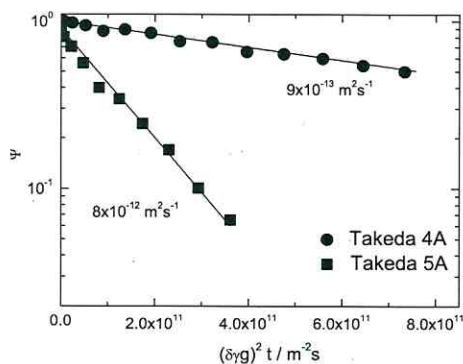


Fig. 7. Diffusion attenuation curves of ethanol in Takeda 4A and Takeda 5A at 298 K. The observation time was equal to 10 ms.

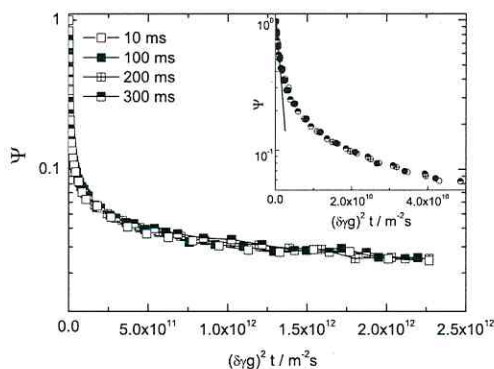


Fig. 8. Diffusion attenuation curves of toluene in MAC-LMA12 at 298 K with different observation times (10, 100, 200, 300 ms). The inset shows the fast component obtained after subtracting the slow component from the total attenuation curve. The observation time was 10 ms.

nent. On the one hand, the absence of the time dependence indicates that there is practically no exchange between the two different species as it was suggested on the basis of the relaxation studies. On the other hand, it provides evidence that the mesopores in MAC-LMA12 represent a well interconnected space, rather than a system of closed separated pores. In the latter case one would have to expect a decrease of the curve slopes with increasing observation times.

The diffusion behaviour of several liquids (acetone, ethanol, toluene, n-decane and nitrobenzene) confined in MAC-LMA12 was compared. Table 2 provides the comparison of the resulting mean diffusivities D_{sorbate} with the bulk diffusivities of these liquids D_{liquid} . Depending on the particular guest, the diffusivities within the pore system are found to be both larger and smaller than the bulk diffusivities. This finding may be related to the fact that due to the presence of the host lattice, guest diffusion may occur both in a liquid (phase 1) attached to the pore system and through the free space (phase 2). With the respective relative amounts of molecules p_1 and diffusivities D_i , the mean diffusivity as accessible by PFG NMR will result to be [22]

$$D_{\text{sorbate}} = p_1 D_1 + p_2 D_2 \quad (15)$$

The diffusivity D_1 in the free space, following gas-phase or Knudsen diffusion [9,22], is notably larger and the diffusivity D_2 in the liquid phase, due to the tortuosity of the pore space, is smaller than the diffusivity D_{liquid} in the bulk phase. Thus, depending on the relative contributions p_1 and p_2 , D_{sorbate} may in fact assume larger or smaller values than D_{liquid} . The magnitude of p_1 increases in proportion with the vapor phase pressure and, hence, also the contribution of the first term in Eq. (15). Hence, it is in complete agreement with our

Table 2

Diffusion coefficients of the liquids when confined in carbon MAC-LMA12 (D_{sorbate}) and in the bulk (D_{liquid}) and their ratio at 298 K, in comparison with their boiling temperature. The diffusion coefficient of the liquid in pores $D_{\text{sorbate}} = (D)$ is the mean value of the diffusivity in the pores and was calculated from the initial slope of the attenuation curve.

	$D_{\text{sorbate}} \times 10^{-9} \times \text{m}^2 \text{ s}^{-1}$	$D_{\text{liquid}} \times 10^{-9} \times \text{m}^2 \text{ s}^{-1}$	$D_{\text{sorbate}}/D_{\text{liquid}}$	Boiling point (°C)
Acetone	5	4.6	1.1	56.5
Ethanol	1.7	1.1	1.5	78.4
Toluene	0.6	2.3	0.26	111
n-Decane	0.24	1.4	0.17	174
Nitrobenzene	0.09	0.8	0.11	211

understanding that, as shown in Table 2, a decrease in the boiling point (which corresponds to a decrease in the vapor pressure at a given temperature) is accompanied with a decrease in D_{sorbate} . The latter, according to Eq. (15), reflects a decrease in p_1 , i.e. in the contribution of the fast (gas-phase) mode of molecular propagation.

4. Conclusions

Carbon materials containing different proportions of micro- and mesoporosity were studied. The combination of different NMR methods was used to explore the pore structure and the interaction of the adsorbate with the pore walls. Pore size distribution in samples RGC30 and MAC-LMA12 was determined by NMR cryoporometry. In MAC-LMA12, a narrow pore size distribution was observed, with a mean pore size of about 2 nm; RGC30 sample has a broad pore size distribution, centered around a mean pore size of about 7 nm. These two values reflect the differences observed in the N_2 (77 K) and CO_2 (273 K) adsorption isotherms.

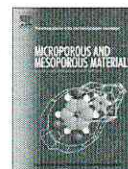
In microporous Takeda 4A, the sorbate relaxation rates were larger and the diffusivities smaller than in Takeda 5A. This evidences that sorbate molecule in Takeda 4A experience stronger restrictions in both their re-orientational and translational motions than in Takeda 5A, as a consequence of the smaller pore size of Takeda 4A. In MAC-LMA12, two molecular species with different relaxation and diffusion properties were observed. The dominating part of molecules confined in MAC-LMA12 exhibited much smaller relaxation rates and larger diffusivities than in Takeda samples. This is attributed to the presence of mesopores which tend to confine the dominating part of the liquid. Besides, diffusion experiments showed the existence of the quite broad distribution of the diffusivities. This is attributed to heterogeneities of the material on length scales notably exceeding the characteristic molecular displacements (in the range of micrometers).

Acknowledgments

Authors thank Dr. R. Valiullin and A. Khohlov for useful discussions. The work was supported by the European Network of Excellence (NoE) Inside Pores (NMP3-CT2004-500895). Financial support from Project (MAT2007-61734) is acknowledged.

References

- [1] H. Marsh, F. Rodriguez-Reinoso, Activated Carbon, Elsevier, London, 2006.
- [2] F. Rodriguez-Reinoso, J.M. Martin-Martinez, M. Molina-Sabio, R. Torregrosa, J. Garrido-Segovia, J. Colloid Interface Sci. 106 (1985) 315.
- [3] J.C. Gonzalez, M.T. Gonzalez, M. Molina-Sabio, F. Rodriguez-Reinoso, A. Sepúlveda-Escribano, Carbon 33 (1995) 1175.
- [4] M. Molina-Sabio, F. Rodriguez-Reinoso, Colloids and Surfaces A: Physicochem. Eng. Aspects 241 (2004) 15.
- [5] R. Ryoo, S. Hoon Joo, S. Jun, J. Phys. Chem. B 103 (1999) 7743.
- [6] C. Liang, S. Dai, J. Am. Chem. Soc. 128 (2006) 5316.
- [7] J.M. Juárez-Galán, A. Silvestre-Albero, J. Silvestre-Albero, F. Rodriguez-Reinoso, Microp. Mesop. Mater. 117 (2009) 519.
- [8] F. Rodriguez-Reinoso, M. Molina-Sabio, Adv. Colloid Interface Sci. 76–77 (1998) 271.
- [9] J. Kärger, D.M. Ruthven, Diffusion in Zeolites, Wiley & Sons, New York, 1992.
- [10] J. Mitchell, S.C. Stark, J.H. Strange, J. Phys. D: Appl. Phys. 38 (2005) 1950.
- [11] R.M.E. Valckenborg, L. Pel, K. Kopinga, J. Phys. D: Appl. Phys. 35 (2002) 249.
- [12] J. Garrido, A. Linares-Solano, J.M. Martin-Martinez, M. Molina-Sabio, F. Rodriguez-Reinoso, R. Torregrosa, Langmuir 3 (1987) 76.
- [13] P. Galvosas, F. Stallmach, G. Seiffert, J. Kärger, U. Kaess, G. Majer, J. Magn. Reson. 151 (2) (2001) 260.
- [14] F. Rodriguez-Reinoso, J. Garrido, J.M. Martin-Martinez, M. Molina-Sabio, R. Torregrosa, Carbon 27 (1989) 23.
- [15] R.V.R.A. Rios, J. Silvestre-Albero, A. Sepúlveda-Escribano, M. Molina-Sabio, F. Rodriguez-Reinoso, J. Phys. Chem. C 111 (2007) 3803.
- [16] J.H. Strange, M. Rahman, E.G. Smith, Phys. Rev. Lett. 71 (1993) 3589.
- [17] C.L. Jackson, G.B. McKenna, J. Chem. Phys. 93 (1990) 9002.
- [18] K. Brownstein, C. Tarr, Phys. Rev. A 19 (1979) 2446.
- [19] H. Carr, E. Purcell, Phys. Rev. 94 (1954) 630.
- [20] M. Cohen, K. Mendelson, J. Appl. Phys. 53 (1982) 1127.
- [21] A. Einstein, Ann. Phys. 17 (1905) 549.
- [22] J. Kärger, H. Pfeifer, W. Heink, Adv. Magn. Reson. 12 (1988) 2.



The evidence of NMR diffusometry on pore space heterogeneity in activated carbon

F. Furtado^{a,b}, P. Galvosas^{b,c}, M. Gonçalves^d, F.-D. Kopinke^a, S. Naumov^b, F. Rodríguez-Reinoso^d, U. Roland^a, R. Valiullin^{b,*}, J. Kärger^b

^a Department of Environmental Engineering, UFZ – Helmholtz-Centre for Environmental Research, Permoserstr. 15, 04318 Leipzig, Germany

^b Department of Interface Physics, University of Leipzig, Linnéstr. 5, D-04103 Leipzig, Germany

^c School of Chemical and Physical Sciences, Victoria University of Wellington, P.O. Box 600, Wellington 6140, New Zealand

^d Departamento de Química Inorgánica, Universidad de Alicante, Apartado 99, 03080 Alicante, Spain

ARTICLE INFO

Article history:

Received 10 June 2010

Received in revised form 11 November 2010

Accepted 12 November 2010

Available online 19 November 2010

Keywords:

PFG NMR

Diffusion

Activated carbon

Pore heterogeneity

ABSTRACT

With the advent of nanoporous materials with hierarchical pore structure, pore space exploration becomes an increasingly complex task which depends on the successful inclusion of novel techniques of sample characterization, in addition to the established ones. We present the results of an in-depth pulsed field gradient (PFG) NMR study of guest diffusion in an activated carbon with a two-modal pore structure (MA2). The pronounced distribution of the local diffusivities is taken as an indication of notable sample heterogeneities. The options of their further characterization by intentionally varying the parameters and conditions of the diffusion measurements are discussed.

© 2010 Elsevier Inc. All rights reserved.

1. Introduction

Diffusion, i.e., the irregular movement of atoms and molecules, is among the fundamental and omnipresent phenomena in nature and technology and occurs in all states of matter. A particular fascination is provided with systems where the sizes of the diffusing molecules are comparable with the characteristic length scale of the host systems by which they are accommodated. This is in particular true for mass transfer in nanoporous materials [1]. Their technological benefit is based on the compatibility of their pore diameters with the size of the guest molecules, by which either catalytic conversion or adsorptive separation is exploited for the generation of value-added products [2,3]. Equally important, the similarity of molecular and pore diameters gives rise to numerous phenomena of fundamental relevance for soft-matter interaction with solid surfaces [4,5], in particular for a better understanding of the conditions for molecular reorientation and redistribution under confinement [6–8].

Being determined by the pore architecture, the rate of molecular propagation may – in turn – be considered as a source of information about pore architecture. In the present study, we have explored these potentials by the application of the pulsed field gradient technique of nuclear magnetic resonance (PFG NMR) to

studying molecular diffusion of cyclohexane in an activated carbon with a two-modal pore structure (MA2). The potentials of PFG NMR for this type of studies are based on two unique properties of this technique. Being able to directly record the probability of molecular displacements during well-defined time intervals (of typically milliseconds till seconds), PFG NMR provides direct information about the rate of molecular propagation (the diffusivity) over distances from about 100 nm to 100 μm [9,10]. In addition, PFG NMR may as well distinguish whether this rate is uniform or whether, over the whole of the sample, there is a distribution of the local propagation patterns giving rise to a sample-related distribution of local diffusivities [11,12]. We are going to exploit this distribution of local diffusivities as a measure of sample heterogeneity.

2. Experimental

2.1. The sample under study

The carbon MA2 (see Fig. 1) has been prepared by carbonisation and subsequent CO₂-activation (43% activation burn-off) of a spherical porous resin obtained by cross-linking of phenol–formaldehyde Novolac precursor with hexamethylenetetramine and with ethylene glycol as solvent – pore former [13]. Fig. 2 shows the N₂ adsorption, at 77 K. The high N₂ uptake at P/P_0 values below 0.1 and over 0.8, reveal high micro- and mesoporosity, each one occupying approximately 50% of total pore volume.

* Corresponding author.

E-mail address: valiullin@uni-leipzig.de (R. Valiullin).

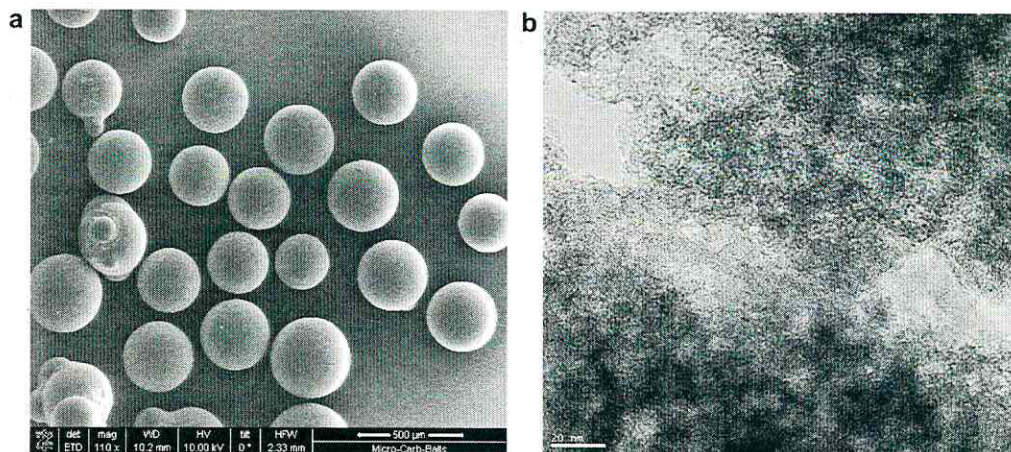


Fig. 1. (a) SEM picture of the carbon particles. (b) TEM picture where both micropore and mesopore structures can be seen.

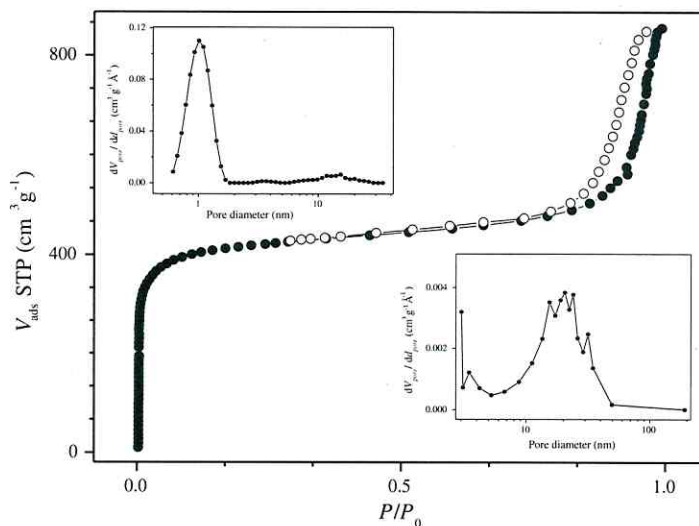


Fig. 2. N₂ adsorption isotherm at 77 K for the carbon sample under study, with closed and open symbols corresponding to the adsorption and desorption branch, respectively. P₀ corresponds to the N₂ saturated vapour pressure at 77 K. The inserts show the micropore and mesopores pore size distribution (upper left side and lower right side, respectively) as obtained by DFT (micropore distribution) and BJH (mesopores distribution).

2.2. PFG NMR diffusion studies

The PFG NMR diffusion studies have been performed with the 13-interval pulse sequence [14] at a proton resonance frequency of 125 MHz by means of the home-built PFG NMR diffusion spectrometer FEGRIS NT [15,16]. Assuming isotropic, normal diffusion and separation times *t* (between the two gradient pulse pairs, determining the “observation” time) notably exceeding those between one gradient pulse pair, the attenuation of the NMR signal (the “spin echo”) obeys Eq. (1) [9,14–16]

$$\Psi(t, g\delta) = \exp(-\gamma^2(2\delta)^2g^2Dt), \tag{1}$$

with *g* and δ denoting the amplitude and the duration of one magnetic field gradient pulse and with γ denoting the gyromagnetic ra-

tio ($2.675 \times 10^8 \text{ T}^{-1}\text{s}^{-1}$ for hydrogen). The self-diffusivity *D* is related by the Einstein equation [6,17]

$$\langle x^2(t) \rangle = 2Dt \tag{2}$$

to the mean squared molecular displacement $\langle x^2(t) \rangle$ in gradient direction during the observation time *t*. Eq. (1) implies homogeneity of the sample under study with respect to a length scale of the order of the molecular displacements under study [18]. This means that, on the average, the probe molecules “experience” the identical pore space on their trajectories during the PFG NMR experiments. If the system deviates from this requirement, instead of Eq. (1) one has to consider

$$\Psi(t, g\delta) = \int_0^\infty p(D) \exp(-\gamma^2(2\delta)^2g^2Dt) dD, \tag{3}$$

where $p(D)dD$ denotes the probability that the diffusivity of the guest molecules within an arbitrarily selected space element (of the order of the considered displacements) is within the interval $D \dots D + dD$. More correctly, one has even to take into account that, due to differences in the nuclear magnetic relaxation times [9,15,16], not only the diffusivities but also the contribution of the molecules to the observed PFG NMR signal from different sample regions may be different. Hence, the function $p(D)$ must be considered to be weighted by differences in the relaxation properties of the different sample regions.

If the PFG NMR signal attenuation follows Eq. (1) a semi-logarithmic plot of the signal intensity versus $\gamma^2(2\delta)^2g^2t$ yields a straight line with the diffusivity as its negative slope. In isotropic systems – as in the case considered, deviations from linearity may indicate deviations from sample homogeneity. This becomes especially true when this deviation will not depend on the observation time t . In this case, the mean diffusivity can be derived from the initial slope of the semi-logarithmic plot of the signal intensity, i.e., for sufficiently small values of $\gamma^2(2\delta)^2g^2t$. We shall extensively make use of this option.

The experimental data as acquired with the PFG NMR technique may be described by a log-normal distribution of diffusion coefficients [19,20]

$$p(D) = \frac{1}{D\sigma\sqrt{2\pi}} \exp\left[-\frac{(\ln D - \ln D_0)^2}{2\sigma^2}\right]. \quad (4)$$

Here, D_0 denotes the median of the diffusivity and σ gives the multiplicative standard deviation, which can empirically be correlated to the degree of heterogeneity of the system under study. It has to be noted that we do not have any particular arguments in favour of Eq. (4), except that it reasonably reproduces the experimental data and has a relatively simple meaning. The obtained parameters D_0 and σ are used to characterize the properties of the diffusion process under study regardless of its actual nature.

For the PFG NMR diffusion studies, a given amount of the host material was filled into sample tubes of 7.5 mm outer diameter and heated in an oven to 383 K in contact with the atmosphere over 24 h. Subsequently, the samples were connected to a vacuum system and dehydrated under high vacuum (of less than 10^{-2} Pa)

at 523 K for around 4 h. After cooling down, the sample was connected to a vessel of known volume, with a given vapour pressure of the diffusant, corresponding to the desired loading amount. After loading was complete, the sample was then cooled to the temperature of liquid nitrogen thus allowing the sealing of the sample.

3. Results and discussion

Irrespective of their great technological relevance, molecular diffusion in activated carbons has never been investigated with the same effort compared to the study of diffusion in zeolites [21]. This is mainly related to the fact that, in contrast to zeolites, activated carbon is not available in the form of well-shaped crystallites. In conventional uptake and release studies this complicates or even excludes the transformation of the directly observable rate constants into well-defined diffusivities. Though, as a technique sensitive to the rate of molecular transportation in the particle interior, PFG NMR is not affected by this complication, its application is severely handicapped by the generally very short transverse nuclear magnetic relaxation times of these materials. Hence, owing to recent improvement of the PFG NMR methodology and the increasing amount of novel structure types also in the field of activated carbons [22], only very recently [23] PFG NMR diffusion studies have been performed with NMR signal attenuations over more than one order of magnitude. There, for the first time, together with the present work indications for a deviation of the attenuation function from the simple exponential dependence as predicted by Eq. (1) for diffusion in a homogeneous system could be observed, opposing previous ones in related systems [24,25].

3.1. Distribution of guest diffusivities in activated carbon of type MA2

Fig. 3 displays the PFG NMR attenuation curve of cyclohexane in MA2 at room temperature for 100% pore filling and an observation time of $t = 10$ ms. The curve is shown to be nicely approximated by Eq. (3) with a distribution function of the local diffusivities as given by Eq. (4). During the fitting procedure, variation of the

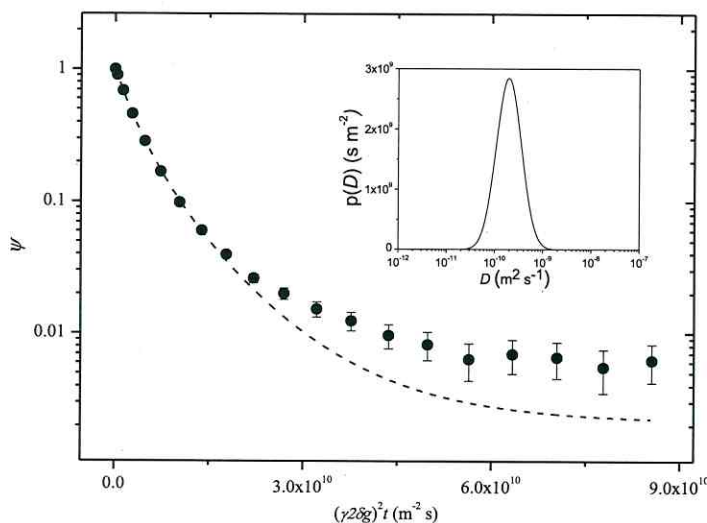


Fig. 3. Spin-echo attenuation of cyclohexane in a fully loaded MA2 sample, at 298 K ($t = 10$ ms) and best fit by Eq. (3), assuming a log-normal distribution of diffusion coefficients (Eq. (4)). The insert shows the distribution of the diffusion coefficients (Eq. (4)).

signal-to-noise ratios (S/N) from 125 to 500 produced the respective variation of resulting D_0 and σ of less than 1% and 9%, respectively. The results presented do refer to S/N inferred from the experimental data which is about 475. Best fit is attained with $D_0 = (2.80 \pm 0.03) \times 10^{-10} \text{ m}^2\text{s}^{-1}$ and a distribution width $\sigma = 0.60 \pm 0.02$. With these parameters it is possible to calculate the average diffusion coefficient $D_m = D_0 e^{\sigma^2/2}$, yielding $D_m = 3.36 \times 10^{-10} \text{ m}^2\text{s}^{-1}$, which would as well follow via Eq. (1) from the slope of the initial decay of the attenuation curve.

With Eq. (4), this result is easily seen to be equivalent with the statement that 68.3% of the measured diffusion coefficients fall into the interval $[D_m/\sigma, D_m/\sigma]$ i.e., $[2.0 \times 10^{-10}, 5.6 \times 10^{-10} \text{ m}^2\text{s}^{-1}]$. Inserting this result into Eq. (2) yields an interval of the square root of mean square displacement considering the range of observation times used from 2.0 to 3.3 μm .

It is noteworthy to emphasize that the diffusion path lengths and, hence, the extensions of these regions are much larger than the diameters of both the micro- and mesopores. The trajectories of all molecules considered will, therefore, consist of displacements within both the micropores and macropores. The diffusivities of molecules confined to pore spaces are known to depend on numerous influences, including the nature of the pore surface, the pore diameters and the tortuosity of the pore space. In the subsequent sections we are going to describe different series of experiments while changing selected influences as a parameter. It is our aim to specify the possible origin of the particular distribution in the diffusivities by exploring the influence of these variations on the resulting diffusivities.

3.2. Variation of the observation time

If one varies the observation time for a diffusion experiment the range of molecular displacement will change until the diffusion path is obstructed. Without obstruction, the mean square displacement will increase according to Eq. (2) and the distribution of diffusion becomes time independent. Fig. 4a represents the spin-echo decays for an observation time range of 5–250 ms. The shape of the echo attenuation, which holds the information on the diffusion coefficient distribution is identical for all observation times within the accuracy of the acquired NMR data. We therefore conclude that the sample morphology is homogeneous for subregions of 2–13 μm , since no observation time dependence for the corresponding mean square displacements from 3 to 170 μm^2 were observed (see Fig. 4b for the linear increase of $\langle x^2 \rangle$ with increasing observation time, as given by Eq. (2)).

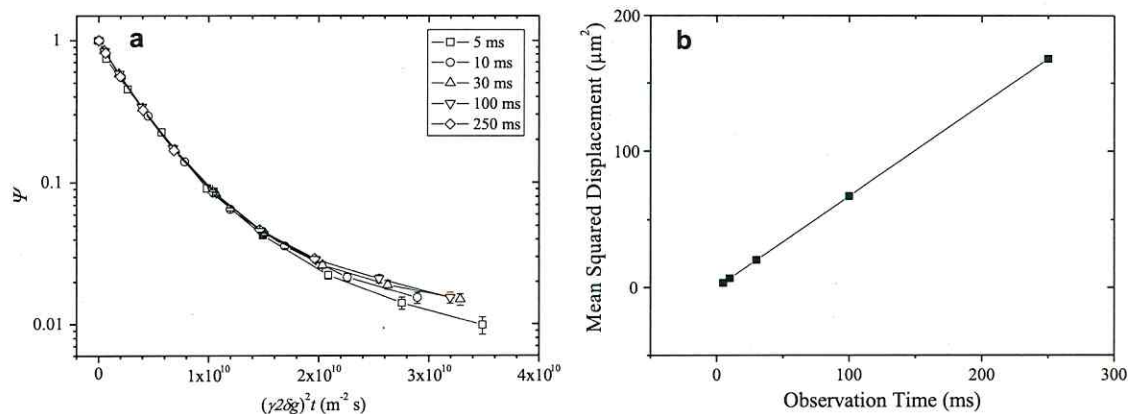


Fig. 4. (a) Spin-echo attenuation of cyclohexane in a fully loaded MA2 sample, at 298 K for different observation times (t) and (b) mean squared displacement for the respective observation times.

As a result, even with the largest diffusion path lengths attainable in the present diffusion studies no change in the distribution function of the resulting local diffusivities could be observed. This means that the correlation lengths of sample homogeneity, i.e., the distance after which a notable change in the host structure will have occurred, have to be much larger than these distances.

3.3. Variation of particle sizes

After the estimate of a lower limit of the correlation length, one may also consider the opposite limiting case, i.e., whether the individual particles (with diameters between 0.15 and 0.50 μm , see Fig. 1) are essentially homogeneous (i.e., with homogeneity correlation lengths notably exceeding their diameters) and that the distribution in the observed diffusivity is caused by a distribution in the structural properties (and, hence, in the diffusion properties) from particle to particle. Their small size prohibits PFG NMR diffusion measurements with each individual host particle.

This problem may be circumvented, however, if the structural peculiarities are correlated with the particle sizes. For the exploration of this option, we have compared the diffusivities in samples containing different particle size fractions. The resulting attenuation plots are shown in Fig. 5. Again, in all samples the attenuation plots and, hence, the distribution functions for the local diffusivities are found to be essentially identical. Hence, any correlation between the size of the host particles and their structural properties may be excluded.

3.4. Variation of the impact of nuclear magnetic relaxation

The distribution in the diffusivities has to be referred to locally varying properties of the host structure. For the exploration of their nature, it would be interesting to find out whether these variations in the host structure give also rise to a distribution of further key parameters of the host-guest system, in addition to the guest diffusivities. In this context, the nuclear magnetic relaxation times are of particular interest since they are known to depend very sensitively on the pore sizes and the pore wall chemistry, generally decreasing with increasing surface-to-volume ratios [5,26]. If the variation in the diffusivities is caused by corresponding variations in the pore geometry and pore wall chemistry, one should, therefore, expect correlations between the diffusivities and nuclear magnetic relaxation times.

Fig. 6 displays PFG NMR attenuation curves where the signal intensity has been modified by dramatically changing the

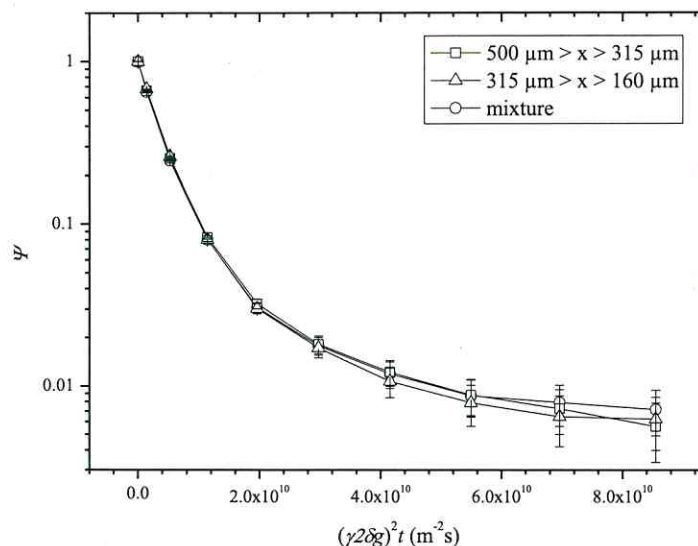


Fig. 5. Effect of particle size on the spin-echo attenuation of cyclohexane in fully loaded samples, at 298 K ($t = 10$ ms).

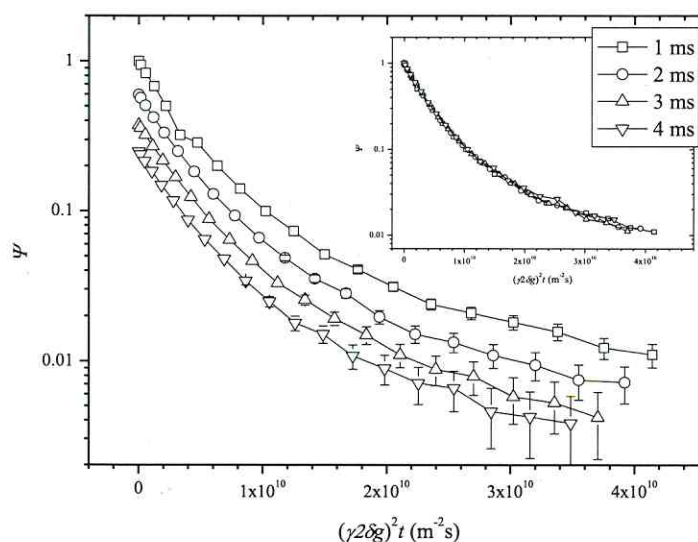


Fig. 6. Spin-echo attenuation of cyclohexane in a fully loaded sample, with different T_2 relaxation windows (variation of the interval between the pair of gradients with opposite sign in the 13-interval pulse sequence [14]). The insert shows the same data, normalized to the echo intensity for the lowest gradient used, for each data set.

contributions of the two nuclear magnetic relaxation mechanisms. Keeping the observation time (and, hence, the time interval relevant for longitudinal nuclear magnetic relaxation) approximately constant, the PFG NMR pulse sequence was modified in such a way that the time interval relevant for transverse nuclear magnetic relaxation was increased by a factor of four (which, in effect, has led to a decrease of the NMR signal (the spin echo) by about one order of magnitude). Note, that we have negligible influence of T_1 on the signal intensity for the parameter variations in these experiments. Fig. 6 shows that this significant variation in the contributions of the two relaxation mechanisms did not yield any

perceptible effect on the shape of the attenuation curve. This means that the contributions of the regions with different diffusivities have in no way been affected by the variation in the weights of the relaxation mechanisms. It is therefore unlikely that the differences in the diffusivities are correlated with a corresponding variation in the pore geometry and pore wall chemistry.

3.5. Variation of substrate loading and temperature

The host material under study is known to contain interpenetrating networks of micro- and mesopores as illustrated in section

2.1. Molecular propagation over distances of micrometers as relevant for the PFG NMR measurements, includes therefore displacements in both pore spaces. The contribution of molecular migration in either of these spaces to the overall mass transfer through the host particles as recorded by PFG NMR depends on both the loading and the temperature of measurement. It is, therefore, worthwhile to explore up to which extent the distribution in the diffusivities is affected by a variation of loading and temperature, in particular the effect of these on the liquid–solid phase transition of geometrically confined cyclohexane.

As an example, fig. 7 shows the PFG NMR attenuation curves for cyclohexane at four different temperatures and for pore loadings varying from 20% to complete saturation. For better comparability, the attenuation curves have been plotted versus $g^2 t D_m$ so that differences in the attenuation curves caused by differences in the absolute values of the diffusivities are compensated. For both the measurements at 0–40 °C, the shape of the attenuation curve is found to remain essentially unaffected by increasing the loading from the lowest value of 20% (where the mesopores are essentially empty) up to complete saturation. The distribution in the diffusivities is thus found to remain unchanged, irrespective of the dramatic difference in the nature of the pore spaces involved.

This finding is complementary to the message of the diffusion studies with varying impact of nuclear magnetic relaxation in sec-

tion 3.4. Irrespective of a significant variation of the contribution of the two pore spaces to overall mass transfer, the shape of the PFG NMR attenuation curves, and hence the distribution of the diffusivities, is found to remain essentially unchanged. One has to exclude, therefore, the possibility that the variation in the diffusivities over the sample may be attributed to a variation of the ratio of the local meso- and microporosity over the sample. In this case, the transition from dominating micro- to dominating mesopore transport should lead to much more distinct changes in the diffusivity distributions.

It is interesting to note that the compatibility in the attenuation curves for different loadings is not preserved with further temperature decrease. At –20 °C, after coinciding in their initial slopes (as the consequence of the unifying representation vs. $g^2 t D_m$), the attenuation curve of the fully saturated sample is found to notably deviate from those with lower loadings, yielding a progressively decreasing slope. With Eqs.(1) and (3), this finding has to be attributed to molecules with notably reduced diffusivities. Fig. 8 compares the relative intensity of the first spin echo, at different temperatures and corresponding loadings. Samples with lower loadings where mesopores remain partially empty (20% and 50%), are less affected by temperature decrease whereas more saturated samples reveal a drastic dependency on temperature. For rationalizing such a behaviour we have to recognize that the

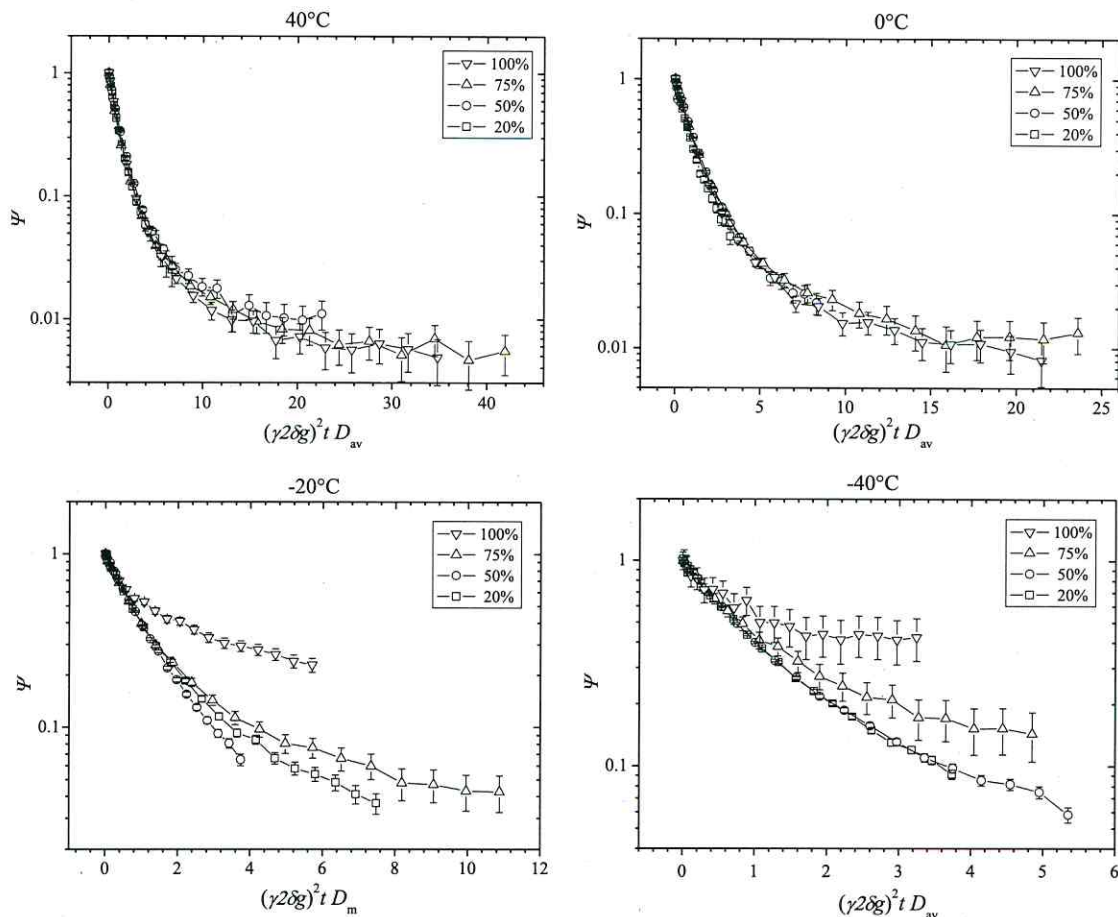


Fig. 7. Influence of temperature on cyclohexane spin-echo attenuation, for different loadings.

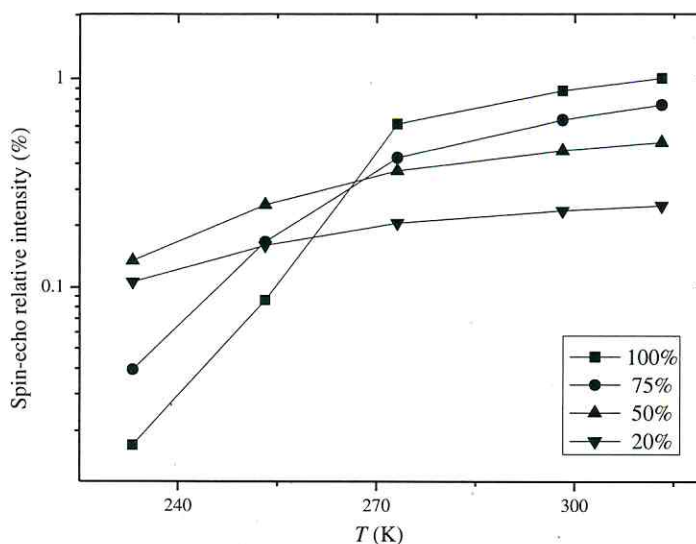


Fig. 8. Temperature dependency of the relative intensity of the first echo of the 13-interval pulse sequence, for different loadings. The intensities are normalized to the value obtained for the fully loaded sample at 313.15 K.

suppression of the freezing point T_f in pores of diameter d from the bulk value T_{fb} (6.6 °C for cyclohexane) is related by following the Gibbs–Thompson equation [27,28].

$$T_f = T_{fb} - K/d, \quad (5)$$

where K is a calibration constant, characteristic of the system under study. Consequently, the phase change will occur at larger pores, which severely reduces the transverse relaxation time, thus suppressing the contribution of the frozen phase to the overall signal intensity. This can clearly be observed on the steep decrease in signal intensity from 0 to –20 °C. Indeed, in the fully saturated sample, a large fraction of the liquid in the mesopores is already frozen (signal intensity loss of about 80%). At these low temperatures, it is important to note that the spin-echo signal intensity on Fig. 8, represents almost exclusively the liquid in the micropores, due to sufficiently short transverse relaxation times in mesopores, at these high loadings. This effect is more pronounced with decreasing temperatures, with the additional solid phase leading to an additional confinement of the remaining fluid phase, reflected by a decrease not only in the transverse relaxation time but also in the diffusivities in these regions and thus in the decaying slope of the PFG NMR signal attenuation curve. In complete agreement with this reasoning, at –40 °C this effect is found to be even more pronounced since now the freezing process is extended to smaller mesopores, leading to an even larger effect of confinement for the remaining fluid phase.

4. Conclusions

With cyclohexane as probe molecules, molecular diffusion in activated carbon MA2 revealed a broad distribution of the local diffusivities as recorded by PFG NMR measurements sensitive to root mean square displacements of up to 13 μm . This distribution was found to remain essentially unaffected by significant variations in the measuring conditions, including observation time, substrate loading, the conditions of nuclear magnetic relaxation and temperature. Deviations below the bulk freezing temperature may be easily referred to an extra-confinement due to the additionally formed

frozen phase. We tentatively attribute the observed distribution of diffusivities to internal transport barriers as observed in zeolites. It is – just due to the observed invariance of the attenuation curves with the experimental conditions – even rather unlikely that this variance is correlated with some local properties of the pore system (such as the mean pore diameters, the pore wall chemistry or the relative density of the micro- and macropores) with correlation lengths of at least the considered displacements of about 10 μm . With its well established application to biological systems [29–31] Fourier transformed q -space plots may be regarded as an alternative methodology for providing further information on the present system, as it also provides information on the micrometer range.

One can rationalize that in addition to the influence of the “regular” pore space, the rate of molecular migration may be affected by further influences, including transport resistances in the form of planes of reduced permeability traversing the host bulk phase. In zeolites, the existence of such “internal transport barriers” has been suggested long time ago to explain the discrepancy between the results of micro- and macroscopic diffusion measurements [32]. Very recently [33], the occurrence of such resistances could be directly evidenced in comparative studies by transmission electron microscopy and PFG NMR diffusion measurements. While it is premature to attribute the observed behaviour in the present case of activated carbon to these additional resistances, as found in zeolites, it may provide an explanation to the experimental evidence and, therefore, be acceptable as a working hypothesis.

Acknowledgements

Financial support from Marie Curie Early Stage Training Program “Risk Assessment and Environmental Safety Affected by Compound Bioavailability in Multiphase Environments” (RAISE-BIO) and by the Deutsche Forschungsgemeinschaft in the frame of the International Research Training Group “Diffusion in Porous Materials” is gratefully acknowledged. We also thank Dr. José Luis Barzola Quiquia for the SEM picture presented in this work.

References

- [1] F. Schuth, K.S.W. Sing, J. Weitkamp, *Handbook of Porous Solids*, Wiley-VCH, Weinheim, Germany, 2002.
- [2] D.M. Ruthven, in: J. Kärger (Ed.), *Leipzig, Einstein, Diffusion*, Leipziger Univ.-Verl., Leipzig, 2010, pp. 123–143.
- [3] J. Weitkamp, *Catalysis and Zeolites: Fundamentals and Applications*, Springer, New York, 1999.
- [4] F. Feil, C. Jung, J. Kirstein, J. Michaelis, C. Li, F. Nolde, K. Müllen, C. Bräuchle, *Micropor. Mesopor. Mater.* 125 (2009) 70–78.
- [5] N. Nestle, A. Kühn, K. Friedemann, C. Horch, F. Stallmach, G. Herth, *Micropor. Mesopor. Mater.* 125 (2009) 51–57.
- [6] D.M. Ruthven, in: H.G. Karge, J. Weitkamp (Eds.), *Adsorption and Diffusion*, Springer, Berlin, Heidelberg, 2008, pp. 1–43.
- [7] J.R. Sangoro, A. Serghei, S. Naumov, P. Galvosas, J. Kärger, C. Wespe, F. Bordusa, F. Kremer, *Phys. Rev. E* 77 (2008) 051202.
- [8] K. Seehamart, T. Nanok, R. Krishna, J.V. Baten, T. Remsungnen, S. Fritzsche, *Micropor. Mesopor. Mater.* 125 (2009) 97–100.
- [9] J. Kärger, in: H.G. Karge, J. Weitkamp (Eds.), *Adsorption and Diffusion*, Springer, Berlin, Heidelberg, 2008, pp. 85–133.
- [10] B. Blümich, in: *Essential NMR for Scientists and Engineers*, Springer, Berlin, 2005.
- [11] P.T. Callaghan, S. Godefroy, B.N. Ryland, *Magn. Reson. Imaging* 21 (2003) 243–248.
- [12] P.T. Callaghan, S. Godefroy, B.N. Ryland, *J. Magn. Reson.* 162 (2003) 320–327.
- [13] S.R. Tennison, O.P. Kozynchenko, V.V. Strelko, A.J. Blackburn, *Porous Carbons*, US 2004/0024074 A1.
- [14] R. Cotts, M. Hoch, T. Sun, J. Markert, *J. Magn. Reson.* 83 (1989) 252–266.
- [15] F. Stallmach, P. Galvosas, *Annu. Rep. NMR Spectrosc.* 61 (2007) 51–131.
- [16] P. Galvosas, F. Stallmach, G. Seiffert, J. Kärger, U. Kaess, G. Majer, *J. Magn. Reson.* 151 (2001) 260–268.
- [17] J. Kärger, *Leipzig, Einstein, Diffusion*, Leipzig: Leipziger Univ.-Verl., 2007.
- [18] J. Kärger, S. Vasenkov, *Micropor. Mesopor. Mater.* 85 (2005) 195–206.
- [19] M. Nydén, O. Söderman, *Macromolecules* 31 (1998) 4990–5002.
- [20] G. Fleischer, F. Rittig, J. Kärger, C.M. Papadakis, K. Mortensen, K. Almdal, P. Štěpánek, *J. Chem. Phys.* 111 (1999) 2789.
- [21] J. Kärger, H.G. Karge, J. Weitkamp, *Adsorption and Diffusion*, Springer, Berlin, Heidelberg, 2008.
- [22] F. Rodríguez-Reinoso, H. Marsh, *Activated Carbon*, Amsterdam, Boston: Elsevier, 2006.
- [23] M. Krutyeva, F. Grinberg, F. Furtado, P. Galvosas, J. Kärger, A. Silvestre-Albero, A. Sepulveda-Escribano, J. Silvestre-Albero, F. Rodríguez-Reinoso, *Micropor. Mesopor. Mater.* 120 (2009) 91–97.
- [24] M. Dubinin, R. Vartapetian, A. Voloshchuk, J. Karger, H. Pfeifer, *Carbon* 26 (1988) 515–520.
- [25] J. Kärger, H. Spindler, *J. Am. Chem. Soc.* 113 (1991) 7571–7574.
- [26] K. Brownstein, C. Tarr, *Phys. Rev. A* 19 (1979) 2446–2453.
- [27] R. Valiullin, S. Naumov, P. Galvosas, J. Kärger, H. Woo, F. Porcheron, P.A. Monson, *Nature* 443 (2006) 965–968.
- [28] J. Strange, M. Rahman, E. Smith, *Phys. Rev. Lett.* 71 (1993) 3589–3591.
- [29] P.W. Kuchel, T.R. Eykyn, D.G. Regan, *Magn. Reson. Med.* 52 (2004) 907–912.
- [30] A. Bar-Shir, Y. Cohen, *NMR Biomed.* 21 (2008) 165–174.
- [31] G. Pages, T.W. Yau, P.W. Kuchel, *Magn. Reson. Med.* 64 (2010) 645–652.
- [32] J. Kärger, D.M. Ruthven, *Zeolites* 9 (1989) 267–281.
- [33] A. Feldhoff, J. Caro, H. Jobic, J. Ollivier, C.B. Krause, P. Galvosas, J. Kärger, *Chem. Phys. Chem.* 10 (2009) 2429–2433.

Tracing Pore-Space Heterogeneities in X-Type Zeolites by Diffusion Studies

Ziad Adem,[†] Jürgen Caro,[‡] Filipe Furtado,[†] Petrik Galvosas,^{†,§} Cordula B. Krause,[†] and Jörg Kärger^{*,†}[†]Department of Interface Physics, University of Leipzig, Linnéstrasse 5, 04103 Leipzig, Germany.[‡]Institute of Physical Chemistry and Electrochemistry, Leibniz University Hanover, Callinstrasse 3-3A, 30167 Hannover, Germany, and [§]MacDiarmid Institute for Advanced Materials and Nanotechnology, School of Chemical and Physical Sciences, Victoria University of Wellington, PO Box 600, Wellington, New Zealand

Received September 23, 2010. Revised Manuscript Received November 10, 2010

Pore-space homogeneity of zeolite NaX was probed by pulsed field gradient (PFG) NMR diffusion studies with *n*-butane as a guest molecule. At a loading of 0.75 molecules per supercage, a wide spectrum of diffusivities was observed. Guest molecules in the (well-shaped) zeolite crystallites were thus found to experience pore spaces of quite different properties. After loading enhancement to 3 molecules per supercage, however, molecular propagation ideally followed the laws of normal diffusion in homogeneous media. At sufficiently high guest concentrations, sample heterogeneity was thus found to be of no perceptible influence on the guest mobilities anymore.

Introduction

The introduction of novel synthesis concepts¹ and the refinement of established ones^{2–4} to attain transport-optimized nanoporous materials led to unprecedented options of their technological application in mass separation and heterogeneous catalysis.⁵ As one of the rate-limiting processes during application, molecular diffusion in such systems has become one of the favorite subjects of investigation.⁶ Thus, it was observed that the bulk phase of zeolite crystallites may notably deviate from the ideal textbook structure. By varying the “observation” time of the measurements, the intracrystalline space was found to be traversed by transport resistances which led to decreasing “effective” diffusivities; the larger displacements are followed in the experiments.^{7–9} Deviating from the “conventional” view that, if at all, additional transport barriers may only occur as “surface barriers”,^{10,11} diffusion studies provided severe evidence of the possibility that such transport resistances, acting in addition to the “drag” exerted by the genuine pore space, may also occur in the crystal interior. Recent high-resolution transmission electron microscopy investigations¹² revealed stacking faults of mirror-twin type on (111)-type planes of the cubic framework of FAU-type zeolites. By the detection of

these faults, for the first time direct evidence of deviations in the structural homogeneity of zeolites was provided which, so far, could only be suggested as a possible hypothesis for explaining the discrepancy between “macroscopic” and “microscopic” diffusivities.¹³

Recently, the pulsed field gradient (PFG) technique of NMR¹⁴ has been applied to diffusion studies in mesoporous host–guest systems. The guest diffusivities could be exploited as a most sensitive probe of the molecular configurations in pore space, exhibiting quite different features in dependence on loading, temperature, and sample “history”. In the present investigation, we have benefited from these special features of PFG NMR by evaluating the deviations from sample homogeneity in detailed diffusion studies with *n*-butane as a probe molecule in large crystals of zeolite NaX.

Materials and Methods

Sample Synthesis and Characterization. The giant X-type zeolite crystals were synthesized following a modified Charnell procedure.¹⁵ The gel composition 1.7 Na₂O:Al₂O₃:1.3 SiO₂:300 H₂O:10 triethanolamine gave after 5 weeks crystallization at 85 °C 70–80 μm large crystals (Figure 1a). To adjust the reactivity of the silicate and aluminate species, metallic aluminum and colloidal silica (LUDOX) have been used. All solutions were filtered using Millipore filters (0.22 μm); the starting hydrogels were prepared at 0 °C and quickly heated to crystallization temperature. Powder X-ray diffraction (Figure 1b) proves the high crystallinity of the X-type crystals prepared (for comparison see ref 16). This high crystallinity does as well appear in the well-shaped form of the crystals (Figure 1a).

PFG NMR Diffusion Studies. The diffusion measurements were performed by means of the home-built PFG NMR spectrometer FEGRIS 400¹⁷ with the 13-interval pulse sequence.¹⁸ In this

*Corresponding author. Tel: +49 341 9732502. Fax: +49 341 9732549. E-mail: kaerger@physik.uni-leipzig.de.

(1) Kaskel, S. In *Handbook of Porous Solids*; Schüth, F., Sing, K. S. W., Weitkamp, J., Eds.; Wiley-VCH: Weinheim, 2002; Vol. 2, pp 1190–1249.

(2) Choi, M.; Srivastava, R.; Ryou, R. *Chem. Commun.* **2006**, 4380–4382.

(3) Sel, O.; Kuang, D.; Thommes, M.; Smarsly, B. *Langmuir* **2006**, *22*, 2311–2322.

(4) Sun, L. H.; Shan, Z.; Maschmeyer, T.; Coppens, M. O. *Langmuir* **2003**, *19*, 8395.

(5) Ertl, G.; Knözinger, H.; Schüth, F.; Weitkamp, J. *Handbook of Heterogeneous Catalysis*; Wiley-VCH: Weinheim, 2008.

(6) Karge, H. G.; Weitkamp, J. *Adsorption and Diffusion*; Springer: Berlin, 2008; Vol. 7, p 400.

(7) Takaba, H.; Yamamoto, A.; Hayamizu, K.; Oumi, Y.; Sano, T.; Akiba, E.; Nakao, S. *Chem. Phys. Lett.* **2004**, *393*, 87–91.

(8) Takaba, H.; Yamamoto, A.; Hayamizu, K.; Nakao, S. *J. Phys. Chem. B* **2005**, *109*, 13871–13876.

(9) Vasenkov, S.; Böhlmann, W.; Galvosas, P.; Geier, O.; Liu, H.; Kärger, J. *J. Phys. Chem. B* **2001**, *105*, 5922–5927.

(10) Barrer, R. M. *Langmuir* **1987**, *3*, 309–315.

(11) Kärger, J. *Langmuir* **1988**, *4*, 1289–1292.

(12) Feldhoff, A.; Caro, J.; Jobic, H.; Krause, C. B.; Galvosas, P.; Kärger, J. *ChemPhysChem* **2009**, *10*, 2429–2433.

(13) Kärger, J.; Ruthven, D. M. *Zeolites* **1989**, *9*, 267–281.

(14) Naumov, S.; Valiullin, R.; Monson, P.; Kärger, J. *Langmuir* **2008**, *24*, 6429–6432.

(15) Yang, X.; Albrecht, D.; Caro, J. *Microporous Mesoporous Mater.* **2006**, *90*, 53–61.

(16) Database of Zeolite Structures: Powder Patterns, homepage of the International Zeolite Association, www.iza-structure.org.

(17) Galvosas, P.; Stallmach, F.; Seiffert, G.; Kärger, J.; Kaess, U.; Majer, G. *J. Magn. Reson.* **2001**, *151*, 260–268.

technique, the two gradient pulses of conventional PFG NMR are replaced by pairs of alternating gradient pulses separated by high-frequency π pulses. In this way, the disturbing influence of the permanent internal field gradients due to indispensable sample heterogeneities is reduced. The observation time was varied between 5 ms and 1 s, and the mean molecular displacements covered in the studies ranged from about 200 nm up to 20 μm . For diffusion in homogeneous, isotropic media, the signal intensity in PFG NMR experiments is known to obey the relation^{6,14,17,18}

$$\Psi(\delta g, t) = \exp(-\gamma^2 \delta^2 g^2 D t) = \exp(-\gamma^2 \delta^2 g^2 \langle r^2(t) \rangle / 6) \quad (1)$$

with g , δ , and t ($\gg \delta$) denoting the amplitude, duration, and separation of the gradient pulses (where, in the 13-interval pulse sequence, δ stands for the sum of the durations of the two gradients of a pair, to ensure conformity with the notation of the simple stimulated echo¹⁷). The second equation results from Einstein's relation⁶

$$\langle r^2(t) \rangle = 6Dt \quad (2)$$

implying proportionality between the mean-square displacement and the observation time. The self-diffusion coefficient D appearing in this relation coincides with the tracer diffusivity defined by Fick's first law.

For the PFG NMR diffusion studies, the zeolite material is contained in closed sample tubes. It is loaded with a well-defined amount of *n*-butane molecules which were introduced into the activated samples by chilling from a calibrated gas volume by means of liquid nitrogen. The samples were activated by heating (10 K/h) under evacuation and by leaving the sample, under continued evacuation, at the final temperature of 400 °C for an additional 10 h.

Results and Discussion

Figure 2 provides typical examples of the primary data observed in our diffusion experiments. As their most striking feature,

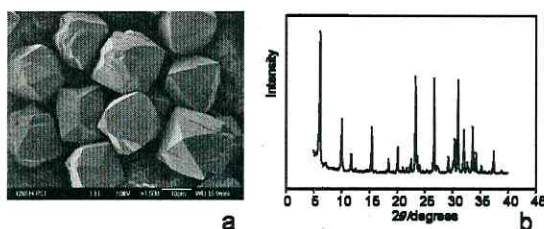


Figure 1. Scanning electron microimage (Jeol JSM 6700F) (a) and X-ray diffraction pattern (b) of the NaX-type sample under study.

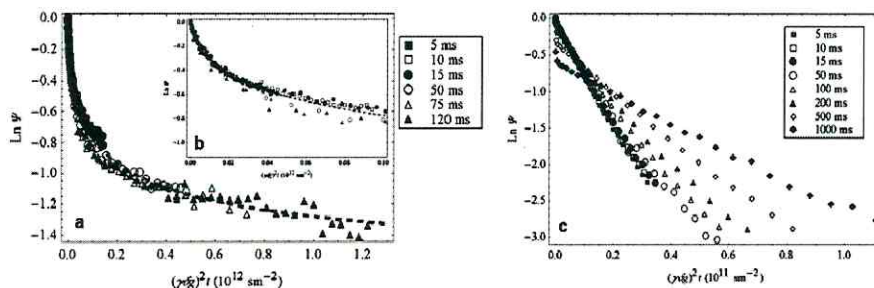


Figure 2. PFG NMR spin-echo attenuation curves for *n*-butane in the NaX sample under study for different observation times as indicated by the different symbols at 298 K and for guest loadings of 0.75 (a, b) and 3 (c) molecules per cavity. The broken lines in (a) and (b) represent the best fit of the attenuation curves for a log-normal distribution of the diffusivities (eqs 3 and 4) to the data points.

the attenuation plots for loadings with 3 molecules per supercage (Figure 2c) are found to follow, essentially, the dependence of eq 1, while there are significant deviations for the smaller loading with 0.75 molecules per supercage (Figure 2a,b). From eq 1 the slope of the attenuation plots is easily seen to be proportional to the diffusivity and, hence, via eq 2, to the mean-square displacements. Correspondingly, at an average loading of 3 molecules per cavity (which corresponds to a relative pore filling of about one-half), anywhere within the sample the guest molecules propagate at identical diffusion rates, while, at the lower loadings, notable differences become perceptible. This means that, within the pore space of the sample accommodated by the guest molecules, there have to be substantial differences which, at low loadings, give rise to the differences observed in the diffusivities. The coincidence in the attenuation curves for different observation times appearing from Figure 2a,b indicates that, during the covered diffusion times, there is essentially no guest exchange between the regions of different mobilities.

The effect of heterogeneity may be quantified by introducing a probability function $p(D)$ with $p(D) dD$ indicating the probability that the diffusivity of a guest molecule, arbitrarily selected within the sample, is in the interval $D \dots D + dD$. In this case, eq 1 may be transferred into the more general form

$$\Psi(\delta g, t) = \int_0^\infty p(D) \exp(-\gamma^2 \delta^2 g^2 D t) dD \quad (3)$$

Often, the so-called log-normal distribution^{19–21}

$$p(D) = \frac{1}{D\sigma\sqrt{2\pi}} \exp\left[-\frac{(\ln D - \ln D_m)^2}{2\sigma^2}\right] \quad (4)$$

is found to serve as a reasonable first-order approach for systems where molecular diffusion has to be described by a distribution of diffusivities rather than by a single one. Here D_m stands for the mean and σ for the width of the distribution. In the limiting case of infinitely narrow distributions, i.e., with $p(D)$ equal to Dirac's delta function, eq 3 coincides with eq 1. This approach is also in the present case found to yield a good fit to the data points as shown in Figure 2a,b by the broken line which corresponds to values of $D_m = 2.54 \times 10^{-11} \text{ m}^2 \text{ s}^{-1}$ and $\sigma = 2.6$. For rationalizing this result we may recollect²¹ that the interval $D_m/\sigma \dots D_m\sigma$ comprises 68.3% of the distribution. In the present contents, this means that the sample heterogeneity appears in a variation of the local diffusivities over a factor of about 7 in two-thirds of the total pore space and that the deviation of the diffusivities in the remaining parts is even more significant!

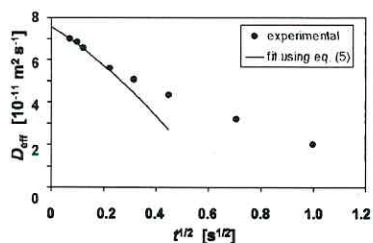


Figure 3. Effective diffusivities in the NaX specimen at 298 K (as resulting, via eq 1, from the slopes of the representation of Figure 2b) and comparison with the best fit of the second-order approach of their time dependence under confinement by spheres (eq 5).

In Figure 2c, the slope of the signal attenuation and hence, via eq 1, the effective diffusivity are seen to decrease with increasing observation time. Exactly this behavior has to be required as a consequence of the fact that intracrystalline diffusion proceeds within the finite volume of the individual crystallites of zeolite NaX rather than in an infinitely extended medium. The confinement leads to mean-square displacements ($\langle r^2(t) \rangle$) lagging progressively behind the displacements in an infinitely extended corresponding medium with increasing observation time t leading, with eq 2, to the observed decrease in the diffusivities. For a quantitative proof of this interrelation one may consider these diffusivities as a function of the square root of the observation time as displayed in Figure 3. For diffusion in spheres of radius R in second-order approximation this dependency obeys the following analytical expression²²

$$\frac{D_{\text{eff}}}{D_0} \approx 1 - \frac{4}{3R} \left(\frac{D_0 t}{\pi} \right)^{1/2} - \frac{D_0 t}{2R^2} \quad (5)$$

with D_0 denoting the genuine diffusivity, unaffected by boundary effects. Figure 3 shows the best fit of eq 3 to the initial four data points, yielding $D_0 = 7.6 \times 10^{-11} \text{ m}^2 \text{ s}^{-1}$ and a value of $R = 6.4 \mu\text{m}$ for the mean crystal radius, which is of the order of magnitude expected from crystal microimages shown in Figure 1a. The approach provided by eq 5 implies that the molecular diffusion path lengths during observation time are still notably exceeded by the crystal radii, i.e., $(D_0 t)^{1/2} \ll R$. Effective diffusivities with further increasing observation times are, therefore, beyond the limits of the applicability of eq 5.

As another feature of Figure 2c, the signal attenuation curves are found to start with an abrupt drop which is increasing with increasing observation time. This first steep decay has to be attributed to that part of the molecules which, during the observation, was able to escape into the intercrystalline space and which, correspondingly, were able to cover particularly long displacements. The contributions to the signal decay are proportional to the fractions of molecules that remain inside the crystals or are able to leave. In the so-called NMR tracer desorption technique^{6,23} this additional information on PFG NMR experiments with beds of nanoporous materials is used to explore the

existence of surface barriers. Assuming an exponential approach

$$p(t) = \exp(-t/\tau) \quad (6)$$

for the relative number of molecules which have remained within one and the same crystallite during the whole observation time t , one may introduce a mean molecular lifetime τ . This quantity can be compared with the mean lifetime resulting under the assumption that molecular exchange is exclusively determined by intracrystalline diffusion^{23,24}

$$\tau_{\text{Diff}} = \frac{R^2}{15D_0} \quad (7)$$

The values resulting in the present study are $\tau = 1.5 \text{ s}$ and $\tau_{\text{Diff}} = 36 \text{ ms}$. Intercrystalline exchange is thus found to be controlled by the permeation of a surface resistance on the individual zeolite crystals rather than by diffusion through the crystal bulk phase. With this finding, belatedly, we also justify the application of eq 5, which does only hold in the limiting case of ideally reflecting boundaries. In the other extreme, namely for diffusion-limited exchange, the right-hand side would maintain its structure, however, with slightly modified prefactors.^{22,25}

To facilitate the discussion of the differences observed with the two loadings, Figure 4 compares the present data with the results of previous diffusion measurements with a sample of NaX stemming from the celebrated laboratory of Professor Zhdanov, Leningrad/St. Petersburg.²⁶ Diffusion measurements with this material revealed, after as long as 30 years, a remarkable reproducibility yielding, with one and the same zeolite specimen, essentially identical diffusivity data.²⁷ Moreover, the diffusion data in these materials were found to be in good agreement with theoretical predictions based on the pore space geometry of the ideal NaX structure.^{28,29} It is in particular the decrease in the mobilities with increasing loading which was widely accepted as a quite general feature of n -alkane diffusion in zeolite NaX,³⁰ caused by the diminishing "free volume". In addition to the much smaller values of the diffusivities, at room temperature, now also this loading tendency is found to be reversed.

Assuming that the diffusivities in the Zhdanov samples are exclusively determined by the friction exerted by the genuine NaX pore network, the lower diffusivities in the zeolites considered in this study (and, most likely, also in numerous other products of zeolite synthesis considered in the past) must additionally be influenced by transport resistances in the interior of the crystals, possibly similarly to the stacking faults revealed in the TEM studies of ref 12. With locally varying separation l between these resistances and, possibly, permeabilities α through these resistances (defined as the ratio between the particle flux through the resistance and the difference in the concentrations on either side^{31,33}), they would give rise to the observed distribution in the diffusivities as soon as the studied displacements exceed these

(18) Cotts, R. M.; Hoch, M. J. R.; Sun, T.; Markert, J. T. *J. Magn. Reson.* **1989**, *83*, 252–266.

(19) Nyden, M.; Soderman, O. *Macromolecules* **1998**, *31*, 4990–5002.

(20) Fleischer, G.; Rittig, F.; Kärger, J.; Papadakis, C. M.; Mortensen, K.; Almdal, K.; Stepanek, P. *J. Chem. Phys.* **1999**, *111*, 2789–2796.

(21) Limpert, E.; Stahel, W. A.; Abbt, M. *BioScience* **2001**, *51*, 341–352.

(22) Mitra, P. P.; Sen, P. N.; Schwartz, L. M. *Phys. Rev. B* **1993**, *47*, 8565–8574.

(23) Krut'eva, M.; Kärger, J. *Langmuir* **2008**, *24*, 10474–10479.

(24) Barrer, R. M. *Zeolites and Clay Minerals as Sorbents and Molecular Sieves*; Academic Press: London, 1978; p 497.

(25) Geier, O.; Snurr, R. Q.; Stallmach, F.; Kärger, J. *J. Chem. Phys.* **2004**, *120*, 1–7.

(26) Zhdanov, S. P.; Khvostochov, S. S.; Feoktistova, N. N. *Synthetic Zeolites*; Gordon and Breach: New York, 1990.

(27) Ulrich, K.; Freude, D.; Galvosas, P.; Krause, C.; Kärger, J.; Caro, J.; Poladli, P.; Papp, H. *Microporous Mesoporous Mater.* **2009**, *120*, 98–103.

(28) Kärger, J.; Pfeifer, H.; Rauscher, M.; Walter, A. *J. Chem. Soc., Faraday Trans. 1* **1980**, *76*, 717–737.

(29) Auerbach, S. M.; Bull, L. M.; Henson, N. J.; Metiu, H. I.; Cheetham, A. K. *J. Phys. Chem.* **1996**, *100*, 5923–5930.

(30) Keil, F. J.; Krishna, R.; Coppens, M. O. *Rev. Chem. Eng.* **2000**, *16*, 71–197.

(31) Crick, F. *Nature* **1970**, *225*, 420.

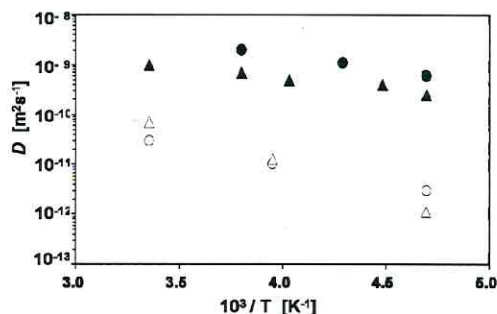


Figure 4. Comparison of the diffusivities of *n*-butane in zeolite NaX (full symbols: specimens synthesized by S. P. Zhdanov;^{26,28} open symbols: this study, sample shown in Figure 1a at loadings of 0.75 (circles) and 3 (triangles) molecules per large cavity. The size of the symbols corresponds to the uncertainty in the diffusivities.

separations but are still short enough to avoid an averaging over the whole spectrum of permeabilities and separations. In such cases, the effective diffusivity simply results by reciprocal addition of the two impeding mechanisms³¹

$$\frac{1}{D_{\text{eff}}} = \frac{1}{D} + \frac{1}{\alpha l} \quad (8)$$

Hence, increasing permeabilities would reduce the contribution of the second term on the right-hand side of eq 8 to the overall diffusivity. Since, in general, the activation energies for permeation through the intracrystalline transport resistances exceed those for diffusion through the genuine pore space,^{12,32} the contribution of the second term on the right-hand side of eq 8 is expected to decrease with increasing temperature. The observation that the effective diffusivities in the present samples increase more strongly with increasing temperature than the diffusivities in the genuine NaX samples considered in ref 28 is in complete agreement with this consideration.

In a similar way one may also rationalize that at the higher loadings the influence of sample heterogeneity is not visible anymore. It is well-known that in narrow pores the diffusivities generally increase with increasing loading (type-v pattern of concentration dependence^{30,33}). Since the formation of internal transport resistances is associated with constrictions in the pore space, the permeability through these barriers is expected to increase with increasing guest concentrations. Hence, with increasing concentration, the weight of barrier permeation (second term in eq 8) on the effective diffusivity is decreasing, while the first term, as a consequence of the well-known decrease of *n*-alkane diffusivities in the genuine pore space of NaX,²⁸ becomes more and more dominating so that, eventually, the influence of the additional transport resistances and, hence, of sample heterogeneities due to structure defects becomes negligibly small—as experimentally observed.

(32) Paoli, H.; Methivier, A.; Jobic, H.; Krause, C.; Pfeifer, H.; Stallmach, F.; Kärger, J. *Microporous Mesoporous Mater.* **2002**, *55*, 147–158.

(33) Kärger, J.; Ruthven, D. M. *Diffusion in Zeolites and Other Microporous Solids*; Wiley & Sons: New York, 1992.

Conclusion

Exploiting *n*-butane as a probe molecule, well-shaped crystals of zeolite NaX are found to exhibit a remarkable heterogeneity. This heterogeneity appears in a broad distribution of the butane diffusivities at low loadings, covering an order of magnitude. These diffusion data are by 1–2 orders of magnitude below the diffusivities observed in NaX specimens which are generally assumed to be close to perfect crystallinity.²⁶ One has to conclude, therefore, that in the NaX specimens considered in the present study guest diffusion is also controlled by internal transport resistances (“barriers”) which act in addition to the permanent “drag” exerted on the diffusing molecules by the genuine pore space. Thus, a variation in both the spacing and the intensity of these resistances over the sample may easily explain the observed distribution in the observed diffusivities. It is interesting to note that these differences disappear with increasing loading. However, such a behavior is not unexpected since in narrow-pore media the diffusivities (and, hence, also the permeabilities) are known to generally increase with increasing loading. As a consequence, the influence of these barriers will decrease with increasing loadings so that, eventually for sufficiently large concentrations, sample heterogeneity will disappear in the diffusion patterns.

In addition to previous studies revealing sample heterogeneities by recording time-dependent intracrystalline diffusivities^{9,34} or by combining the PFG NMR diffusion data with the results of quasi-elastic neutron scattering and high-resolution microscopy,¹² we have observed that, for one and the same guest molecule, the effect of sample heterogeneity on the observed diffusion patterns may dramatically depend on the loading. The decrease of this influence with increasing loading is shown to be in agreement with quite general features of mass transfer in pore spaces.³⁰

Crystals which, judging from both their external habit and their X-ray diffraction patterns, appear to be ideal are thus found to occur with vast differences in their real structure, ranging from perfect crystallinity as observed, e.g., with the diffusion measurements in ref 28 and their repetition in ref 27 to pronounced heterogeneities as substantiated with the present studies following previous comparative diffusion measurements by QENS and PFG NMR and investigations by high-resolution transmission electron microscopy.¹² It is noteworthy that in these studies both ideal crystallinity and deviations from crystallinity have been observed irrespective of the size of the given crystals. The correlation between the deviations from ideal crystallinity and the resulting diffusion patterns is thus expected to be quite complex and should be kept in mind quite generally in diffusion studies with such materials.

Acknowledgment. Financial support by Deutsche Forschungsgemeinschaft (International Research Group “Diffusion in Zeolites”) and by “Fonds der Chemischen Industrie” are gratefully acknowledged. Xiaobo Yang (Hanover) is thanked for NaX synthesis and Aisheng Huang (Hanover) for taking the XRD and SEM.

(34) Vasenkov, S.; Kärger, J. *Microporous Mesoporous Mater.* **2002**, *55*, 139–145.

Guest Diffusion in Interpenetrating Networks of Micro- and Mesopores

Filipe Furtado,^{†,‡} Petrik Galvosas,^{‡,§} Maraisa Gonçalves,^{||} Frank-Dieter Kopinke,[†] Sergej Naumov,[‡] Francisco Rodríguez-Reinoso,^{||} Ulf Roland,[†] Rustem Valiullin,^{*,‡} and Jörg Kärger[‡]

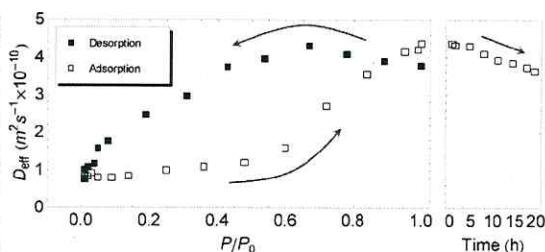
[†]Department of Environmental Engineering, UFZ—Helmholtz Centre for Environmental Research, Permoserstrasse 15, 04318 Leipzig, Germany

[‡]Department of Interface Physics, University of Leipzig, Linnéstrasse 5, D-04103 Leipzig, Germany

[§]MacDiarmid Institute for Advanced Materials and Nanotechnology, School of Chemical and Physical Sciences, Victoria University of Wellington, P.O. Box 600, Wellington 6140, New Zealand

^{||}Departamento de Química Inorgánica, Universidad de Alicante, Apartado 99, 03080 Alicante, Spain

ABSTRACT: Pulsed field gradient NMR is applied for monitoring the diffusion properties of guest molecules in hierarchical pore systems after pressure variation in the external atmosphere. Following previous studies with purely mesoporous solids, also in the material containing both micro- and mesopores (activated carbon MA2), the diffusivity of the guest molecules (cyclohexane) is found to be most decisively determined by the sample "history": at a given external pressure, diffusivities are always found to be larger if they are measured after pressure decrease (i.e., on the "desorption" branch) rather than after pressure increase (adsorption branch). Simple model consideration reproduces the order of magnitude of the measured diffusivities as well as the tendencies in their relation to each other and their concentration dependence.



INTRODUCTION

The need for transport-optimized materials for molecular separation and for molecular conversion by heterogeneous catalysis has initiated the development of novel strategies for the production of such materials.¹ Combining the benefit of micropores for molecular separation and conversion and of mesopores for transport acceleration, materials of hierarchical pore architecture have attained particular interest.² The interpenetration of micro- and mesopore spaces leads to very special patterns of mass transfer which, in such complex systems, are by far more complicated to be assessed than in purely microporous or mesoporous materials. This includes, in particular, the exploration of the interrelation between sorption hysteresis and mass transfer. In the literature, time-dependent hysteresis is referred to both as structural changes (such as deformations and swelling) in the host material^{3,4} and as diffusion resistances in the pore space.⁵ To the best of our knowledge, never before have mass transfer and sorption hysteresis in hierarchical pore systems been directly correlated by experimental measurement.

The present work is dedicated to this issue, exploiting the pulsed field gradient technique of NMR (PFG NMR)^{6–8} as a sophisticated tool for the in situ observation of molecular displacements over microscopic dimensions. The covered diffusion path lengths are thus large enough to ensure tracing of the combined effect of mass transfer in the micro- and mesopores.

They are small enough, however, to remain unaffected by the influence of unwanted boundary effects by the external surface of the host particles and the interparticle space.

MATERIALS AND METHODS

The host system under study was an activated carbon (MA2), prepared by carbonization and subsequent CO₂ activation (43% activation burnoff) of spherical porous resin obtained by cross-linking of phenol-formaldehyde Novolac precursor with hexamethylenetetramine and with ethylene glycol as solvent–pore former.^{9,10} It consists of spherical particles (Figure 1, left) with diameters of 0.15–0.50 mm (mean 0.32 mm).

In both nitrogen adsorption at 77 K (Figure 2) and transmission electron microscopy (Figure 1, right), micro- and mesoporosity appear in an almost perfect mixture (1:1), with respective volumes $V_{\text{micro}} = 0.64 \text{ cm}^3 \text{ g}^{-1}$ and $V_{\text{meso}} = 0.59 \text{ cm}^3 \text{ g}^{-1}$, which correspond to two pore diameter ranges centered around 1 and 20 nm, in the obtained pore size distributions (inserts to Figure 2). Furthermore, the micropore volume was also accessed by CO₂ adsorption at 273 K giving rise to an expected slightly lower value of $V_{\text{micro}} = 0.57 \text{ cm}^3 \text{ g}^{-1}$. This value remains in good agreement with the estimation from the N₂ adsorption data, since the adsorption of CO₂ at 273 K is limited to the narrow (<1 nm)

Received: June 17, 2010

Published: February 7, 2011

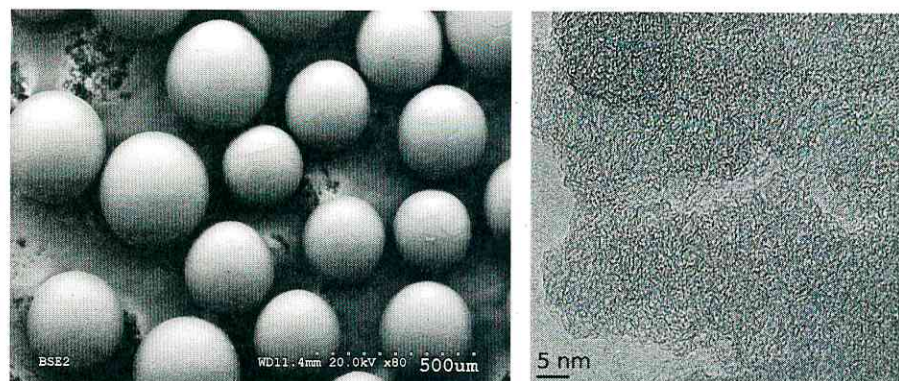


Figure 1. Images of the host system under study (activated carbon of type MA2^{9,10}) as obtained by (left) scanning electron microscopy and (right) by transmission electron microscopy, revealing both micro- and mesopores.

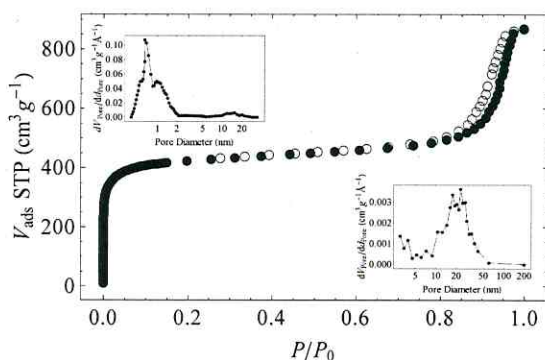


Figure 2. N₂ adsorption isotherm at 77 K for the carbon sample under study, with closed and open symbols corresponding to the adsorption and desorption branch, respectively. The insets show the micropore and mesopores pore size distributions (upper left side and lower right side, respectively) as obtained by DFT¹³ (micropore distribution) and BJH¹⁴ (mesopores distribution). Note that the area under both peaks, in the upper-left inset, is approximately the same.

micropores;^{11,12} the distinction of narrow and wide microporosity is clear in the DFT¹³ pore size distribution inset of Figure 2.

The diffusion measurements have been performed by means of PFG NMR technique,^{6–8} using cyclohexane (with a saturation pressure of $P_0 = 130$ mbar, at 298 K) as a probe molecule. By considering large ensembles of molecular entities, experiments of this type are complementary to single-molecule observation¹⁵ and yield the complete statistical information relevant for the selected space and time scales. The primary quantity recorded by PFG NMR is the intensity of the NMR signal (the spin echo). This quantity, plotted as a function of the intensity of the field gradient pulses, is the Fourier transform of the propagator,⁷ i.e., the probability distribution of molecular displacements as a function of the observation time. Typical space and time scales as accessible by PFG NMR are micrometers and milliseconds. The mean square displacement $\langle r^2(t) \rangle$ results as the mean squared width of this distribution and follows directly from the signal attenuation in the limit of sufficiently small gradient intensities (initial decay of the NMR signal intensity in a semilogarithmic representation versus the squared magnetic field gradient intensity).^{6,7}

PFG NMR diffusion data in complex systems are commonly represented by so-called effective diffusivities defined by the relation

$$D_{\text{eff}} = \langle r^2(t) \rangle / 6t \quad (1)$$

as the ratio between the mean square displacement $\langle r^2(t) \rangle$ of the molecules under study and the observation time t . In homogeneous systems, eq 1 represents Einstein's diffusion equation^{16,17} and D_{eff} coincides with the genuine coefficient of self-diffusion (also referred to as the self-diffusivity). In heterogeneous systems, D_{eff} is the mean value of the diffusivities of all probe molecules under study. The diffusion measurements have been performed with the 13-interval pulse sequence¹⁸ at a proton resonance frequency of 125 MHz by means of the home-built PFG NMR diffusion spectrometer FEGRIS NT.^{19,20} Prior to the measurements, the host material under study was kept in an oven at 383 K in contact with atmosphere over 24 h and, subsequently, under high vacuum ($<10^{-2}$ Pa) at 523 K for 4 h. The diffusion measurements were generally performed by connecting the sample with a reservoir containing the guest molecule under well-defined pressure. By varying the pressure, a continuous variation of the sample loading was possible. By approaching a certain pressure either from smaller or larger values (i.e., by adsorption or desorption) different sample "histories" could be considered. Since the intensity of the NMR signal following the first ($\pi/2$) pulse of the PFG NMR pulse sequence (the "free induction decay") is directly proportional to the number of guest molecules, the NMR technique may as well be exploited to determine the guest loading. This occurs under exactly those conditions under which the diffusion experiments are performed and allows the immediate correlation of diffusion and adsorption under a well-defined external atmosphere.²¹

Complementary to these studies, selected diffusion measurements have been performed in closed PFG NMR samples as well. After subjecting the host material to exactly the same activation procedure as described above, these samples have been prepared by introducing a well-defined amount of guest molecules into the host material by freezing with liquid nitrogen and subsequent sealing of the sample tubes.

RESULTS

Figure 3 provides a survey of the diffusivities (D_{eff}) of cyclohexane in activated carbon MA2 measured under variation of the external gas phase pressure, jointly with the corresponding loadings (Θ). The loadings are represented as the ratio between the amount actually adsorbed and its maximum value attained by guest pressures close to saturation. Inevitable long-term

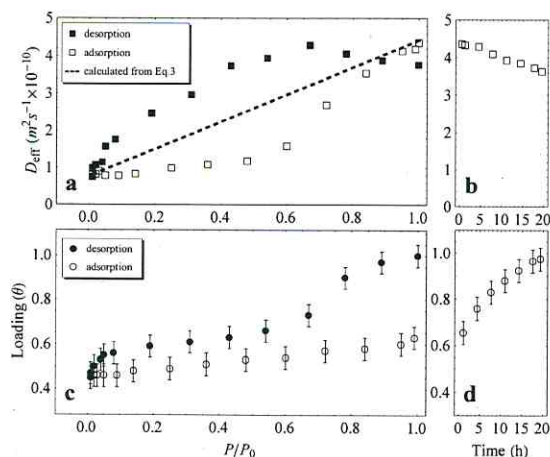


Figure 3. (a) Diffusivities of cyclohexane at 298 K in MA2 as a function of the relative external pressure during adsorption and desorption and the diffusivities resulting via eq 3 (dashed line). (b) Evolution of the diffusivities with time after the last pressure step (to $P/P_0 \approx 1$) on the adsorption branch. (c) Cyclohexane loading isotherm at 298 K in MA2 as a function of the external pressure during adsorption and desorption, measured 10 min after each pressure variation. (d) Loading evolution with time after the pressure step to $P/P_0 \approx 1$ on the adsorption branch.

instabilities cause the uncertainty indicated for the loadings. The uncertainty in the measured diffusivities relative to each other is smaller than the size of the symbols.

Usually, the measurements were performed 10 min after the pressure step. The development of the loading during this time interval is represented by the development of the free induction decay (FID) shown in Figure 4. Pressure steps during adsorption (Figure 4a) are found to lead to an only slight change in loading, which must be expected to continue after the considered time interval of 10 min. In general, pressure steps during desorption are followed by a much more pronounced changes in loading (Figure 4b). The normalized representation in Figure 4c shows that this effect is particularly pronounced for pressure steps around $P/P_0 = 0.7$.

Limitation in the measuring time allowed an extension of the equilibration time only for selected cases. One example is provided by Figures 3b and d, where the final adsorption step to saturation is found to require equilibration times of days, accompanied by distinct changes in the diffusivities. A second experiment of this type has been performed during desorption following the pressure step from $P/P_0 = 0.74$ to 0.67 . Here, following the initial change as displayed by Figure 4c, during the considered time interval of 20 h no further change in loading and diffusivity became visible within the accuracy of these measurements ($\pm 5\%$).

Complementary to the diffusion measurements at well-defined external pressures, Figure 5 provides a survey of the diffusivity data obtained for the closed samples. Also included in this representation are the diffusivity data of Figure 3a. The error bars in the loading (resulting by turning the vertical error bars of Figure 3c into horizontal direction) are omitted. Note that diffusion measurements with loadings notably below saturation of the micropores could not be performed by the experimental setup designed for pressure variation (data of Figure 3a). The spatial

constraint given by the PFG NMR spectrometer did not allow a satisfactorily accurate adjustment and maintenance of the small guest pressures necessary for attaining these low loadings.

DISCUSSION

Following investigations with purely mesoporous host systems (Vycor porous glass)²² and system containing both meso- and macro-porosity,²³ with the data shown in Figure 3a for the first time hysteresis effects are also observed for diffusion in hierarchical pore networks involving both micro- and mesoporous spaces. It turns out that, for a given external pressure, the measured diffusivities notably depend on the "history" of the system: if the pressure is attained by pressure decrease from larger values (i.e., on the "desorption branch"), then the diffusivities are found to be notably larger than after approaching the same pressure from lower values, i.e., on the adsorption branch.

For rationalizing the observed diffusion behavior, we have to correlate the experimentally accessible quantity, the mean square displacement, with its constituents, i.e., the displacements in the micro- and mesopores. The distances over which, in PFG NMR measurements, the guest molecules are followed are typically of the order of micrometers so that the diffusion paths consist, in general, of displacements in both the micro- and mesoporous spaces. We, correspondingly, note:

$$\begin{aligned} \langle r^2(t) \rangle &= \langle (r_{\text{micro}}(t) + r_{\text{meso}}(t))^2 \rangle \\ &= \langle r_{\text{micro}}^2(t) \rangle + \langle r_{\text{meso}}^2(t) \rangle \end{aligned} \quad (2)$$

where $r_{\text{micro}}(t)$ and $r_{\text{meso}}(t)$ represent the (vector) sum over all individual constituents of overall displacement in the micro- and mesoporous spaces, respectively, during time t . The second relation holds rigorously if subsequent displacements in the micro- and mesopores are uncorrelated. This requirement is fulfilled for mutually interpenetrating pore networks and corresponds to the model of parallel diffusion resistances. Dividing eq 2 by the observation time and comparison with eq 1 finally yields:

$$\begin{aligned} D_{\text{eff}} &= \frac{t_{\text{micro}}}{t} D_{\text{micro}} + \frac{t_{\text{meso}}}{t} D_{\text{meso}} \\ &= p_{\text{micro}} D_{\text{micro}} + p_{\text{meso}} D_{\text{meso}} \end{aligned} \quad (3)$$

where the quantities $t_{\text{micro(meso)}}$, $D_{\text{micro(meso)}}$, and $p_{\text{micro(meso)}}$ denote, respectively, the total lifetime (during t), the self-diffusivity and the relative amount of molecules in the micro-(meso-) mesopores. The second equation results in consequence of the detailed-balance requirement $p_{\text{micro}}/t_{\text{micro}} = p_{\text{meso}}/t_{\text{meso}}$.

With eq 3, the general tendency in the variation of the diffusivities with varying loading, as revealed by Figure 5, may be easily rationalized. For loadings sufficiently below total filling of the microporous space (i.e., up to $\Theta \approx 0.5$), the pressure and, hence, the relative amount p_{meso} of molecules in the mesopores is so small that the second term in eq 3 may be neglected. Mass transfer in the pore system is essentially controlled, therefore, by micropore diffusion. The increase with increasing loading observed in this loading range corresponds to the well-known pattern III of the concentration dependence of pore space diffusion as discussed by Kärger and Ruthven²⁴ and may be referred to the (transport-impeding) influence of strong adsorption sites which decreases with increasing loading.

In Figure 5, this range of micropore-controlled diffusion is followed by a region ($0.5 < \Theta < 0.6$) of steep increase of the diffusivity with increasing loading: loading enhancement by 20%

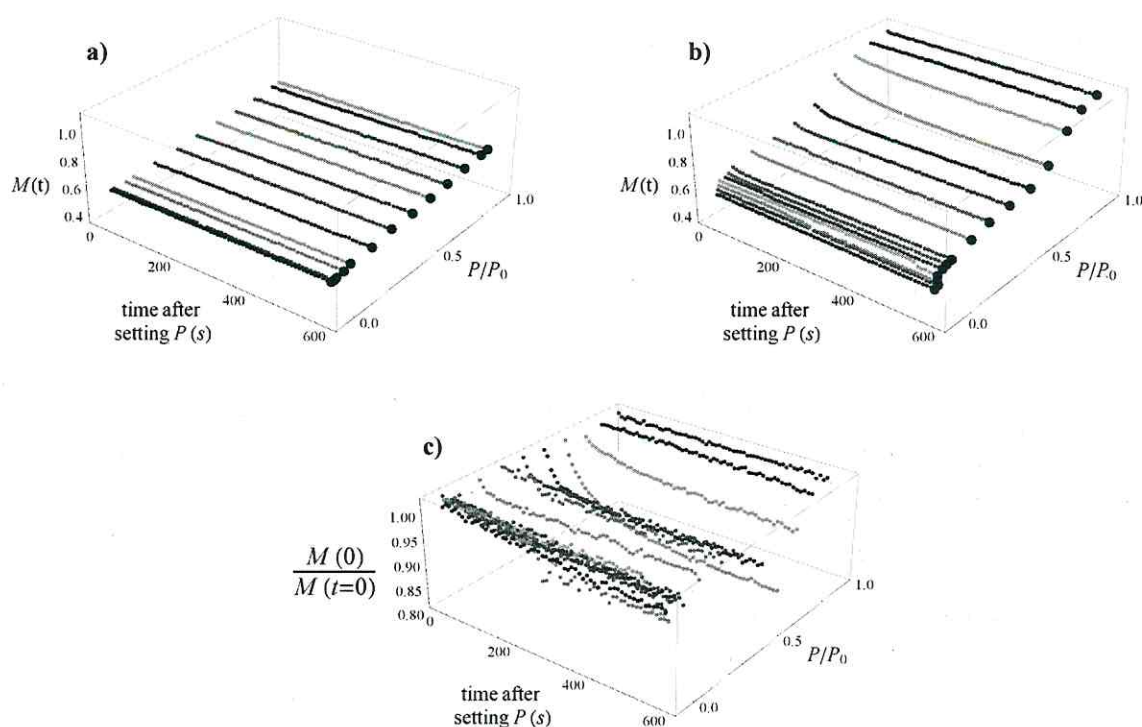


Figure 4. Changes in loading of the host material following pressure steps during adsorption (a) and desorption (b, c). The blue data points are used as loading in Figure 3c).

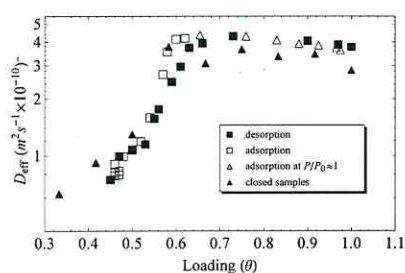


Figure 5. Measured diffusivities as a function of sample loading, obtained by continually varying the external pressure and on closed samples, prepared with a defined amount of cyclohexane.

increases the diffusivity by a factor of 5. This enhancement may immediately be attributed to the onset and a dramatic increase of the contribution of mesopore diffusion to mass transfer, i.e., to the second term on the right-hand side of eq 3. We have to note that the relative amount of molecules in the mesopores is still much smaller than in the micropores ($p_{meso} \ll p_{micro}$). This, however, is now becoming to be overcompensated by the fact that molecular propagation in the (still empty) mesopores is much larger than in the micropores and that, therefore, $D_{meso} \gg D_{micro}$.

The steep increase in the diffusivity for $0.5 < \Theta < 0.6$ is followed by a moderate decrease in the diffusivities, which attain their minimum for $\Theta = 1$. This behavior appears even

more pronounced in the presentations of Figure 3 and is immediately correlated with the onset of capillary condensation. Again, the behavior may be rationalized by eq 3: capillary condensation leads to a break down in the mesopore diffusivity from Knudsen to bulk diffusion. As a consequence, the decrease in D_{meso} may affect that, irrespective of an increase of p_{meso} toward (for the given system) $p_{meso} \approx p_{micro} \approx 0.5$, the second term on the right-hand side of eq 3 decreases with further increasing loading.

As already discussed, Figure 3 shows that cyclohexane diffusivity plotted versus external pressure does remarkably depend on the sample preparation history. It should be noted that Figure 5 rather indicates that the measured diffusivities on the desorption and adsorption branches, as well as on closed samples in this particular system do not significantly differ from each other (within the experimental precision), for a given loading. Therefore, provided that the system has been given enough time to equilibrate, on the basis of the results obtained, one may anticipate that sample preparation history should not affect the diffusivity of the guest molecule. This, however, is a matter of ongoing discussions in the literature with a particular emphasis that, in random mesoporous structures, no thermal equilibration can be obtained on the laboratory time scale.^{22,30}

The scenario of molecular dynamics as deduced from the experimental data may be supported by order-of-magnitude estimates which can be shown to cover the two limiting cases in which the guest molecules are assumed to accommodate the mesopores exclusively in either the gaseous or liquid state. Disregarding any mass transfer along the inner surface of the

mesopores, in the first case, the relative amount of molecules in the mesopores may be noted as a function of the volumes V_{meso} and V_{micro} of the meso- and micropores and the pressure P in the mesopores by the relation:²¹

$$p_{\text{meso}} = \frac{V_{\text{meso}}}{V_{\text{micro}} + V_{\text{meso}}} \frac{MP}{RT\rho_{\text{liq}}} \ll 1 \quad (4)$$

with R denoting the gas constant, T the absolute temperature, M the molecular weight, and ρ_{liq} the density of liquid cyclohexane. Mesopore diffusion may be approached by the classical Knudsen relation:

$$D_{\text{meso}} = D_{\text{Knudsen}} / \tau = \frac{d}{3\tau} \sqrt{\frac{8RT}{\pi M}} \quad (5)$$

where, in addition, a tortuosity factor τ has been introduced to take account of an additional enhancement of the diffusion path lengths due to pore tortuosity.²⁵

Figure 3a shows the effective diffusivities resulting from eq 3, in combination with eqs 4 and 5, by the dashed straight line. The starting point in the low-pressure region is chosen to coincide with the effective diffusivity which may be attributed to micropore diffusion at micropore saturation. By assuming that the mesopores are exclusively filled by gas phase, p_{meso} remains much less than p_{micro} (i.e., $p_{\text{meso}} \ll p_{\text{micro}} \approx 1$, with the latter relation following due to $p_{\text{micro}} + p_{\text{meso}} = 1$). With eqs 3 to 5, D_{eff} thus results as a function linearly increasing with the pressure. Its slope is given by the ratio d/τ . With a pore diameter of $d = 20$ nm (see Figure 2), the effective diffusivity is found to reach the experimental value at saturation pressure by assuming a tortuosity factor of $\tau = 1.3$. Since our estimates had to neglect possible contributions of surface diffusion to mass transfer in the mesopores, including correlation effects which may affect the applicability of eq 5,^{26–28} the resulting tortuosity factor is only an estimate of the lower limit and thus in satisfactory agreement with the values (about 2 to 4) commonly found in the literature.²⁵

With the onset of capillary condensation, after a waiting time of 20 h (Figure 3b), the effective diffusivity decreases to a value of $D_{\text{eff}} = 3.6 \times 10^{-10} \text{ m}^2 \text{ s}^{-1}$. In the limiting case of micro- and mesopore saturation, eq 3 becomes:

$$D_{\text{eff}} = \frac{V_{\text{micro}}}{V_{\text{micro}} + V_{\text{meso}}} D_{\text{micro}} + \frac{V_{\text{meso}}}{V_{\text{micro}} + V_{\text{meso}}} D_{\text{meso}} \quad (6)$$

where, for simplicity, the guest densities in the two pore spaces are assumed to coincide. With the relevant values of $D_{\text{micro}} = 7.9 \times 10^{-11} \text{ m}^2 \text{ s}^{-1}$, $V_{\text{micro}} = 0.64 \text{ cm}^3 \text{ g}^{-1}$ and $V_{\text{meso}} = 0.59 \text{ cm}^3 \text{ g}^{-1}$, eq 6 is found to yield the experimentally determined value of $D_{\text{eff}} = 3.6 \times 10^{-10} \text{ m}^2 \text{ s}^{-1}$ by implying a value of $D_{\text{meso}} = 6.6 \times 10^{-10} \text{ m}^2 \text{ s}^{-1}$ for the liquid diffusivity in the mesopores. This value is by a factor of 2 below the diffusivity in the bulk liquid ($D_{\text{cyclohexane}} = 1.4 \times 10^{-9} \text{ m}^2 \text{ s}^{-1}$)²⁹ which, again, may be easily referred to the effect of tortuosity. The order of magnitude of the measured diffusivities is thus found to be nicely reflected by our simplifying model based on eq 3 and by considering the two extreme cases that mass transfer in the mesopores is controlled by either Knudsen diffusion (mesopores exclusively containing gas phase) or by bulk diffusion (mesopores exclusively containing liquid phase).

As the most remarkable feature of Figure 3a, the measured diffusivities are found to deviate in a well-defined way from the straight line which, via eqs 3–5, represents the diffusivities

predicted by assuming that the gas pressure within the mesopores coincides with the pressure externally applied. The experimental results deviate to smaller values on the adsorption branch, i.e., in a sequence of steps with increasing pressure, while they are above this line on the desorption branch. Such history dependence in the measured diffusivities (“diffusion hysteresis”) has, for the first time, been observed in purely mesoporous systems.²²

With the present work, this phenomenon is now also demonstrated to occur in hierarchical pore networks. In contrast to the purely mesoporous materials, in the hierarchical materials under study, the mesoporous space is imbedded in a microporous matrix. The micropores provide the system with additional diffusion pathways, the efficiency of which may be quantified by the micropore diffusivities also measured in this study (diffusivities in Figure 5 for $\Theta < 0.5$). The additional diffusion pathways provided by the micropores may be expected to promote equilibration. It turns out, however, that this effect is not strong enough and does not prevent the formation of hysteresis effects. This finding confirms the conclusion of the previous studies with purely mesoporous materials:²² system equilibration during hysteresis is not correlated with the guest diffusivities. It is the rate of collective rearrangement of molecular ensembles rather than of individual molecules which promotes the systems into states of lower free energy. It is well established that the propagation rate of the latter process is dramatically decreasing with increasing time^{22,30–32} excluding equilibrium establishment over feasible observation times.

Deviating from the observations with the pure mesoporous material (Vycor porous glass, see Figure 1b of ref 22), the diffusivities on the desorption branch are now (Figure 3a) found to be notably larger (rather than smaller) than those on the adsorption branch. This difference, however, may be nicely referred to a quite general pattern of diffusion hysteresis which may be deduced from both the previous studies with the purely mesoporous material²² and the present investigations with hierarchical pore spaces: since, upon pressure variation, the system tends to remain in the old state, the diffusivities likewise tend to be shifted toward the previously measured values. The relation between the diffusivities on the adsorption and desorption branches may therefore easily be correlated with the overall trends in the concentration dependence. In Vycor porous glass,²² the diffusivity at complete saturation is found to be notably smaller than over most of the covered pressure range while, just vice versa, in the material considered in this work, the diffusivity at complete saturation is notably larger than over most of the pressure range considered.

The deviation of the experimental data from the theoretical estimate (broken line in Figure 3a) toward larger values on the desorption branch and toward smaller values on the adsorption branch is in complete agreement with the understanding that, upon pressure decrease, the actual pressure within the mesopores is above the external pressure, while it is below the external pressure upon pressure increase: system “memory” tends to maintain the previous state. The time interval between pressure variation and measurement (in general 10 min) has thus turned out to be too small to ensure complete equilibration.

Figures 3b,d and 4 display the experimental data that have been obtained in selected series of measurement with observation times extended to 20 h. As a most intriguing difference in system evolution, pressure steps are found to lead to a pronounced short-term response during desorption (Figure 4b, c) while,

during adsorption (Figures 3b, d and 4a), loading and diffusivities vary extremely slowly with increasing observation time. A reliable explanation of this difference requires long-term measurements with correspondingly long observation times which are under consideration for future studies. Possible explanations may include variations in the host structure upon sorption³ and/or kinetic restrictions in the micropore space as suggested in ref 33.

For the time constant ("first statistical moment"³⁴) of the decay following the desorption step at $P/P_0 = 0.67$ in Figure 4b, c, one obtains a value of $\tau_{\text{des}} \approx 100$ s. For diffusion-limited desorption by spherical particles of radius R , this time constant is given by the relation:³⁴

$$\tau_{\text{des}}^{\text{diff}} = \frac{R^2}{15D_{\text{des}}} \quad (7)$$

with D_{des} denoting the diffusivity relevant for the desorption process considered. With a mean radius of 0.16 mm as relevant for our host particles and the above value of $\tau_{\text{des}} \approx 100$ s, eq 7 yields a diffusivity $D_{\text{des}} = 1.7 \times 10^{-11} \text{ m}^2 \text{ s}^{-1}$. It is interesting to note that this value is still—although slightly smaller—of the order of the micropore diffusivities ($D_{\text{micro}} = 7.9 \times 10^{-11} \text{ m}^2 \text{ s}^{-1}$). The given differences might, moreover, be referred to the different nature of the two diffusivities: the self-diffusivity resulting by PFG NMR is an equilibrium quantity, while D_{des} results from the rate of desorption and is, therefore, generally referred to as a transport (or Fickian) diffusivity.^{28,35} On the basis of the experimental data so far available, however, the indicated correlation with the short-time behavior in the relaxation curves shown in Figure 4b, c cannot be anything more than a tentative approach. Similarly, there is no sound basis to exclude that the observed fast relaxation is followed by another, very slow one, with time constants far too large to be accessible in our measurements. The possibility of diverging time constants is well established in the literature.^{22,36}

CONCLUSIONS

In the course of recent decades, diffusion measurements in apparently simple materials such as purely microporous solids revealed a multitude of diverging results^{37,38} and, eventually, led to the insight that the real structure of such materials may notably deviate from the patterns resulting from conventional structure analysis and generally found in textbooks.^{39,40} It is worth mentioning that, in general, these complications do not concern diffusion measurements by Quasi-Elastic Neutron Scattering (QENS)⁴¹ where the covered diffusion paths are of the order of nanometers. Structural deviations such as stacking faults⁴⁰ which may become rate controlling in PFG NMR diffusion measurements (and even more pronounced in the more "macroscopic" techniques) would thus affect an only negligibly fraction of the recorded trajectories and would not appear in the QENS diffusion data. This virtue of QENS is impressively demonstrated by the excellent agreement between QENS measurement of guest diffusion in zeolites and Molecular Dynamics simulations which are based on the ideal pore structure.⁴²

Mesoporous and, in particular, hierarchical host materials may additionally complicate the conditions for reliable diffusion measurements. Since the range of diffusion measurement by QENS is, at best, limited to distances comparable with the mesopore diameters, this technique is unable to provide direct information about the rate of long-range diffusion within the individual host particles.

Covering diffusion path lengths from fractions to hundreds of micrometers, PFG NMR is the method of choice for the measurement of molecular transport in such systems. Following previous studies with purely mesoporous materials,^{22,43,44} PFG NMR has now been employed to investigate the mobility of guest molecules in a material with an interpenetrating network of micro- and mesopores as a function of the sample history. Over essentially the whole pressure range covered in the experiments, for one and the same externally applied pressure, the molecular diffusivities measured on the desorption branch, i.e., following a decrease in the external pressure, notably exceeded the diffusivities on the adsorption branch. We were able to rationalize both the trends in the concentration dependence and the relation between the diffusivities on the basis of simple microkinetic models.

The waiting times of generally 10 min, as allowed by the conditions under which the experiments had to be performed, not unexpectedly turned out to be much too short for equilibration. Even with waiting times of up to 20 h, allowed for in selected cases, there was no clear evidence of final equilibration. We have confined ourselves to weak conjectures about the mechanisms behind the ongoing equilibration process, including the option of sorption-induced structural changes in the host material, and hope that the presented experimental data help to intensify investigations on a challenging field of current research.

AUTHOR INFORMATION

Corresponding Author

valiullin@uni-leipzig.de

ACKNOWLEDGMENT

Financial support from Marie Curie Early Stage Training Program "Risk Assessment and Environmental Safety Affected by Compound Bioavailability in Multiphase Environments" (RA-ISEBIO), by the Deutsche Forschungsgemeinschaft, and by the Fonds der Chemischen Industrie is gratefully acknowledged.

REFERENCES

- (1) Schüth, F.; Sing, K. S. W.; Weitkamp, J. *Handbook of Porous Solids*; Wiley-VCH: Weinheim, Germany, 2002.
- (2) Wang, G.; Johannessen, E.; Kleijn, C.; Deleeuw, S.; Coppens, M. *Chem. Eng. Sci.* **2007**, *62* (18–20), 5110–5116.
- (3) Gregg, S. *Adsorption, Surface Area, And Porosity*; Academic Press: London, New York, 1982.
- (4) Tvardovski, A. J. *Colloid Interface Sci.* **2001**, *241* (2), 297–301.
- (5) Ravikovitch, P. I.; Neimark, A. V. *Adsorption* **2005**, *11* (S1), 265–270.
- (6) Dvoyashkin, M.; Valiullin, R.; Kärger, J.; Einicke, W. D.; Gläser, R. *J. Am. Chem. Soc.* **2007**, *129* (34), 10344–10345.
- (7) Kärger, J.; Pfeifer, H.; Heink, W. *Adv. Magn. Reson.* **1988**, *12*, 2–89.
- (8) Stejskal, E. O.; Tanner, J. E. *J. Chem. Phys.* **1965**, *42* (1), 288.
- (9) Rodríguez-Reinoso, F.; Marsh, H. *Activated Carbon*; Elsevier: Amsterdam, Boston, 2006.
- (10) Tennison, S. R.; Kozynchenko, O. P.; Strelko, V. V.; Blackburn, A. J. *Porous carbons*. U.S. Patent 2004/0024074 A1.
- (11) Garrido, J.; Linares-Solano, A.; Martín-Martínez, J. M.; Molina-Sabio, M.; Rodríguez-Reinoso, F.; Torregrosa, R. *Langmuir* **1987**, *3* (1), 76–81.
- (12) Rodríguez-Reinoso, F.; Garrido, J.; Martín-Martínez, J.; Molinasabio, M.; Torregrosa, R. *Carbon* **1989**, *27* (1), 23–32.
- (13) Lastoskie, C.; Gubbins, K. E.; Quirke, N. *J. Phys. Chem.* **1993**, *97* (18), 4786–4796.

- (14) Barrett, E. P.; Joyner, L. G.; Halenda, P. P. *J. Am. Chem. Soc.* **1951**, *73* (1), 373–380.
- (15) Jung, C.; Kirstein, J.; Platschek, B.; Bein, T.; Budde, M.; Frank, I.; Müllen, K.; Michaelis, J.; Bräuchle, C. *J. Am. Chem. Soc.* **2008**, *130* (5), 1638–1648.
- (16) Einstein, A. *Ann. Phys. (Berlin)* **1905**, *322* (8), 549–560.
- (17) Kärger, J. *Leipzig, Einstein, Diffusion*; Leipziger University-Verlag: Leipzig, 2007.
- (18) Cotts, R.; Hoch, M.; Sun, T.; Markert, J. *J. Magn. Reson.* **1989**, *83* (2), 252–266.
- (19) Galvosas, P.; Stallmach, F.; Seiffert, G.; Kärger, J.; Kaess, U.; Majer, G. *J. Magn. Reson.* **2001**, *151* (2), 260–268.
- (20) Stallmach, F.; Galvosas, P. *Annu. Rep. NMR Spectrosc.* **2007**, *61*.
- (21) Valiullin, R.; Kortunov, P.; Kärger, J.; Timoshenko, V. *J. Chem. Phys.* **2004**, *120* (24), 11804–11814.
- (22) Valiullin, R.; Naumov, S.; Galvosas, P.; Kärger, J.; Woo, H. J.; Porcheron, F.; Monson, P. A. *Nature* **2006**, *443* (7114), 965–968.
- (23) Valiullin, R.; Dvoyashkin, M.; Kortunov, P.; Krause, C.; Kärger, J. *J. Chem. Phys.* **2007**, *126* (5), 054705.
- (24) Kärger, J.; Ruthven, D. M. *Diffusion in Zeolites and Other Microporous Solids*; Wiley: New York, 1992.
- (25) Satterfield, C. *Mass Transfer in Heterogeneous Catalysis*; R.E. Krieger Pub. Co.: Huntington, N.Y., 1981.
- (26) Ruthven, D. M.; DeSisto, W. J.; Higgins, S. *Chem. Eng. Sci.* **2009**, *64* (13), 3201–3203.
- (27) Bhatia, S. K.; Nicholson, D. *AIChE J.* **2006**, *52* (1), 29–38.
- (28) Krishna, R. *J. Phys. Chem. C* **2009**, *113* (46), 19756–19781.
- (29) Holz, M.; Heil, S. R.; Sacco, A. *Phys. Chem. Chem. Phys.* **2000**, *2* (20), 4740–4742.
- (30) Naumov, S.; Valiullin, R.; Monson, P. A.; Kärger, J. *Langmuir* **2008**, *24* (13), 6429–6432.
- (31) Woo, H. J.; Monson, P. *Phys. Rev. E* **2003**, *67* (4), 041207.
- (32) Neimark, A. V.; Ravikovitch, P. I.; Vishnyakov, A. *Phys. Rev. E* **2002**, *65* (3 Pt 1), 031505.
- (33) Nguyen, T. X.; Bhatia, S. K. *Langmuir* **2008**, *24* (1), 146–154.
- (34) Barrer, R. *Zeolites and Clay Minerals As Sorbents and Molecular Sieves*; Academic Press: London, New York, 1978.
- (35) Chmelik, C.; Bux, H.; Caro, J.; Heinke, L.; Hibbe, F.; Titze, T.; Kärger, J. *Phys. Rev. Lett.* **2010**, *104*, 8.
- (36) Dvoyashkin, M.; Khokhlov, A.; Valiullin, R.; Kärger, J. *J. Chem. Phys.* **2008**, *129* (15), 154702.
- (37) Kärger, J. *Adsorption* **2003**, *9*, 29–35.
- (38) Ruthven, D. M. *Molecular Sieves—Science and Technology: Adsorption and Diffusion*; Springer-Verlag: Berlin, Heidelberg, 2008; Vol. 7.
- (39) Agger, J. R.; Hanif, N.; Cundy, C. S.; Wade, A. P.; Dennison, S.; Rawlinson, P. A.; Anderson, M. W. *J. Am. Chem. Soc.* **2003**, *125* (3), 830–839.
- (40) Feldhoff, A.; Caro, J.; Jobic, H.; Ollivier, J.; Krause, C. B.; Galvosas, P.; Kärger, J. *ChemPhysChem* **2009**, *10* (14), 2429–2433.
- (41) Jobic, H. *Molecular Sieves—Science and Technology: Adsorption and Diffusion*; Springer-Verlag: Berlin, Heidelberg, 2008; Vol. 7.
- (42) Jobic, H.; Theodorou, D. N. *Microporous Mesoporous Mater.* **2007**, *102* (1–3), 21–50.
- (43) Valiullin, R.; Kärger, J.; Gläser, R. *Phys. Chem. Chem. Phys.* **2009**, *11* (16), 2833.
- (44) Dvoyashkin, M.; Khokhlov, A.; Naumov, S.; Valiullin, R. *Microporous Mesoporous Mater.* **2009**, *125* (1–2), 58–62.

Zusammenfassung der wissenschaftlichen Ergebnisse
zur Dissertation

**Nuclear Magnetic Resonance Studies of Molecular Transport in Activated Carbon and
Other Porous Media**

Der Fakultät für Chemie und Mineralogie der Universität Leipzig
vorgelegt von

Dipl.-Chem. Filipe Ricardo Correia Duarte Furtado

im April, 2011

Angefertigt am Department für Technische Umweltchemie, Helmholtz-Zentrum für
Umweltforschung UFZ

Abstract

Mass transfer in porous media has a significant impact in phenomena such as pollutant bioavailability in soils and heterogeneous chemical catalysis. In these cases, the mechanisms for molecular transport are frequently of a complex nature and remain poorly understood. Thus, growing environmental awareness and the rising demand for more efficient catalytic processes have triggered investigations in this and related fields. Recently, efforts in the synthesis of activated carbons mainly for applications in chemical catalysis successfully yielded materials of a hierarchical pore structure, from natural [1] and synthetic [2] origin. Accompanying the advent of such materials, the present thesis focuses mainly on the investigation of diffusive transport in activated carbons with a bi-modal pore size distribution from lignocellulosic (MAC-LMA12) and polymeric (MA2) precursors. This was achieved by using the ability of Pulsed Field Gradient Nuclear Magnetic Resonance (PFG NMR) technique to trace molecular displacements in a microscopic, non-invasive way. In addition to this method, and bearing the study of environmental systems in mind, the phenomenon of Paramagnetic Relaxation Enhancement (PRE) was used to develop a new NMR-based approach to investigate molecular transport in water-saturated porous media, without recurring to the use of PFG. The experimental accomplishments and findings are summarized below.

Results

The spin-echo attenuation curves of cyclohexane in the MA2 sample and of toluene in MAC-LMA12 sample revealed a pronounced deviation from a mono-exponential decay, which implies a broad distribution of diffusion coefficients. Resembling other systems in the literature [3], the assumption of a log-normal distribution of diffusion coefficients yielded a good approximation to the experimental data in the case of the MA2 sample (Figure 1.a). This distribution remained unchanged upon variation of several parameters such as the observation time, the influence of the nuclear magnetic transverse relaxation time and the particle size. In particular, the observation time independency indicates that the sample morphology is homogeneous for sub-regions of 2 to 13 μm and that the distance after which significant transport barriers occur should be larger than the referred upper limit.

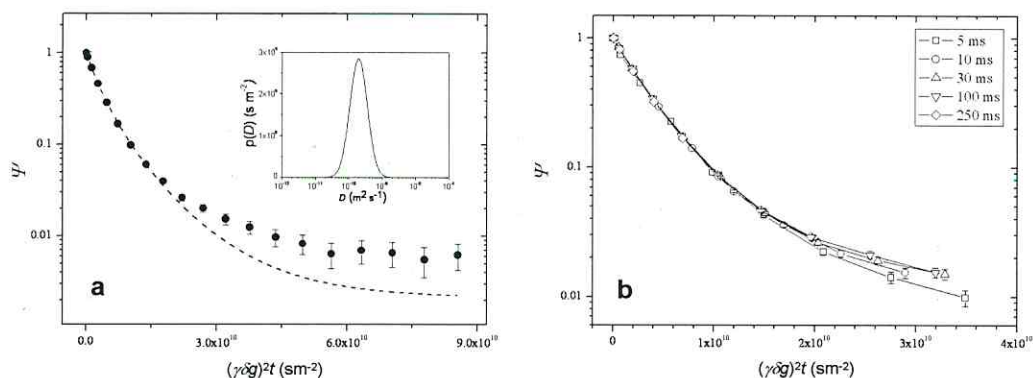


Figure 1 – a) Spin-echo attenuation of cyclohexane in a fully loaded MA2 sample, at 298 K ($t = 10$ ms) and best fit by assumption of a log-normal distribution of diffusion coefficients. The insert shows the distribution of the diffusion coefficients. b) Spin-echo attenuation of cyclohexane in a fully loaded MA2 sample, at 298 K for different observation times (t).

A similar behavior of a guest molecule (n -butane) was observed in a purely microporous zeolite (NaX) for lower loadings. This confirms the existence of internal transport barriers (as indicated in Ref. [4]), revealing considerable deviations from the idealized structure of these materials. Similarly to the activated carbon system, the primary NMR data obtained from n -butane in zeolite NaX was successfully fitted by a log-normal distribution function (Figure 2.a, 2.b). At higher loadings, n -butane diffusivity showed a bimodal character, rather than being

log-normally distributed, accompanied by an observation time dependency. These results are interpreted in light of known models [5] for interparticle or long-range diffusion.

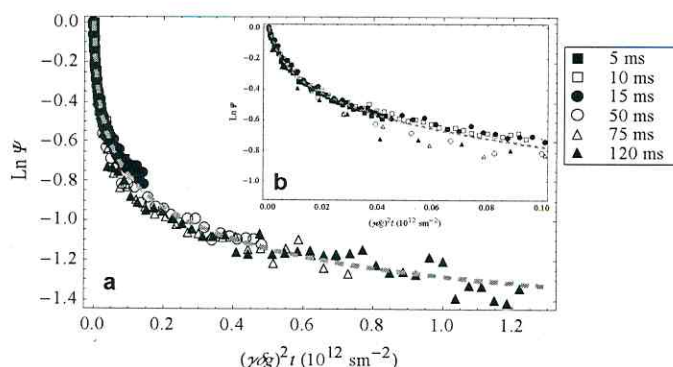


Figure 2. PFG NMR spin-echo attenuation curves for *n*-butane in the NaX sample under study for different observation times as indicated by the different symbols at 298 K and for guest loadings of 0.75 molecules per cavity. The broken line represents the best fit of the attenuation curves for a log-normal distribution of the diffusivities to the data points. The inset (b) shows a detail of the region from 0 till 10^{11} (sm^{-2}) of the effective gradient strength in a).

Containing an almost perfectly defined mixture of micro- and mesopores, the MA2 activated carbon is an exciting system for the investigation of hysteresis phenomena, which are known to occur in purely mesoporous materials. An experimental correlation between the system uptake and the mass transfer occurring inside the pore structure was established. This was achieved by a procedure resembling the isothermal gas adsorption in which, upon system saturation, the external pressure of cyclohexane is varied subsequently to lower values until loading reached about 50% (corresponding to empty mesopores) followed by a stepwise increase of the pressure, till saturation is reached. In each pressure step the loading of sample was determined by the initial intensity of the NMR free induction decay (FID) whereas the average diffusivity was determined by NMR diffusometry. The results are shown in Figure 3 and indicate that the chosen waiting times (10 minutes) between each pressure step on the desorption branch were sufficient to show significant effect on the loading of the system, while this was not the case in the adsorption branch. This resulted in the observation of hysteresis in the loading and diffusivity data. In the case of adsorption, only waiting times of up to 20h at pressures close to

saturation, had a significant effect on the experimentally determined loadings. Resembling purely mesoporous systems [5], loading and diffusivity appear to be directly correlated with the “history” of the sample: they are found to be larger upon decreasing pressure (desorption) than for increasing pressure (adsorption). The maximum in the diffusivities observed in the adsorption branch was predicted by simple model considerations which take into account the contributions of micropore- and gas-diffusivity in the mesopores (see Figure 3.a, dashed line).

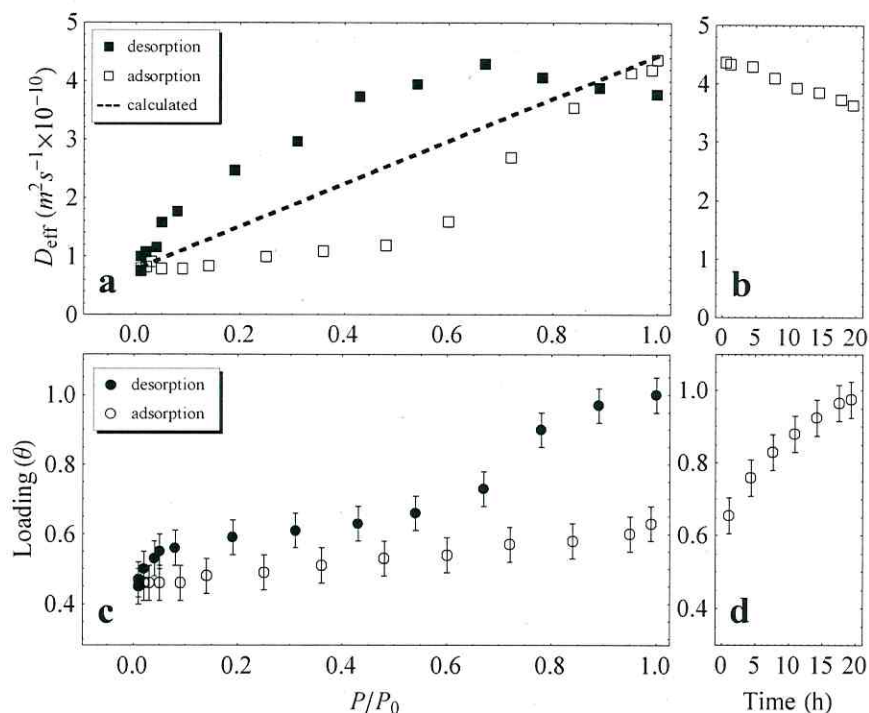


Figure 3. a) Diffusivities of cyclohexane at 298 K in MA2 as a function of the relative external pressure during adsorption and desorption and the calculated diffusivities by considering micropore- and gas-diffusivity in the mesopores, as a function of the external cyclohexane pressure. b) Evolution of the diffusivities with time after the last pressure step (to $P/P_0 \approx 1$) on the adsorption branch. c) Cyclohexane loading isotherm at 298 K in MA2 as a function of the external pressure during adsorption and desorption, measured 10 min after each pressure variation. d) Loading evolution with time after the pressure step to $P/P_0 \approx 1$ on the adsorption branch.

In addition to these results, the dependence of diffusivity on decreasing loading and pressure (desorption branch) was fitted by combining the determined micropore diffusivity with literature models used to describe the diffusivity in purely mesoporous materials [7,8], in which the contributions arising from both the bulk liquid and the gas phase in the pores, are taken into account. Consideration of the estimated pore size distribution and the respective diffusivities, led to a good agreement with the experimentally obtained data (Figure 4) and yielded a tortuosity value ($\tau_{\text{des}}=1.5$) which is in good agreement with the value found to explain the maximum in the diffusivity observed in the adsorption branch ($\tau_{\text{ads}}=1.3$). Upon complete system saturation, the diffusivities from micro- and mesopores were estimated based on their relative volume, known from the N_2 adsorption isotherm. Mesopore diffusivity was found to be reduced by a factor of 2, which shows a good agreement to values of tortuosity found for both adsorption and desorption in the gas phase.

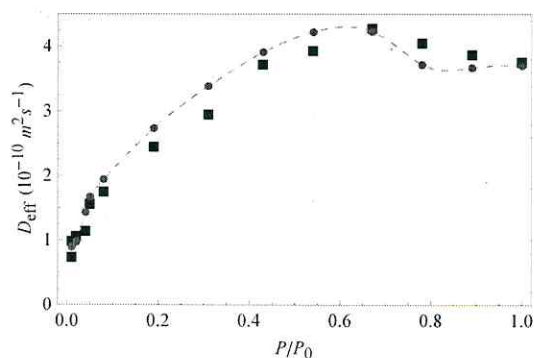


Figure 4 – Comparison between effective diffusivities: experimental data determined (squares) and model estimates (dots, dashed line), by considering the contribution of molecular transport by Knudsen diffusion in the pore gas phase.

In addition to the results obtained by PFG NMR, an alternative method to the latter was developed in order to measure the diffusivities of chemical compounds in lower concentrations. The transport diffusivity of the paramagnetic molecule 2,2,6,6-tetramethylpiperidine-1-oxyl (TEMPO) was measured by monitoring its influence on the NMR transverse relaxation time (T_2) on surrounding water protons due to the PRE. Due to the nature of the PRE effect, a few paramagnetic molecules are already able to simultaneously reduce the T_2 of many NMR-active

nuclei, allowing, e.g., the detection of TEMPO in water in concentrations as low as 70 ppm. The changes in the NMR transverse relaxation times of water protons due to migration of TEMPO were measured via the CPMG pulse sequence, in both a homogenous phase and in a water-saturated sand column. The transport diffusivity was estimated by fitting the experimental data (Figure 5) in by considering models in accordance with the systems investigated. The method yielded results in agreement to the literature values, and thus opens a new approach to investigate molecular dynamics of probe molecules in low concentrations, as a method to provide information on the interactions with matrices of environmental relevance.

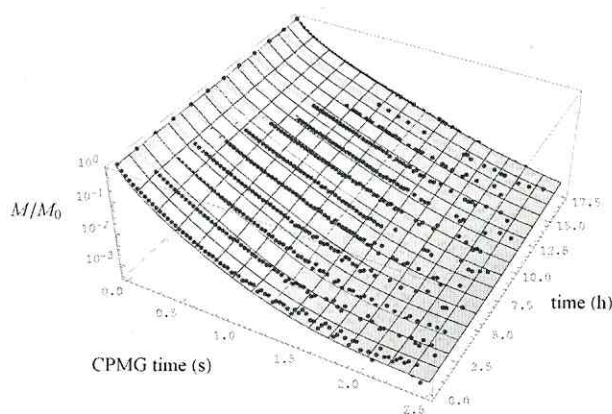


Figure 5 – Measured CPMG data of a water in a saturated sand column as a function of diffusion time (●) and respective fit (semi-transparent surface ⊗).

Summary

The present work explores different aspects of the applicability of NMR in studying of molecular dynamics, with emphasis on, but not limited to, NMR Diffusometry. The difficulties in using the latter technique under experimentally challenging conditions due to the intrinsic properties of the activated carbons were successfully overcome and a significant contribution to understand mass transfer phenomena in systems with bi-modal pore size distributions has been given. While further theoretical and experimental investigations would be needed to fully clarify the hysteretic behavior observed in the investigated system, the present work adds an important experimental contribution on this topic. The newly developed methodology represents a feasible

alternative to the use of PFG and brings NMR methods closer to environmentally relevant applications, opening new possibilities to investigate such complex systems at low concentrations.

Literature

- [1] J.M.Juárez-Galán, A. Silvestre-Albero, J. Silvestre-Albero, and F. Rodríguez-Reinoso, Synthesis of activated carbon with highly developed "mesoporosity", *Microporous Mesoporous Mater.*, **2009**, *117*, 519.
- [2] S. R. Tennison, O. P. Kozynchenko, V. V. Strelko, and A. J. Blackburn, Porous carbons, US Patent 2004/0024074 A1.
- [3] G. Fleischer, F. Rittig, J. Kärger, C. M. Papadakis, K. Mortensen, K. Almdal, and P. Štěpánek, Self-diffusion of an asymmetric diblock copolymer above and below the order-to-disorder transition temperature, *J. Chem. Phys.*, **1999**, *111*, 2789.
- [4] Vasenkov, S., Kärger, J., Evidence for the existence of intracrystalline transport barriers in MFI-type zeolites: a model consistency check using MC simulations, *Microporous Mesoporous Mater.* **2002**, *55*, 139.
- [5] J. Kärger, Diffusion measurements by NMR techniques, in *Adsorption and Diffusion*, 7 ed. H. G. Karge and J. Weitkamp, Eds. Berlin, Heidelberg: Springer Berlin Heidelberg, **2008**, pp. 85-133
- [6] R. Valiullin, S. Naumov, P. Galvosas, J. Kärger, H. J. Woo, F. Porcheron, and P. A. Monson, Exploration of molecular dynamics during transient sorption of fluids in mesoporous materials, *Nature*, **2006**, *443*, 965.
- [7] R. Valiullin, P. Kortunov, J. Kärger, and V. Timoshenko, Concentration-dependent self-diffusion of liquids in nanopores: a nuclear magnetic resonance study, *J. Chem. Phys.*, **2004**, *120*, 11804.
- [8] R. Valiullin, J. Kärger, and R. Gläser, Correlating phase behaviour and diffusion in mesopores: perspectives revealed by pulsed field gradient NMR, *Phys. Chem. Chem. Phys.*, **2009**, *11*, 2833.

Publication List

- 1) M. Krutyeva, F. Grinberg, F. Furtado, P. Galvosas, J. Kärger, A. Silvestre-Albero, A. Sepulveda-Escribano, J. Silvestre-Albero, F. Rodríguez-Reinoso, Characterisation of carbon materials with the help of NMR methods, *Micropor. Mesopor. Mat.*, 2009, 120, 91.
- 2) F. Furtado, P. Galvosas, M. Gonçalves, F.-D. Kopinke, S. Naumov, F. Rodríguez-Reinoso, U. Roland, R. Valiullin, J. Kärger, The evidence of NMR diffusometry on pore space heterogeneity in activated carbon, *Micropor. Mesopor. Mat.*, 2011, 141, 184.
- 3) Z. Adem, J. Caro, F. Furtado, P. Galvosas, C. Krause, J. Kärger, Tracing pore-space heterogeneities in X-type zeolites by diffusion studies, *Langmuir*, 2011, 27, 416.
- 4) F. Furtado, P. Galvosas, M. Gonçalves, F.-D. Kopinke, S. Naumov, F. Rodríguez-Reinoso, U. Roland, R. Valiullin, J. Kärger, Guest Diffusion in Interpenetrating Networks of Micro- and Mesopores, *J. Am. Chem. Soc.*, 2011, 133, 2437.
- 5) F. Furtado, P. Galvosas, F. Stallmach, U. Roland, F.-D. Kopinke, J. Kärger, Paramagnetic Relaxation Enhancement (PRE) as a tool for probing diffusion in environmentally relevant porous media, *Environ. Sci. Technol.* (submitted).

Oral Presentations

- 1) RAISEBIO Summerschool - *Chemicals in Soil: Interactions, Availability and Residue Formation*, 24th – 27th of September 2007, Leipzig
- 2) RAISEBIO Summerschool - *Chemicals in Soil: Interactions, Availability and Residue Formation*, 22th – 25th of September 2008, Leipzig
- 3) 9th Workshop from the International Research Training Group (IRTG) "*Diffusion in Porous Materials*", 4th – 6th of February 2009, Leipzig
- 4) 5th UFZ Doc-Conference, 28th of April 2009, Leipzig
- 5) Final RAISEBIO Symposium - Microbial Contaminant Degradation at Biogeochemical Interfaces, 2nd -4th March 2010, Leipzig

Errata

- on Chapter 1, page 9, on the legend of Figure 3

“SEM image of faujasite” should read “TEM image of faujasite”

- on Chapter 2, Publication 5, page 137, Equation (7) should read

$$\tau_D = \frac{d_{\min}^2}{D_{\text{TEMPO}} + D_{\text{water}}} \quad (7)$$

